INFORMATION TO USERS

This reproduction was made from a copy of a document sent to us for microfilming. While the most advanced technology has been used to photograph and reproduce this document, the quality of the reproduction is heavily dependent upon the quality of the material submitted.

The following explanation of techniques is provided to help clarify markings or notations which may appear on this reproduction.

1. The sign or "target" for pages apparently lacking from the document photographed is "Missing Page(s)". If it was possible to obtain the missing page(s) or section, they are spliced into the film along with adjacent pages. This may have necessitated cutting through an image and duplicating adjacent pages to assure complete continuity.

2. When an image on the film is obliterated with a round black mark, it is an indication of either blurred copy because of movement during exposure, duplicate copy, or copyrighted materials that should not have been filmed. For blurred pages, a good image of the page can be found in the adjacent frame. If copyrighted materials were deleted, a target note will appear listing the pages in the adjacent frame.

3. When a map, drawing or chart, etc., is part of the material being photographed, a definite method of "sectioning" the material has been followed. It is customary to begin filming at the upper left hand corner of a large sheet and to continue from left to right in equal sections with small overlaps. If necessary, sectioning is continued again—beginning below the first row and continuing on until complete.

4. For illustrations that cannot be satisfactorily reproduced by xerographic means, photographic prints can be purchased at additional cost and inserted into your xerographic copy. These prints are available upon request from the Dissertations Customer Services Department.

5. Some pages in any document may have indistinct print. In all cases the best available copy has been filmed.

University Microfilms International
300 N. Zeeb Road
Ann Arbor, MI 48106

Downloaded from SHAREOK. Persistent Handle URL: https://hdl.handle.net/11244/5123

8314773

Karber, Lionel Gordon

DIFFERENTIAL PULSE VOLTAMMETRIC OXIDATION OF POLYINOSINIC ACID AND ITS COMPONENTS AND ELECTROCHEMISTRY OF 6-METHYL-5,6,7,8-TETRAHYDROPTERIN AND 5-METHYL-5,6,7,8-TETRAHYDROPTERIN

The University of Oklahoma PH.D. 1983

University
Microfilms
International 300 N. Zeeb Road, Ann Arbor, MI 48106

PLEASE NOTE:

In all cases this material has been filmed in the best possible way from the available copy. Problems encountered with this document have been identified here with a check mark __√__.

1. Glossy photographs or pages _____
2. Colored illustrations, paper or print _____
3. Photographs with dark background ✓
4. Illustrations are poor copy _____
5. Pages with black marks, not original copy _____
6. Print shows through as there is text on both sides of page _____
7. Indistinct, broken or small print on several pages ✓
8. Print exceeds margin requirements _____
9. Tightly bound copy with print lost in spine _____
10. Computer printout pages with indistinct print _____
11. Page(s) _____ lacking when material received, and not available from school or author.
12. Page(s) _____ seem to be missing in numbering only as text follows.
13. Two pages numbered _____. Text follows.
14. Curling and wrinkled pages _____
15. Other _____

University
Microfilms
International

THE UNIVERSITY OF OKLAHOMA

GRADUATE COLLEGE

DIFFERENTIAL PULSE VOLTAMMETRIC OXIDATION OF POLYINOSINIC ACID AND ITS COMPONENTS

AND

ELECTROCHEMISTRY OF 6-METHYL-5,6,7,8-TETRAHYDROPTERIN AND 5-METHYL-5,6,7,8-TETRAHYDROPTERIN

A DISSERTATION

SUBMITTED TO THE GRADUATE FACULTY

in partial fulfillment of the requirements for the

degree of

DOCTOR OF PHILOSOPHY

BY

LIONEL GORDON KARBER

Norman, Oklahoma

1982

DIFFERENTIAL PULSE VOLTAMMETRIC OXIDATION OF

POLYINOSINIC ACID AND ITS COMPONENTS

AND

ELECTROCHEMISTRY OF 6-METHYL-5,6,7,8-TETRAHYDROPTERIN

AND 5-METHYL-5,6,7,8-TETRAHYDROPTERIN

APPROVED BY

DISSERTATION COMMITTEE

ACKNOWLEDGEMENTS

I would like to express my gratitude to Dr. Glenn Dryhurst for suggesting the research problems in this work and for his guidance throughout my graduate career.

A special thanks must go to the late J. Clarence Karcher whose endowment to the University of Oklahoma provided financial support for me in the form of a three year fellowship. My appreciation also goes to Dr. Glenn Dryhurst for financial assistance in the form of a research assistantship.

My appreciation especially goes out to Henry Marsh, Jr. who patiently taught me many of the electrochemical techniques used throughout this work. Thanks also go to Henry Marsh, Jr., Deniz Ege-Serpkenci, Arnold Conway, and Raymond Chen for their friendship during my graduate career.

I would like to thank the entire staff of the Chemistry Department for their support, especially the secretaries, Fred Dillon in the electronics shop, and Dr. Tom Karns.

I also wish to thank my parents, Mr. and Mrs. Reuben Karber, and my wife's parents, Mr. and Mrs. A. W. Dugger for their support and encouragement.

Most important of all I want to thank my wife, Debbie, whose patience, understanding, and encouragement were indispensable these

last five years. I also want to thank my son, Jeremy, whose cheeriness kept us going many times when we were discouraged. I could never have finished this work without the encouragement of my loving family.

TABLE OF CONTENTS

Page

LIST OF TABLES . . . . . .

LIST OF ILLUSTRATIONS . . . . . .

PART I. DIFFERENTIAL PULSE VOLTAMMETRIC OXIDATION OF POLYINOSINIC ACID AND ITS COMPONENTS 1

Chapter

I. INTRODUCTION 1

II. RESULTS AND DISCUSSION 6

III. EXPERIMENTAL 46

IV. SUMMARY 51

V. REFERENCES 53

PART II. ELECTROCHEMISTRY OF 6-METHYL-5,6,7,8-TETRAHYDROPTERIN 55

Chapter

I. INTRODUCTION 55

II. RESULTS 75

III. DISCUSSION 143

IV. EXPERIMENTAL 149

V. SUMMARY 155

VI. REFERENCES 156

TABLE OF CONTENTS (continued)

	Page
PART III. ELECTROCHEMISTRY OF 5-METHYL-5,6,7,8-TETRAHYDROPTERIN	161
Chapter	
I. INTRODUCTION	161
II. RESULTS AND DISCUSSION	166
III. EXPERIMENTAL	301
IV. SUMMARY	304
V. REFERENCES	305

LIST OF TABLES

Table		Page
PART I.		
1.	pK_a Values for Poly(I) and its Monomeric Components . .	4
2.	U.v. Spectral Data for Hypoxanthine and Its Derivatives.	4
3.	Determination of Hypoxanthine in Poly(I) Samples by Differential Pulse Voltammetric Oxidation at the PGE . .	45
PART II.		
1.	U.v. Spectral Data for 6-MTHP	73
2.	U.v. Spectral Data for 6-MDHP	73
3.	U.v. Spectral Data for 6-MP	74
4.	Coulometric n-values Observed Upon Electrolysis of 6-MTHP at Peak I_a and Peak III_a Potentials	103
5.	Coulometric n-values Observed Upon Electrolysis of 0.5 mM 6-MDHP at Peak II_a and Peak III_a Potentials . . .	107
6.	Fraction of 6-MP and 6-MDHP Found in 6-MTHP Solutions Utilizing a High Performance Chromatographic Method . .	109
7.	Observed First Order Rate Constants for Chemical Reaction of the Intermediate Generated Upon Peak I_a Oxidation of 1.0 mM 6-MTHP as a Function of pH	122
8.	Observed First Order Rate Constants for Chemical Reaction of the Intermediate Generated Upon Peak I_a Oxidation of 0.5 mM 6-MTHP as a Function of pH	123
9.	Observed First Order Rate Constants for Chemical Reaction of the Intermediate Generated Upon Peak I_a Oxidation of 0.1 mM 6-MTHP as a Function of pH	124

LIST OF TABLES (continued)

Table		Page
10.	Observed Pseudo-first Order Rate Constants for Chemical Reaction of the Intermediate Generated Upon Peak I_a Oxidation of 6-MTHP as a Function of Buffer Ionic Strength at pH 7.0	131
11.	Observed First Order Rate Constants for Chemical Reaction of the Intermediate Formed Upon Peak II_a and Peak III_a Electrooxidation of 6-MDHP	142
PART III.		
1.	n-Values for Electrolysis of Fresh Solutions of 0.75 mM 5-MTHP in pH 4.7 Phosphate	189
2.	Coulometric n-values Observed Upon Electrooxidation of 1.0 mM 5-MTHP in Phosphate Buffers	191
3.	First Order Rate Constants Obtained for the Chemical Rearrangement of Intermediates Generated Upon Electrooxidation of 1.0 mM 5-MTHP at Peak I_a	202
4.	Molecular Ions for GC-MS Peaks Which Increase During Peak I_a Electrolysis of 15 mg 5-MTHP in pH 4.7 NaCl, 0.5 M	221
5.	Comparison of Fully Electrolyzed Samples at Different Silylation Temperatures from Electrolysis of 15 mg 5-MTHP in pH 4.7 NaCl	223
6.	Possible Molecular Weights Which Could Yield the Observed Molecular Ions When Silylated with MTBSTFA	224
7.	Possible Empirical Formulas for Molecular Weight = 116 g/mole Containing C, H, N, and O	277
8.	Isotopic Abundances	278
9.	Possible Empirical Formulas With the Lowest P_{M+1}/P_{M+2} Ratio	280
10.	Calculated Isotopic Abundances for the Silylated Derivatives	281
11.	Possibilities for Compounds with Molecular Formulas $C_2H_4N_4O_2$ and $C_3H_4N_2O_3$	282

LIST OF ILLUSTRATIONS

Figure — Page

PART I.

1. (A) Excitation potential waveform for differential pulse polarography. (B) Current as a function of time during the drop lifetime 7

2. Typical differential pulse polarogram 9

3. E_p *vs.* pH relationship for the differential pulse voltammetric oxidation peaks of hypoxanthine at a sweep rate of 5 mV s^{-1}. (A) 0.037 mM hypoxanthine and (B) 3.68 mM hypoxanthine 12

4. Differential pulse valtammograms of 3.68 mM hypoxanthine at 5 mV s^{-1}. (A) pH 4.94, (B) pH 7.00, and (C) pH 9.03 14

5. (A) Peak current *vs.* concentration curves for the differential pulse voltammetric oxidation peak of hypoxanthine at the PGE in pH 7 phosphate buffer obtained at a sweep rate of 5 mV s^{-1}. (B) Expanded low concentration region of A 16

6. Differential pulse voltammograms of inosine in pH 10.9 phosphate buffer at a sweep rate of 5 mV s^{-1}. (A) 2.03 mM inosine and (B) 0.20 M inosine 17

7. Peak potential, E_p *vs.* pH relationship for the differential pulse voltammetric oxidation peaks of inosine observed in phosphate buffers at a sweep rate of 5 mV s^{-1}. (A) 0.20 mM inosine and (B) 2.03 mM inosine 19

8. Peak current *vs.* concentration curves for the differential pulse voltammetric oxidation peaks of inosine at the PGE in pH 11.0 phosphate buffer obtained at a sweep rate of 5 mV s^{-1} 21

9. E_p *vs.* pH relationship for the differential pulse voltammetric oxidation peaks of inosine-5'-monophosphate (IMP) observed at 5 mV s^{-1}. (A) 0.095 mM IMP and (B) 0.95 mM IMP 22

LIST OF ILLUSTRATIONS (continued)

Figure — Page

10. Differential pulse voltammogram of 0.95 mM IMP in pH 8.45 phosphate buffer obtained at a sweep rate of 5 mV s^{-1} 24

11. i_p vs. concentration curves for the differential pulse voltammetric oxidation peaks of IMP at the PGE in pH 7.0 phosphate buffer obtained at a sweep rate of 5 mV s^{-1}. (A) Oxidation peak I plus II and (B) oxidation peak A . 26

12. Differential pulse voltammograms of 2.0 mM IMP in pH 7.0 phosphate buffer obtained at a sweep rate of 5 mV s^{-1}. (A) Before electrolysis at peak A and (B) after electrolysis at peak A 28

13. Differential pulse voltammograms of 0.50 mM IMP in pH 7.0 phosphate buffer observed at a sweep rate of 5 mV s^{-1}. (A) IMP alone and (B) 0.0049 mM hypoxanthine + IMP 29

14. Differential pulse voltammograms of 0.99 mM IMP in pH 7.0 phosphate buffer obtained at a sweep rate of 5 mV s^{-1}. (A) IMP alone and (B) 0.025 mM adenine + IMP . . . 31

15. i_p vs. concentration curve for the differential pulse voltammetric oxidation peak of adenine which was added in known concentrations to an IMP solution. Voltammograms were obtained in pH 7.0 phosphate buffer at a sweep rate of 5 mV s^{-1} 32

16. Differential pulse voltammogram of 1.65 mM poly(I) in pH 6.25 phosphate buffer obtained at a sweep rate of 5 mV s^{-1} 34

17. E_p vs. pH relationship for the single differential pulse voltammetric oxidation peak of poly(I) obtained at a sweep rate of 5 mV s^{-1} 35

18. E_p vs. pH relationship for the single differential pulse voltammetric oxidation peak of 5.0 mM poly(I) obtained at 5 mV s^{-1} 36

19. i_p vs. buffer ionic strength for the single differential pulse voltammetric oxidation peak of 1.65 mM poly(I) in pH 6.3 phosphate buffer 38

20. i_p vs. concentration curve for the differential pulse voltammetric oxidation peak of poly(I) in phosphate buffers of ionic strength 0.5 M. (A) pH 5.3 and (B) pH 7.0 39

LIST OF ILLUSTRATIONS (continued)

Figure — Page

21. i_p vs. hypoxanthine concentration in pH 7.0 phosphate buffer containing 2.0 mM poly(I) 42

22. Hypoxanthine peak current vs. poly(I) concentration in pH 7.0 phosphate buffer. The hypoxanthine concentration was held constant at (A) 0.040 mM and (B) 0.010 mM . . . 43

23. i_p vs. hypoxanthine concentration in pH 7.0 phosphate buffer at a constant poly(I) concentration of 5.0 mM . . 44

PART II.

1. Original reaction scheme proposed by Kaufman for the participation of tetrahydropterin cofactors in the enzymic hydroxylation of phenylalanine 57

2. Reaction scheme showing the five possible quinonoid-dihydropterins which might be formed 59

3. Later reaction scheme proposed by Kaufman to explain how molecular oxygen might be involved in the hydroxylation of phenylalanine 61

4. Hamilton's reaction scheme for enzymic hydroxylation of phenylalanine involving tetrahydropterin hydroperoxides 63

5. Bailey-Ayling reaction scheme to explain cofactor properties of pyrimidines 64

6. Proposed reaction mechanism for the intermediacy of radicals in the auto-oxidation of tetrahydrobiopterin and tetrahydrofolic acid 66

7. Simplified reaction scheme to explain the formation of 7,8-dihydroxanthopterin and xanthopterin from 7,8-dihydropterin 69

8. (A) Cyclic voltammogram of 0.5 mM 7,8-dihydroxanthopterin at the PGE. (B) Cyclic voltammogram of electrolysis product of 7,8-DHP. Voltammograms were obtained in pH 6.0 phosphate buffer at a sweep rate of 200 mV s^{-1} 70

9. Linear sweep voltammograms of 1.0 mM 6-MTHP at a PGE in phosphate buffer at a sweep rate of 5 mV s^{-1}. (A) pH 3.0 and (B) pH 5.6 76

10. Cyclic voltammogram of 1.0 mM 6-MTHP in pH 3.0 phosphate buffer showing peaks V_c and VI_c. Sweep rate 200 mV s^{-1} 77

LIST OF ILLUSTRATIONS (continued)

Figure — Page

11. Variation of E_p vs. pH for the voltammetric oxidation peaks of 1.0 mM 6-MTHP observed at a sweep rate of 5 mV s^{-1} 78

12. Linear sweep voltammograms of 0.5 mM 6-MDHP in phosphate buffers at a sweep rate of 5 mV s^{-1}. (A) pH 3.1, (B) pH 5.6, and (C) pH 6.9 81

13. E_p vs. pH relationship for the voltammetric oxidation peaks of 0.5 mM 6-MDHP observed at a sweep rate of 5 mV s^{-1} 82

14. Cyclic voltammogram of 1.0 mM 6-MTHP in pH 2.0 phosphate buffer at a sweep rate of 200 mV s^{-1} 83

15. Cyclic voltammograms of 0.5 mM 6-MDHP in pH 3.0 phosphate buffer. (A) 200 mV s^{-1} and (B) 1 V s^{-1} 85

16. Linear sweep voltammograms of 6-MTHP at the PGE in pH 3.0 phosphate buffer. (A) 0.35 mM 6-MTHP and (B) 9.7 mM 6-MTHP 88

17. i_p vs. concentration dependence for the oxidation peaks of 6-MTHP in pH 3.0 phosphate buffer at a sweep rate of 5 mV s^{-1} 89

18. i_p vs. concentration for peak I_a of 6-MTHP in pH 3.0 phosphate buffer at a sweep rate of 5 mV s^{-1} 90

19. i_p vs. concentration curves for the voltammetric oxidation peaks of 6-MDHP in pH 3.0 phosphate buffer at a sweep rate of 5 mV s^{-1} 92

20. Peak current function vs. the square root of the sweep rate for the voltammetric oxidation peaks of 1.0 mM 6-MTHP in pH 3.0 phosphate buffer 94

21. Linear sweep voltammograms of 0.5 mM 6-MDHP in pH 3.0 phosphate buffer at a sweep rate of (A) 20 mV s^{-1}, (B) 50 mV s^{-1}, and (C) 100 mV s^{-1} 96

22. Peak current function vs. the square root of the sweep rate for the voltammetric oxidation peaks of 0.5 mM 6-MDHP in pH 3.0 phosphate buffer 98

23. i_p vs. sweep rate for peak III_a' of 0.5 mM 6-MDHP in pH 3.0 phosphate buffer 99

LIST OF ILLUSTRATIONS (*continued*)

Figure — Page

24. Cyclic voltammograms of 0.5 mM 6-MDHP in pH 2.0 phosphate buffer at a sweep rate of 200 mV s^{-1}. (A) hold 0 seconds and (B) hold 10 seconds 101

25. Linear sweep voltammograms of 1.0 mM 6-MTHP in pH 3.0 phosphate buffer in the RVC thin-layer cell at 5 mV s^{-1}. (A) Fresh solution and (B) after running one voltammogram 104

26. HPLC chromatogram of 0.1 mM 6-MTHP in pH 5.6 phosphate buffer utilizing pH 6.1 phosphate buffer of ionic strength 0.1 M as the eluant. (A) Before injection of sodium dithionite and (B) after injection of dithionite 111

27. Method used for determining peak area of HPLC chromatogram 112

28. U.v. spectra of 0.5 mM 6-MDHP in pH 2.0 phosphate buffer in 1 mm quartz cells. (A) During electrolysis at peak II_a potentials (0.35V), (B) before and after electrolysis at peak III_a potentials (0.60V), and (C) after electrolysis at a potential positive of peak III_a (0.85V) . 114

29. Spectrum of 0.5 mM 6-MTHP electrolyzing at 0.37V at a RVC electrode in a thin-layer cell in pH 3.1 phosphate buffer 115

30. Spectra of 0.51 mM 6-MTHP electrolyzing at 0.27V at a RVC electrode in a thin-layer cell in pH 4.7 phosphate buffer 118

31. Spectra of 0.52 mM 6-MTHP electrolyzing at 0.08V at a RVC electrode in a thin-layer cell in pH 9.1 phosphate buffer 119

32. (A) A vs. t curve for the decay of the intermediate species generated upon electrolysis of 1.0 mM 6-MTHP at 0.32V for 20s in pH 4.0 phosphate buffer. (B) Ln $|A-A_\infty|$ vs. t for the decay curve in A 121

33. (A) A vs. t curve for the decay of the intermediate generated upon electrolysis of 1.0 mM 6-MTHP at 0.01V for 50s in pH 9.9 phosphate buffer. (B) Ln $|A-A_\infty|$ vs. t for the decay curve in A 126

34. A vs. t curve for the decay of the intermediate generated upon electrolysis of 0.1 mM 6-MTHP at 0.28V for 20s in pH 4.6 phosphate buffer 127

LIST OF ILLUSTRATIONS (continued)

Figure Page

35. Variation of rate constant vs. pH for the rearrangement of the intermediate generated upon peak I_a electrooxidation of 1.0 mM 6-MTHP 128

36. Variation of the rate constant vs. ionic strength for the rearrangement of the intermediate generated upon peak I_a electrooxidation of 1.0 mM 6-MTHP in pH 7 phosphate buffer 130

37. (A) Spectra of 0.052 mM 6-MTHP oxidizing in a solution of 0.039 mM I_2/0.2 mM I^- buffered to pH 7 with phosphate obtained in a 1 cm quartz cuvette. (B) Same as A except now a peak is observed at 242 nm 135

38. Spectra of 0.5 mM 6-MDHP electrolyzing at peak II_a potentials at a RVC electrode in a thin-layer cell in phosphate buffers. (A) pH 2.0 and (B) pH 5.6 138

39. (A) A vs. t curve for the decay of the intermediate generated upon electrolysis of 0.5 mM 6-MDHP at 0.40V for 50s in pH 4.5 phosphate buffer. (B) Ln $|A-A_\infty|$ vs. t for the decay curve in A 140

40. Reaction scheme proposed to explain the oxidation and reduction peaks observed upon cyclic voltammetry of 6-MTHP at the PGE 144

41. Design of RVC thin-layer cell for spectroelectrochemical studies in the absence of atmospheric oxygen . . . 151

PART III.

1. Linear sweep voltammograms of 1.0 mM 5-MTHP in phosphate buffers at a sweep rate of 5 mV s^{-1}. (A) pH 1.4 and (B) pH 4.6 167

2. Variation of E_p vs. pH for the voltammetric oxidation peaks of 1.0 mM 5-MTHP observed at a sweep rate of 5 mV s^{-1} 168

3. Variation of E_p vs. pH for voltammetric oxidation peaks V_a, VI_a, and VII_a of 1.0 mM 5-MTHP observed at a sweep rate of 5 mV s^{-1} 170

4. Cyclic voltammograms of 1.0 mM 5-MTHP in phosphate buffers observed at a sweep rate of 200 mV s^{-1}. (A) pH 1.4, (B) pH 4.7, and (C) pH 9.2 171

LIST OF ILLUSTRATIONS (continued)

Figure — Page

5. Cyclic voltammogram of 0.9 mM 5-MTHP in pH 4.6 phosphate buffer. Potential was switched before scanning through peaks VI_a and VII_a. Sweep rate: 200 mV s^{-1} — 173

6. Variation of i_p vs. concentration for peak I_a of 5-MTHP in pH 4.7 phosphate buffer observed at a sweep rate of 5 mV s^{-1} . . . . . — 176

7. Cyclic voltammograms of 5-MTHP in pH 4.7 phosphate buffer. Sweep rate: 20 mV s^{-1}. 5-MTHP concentration (A) 0.075 mM and (B) 0.77 mM . . . . . — 177

8. Cyclic voltammograms of 5-MTHP in pH 4.7 phosphate buffer. Sweep rate: 200 mV s^{-1}. 5-MTHP concentration (A) 0.075 mM, (B) 0.77 mM, and (C) 2.4 mM . . . . . — 178, 179

9. (A) peak current and (B) peak current function for peak I_a of 1.0 mM 5-MTHP vs. the square root of the sweep rate at pH 4.7 . . . . . — 181

10. Cyclic voltammograms of 1.0 mM 5-MTHP in pH 4.7 phosphate buffer. Sweep rate: (A) 50 mV s^{-1} and (B) 10 mV s^{-1} — 182

11. Cyclic voltammograms of 1.0 mM 5-MTHP in pH 4.7 phosphate. Sweep rate: (A) 500 mV s^{-1}, (B) 2 V s^{-1}, and (C) 20 V s^{-1} . . . . . — 183

12. Cyclic voltammogram of 0.75 mM 5-MTHP in pH 4.7 phosphate buffer after electrooxidation at 0.20V. Sweep rate: 200 mV s^{-1}. (A) Initial sweep negative and (B) initial sweep positive . . . . . — 185

13. Cyclic voltammograms of 0.75 mM 5-MTHP in pH 4.7 phosphate buffer after electrooxidation at 0.20V/SCE. Sweep rate: 200 mV s^{-1}. Illustrates the reversibility of peaks III_a and IV_a . . . . . — 186

14. Cyclic voltammograms of 2.3 mM 5-MTHP in pH 4.7, 0.5 M NaCl. Sweep rate: 200 mV s^{-1}. (A) Before electrolysis and (B) after electrolysis at 0.26V/SCE ($E_p/2$) . . . — 187

15. Linear sweep voltammogram of 0.99 mM 5-MTHP in pH 4.2 phosphate at a RVC electrode in a thin-layer cell at a sweep rate of 5 mV s^{-1} . . . . . — 190

16. Spectra observed during peak I_a electrolysis and decay of the intermediate generated from 1.0 mM 5-MTHP in pH 4.7 phosphate buffer at a RVC electrode in a thin-layer cell . . . . . — 194

LIST OF ILLUSTRATIONS (continued)

Figure Page

17. Spectra observed during complete electrolysis of 1.0 mM 5-MTHP in pH 4.7 phosphate buffer at a RVC electrode in a thin-layer cell 195

18. Spectra observed during peak I_a electrolysis of 1.0 mM 5-MTHP and subsequent decay of the intermediate generated in pH 7.8 phosphate buffer at a RVC electrode in a thin-layer cell 198

19. Spectra observed during complete electrolysis of 1.0 mM 5-MTHP in pH 7.8 phosphate buffer at a RVC electrode in a thin-layer cell 199

20. (A) A vs. t curve observed after electrooxidation of 1.0 mM 5-MTHP in pH 6.9 phosphate buffer at peak I_a potentials. (B) Ln $|A-A_\infty|$ vs. t plot for the decay curve in A 200

21. Typical ion current chromatogram of a MTBSTFA silylated product only partially separated from phosphate buffer showing the phosphate peak at 29 minutes 204

22. Mass spectrum of phosphate triply silylated with MTBSTFA at R_t=30 minutes 205

23. Total ion current chromatogram of aliquots of 5-MTHP electrolyzed at peak I_a in a low phosphate buffer and silylated with MTBSTFA. (A) Before electrolysis and (B) after approximately 10% of the 5-MTHP was oxidized 208

24. Total ion current chromatogram of 5-MTHP starting material silylated with MTBSTFA in pyridine at room temperature for 75 minutes 209

25. Mass spectrum of 5-MTHP silylated in one position with MTBSTFA at R_t=33.1 minutes 210

26. Mass spectrum of 5-MTHP silylated in two positions with MTBSTFA at R_t=37.2 minutes 211

27. Mass spectrum of 5-MTHP silylated in three positions with MTBSTFA at R_t=40.3 minutes 212

28. Comparison of total ion current chromatograms of samples taken during peak I_a electrolysis of 5 mg of 5-MTHP in pH 4.7 NaCl and silylated with MTBSTFA. Percent 5-MTHP electrolyzed: (A) 0%, (B) 12%, (C) 23%, and (D) 31% . . 214

LIST OF ILLUSTRATIONS (continued)

Figure Page

29. Comparison of total ion current chromatograms of samples taken during peak I_a electrolysis of 10 mg of 5-MTHP in pH 4.7 NaCl and silylated with MTBSTFA. Percent 5-MTHP electrolyzed: (A) 0%, (B) 32%, and (C) 58% . . . 215

30. Mass spectrum of peak at R_t=36.9 minutes from chromatogram of Figure 29C 216

31. Total ion current chromatogram of a sample from peak I_a electrolysis of 10 mg of 5-MTHP in pH 4.7 NaCl at 77% completion silylated with MTBSTFA 218

32. Comparison of total ion current chromatograms of samples taken during peak I_a electrolysis of 15 mg of 5-MTHP in pH 4.7 NaCl and silylated with MTBSTFA. Percent 5-MTHP electrolyzed: (A) 0%, (B) 30%, (C) 67%, and (D) 100% 220

33. Total ion current chromatogram of a fully electrolyzed sample from peak I_a electrolysis of 15 mg of 5-MTHP in pH 4.7 NaCl silylated with MTBSTFA at room temperature for 30 minutes 222

34. Comparison of total ion current chromatograms of samples taken during peak I_a electrolysis of 15 mg of 5-MTHP in pH 4.7 NaCl and silylated with BSA. Percent 5-MTHP electrolyzed: (A) 0%, (B) 30%, and (C) 67% . . . 226

35. Mass spectrum of peak at R_t=30.1 minutes from chromatogram of Figure 34C 227

36. Total ion current chromatogram of an authentic sample of pterin silylated with MTBSTFA in pyridine at 100°C for 15 minutes 229

37. Mass spectrum of an authentic sample of pterin silylated with MTBSTFA. R_t=36.0 minutes in Figure 36 . . . 230

38. Total ion current chromatogram of an authentic sample of xanthopterin silylated with MTBSTFA in pyridine at room temperature for 30 minutes 232

39. Mass spectrum of the doubly silylated derivative of an authentic sample of xanthopterin at R_t=39.1 minutes in Figure 38 234

40. Liquid chromatogram of the products from peak I_a electrooxidation of 0.75 mM 5-MTHP in pH 4.7 phosphate buffer. Separation used distilled water on Sephadex G-10 237

LIST OF ILLUSTRATIONS (continued)

Figure Page

41. Liquid chromatogram of the products from peak I_a electrolysis of 1.5 mM 5-MTHP in pH 4.7 NaCl. Separation used distilled water on Sephadex G-10 239

42. Liquid chromatogram of the products from peak I_a electrooxidation of 1.5 mM 5-MTHP in pH 4.7 NaCl. Separation used distilled water on Sephadex G-10. These products had been stored in solution for several weeks . . 240

43. (A) U.v. spectrum of authentic pterin in distilled water. (B) U.v. spectrum of LC peak 9 from separation of peak I_a electrolysis of 15 mg of 5-MTHP in pH 4.7 NaCl . . . 242

44. U.v. spectra in pH 4.7 phosphate buffer of (A) authentic pterin and (B) LC peak 9 244

45. Total ion current chromatogram of product isolated from LC peak 9 and silylated with MTBSTFA in pyridine at 100°C for 13 minutes 245

46. Mass spectrum of peak at R_t=35.8 minutes from the chromatogram of LC peak 9 (Figure 41) silylated with MTBSTFA in pyridine 246

47. Cyclic voltammograms in pH 4.6 phosphate buffer at a sweep rate of 200 mV s^{-1}. (A) LC peak 9 and (B) authentic pterin 248

48. Total ion current chromatogram of product isolated from LC peak 2' and silylated with MTBSTFA at room temperature for 30 minutes 252

49. Mass spectrum of peak at R_t=41.8 minutes from the chromatogram of LC peak 2' (Figure 48) silylated with MTBSTFA 253

50. Mass spectrum of the triply silylated derivative of an authentic sample of xanthopterin. R_t=41.6 minutes in the chromatogram of Figure 38 254

51. Cyclic voltammogram of authentic xanthopterin in pH 4.7 phosphate buffer at a sweep rate of 200 mV s^{-1} 255

52. Total ion current chromatogram of product isolated from LC peak 10 and silylated with MTBSTFA at room temperature for 20 minutes 257

53. Mass spectrum of the doubly silylated derivative of product isolated from LC peak 10 at a R_t=38.7 minutes in the chromatogram of Figure 52 259

LIST OF ILLUSTRATIONS (continued)

Figure		Page
54.	U.v. spectrum of LC peak 10 in pH 4.7 phosphate buffer	260
55.	Cyclic voltammograms of LC peak 10 product in pH 4.6 phosphate buffer obtained at a sweep rate of 200 mV s^{-1}	261
56.	Cyclic voltammogram of LC peak 10 product in pH 4.6 phosphate buffer in which the sweep was reversed immediately after passing through the oxidation peak at 0.42V. Sweep rate: 200 mV s^{-1}	263
57.	Cyclic voltammogram of a saturated solution of leucopterin in pH 4.6 phosphate buffer at a sweep rate of 200 mV s^{-1}	264
58.	U.v. spectrum of LC peak 6 in water	267
59.	U.v. spectrum of guanidine sulfate in distilled water	268
60.	Total ion current chromatogram of product isolated from LC peak 6 and silylated with MTBSTFA at 85°C for 10 minutes	270
61.	Mass spectrum of peak at 28.4 minutes from the chromatogram of LC peak 6 (Figure 60)	271
62.	Mass spectrum of the triply silylated derivative of guanidine (MTBSTFA in pyridine at room temperature for 15 minutes) at a R_t=28.3 minutes	272
63.	Total ion current chromatogram of product isolated from LC peak 4 and silylated with MTBSTFA in pyridine at room temperature for 30 minutes	274
64.	Total ion current chromatogram of product isolated from LC peak 4 and silylated with BSA in pyridine at room temperature for 1½ hours	275
65.	Total ion current chromatogram of product isolated from LC peak 3 and silylated with MTBSTFA in pyridine at 100°C for 11 minutes	285
66.	Total ion current chromatogram of product isolated from LC peak 3 and silylated with BSA at 120°C for 16 minutes	286
67.	Total ion current chromatogram of the sodium hydroxide decomposed product of LC peak 3. Silylation was carried out with MTBSTFA at 85°C for 10 minutes	287

LIST OF ILLUSTRATIONS (continued)

Figure		Page
68.	I.r. spectrum of LC peak 3 product in KBr disc	290
69.	Proposed reaction scheme to explain the observed products for oxidation of 5-MTHP at peak I_a in which the methyl group is lost	296
70.	Proposed reaction scheme to explain the observed products for oxidation of 5-MTHP at peak I_a in which the methyl group is retained	299

DIFFERENTIAL PULSE VOLTAMMETRIC OXIDATION OF POLYINOSINIC ACID AND ITS COMPONENTS

AND

ELECTROCHEMISTRY OF 6-METHYL-5,6,7,8-TETRAHYDROPTERIN AND 5-METHYL-5,6,7,8-TETRAHYDROPTERIN

PART I

DIFFERENTIAL PULSE VOLTAMMETRIC OXIDATION OF POLYINOSINIC ACID AND ITS COMPONENTS

CHAPTER I

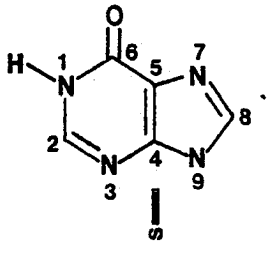
INTRODUCTION

Investigations into the chemistry of biosynthetic and naturally occurring polynucleotides is fairly widespread. The electrochemical oxidation of various DNA's and RNA's, as well as poly(G), poly(A), and poly(X) have been investigated recently.[1-6] Studies of those molecules containing base residues not normally encountered in naturally occurring nucleic acids can give insight into the structure and biological action of the latter biopolymers. One of the least studied of the biosynthetic polymers is polyinosinic acid, poly(I),

which is the subject of this work.[7]

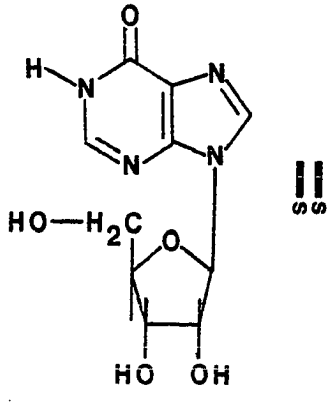
Our laboratory has studied the electrochemical oxidation of a number of purine bases,[8-14] nucleosides,[15-17] and nucleotides. In several cases the enzymic oxidation has also been studied and the results are the same as for the electrochemical oxidation.[18-21] The logical extension of this work is the study of the electrochemical oxidation of various polynucleotides. It is known that the structure of synthetic polynucleotides made from their corresponding nucleoside-5'-diphosphates are closely related structurally to RNA.[22] Perhaps the study of synthetic polynucleotides can give information which can be used to deduce the tertiary structure and conformation of polymers such as DNA and RNA.

The purine base in poly(I) is hypoxanthine (I) whose structure is shown below:

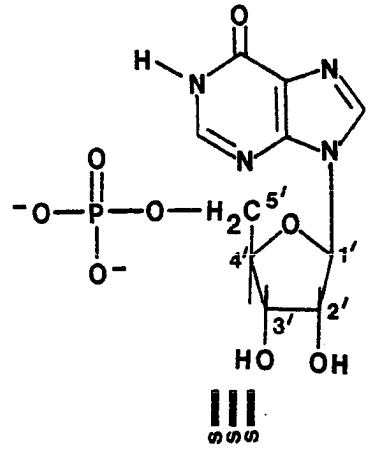


The numbering system for all purine derivatives most commonly used today is also shown in I.[23]

Inosine (II) is the riboside of hypoxanthine and has the structure with the ribose moiety at the N(9)-position:



Inosine-5'-monophosphate (III) (IMP) is the nucleotide of inosine with a phosphate group at the 5'-position:



III

pK_a values for these species can be seen in Table 1. U.v. spectral data reported in the literature are listed in Table 2.

Poly(I) has as its repeating unit IMP. Its tertiary structure has been the subject of several investigations and has not been unequivocally determined. Rich originally proposed a three-stranded, right-handed helical structure which he deduced from X-ray diffraction measurements.[29] Later Thiele and Guschlbauer proposed a four-stranded, left-handed helical structure calculated from data obtained with more sophisticated X-ray diffraction instrumentation.[7] The most recent report by Arnott et al. supports a four-stranded, right-handed helix.[30]

In solution the structure of poly(I) is thought to be highly dependent on a number of parameters including pH, temperature, and the ionic strength of the solution. As the pH increases from 6.7 to 10.2 the sedimentation coefficient for poly(I) decreases indicating that some breakdown of the organized helical structure takes place.[29] However, if the ionic strength of a solution containing poly(I) increases,

Table 1

pK_a Values

Compound	pK_a	Position in molecule	Reference
Hypoxanthine	1.98	$=O^+H$	24
	8.94	N(1)	
	12.10		
Inosine	1.2	$=O^+H$	25
	8.75	N(1)	
	12.33	sugar group	
Inosine-5'-mono-phosphate	1.54	primary PO_4^{3-} group	25
	6.04	secondary PO_4^{3-} group	
	8.88	N(1)	
	12.2	sugar group	
Poly(I)	10.24		27

Table 2

U.v. Spectral Data for Hypoxanthine and Its Derivatives

Compound	pH	λ_{max}	$\varepsilon_{max} \times 10^{-3}$	Reference
Hypoxanthine	1	248	10.8	26
	11	258	11.0	
Inosine	3	248	12.2	26
	12	253	13.1	
Inosine-5'-monophosphate	2	249	11.7	26
	11	254	12.3	
Poly(I)	7	247	7.6	28

the concentration of the organized form increases.[29] Below an ionic strength of 0.006 M in NaCl and between 3-20°C it is considered to exist as a single-stranded, poorly stacked helix.[7] Above an ionic strength of 0.7-0.8 M it is probably present largely in the closely packed, organized helical structure.[7,29] Since poly(I) can assume several protonation states it exhibits melting curves showing at least two steps.[7]

Earlier investigations of polyriboxanthylic acid revealed that commercial samples are often contaminated with traces of xanthine and xanthosine-5'-monophosphate.[5,31] Accordingly with the study of the basic electrochemical properties of poly(I) and its constituents, i.e., hypoxanthine, inosine, and IMP, it was felt an electroanalytical method for determining their presence in poly(I) samples in trace quantities could be useful. Studies of the chemical and biological properties may be affected by contamination with the purine bases and their derivatives thus demonstrating the importance of a quick analytical method. U.v. spectroscopy is not very useful because the peak maxima for hypoxanthine and poly(I) at pH 7.0 are 249.5 nm and 247 nm, respectively.

CHAPTER II

RESULTS AND DISCUSSION

Differential Pulse Voltammetry

Differential pulse voltammetry at a stationary pyrolytic graphite microelectrode (PGE) was used almost exclusively throughout this investigation. Differential pulse voltammetry utilizes the same type of instrumentation as differential pulse polarography except for the substitution of a stationary solid electrode for the dropping mercury electrode (DME).

Differential pulse techniques are more sensitive than linear sweep voltammetry because they can discriminate against capacitive current, the current which charges the electrical double layer.[9] A linear voltage ramp changing at the rate of 3-5 mV s^{-1} is applied to the electrode just as in linear sweep voltammetry, except that a square wave pulse of short duration is imposed on it at periodic intervals. This pulse, usually having an amplitude of 5-100 mV, is applied near the end of the drop lifetime (when a DME is used) and has a duration of ca. 60 ms. For the Princeton Applied Research 174A Polarographic Analyzer the pulse duration is 57 ms and current sampling occurs during the 17 ms immediately prior to initiation of the voltage pulse and 17 ms prior to termination of the pulse (Figure 1A).

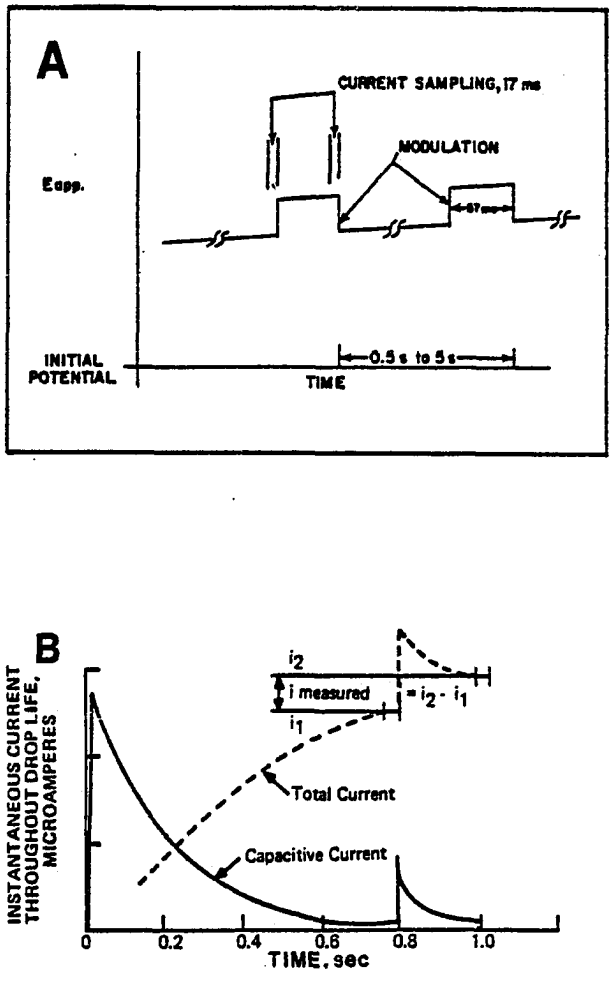


Figure 1. (A) Excitation potential waveform for differential pulse polarography. The values for the current sampling time and pulse time are for the PAR 174A Polarographic Analyzer. (B) Behavior of current as a function of time before and after initiation of pulse at a potential where a faradaic reaction can occur. Note: pulse time has been exaggerated for clarity.

The current vs. time relationship for a single pulse is shown in Figure 1B. At the foot of a DC polarographic wave when no faradaic reaction is occurring, i_2-i_1 is about zero, where i_1 is the current measured in the sampling period immediately prior to the pulse and i_2 is the current measured during the sampling period at the end of the pulse. Initiation of the voltage pulse does not cause any faradaic current to occur and the additional capacitive current caused by the pulse decays very rapidly, effectively approaching zero, therefore $i_1 \simeq i_2 \simeq 0$ and $i_2-i_1 \simeq 0$. As the potential approaches the value where a faradaic process occurs, i.e., the rising portion of a DC polarogram, the voltage pulse can cause additional faradaic current which decays in a Cottrellian manner. However the current measured at the end of the voltage pulse, i_2, is still larger than i_1, which is the current measured during the sampling period prior to the pulse. Therefore i_2-i_1 now has a finite value which is directly proportional to the faradaic current. This is the measured quantity which is observed on the recorder. As the potential continues to increase to the point where it is on the plateau of the DC polarographic wave, the voltage pulse does not cause a significant increase in the faradaic process and consequently i_2-i_1 again approximates zero.

Thus a differential pulse polarogram or voltammogram has the appearance of a peak rather than a wave (Figure 2). The peak potential, E_p, of a differential pulse voltammogram should correspond approximately with the half-wave potential, $E_{1/2}$, of a DC polarographic wave. This follows from the fact that i_2-i_1 reaches a maximum at E_p which should be the point on a DC polarographic wave where the current is

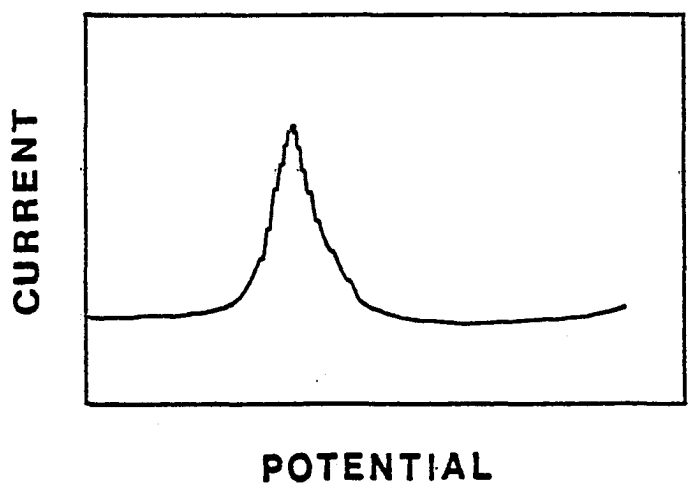


Figure 2. Typical differential pulse polarogram.

changing the quickest. That point should be close to, but not necessarily equal to, the half-wave potential.

Differential pulse voltammetry was used in this investigation because it has a considerably greater sensitivity than linear sweep voltammetry. Yao et al.[4] have reported on the electrooxidation of DNA using linear sweep voltammetry, but differential pulse voltammetry seems to give more well defined peaks for polynucleotides.[1,5] Before an attempt was made to detect or determine hypoxanthine, inosine, or IMP in the presence of poly(I) it was necessary to do a detailed differential pulse voltammetric study of each component separately.

Differential Pulse Voltammetry of Hypoxanthine

Background. Hypoxanthine was the first component of poly(I) studied in detail.[32] Later Conway et al.[13,14] studied the electrochemical oxidation of hypoxanthine to determine the mechanism and reaction products. This work contained a study of the dependence of the peak potential on the pH of the solution determined at a pyrolytic graphite electrode (PGE) using linear sweep voltammetry.

The pH dependence of the first oxidation peak is given by:[13]

$$E_p \text{ (pH 2.5-7.5)} = [1.34-0.056 \text{ pH}]V$$

$$E_p \text{ (pH 8.5-11.0)} = [1.53-0.064 \text{ pH}]V$$

However the paper which reported this work gives a pH dependence which is slightly different below pH 8:[14]

$$E_p \text{ (pH 2.5-ca. 8)} = [1.30-0.056 \text{ pH}]V$$

Another earlier report has given the pH dependence of the half-peak potential ($E_{p/2}$) at 3.3 mV s^{-1} sweep rate[9,33] as

$$E_{p/2} \text{ (pH 0-5.7)} = [1.27-0.067 \text{ pH}]V$$

with a hypoxanthine concentration of 0.51 mM.

These peak potentials are for the linear sweep voltammetry at a sweep rate of 5 mV s^{-1} and are not the same as the peak potential in differential pulse voltammetry. Results were also reported for the pH dependence of hypoxanthine under differential pulse voltammetric oxidation conditions and they are:[13]

$$E_p \text{ (pH 2.0-8.0)} = [1.38-0.060 \text{ pH}]V$$
$$E_p \text{ (pH 10-12)} = [1.62-0.075 \text{ pH}]V$$

However, no concentration was reported. Therefore the first study on hypoxanthine was the variation of the differential pulse voltammetric oxidation peak potential with pH at several concentrations.

pH study. Hypoxanthine was studied under differential pulse voltammetric oxidation conditions at two different concentrations, 0.005 mg ml^{-1} (0.037 mM) and 0.5 mg ml^{-1} (3.68 mM) at 25°C over the pH range 1.5 to 12. At the lowest concentration hypoxanthine shows only one oxidation peak with a pH dependence of (Figure 3A):

$$E_p \text{ (pH 1.5-7.7)} = [1.40-0.067 \text{ pH}]V$$
$$E_p \text{ (pH 7.7-9.0)} = 0.88 \pm 0.01V$$
$$E_p \text{ (pH 9-12)} = [1.49-0.067 \text{ pH}]V$$

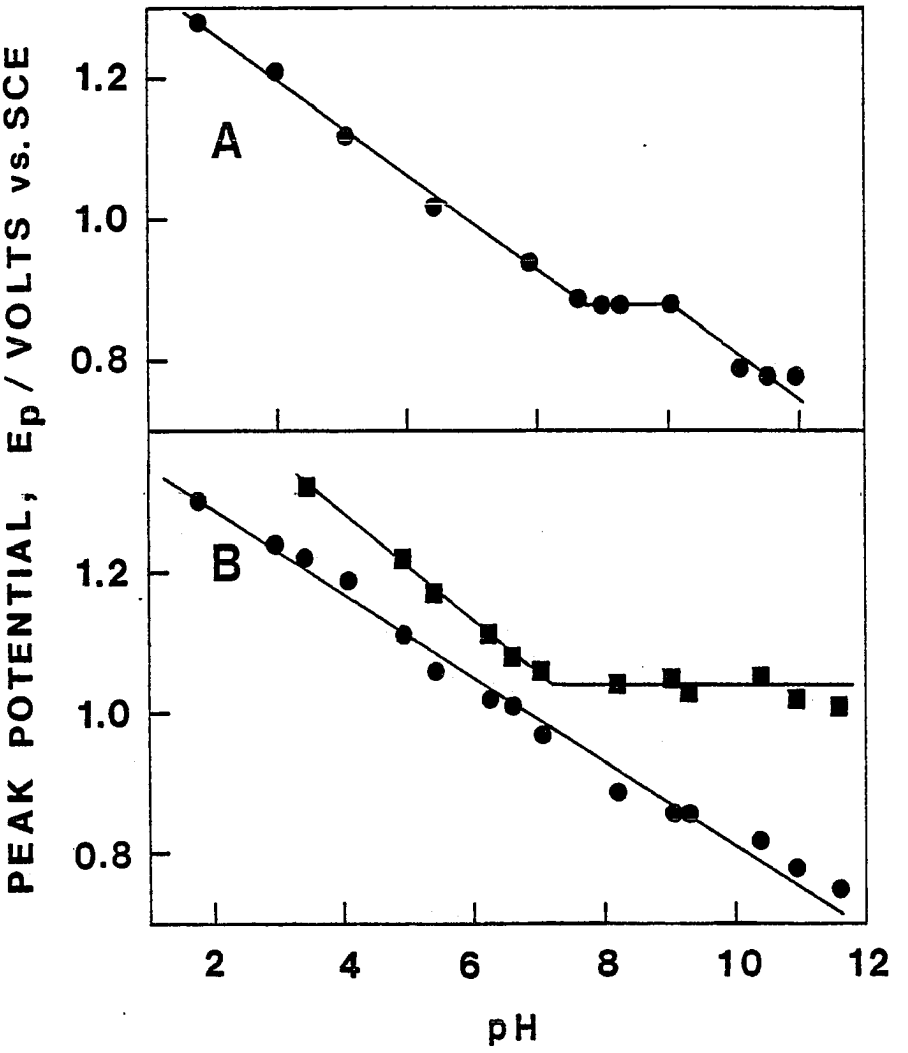


Figure 3. Peak potential, E_p, vs. pH relationship for the differential pulse voltammetric oxidation peaks of hypoxanthine observed in phosphate buffers of ionic strength 0.5 M at a sweep rate of 5 mV s^{-1}. (A) Data obtained at a hypoxanthine concentration of 37 μM. (B) Data obtained at a hypoxanthine concentration of 3.68 mM. Peak I, ● ; Peak II, ■ .

These solutions need to be made up fresh every day because the hypoxanthine oxidation peak disappears in about a day at the 0.037 mM concentration level. However, at 3.68 mM the differential pulse voltammetric oxidation peak does not appear to change even after several days. It has been reported in the literature that hypoxanthine is one of the most stable of the purine bases toward concentrated acid or alkali.[24] When a solution of 0.037 mM hypoxanthine was refrigerated overnight it was found that the differential pulse voltammetric oxidation peak did not disappear. However, since this work was analytical in nature, fresh solutions were prepared every day to remove this variable as a possible source of error.

When the hypoxanthine concentration was increased to 0.50 mg ml^{-1} (3.68 mM) the differential pulse voltammetry shows two oxidation peaks throughout most of the pH range (Figure 4). The pH dependence for these peaks is given by the following equations and Figure 3B:

Peak I (pH 1.5-1.2): $E_p = [1.40-0.060\ pH]V$

Peak II (pH 3.4-7.2): $E_p = [1.59-0.077\ pH]V$

(pH 7.2-12): $E_p = 1.04 \pm 0.02V$

Peak I appears to be an adsorption prepeak of the peak II process indicating that the oxidation product(s) of hypoxanthine is/are adsorbed at the electrode surface.[34]

Concentration study. At any pH the differential pulse voltammetric oxidation peak of hypoxanthine is well separated from the peak for poly(I) (almost 0.4V) therefore pH 7 was chosen for a concentra-

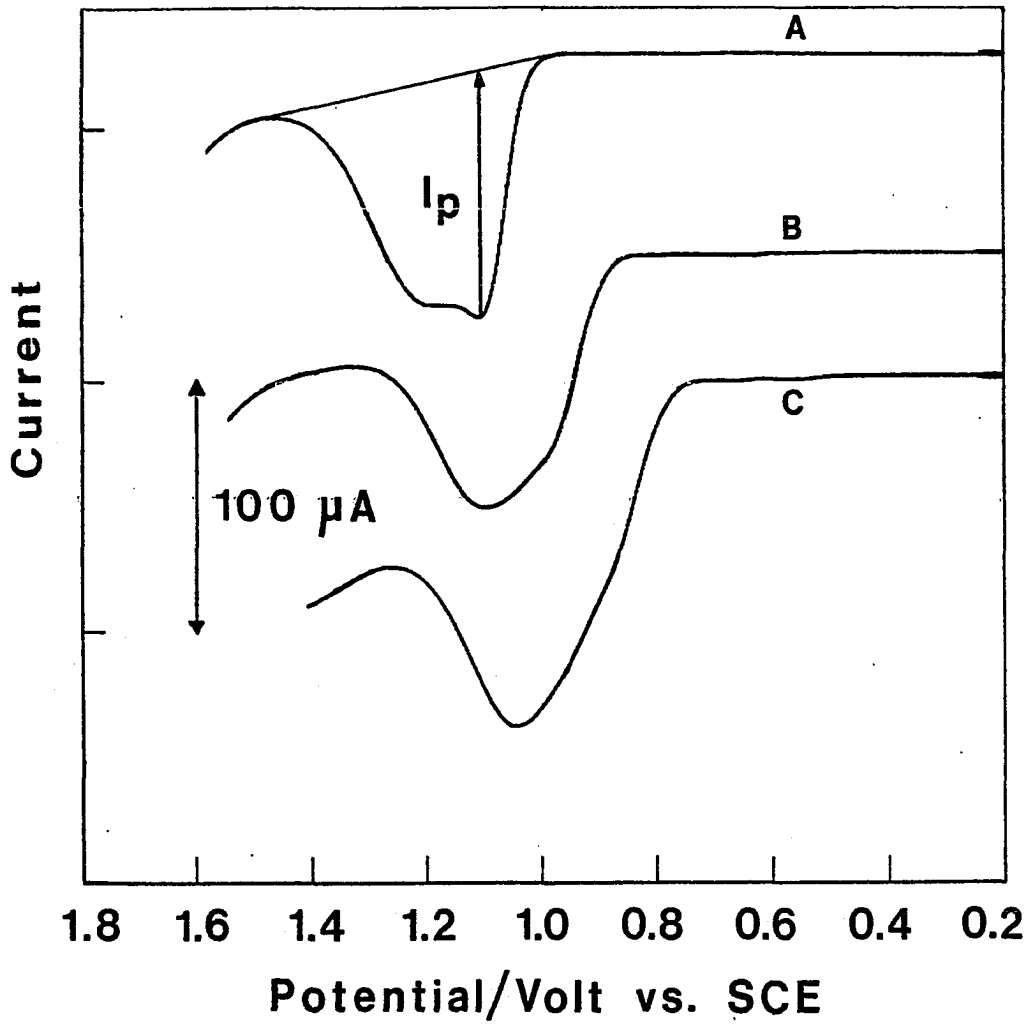


Figure 4. Differential pulse voltammograms of 3.68 mM hypoxanthine in phosphate buffers with an ionic strength of 0.5 M at a sweep rate of 5 mV s^{-1}. (A) pH 4.94, (B) pH 7.00, and (C) pH 9.03. Axis marker indicates zero current.

tion study since this is close to physiological pH. The peak current, i_p, vs. concentration dependence can yield information about the electron transfer process, i.e., whether adsorption is occurring and to what extent. Also for analytical purposes a linear calibration curve of i_p vs. concentration is desirable.

The peak current was measured at the maximum point of the distorted voltammetric peak since peak I and II were never completely resolved (Figure 4A illustrates this). The peak current dependence is linear up to ca. 0.15 mM (Figure 5B). At higher hypoxanthine concentrations the curve begins to deviate from linearity and approaches a constant value at ca. 1.0 mM (Figure 5A). This is indicative of an adsorption process since the peak current only increases to the point where the electrode surface is completely covered with adsorbed molecules. Adsorption of hypoxanthine occurs to glass surfaces as well and can cause cross contamination of test solutions (see later discussion).

Differential Pulse Voltammetry of Inosine

Inosine is the riboside of hypoxanthine and was the next component of poly(I) to be studied in detail. Differential pulse voltammetry was done on inosine at two concentrations throughout the pH range 1-12. At the lower concentration of 0.05 mg ml^{-1} (0.20 mM) inosine shows two differential pulse voltammetric oxidation peaks with peak I being the major peak (Figure 6B). When the concentration of inosine is raised to 0.50 mg ml^{-1} (2.03 mM) peak II becomes the major peak (Figure 6A).

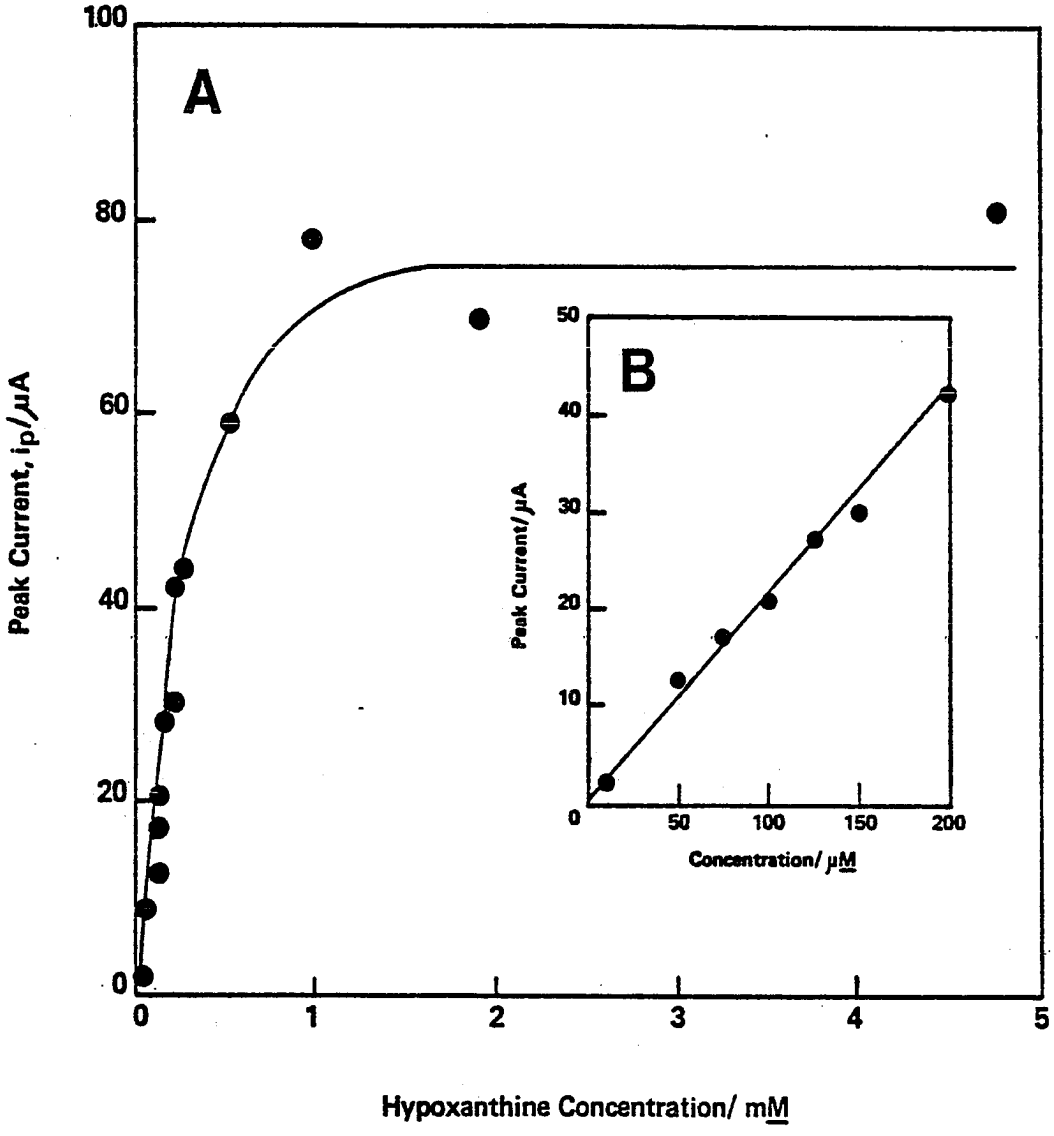


Figure 5. (A) Peak current, i_p, vs. concentration curves for the differential pulse voltammetric oxidation peak of hypoxanthine at the PGE in pH 7.0 phosphate buffer with an ionic strength of 0.5 M. Data was obtained at a sweep rate of 5 mV s^{-1} and a temperature of 25°C. (B) Expanded low concentration region of A.

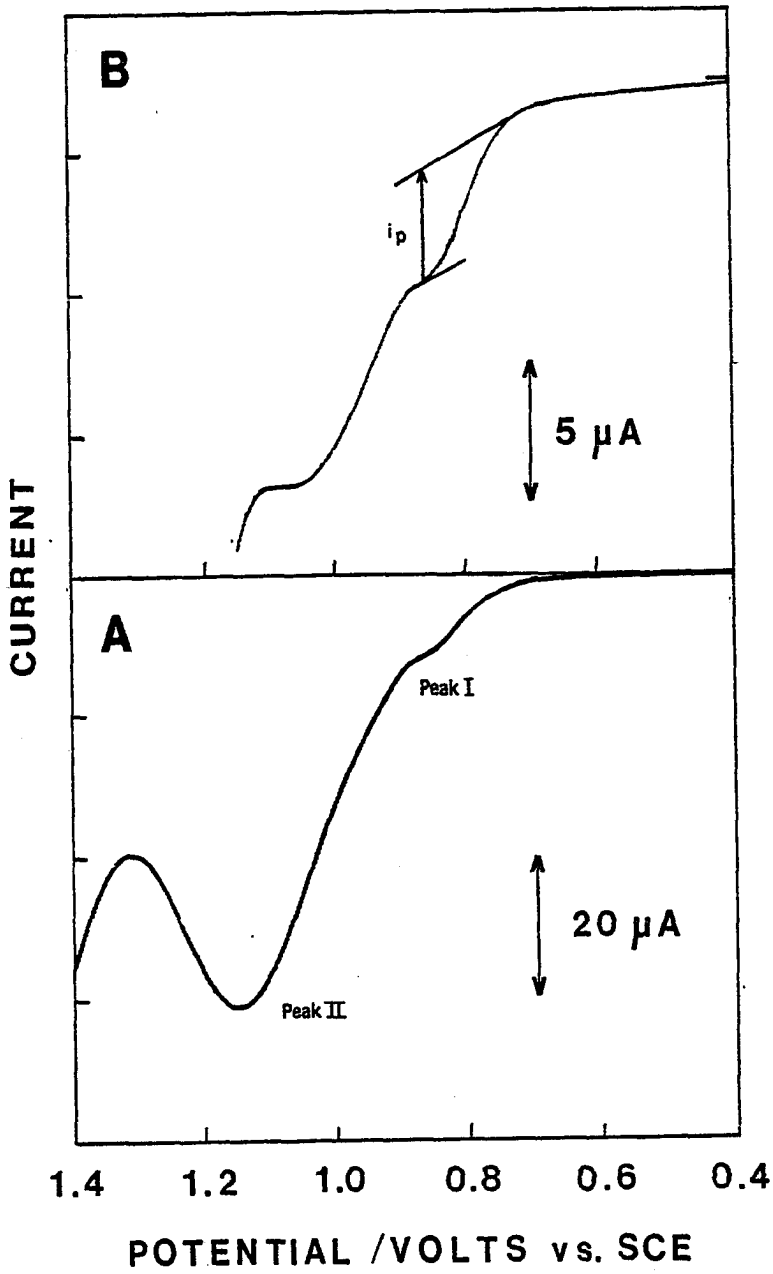


Figure 6. Differential pulse voltammograms of inosine in pH 10.9 phosphate buffer, μ=0.5 M at a sweep rate of 5 mV s^{-1}. (A) 2.03 mM inosine and (B) 0.20 mM inosine. Illustrates how the peak current for peak I was estimated.

pH study. The pH dependence was studied to see if a pH could be determined at which the peak potential of either peak I or II (especially peak I) of inosine is different enough from poly(I) that it can be determined in the presence of poly(I). At the lower concentration of 0.20 mM inosine peak I exhibits a pH dependence of (Figure 7A):

Peak I (pH 3-10): E_p = [1.67-0.061 pH]V

(pH 10-12): E_p = [1.47-0.057 pH]V

Peak II (pH 7.5-12): E_p = [1.84-0.072 pH]V

The pH dependence of the peaks at a concentration of 2.03 mM inosine (Figure 7B) is:

Peak I (pH 6.3-11.5): E_p = [1.73-0.078 pH]V

Peak II (pH 2.9-11.5): E_p = [1.62-0.043 pH]V

At this concentration peak II appears throughout the pH range studied.

At pH 11 inosine exhibits two reasonably well resolved differential pulse voltammetric oxidation peaks especially at the 0.20 mM concentration level. The first oxidation peak occurs at 0.84V and peak II appears at a potential of 1.05V (Figure 6B). Peak II occurs at almost the same potential as the single oxidation peak of poly(I) (1.03V at pH 11), however peak I is separated by ca. 190 mV.

Concentration study. Since the peak separation between inosine peak I and the oxidation peak of poly(I) is greatest at pH 11, a peak current vs. concentration study was done on peaks I and II

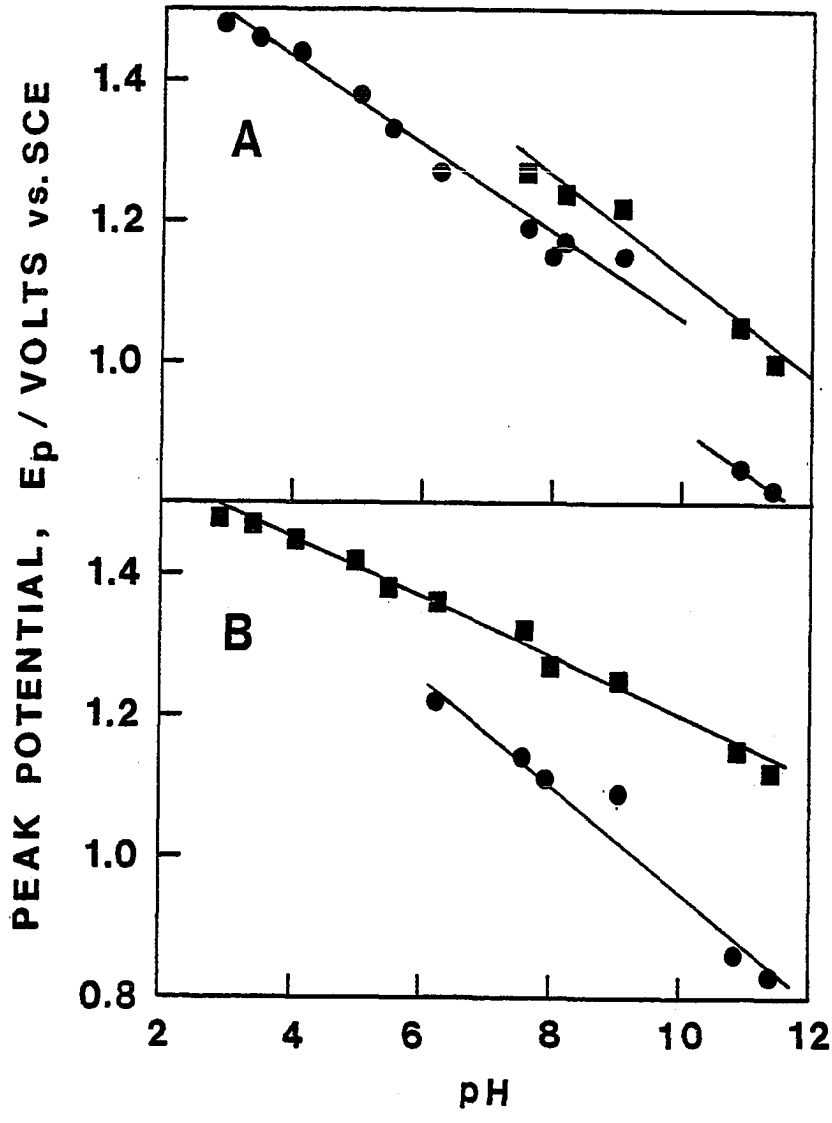


Figure 7. Peak potential, E_p, vs. pH relationship for the differential pulse voltammetric oxidation peaks of inosine observed in phosphate buffers of ionic strength of 0.5 M at a sweep rate of 5 mV s-1. (A) Data obtained at an inosine concentration of 0.20 mM. (B) Data obtained at an inosine concentration of 2.03 mM. Peak I, ● ; Peak II, ■ .

of inosine at pH 11. Peak II exhibits an i_p vs. concentration behavior which is very nearly linear throughout the concentration range studied (Figure 8). The maximum concentration studied was 0.66 mM and the behavior observed for peak II is indicative of a diffusion controlled electrode process. However peak I exhibits a highly variable behavior where the peak current becomes essentially constant above an inosine concentration of 0.1 mM. Figure 6B illustrates how the peak current was estimated for peak I. Behavior where the peak current approaches a constant value with increasing concentration is indicative of an adsorption process. Thus peak I appears to be an absorption prepeak of peak II. An adsorption prepeak occurs when the product of the electrode process is more strongly adsorbed than the reactant.[34]

Differential Pulse Voltammetry of IMP

pH study. The pH dependence of the differential pulse voltammetric oxidation peaks of IMP is different from that of hypoxanthine or inosine. At the lowest concentration of 0.05 mg ml^{-1} (0.095 mM) IMP exhibits only a single oxidation peak. E_p for this peak varies with pH according to the following equations:

$$E_p \text{ (pH 2.5-4.2)} = [1.54-0.029 \text{ pH}]V$$

$$E_p \text{ (pH 4.2-7.1)} = [1.80-0.090 \text{ pH}]V$$

$$E_p \text{ (pH 7.1-9.4)} = 1.17 \pm 0.01V$$

$$E_p \text{ (pH 9.4-11.6)} - [1.98-0.087 \text{ pH}]V$$

This behavior is illustrated graphically in Figure 9A. The obvious breaks in the E_p vs. pH plots noted in both Figures 9A and B (vide

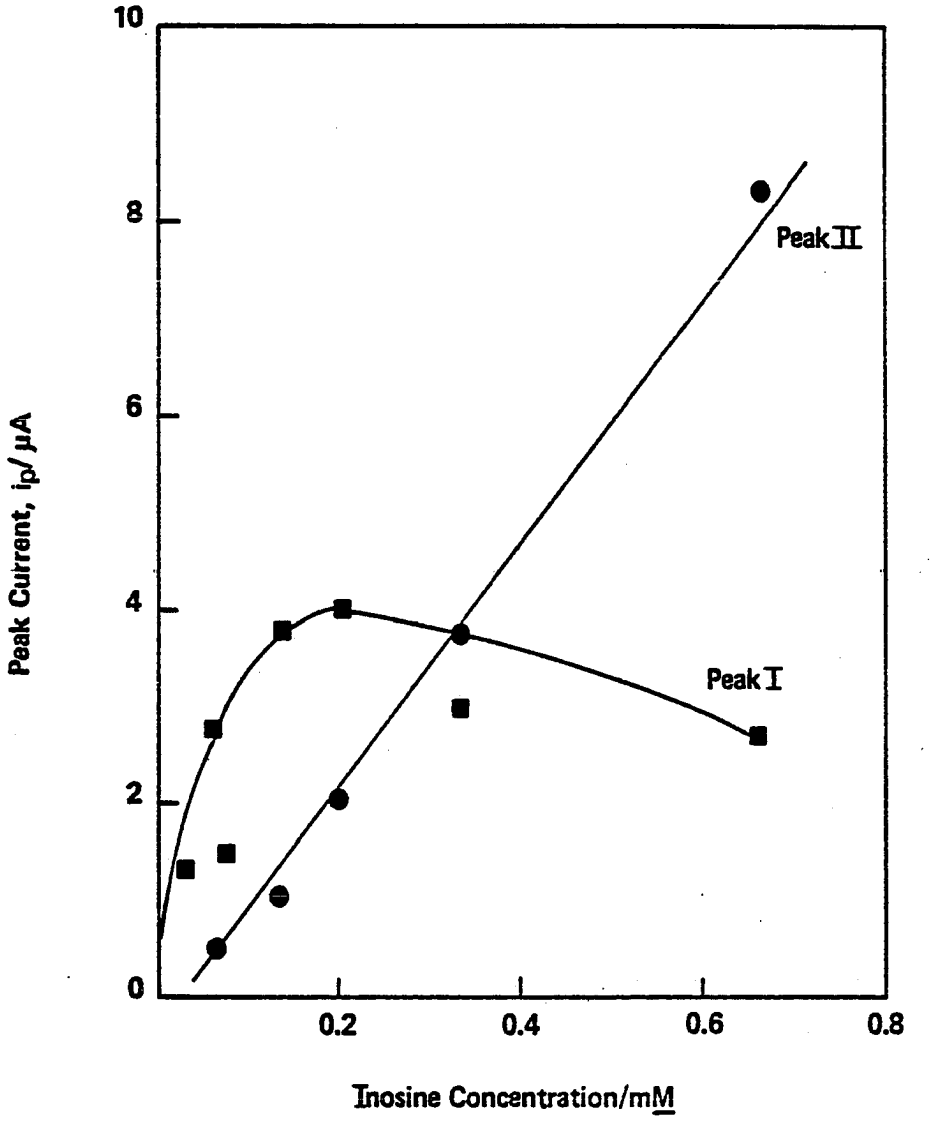


Figure 8. Peak current, i_p, vs. concentration curves for the differential pulse voltammetric oxidation peaks of inosine at the PGE in pH 11.0 phosphate buffer, μ=0.5 M. Data obtained at a sweep rate of 5 mV s^{-1} and a temperature of 25°C. Peak I, ■ ; Peak II, ● .

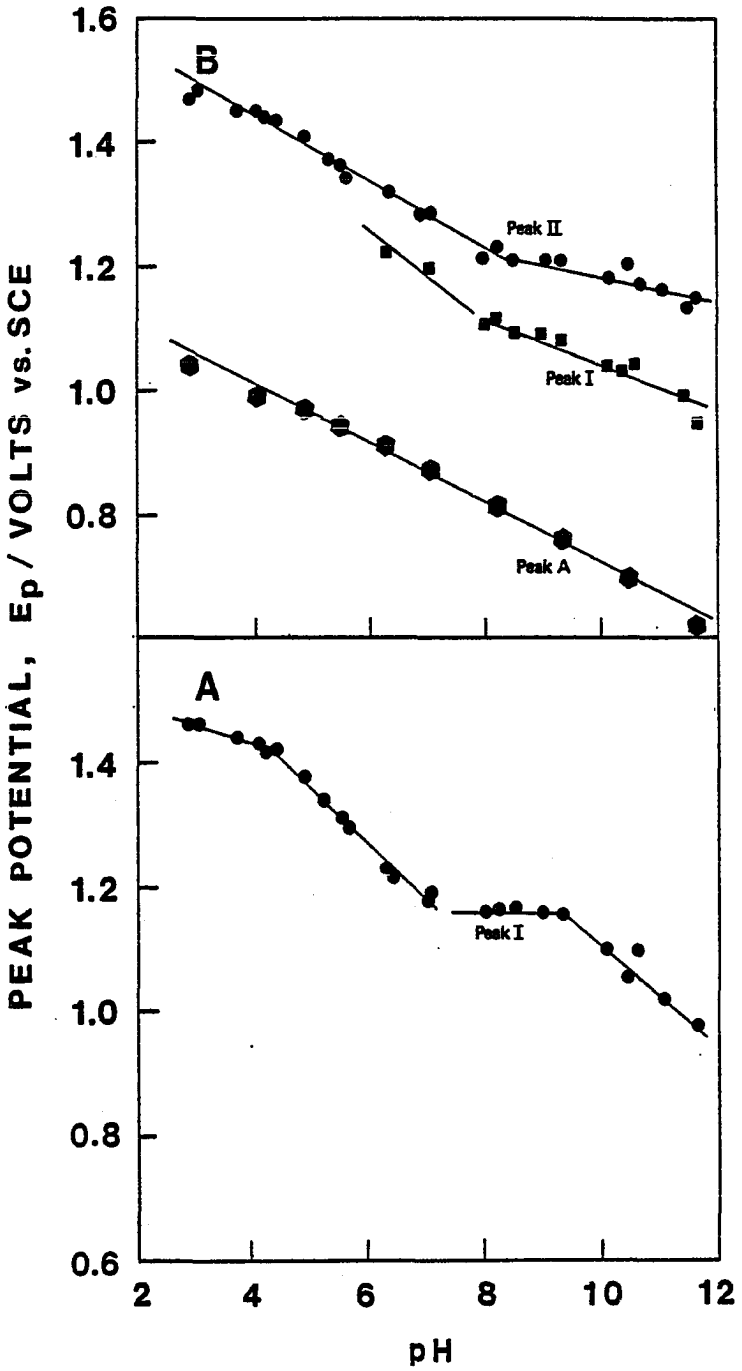


Figure 9. Peak potential, E_p, vs. pH relationship for the differential pulse voltammetric oxidation peaks of inosine-5'-monophosphate (IMP) observed in phosphate buffers of ionic strength 0.5 M at a sweep rate of 5 mV s^{-1}. (A) Data obtained at an IMP concentration of 0.095 mM. Peak I, ● . (B) Data obtained at an IMP concentration of 0.95 mM. Peak I, ■ ; Peak II, ● ; Peak A, ⬢ .

infra) between pH 8 and 9 agree approximately with the pK_a of IMP of 8.88.[25]

A pH study was also done for an IMP solution with a concentration of 0.5 mg ml^{-1} (0.95 mM). At this IMP concentration as many as three differential pulse voltammetric oxidation peaks are observed. The most negative of these peaks is designated peak A and is much smaller than peaks I and II. Peak A shows a pH dependence of:

$$E_p \text{ (pH 2.9-11.6)} = [1.20-0.048 \text{ pH}]V$$

Peak I is observed as an inflection on the rising portion of oxidation peak II above ca. pH 6. The E_p vs. pH behavior is illustrated in Figure 9B and is given by the following equations:

$$\text{Peak I (pH 6.3-7.1):} \quad E_p = [1.71-0.075 \text{ pH}]V$$
$$\text{(pH 7.8-11.6):} \quad E_p = [1.50-0.047 \text{ pH}]V$$
$$\text{Peak II (pH 2.9-8.2):} \quad E_p = [1.65-0.052 \text{ pH}]V$$
$$\text{(pH 8.2-11.6):} \quad E_p = [1.44-0.026 \text{ pH}]V$$

The peak equations given above for the pH dependence of peak I are only approximate because of the fact that peak I occurs as a shoulder on the rising portion of peak II.

Careful examination of voltammograms of IMP at high and low concentrations revealed that the single peak at low concentrations corresponds to peak I at higher concentrations. Figure 10 is a typical voltammogram of 0.95 mM IMP and illustrates the difficulty of measuring the peak potential and peak current for peak I. As the concentration increases, peak II clearly becomes more dominant. Therefore, it appears

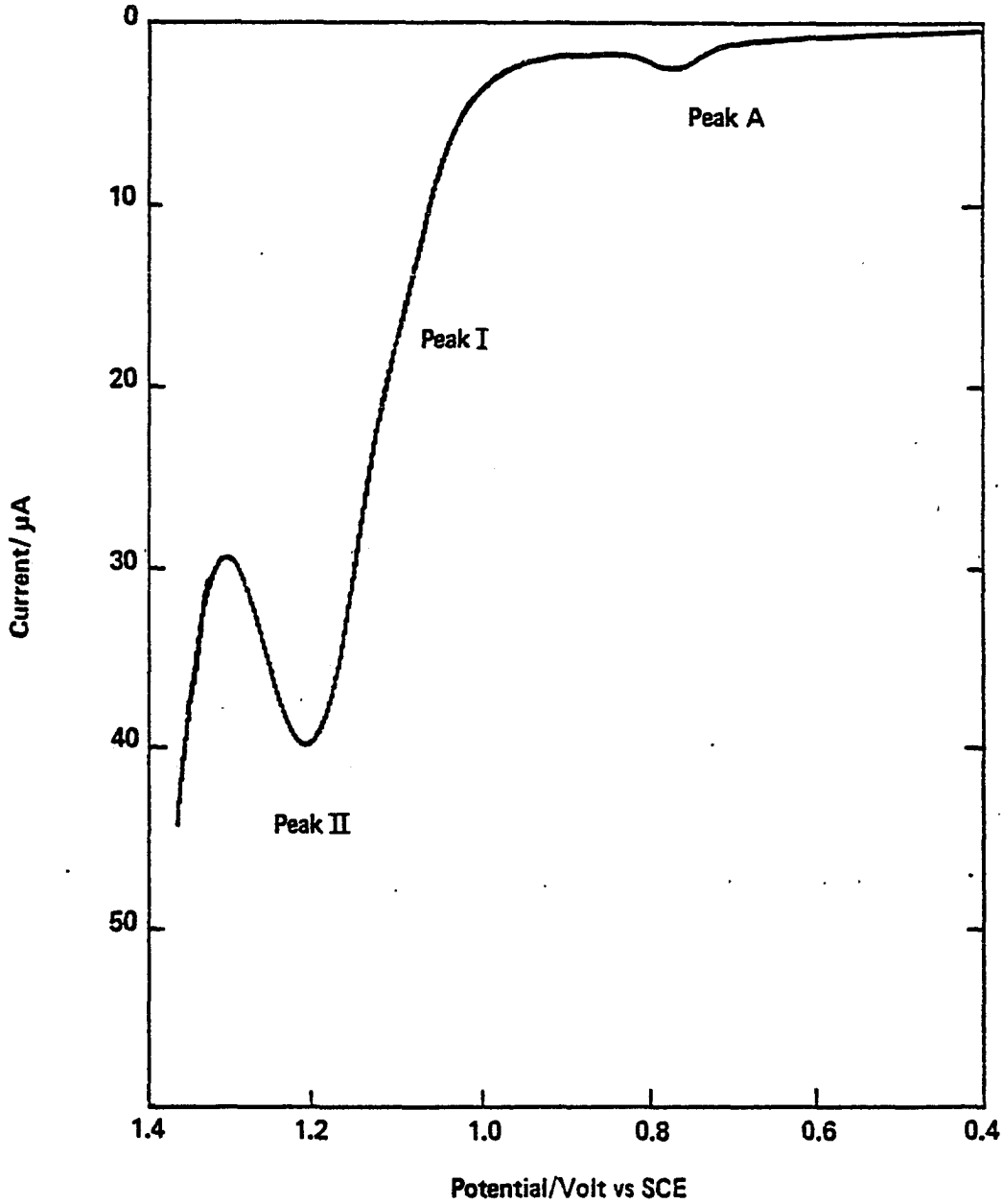


Figure 10. Differential pulse voltammogram of 0.95 mM IMP in pH 8.45 phosphate buffer of ionic strength 0.5 M obtained at a sweep rate of 5 mV s^{-1}.

that peak I is an adsorption prepeak.

Concentration study. The greatest separation between the oxidation peaks for poly(I) and peak II of IMP is ca. 90 mV at pH 7. Poly(I) has a peak potential of 1.28V at this pH and peak II of IMP has a peak potential of 1.19V. Consequently, a detailed peak current vs. concentration study of IMP was carried out at pH 7. Peak I was so poorly resolved from peak II that an estimation of its peak current could not be obtained. The current reported for peak II is really a composite of peaks I and II and represents the maximum point on the distorted voltammogram. The linear range of i_p vs. concentration for peak II extends only to about 50 μM (Figure 11A) which is a smaller range than for either hypoxanthine or inosine. This would indicate the possibility that IMP is more strongly adsorbed at the PGE than the purine base or nucleoside. The peak potential for peak II shifts with increasing concentration from 1.18V at low concentration (0.05 mM) to 1.32V at the highest concentration (5.0 mM). The disappearance of peak I as the IMP concentration is increased strongly suggests that it is an adsorption prepeak.

Peak A, however, varies from 0.85V to 0.88V over this same concentration range and exhibits a much greater linear peak current vs. concentration dependence extending to ca. 0.5 mM (Figure 11B). To determine if peak A was really an oxidation peak of IMP or an impurity, a controlled potential electrolysis of 2.0 mM IMP was carried out at 0.88V for ca. 20 hrs. All traces of peak A disappeared upon electro-oxidation, but the differential pulse voltammetry shows that peaks

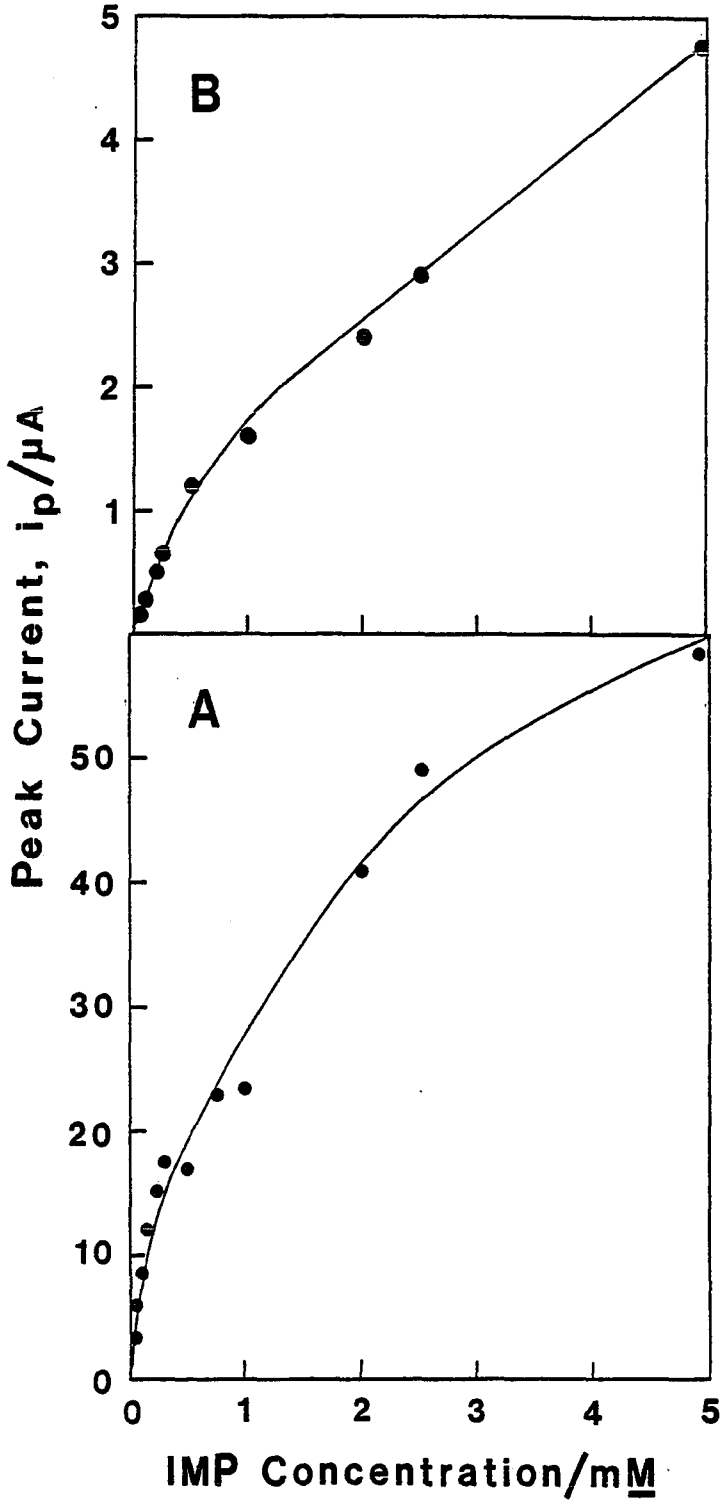


Figure 11. Peak current, i_p, vs. concentration curves for the differential pulse voltammetric oxidation peaks of IMP at the PGE in pH 7.0 phosphate buffer of ionic strength 0.5 mM. Data obtained at a sweep rate of 5 mV s^{-1}. (A) Oxidation peak I plus II and (B) oxidation peak A.

I and II of IMP remain unchanged (Figure 12). U.v. spectra obtained before and after the electrolysis are virtually identical indicating that no IMP was oxidized during the electrolysis of the species responsible for peak A. All evidence points to the fact that peak A is not an oxidation peak of IMP, but is in fact a trace contaminant which is electroactive.

Identification and Quantitation of Contaminants

A prime candidate for the species responsible for peak A was thought to be hypoxanthine. Hypoxanthine alone in solution exhibits an oxidation peak at a potential as low as 0.92V when the hypoxanthine concentration is very low (below ca. 5 μM). Figure 13A is a voltammogram of 0.5 mM IMP before addition of hypoxanthine. To investigate the possibility of hypoxanthine contamination, a 0.5 mM IMP solution was spiked with enough hypoxanthine to give a hypoxanthine concentration of ca. 5 μM. This is the hypoxanthine concentration which shows a comparable peak current to that exhibited by peak A. The resulting voltammogram exhibited two oxidation peaks of ca. equal size with peak potentials of 0.86V and 0.96V (Figure 13B). The oxidation peak at 0.96V was the result of the added hypoxanthine and proved conclusively that peak A was not a result of hypoxanthine contamination.

The impurity which was electrooxidized at 0.88V in pH 7 phosphate buffer was suspected of being a purine base because of the synthesis route of IMP. Using the equations for the pH dependence of the peak potential of various purines, adenine was found to have a peak potential of 0.88V at pH 7.0 according to the equation E_p =

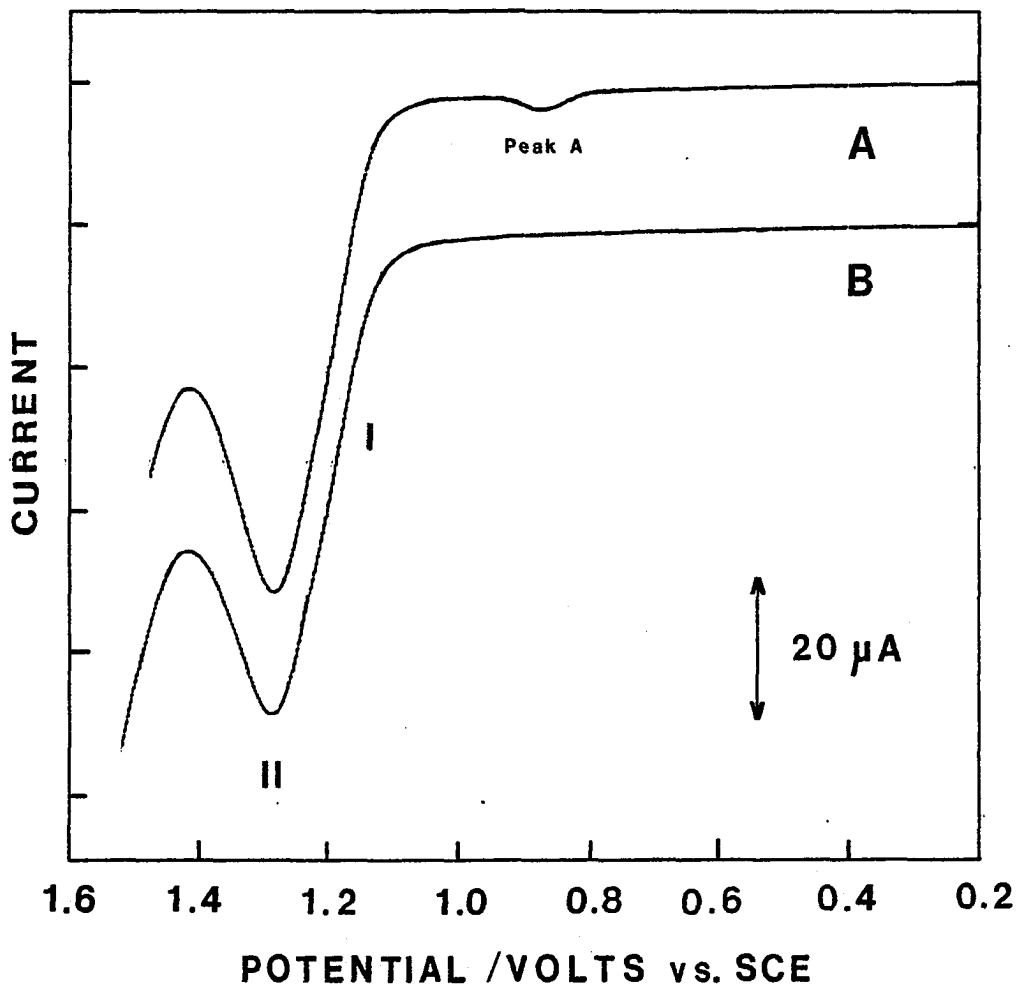


Figure 12. Differential pulse voltammograms of 2.0 mM IMP in pH 7.0 phosphate buffer of ionic strength 0.5 M at a sweep rate of 5 mV s^{-1}. (A) Before electrolysis at 0.88V vs. SCE. (B) After 21 hours electrolysis at 0.88V vs. SCE.

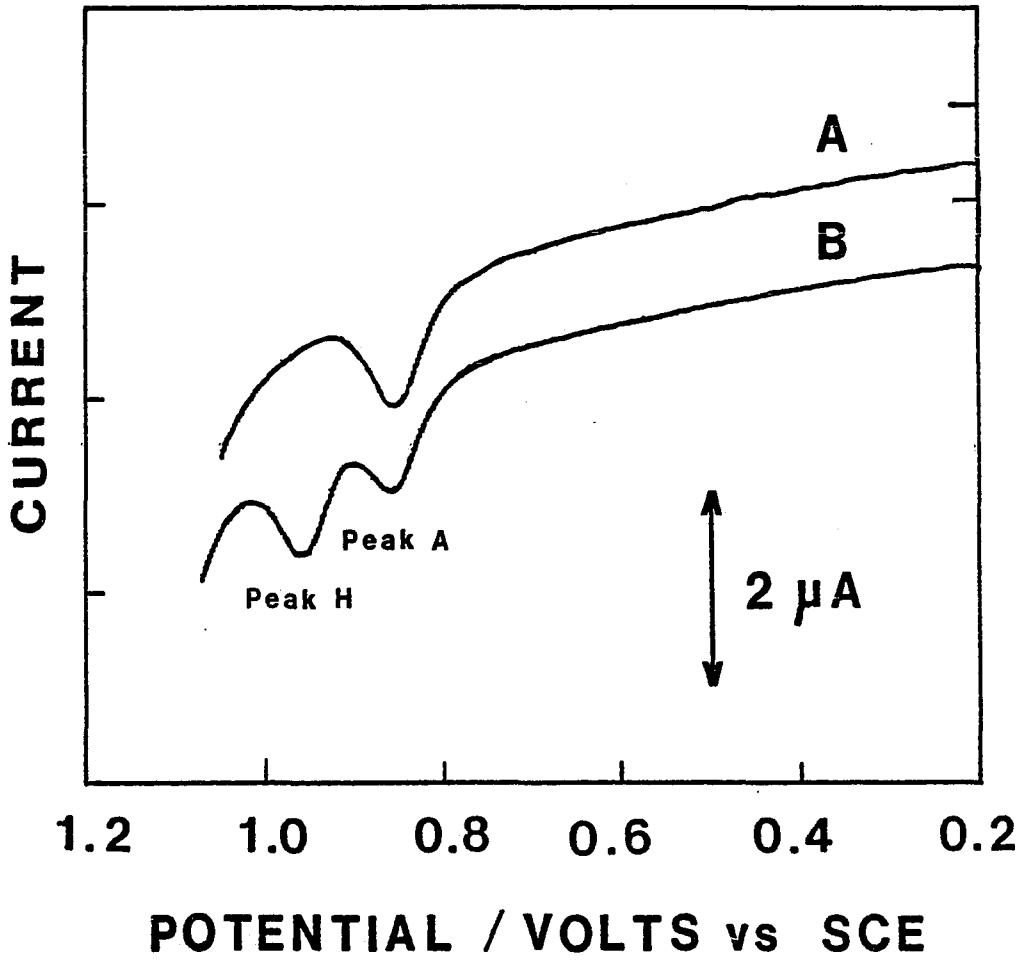


Figure 13. Differential pulse voltammograms of 0.50 mM IMP in pH 7.0 phosphate buffer, μ=0.5 M. The major peaks of IMP are off-scale at 1.1V. Data was obtained at a sweep rate of 5 mV s^{-1}. (A) IMP alone and (B) 4.9 μM hypoxanthine + IMP.

(1.338-0.063 pH)V.[9,35] This is the peak potential from a linear sweep voltammogram and would not compare exactly with the peak potential of the compound under differential pulse voltammetric conditions. The adenine concentration was also much higher, ca. 0.25 mM, and thus it would not be unusual for the pH dependence to be somewhat different from that reported above for peak A. To show that peak A might be adenine the IMP solution was spiked with a very small amount of adenine which would give a comparable peak current to that observed for peak A. Under these conditions only one differential pulse voltammetric oxidation peak is observed except the peak current is much greater (Figure 14). This is not conclusive proof that peak A is a result of adenine contamination, but suggests it is a good possibility.

Assuming the contamination is adenine, a method was developed for quantitation of adenine in IMP using a standard addition method. Several known quantities of adenine were added to 0.95 mM IMP solutions and the combined peak current for adenine and peak A was measured. After subtracting the contribution of the peak current for peak A, the resulting value is the peak current for the added quantity of adenine. These values were used to prepare the calibration curve of adenine peak current vs. concentration shown in Figure 15. This calibration curve is linear up to ca. 20 μM adenine. Assuming once again that adenine is responsible for peak A, the concentration of adenine which would give the same peak current is found from the calibration curve to be 3.3 μM. Thus adenine is suggested to be a contaminant at a level of 0.09% by weight.

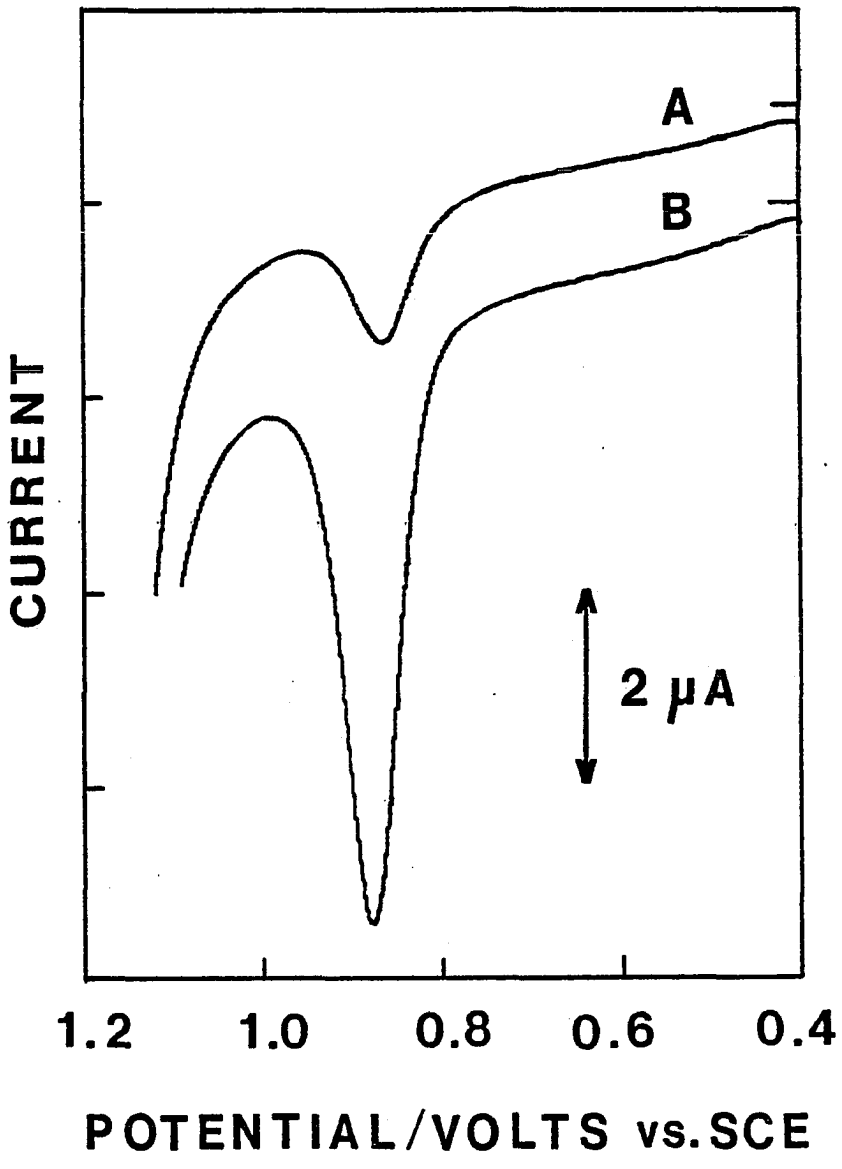


Figure 14. Differential pulse voltammograms of 0.99 mM IMP in pH 7.0 phosphate buffer, μ=0.5 M. Data was obtained at a sweep rate of 5 mV s^{-1}. The major peaks of IMP are off-scale at 1.1V. (A) IMP alone and (B) 25 μM adenine + IMP.

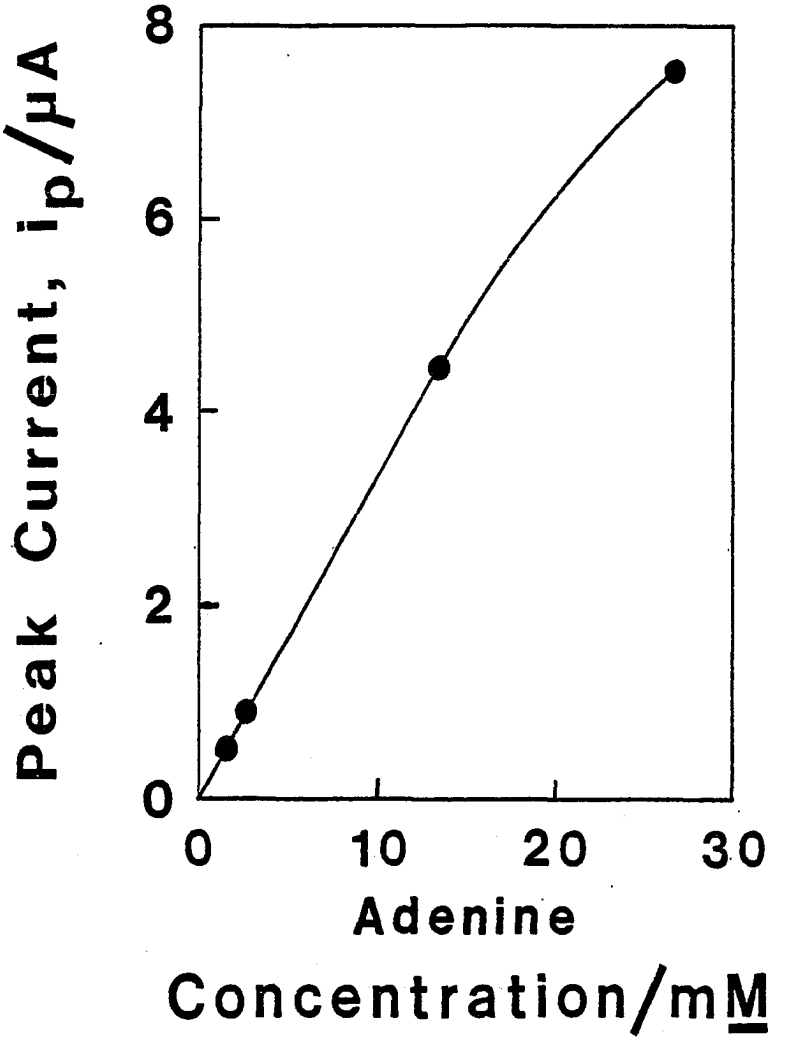


Figure 15. Peak current vs. concentration curve for the differential pulse voltammetric oxidation peak of adenine which was added in known concentrations to an IMP solution. Voltammograms were run in pH 7.0 phosphate buffer of ionic strength 0.5 M at a sweep rate of 5 mV s^{-1}. The contribution of the peak current for peak A was subtracted out.

Differential Pulse Voltammetry of Poly(I)

pH study. Poly(I) exhibits a single, well-defined differential pulse voltammetric oxidation peak between pH 2 and 14 (Figure 16). The concentration of poly(I) was determined from u.v. spectroscopy at 247 nm in pH 7.0 phosphate buffer having an ionic strength of 0.2 M.[28] Under these conditions the molar absorptivity is 7.6×10^3 ℓ $mole^{-1}$ cm^{-1} and thus a 1.0 mg ml^{-1} solution of poly(I) is 3.3 mM. This concentration refers to the concentration of the monomer, IMP. At poly(I) concentrations of 0.165 mM and 1.65 mM the pH dependence of the peak potential is described by the following expression:

$$E_p \text{ (pH 2.9-7.2)} = [1.56-0.039 \text{ pH}]V$$

Above pH 7.2 the peak potential is dependent on concentration:

$$0.165 \text{ mM (pH 7.2-14):} \quad E_p = [1.87-0.082 \text{ pH}]V$$
$$1.65 \text{ mM (pH 7.2-14):} \quad E_p = [1.66-0.057 \text{ pH}]V$$

These expressions are illustrated graphically in Figure 17.

The pH dependence for the oxidation peak of poly(I) was also investigated at a concentration of 5 mM. This was done because calibration curves for determination of hypoxanthine in poly(I) were run at a poly(I) concentration of 5 mM (vide infra). Under these conditions the E_p vs. pH equation becomes (Figure 18):

$$E_p \text{ (pH 2-10)} = [1.60-0.047 \text{ pH}]V$$

Ionic strength study. A differential pulse voltammetric

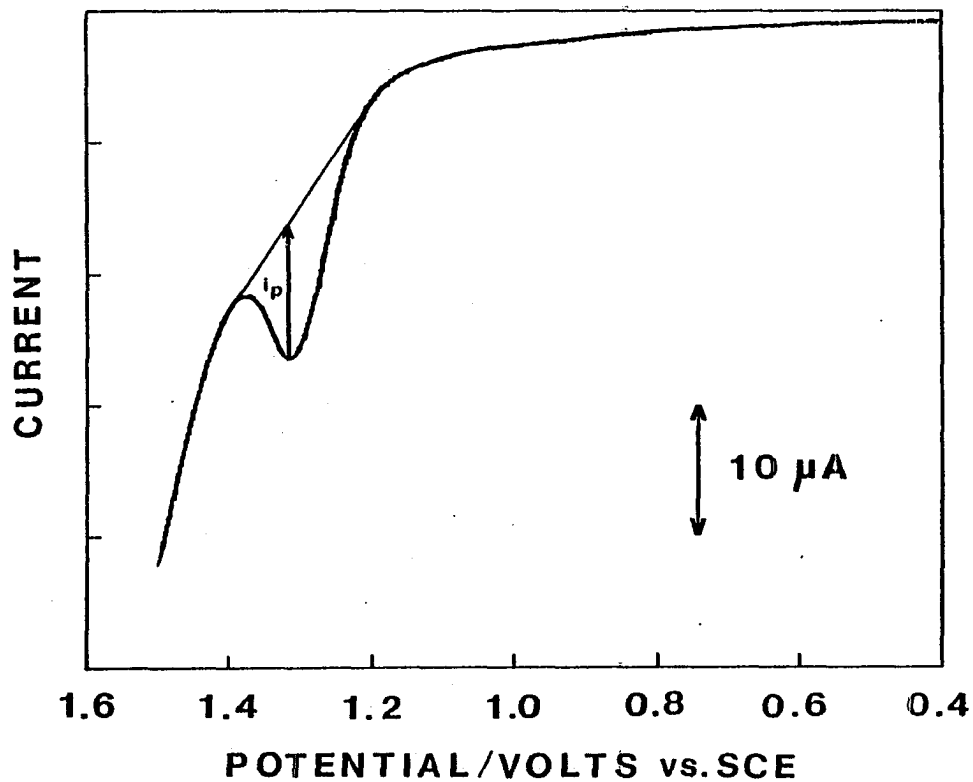


Figure 16. Differential pulse voltammogram of 1.65 m$\underline{M}$ poly(I) in pH 6.25 phosphate buffer, μ=0.5 $\underline{M}$. Data obtained at a sweep rate of 5 mV s-1.

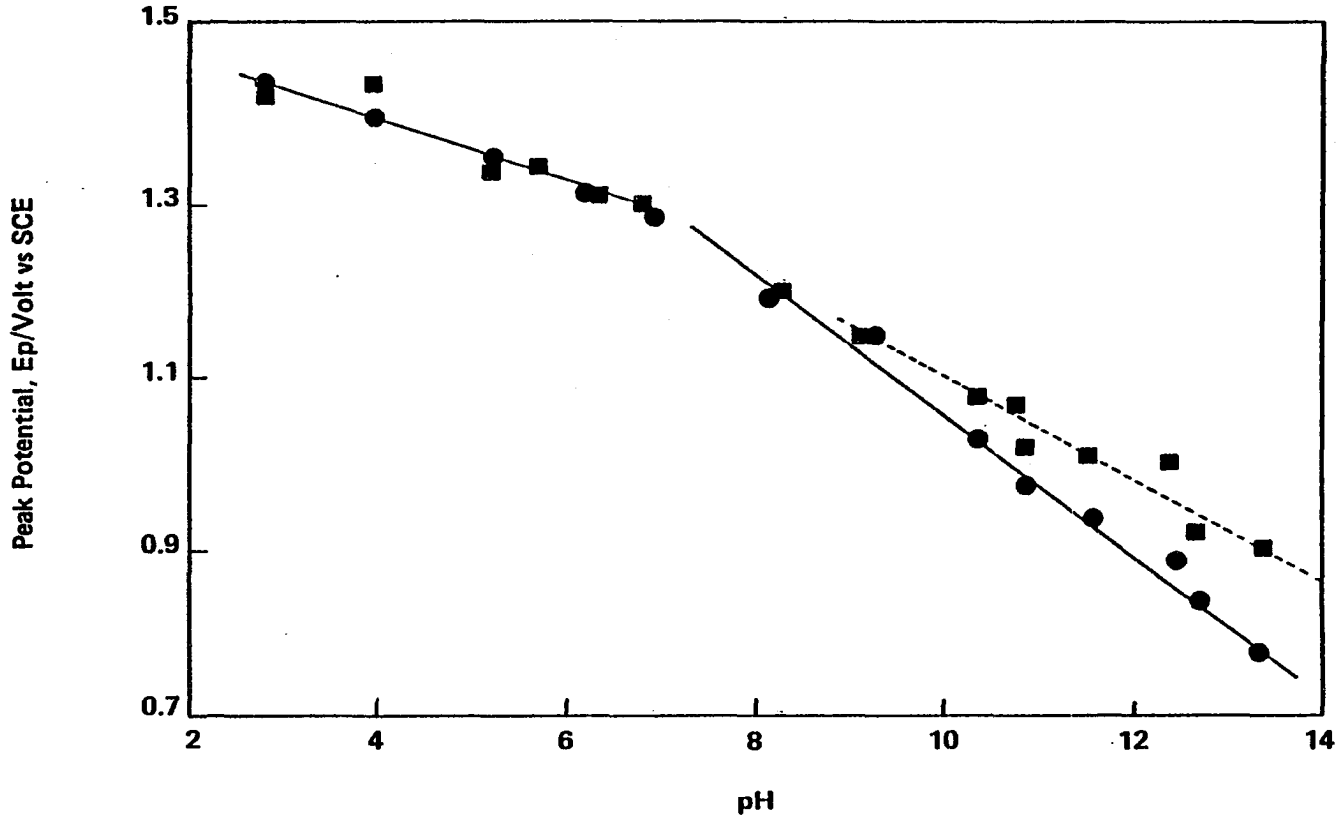


Figure 17. Peak potential, E_p, vs. pH relationship for the single differential pulse voltammetric oxidation peak of poly(I) obtained in phosphate buffers of ionic strength 0.5 M at a sweep rate of 5 mV s^{-1}. (■) 1.65 mM poly(I). (●) 0.165 mM poly(I).

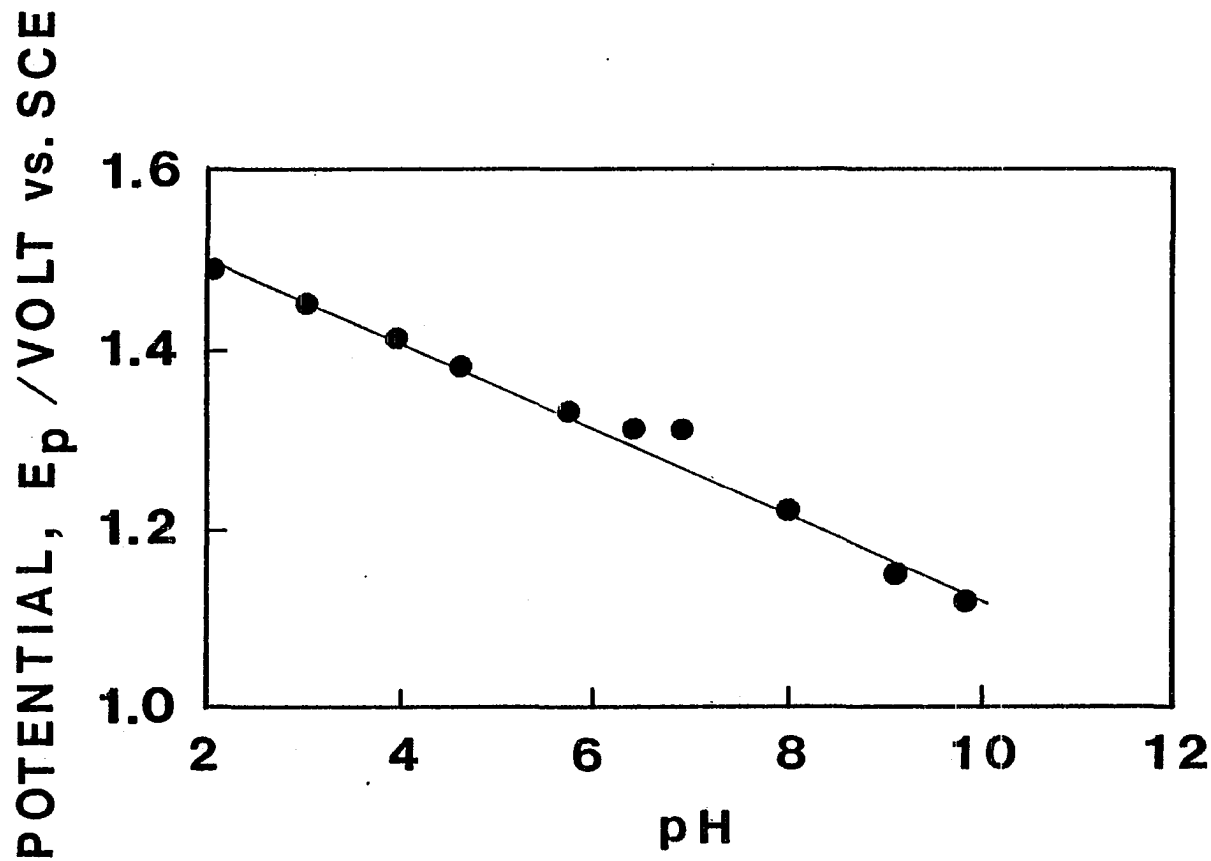


Figure 18. Peak potential, E_p, vs. pH relationship for the single differential pulse voltammetric oxidation peak of 5.0 mM poly(I) in phosphate buffers, μ=0.5 M. Data obtained at a sweep rate of 5 mV s^{-1}.

study of poly(I) in phosphate buffers of various ionic strengths was done to determine an ionic strength where the peak current would remain constant even with slight variations in the ionic strength. For example, at pH 6.3 the peak current for 1.65 mM poly(I) increases with the ionic strength of the buffer up to ca. 0.4 M. Above this ionic strength the peak current becomes essentially independent of the ionic strength (Figure 19). A buffer ionic strength of 0.5 M was thus chosen for analytical studies because of the larger peak current and hence the greatest analytical sensitivity. At this ionic strength small variations in ionic strength do not affect the peak current for poly(I).

Concentration study. Differential pulse voltammetric peak current vs. concentration studies of poly(I) were undertaken to determine the amount of adsorption which occurs at the electrode. The peak current was found to be highly dependent on the pH of the solution. At low pH the peak current is largest and decreases with pH similar to the behavior for hypoxanthine, inosine, and IMP. This behavior suggests that adsorption of all the species studied is greater at low pH with a corresponding increase in the experimental peak current. For example, at pH 5.3 poly(I) exhibits a maximum peak current at ca. 1.6 mM (Figure 20A). The maximum value for the peak current of poly(I) in pH 7 buffers occurs at ca. 2.0 mM (Figure 20B). These results indicate that at concentrations above 2.0 mM the electrode surface is completely covered with adsorbed poly(I) molecules or its electrooxidation product(s).

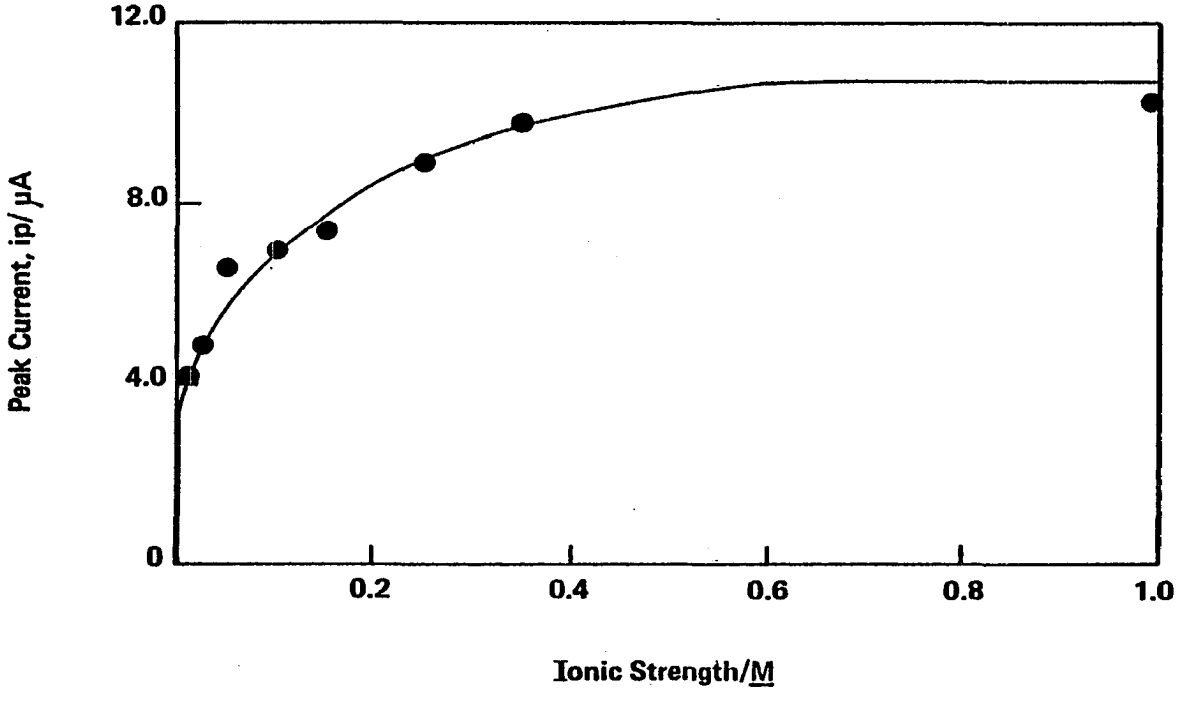


Figure 19. Peak current, i_p, vs. buffer ionic strength for the single differential pulse voltammetric oxidation peak of 1.65 mM poly(I) in pH 6.3 phosphate buffer.

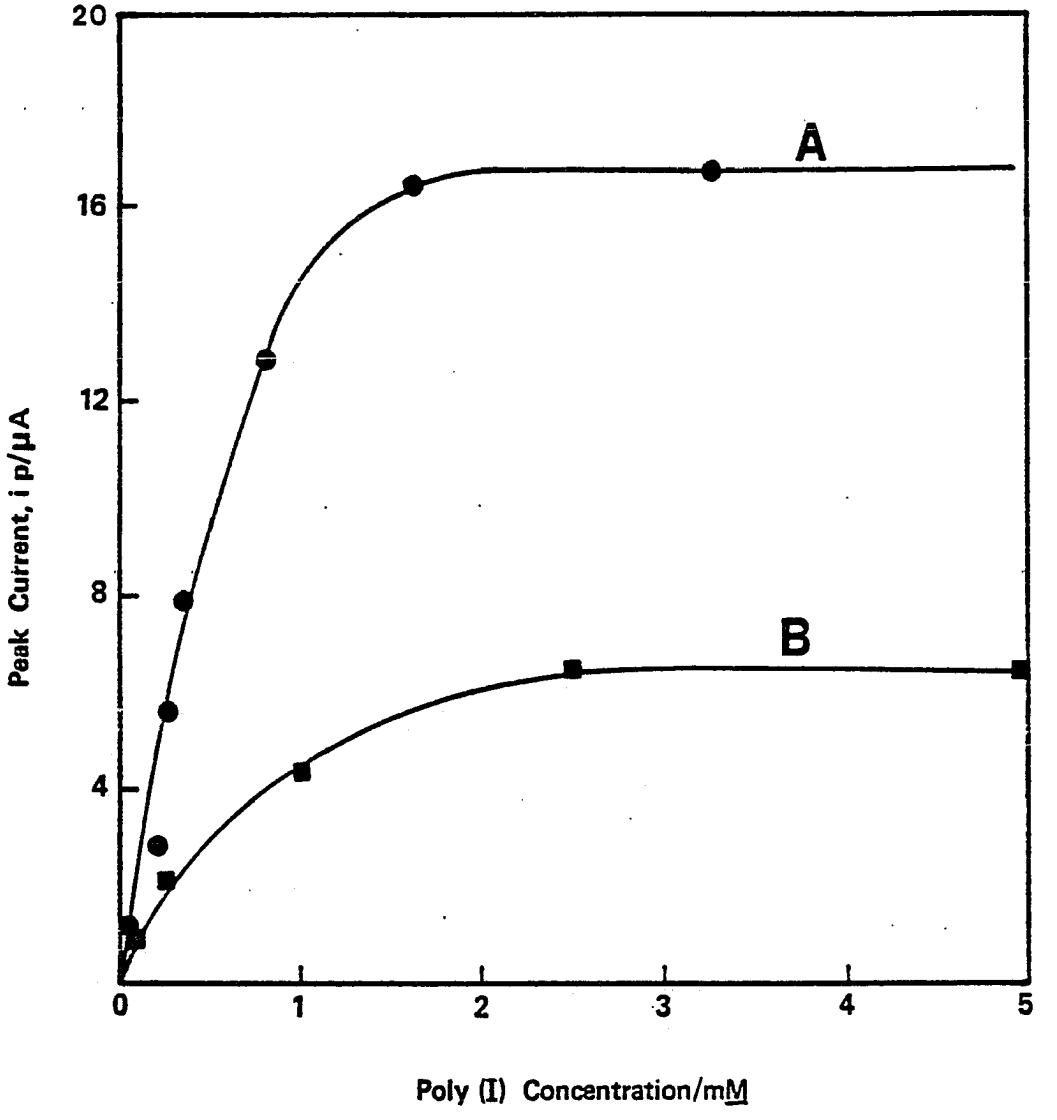


Figure 20. Peak current, i_p, vs. concentration curve for the differential pulse voltammetric peak of poly(I) in phosphate buffers of ionic strength 0.5 M. (A) pH 5.3 and (B) pH 7.0.

Studies of Hypoxanthine in Poly(I)

The peak potential *vs.* pH dependence curves for hypoxanthine, inosine, IMP, and poly(I) reveal that the major peaks of inosine, IMP, and poly(I) occur at very nearly the same potential over the entire pH range. This implies that traces of inosine and/or IMP cannot be determined in poly(I) using differential pulse voltammetry. As mentioned above it has been found that polynucleotides, nucleotides, and nucleosides are usually contaminated with traces of the corresponding purine base. Thus it was decided that the determination of trace amounts of hypoxanthine in poly(I) would be of primary concern.

Because many of our mechanistic studies are carried out at physiological pH the investigation of hypoxanthine/poly(I) mixtures was carried out at pH 7. Figure 20A,B indicate that above a poly(I) concentration of *ca.* 2 m*M* the peak current for its oxidation peak has reached its limiting value. This would seem to indicate that the electrode surface is completely covered with adsorbed poly(I) molecules or its electrooxidation products. If this is the case then the extent of hypoxanthine adsorption at the PGE might be decreased. Decreasing the extent of the adsorption of hypoxanthine should extend the linear range of the hypoxanthine peak current *vs.* concentration curve above that shown in Figure 5. A linear calibration curve is desirable from an analytical viewpoint because of the greater simplicity it affords.

Peak current studies. The initial study of the oxidation peak current for hypoxanthine in poly(I) was done at a poly(I) concentration of 2.0 m*M*. Under these conditions the hypoxanthine peak current *vs.*

concentration curve was linear only to ca. 50 μM (Figure 21). It was also observed that the peak current for the poly(I) peak decreased with increasing hypoxanthine concentration (Figure 21). This behavior suggests that the adsorption of poly(I) and hypoxanthine is competitive at the PGE surface.

The competitive adsorption observed was further investigated by varying the poly(I) concentration and holding the concentration of hypoxanthine at a constant level. The hypoxanthine concentration was held at either 10 μM or 40 μM (both hypoxanthine concentrations are on the linear region of the peak current vs. concentration curve shown in Figure 21) and the poly(I) concentration was varied between 0.25 mM and 5.0 mM. At the 40 μM hypoxanthine concentration level the peak current for hypoxanthine varied the most and reached a limiting minimum value above ca. 2.5 mM poly(I) (Figure 22A). A constant value for the hypoxanthine peak current at the 10 μM concentration level was reached at ca. 1 mM poly(I) (Figure 22B). It appears that if the concentration of poly(I) is held at a level of 5 mM, which approaches the limit of solubility at pH 7, competitive adsorption of hypoxanthine is minimized. Even at this poly(I) concentration the peak current vs. concentration curve for hypoxanthine is once again linear only to about 25 μM (Figure 23).

In order to test the usefulness of differential pulse voltammetry at the PGE for the analytical determination of hypoxanthine in poly(I), a series of test solutions were prepared which were 5 mM in poly(I) and ranged from 9 to 24 μM in hypoxanthine. These solutions were analyzed by measuring the peak current for the hypoxanthine oxida-

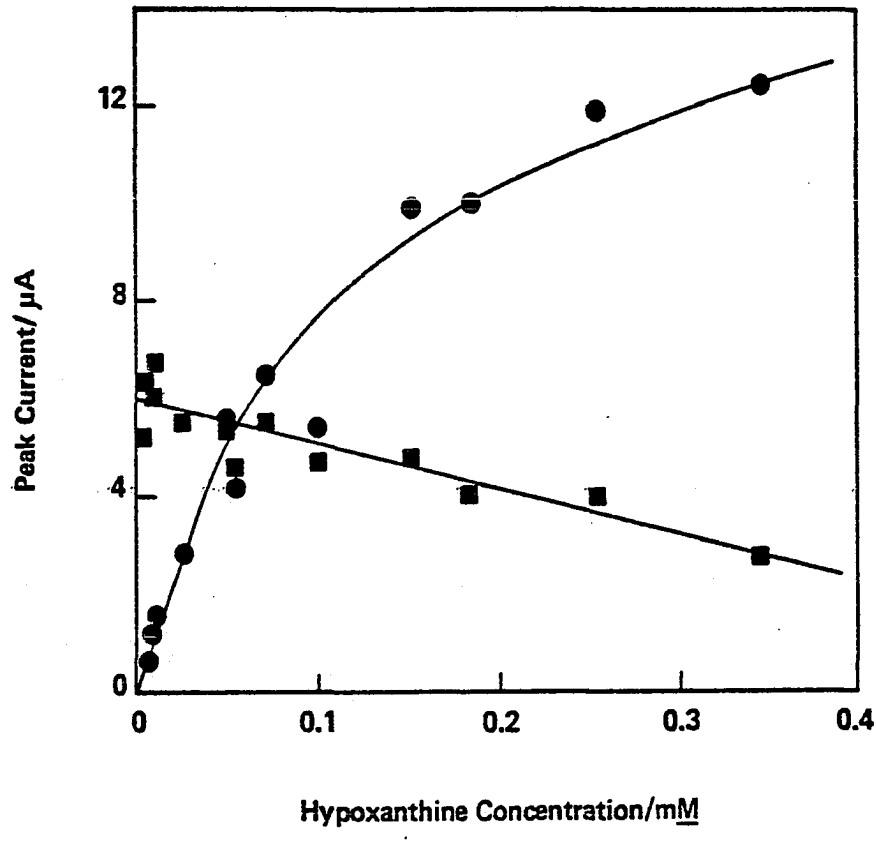


Figure 21. Peak current vs. hypoxanthine concentration in pH 7.0 phosphate buffer, μ=0.5 M containing 2.0 mM poly(I). ● Peak current for hypoxanthine peak I. ■ Peak current for poly(I) peak.

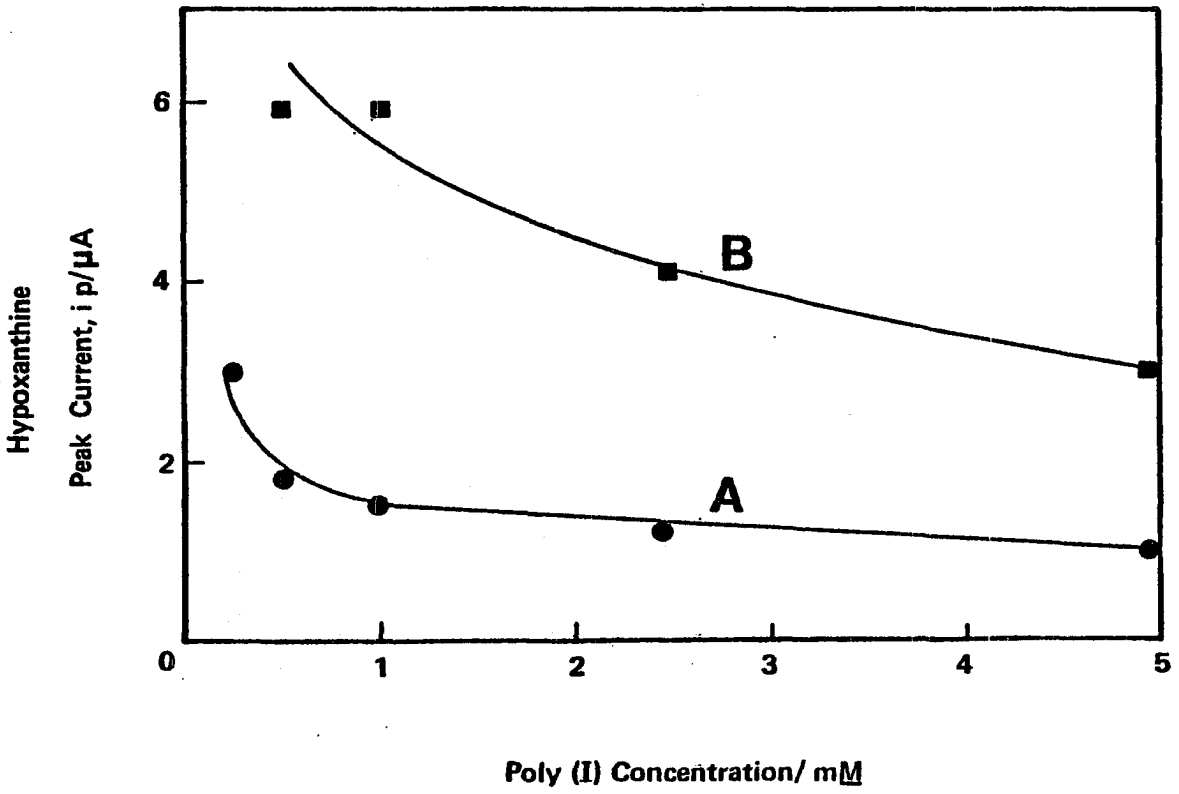


Figure 22. Hypoxanthine peak current vs. poly(I) concentration in pH 7.0 phosphate buffer, μ=0.5 M. The concentration of hypoxanthine was held constant at (A) ■ 40 µM and (B) ● 10 µM.

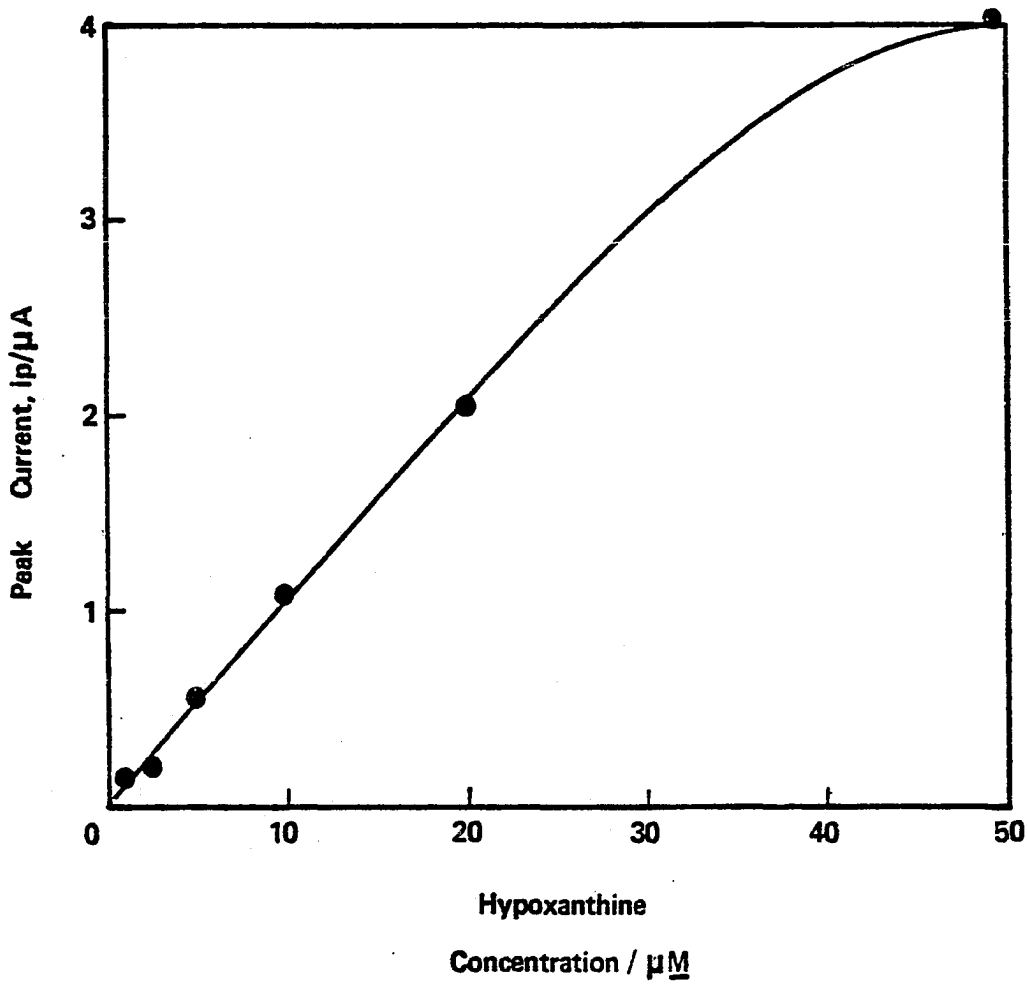


Figure 23. Peak current, i_p, vs. hypoxanthine concentration curve in pH 7.0 phosphate buffer, μ=0.5 M at a constant poly(I) concentration of 5.0 mM.

tion peak and comparing to a calibration curve similar to Figure 23. Results for the three unknowns are given in Table 3. These results indicate that hypoxanthine can be determined at concentrations less than 0.5% in poly(I) with an accuracy of better than ±4%.

Table 3

Determination of Hypoxanthine in Poly(I) Samples[a] by Differential Pulse Voltammetric Oxidation at the PGE

Sample	Concentration of Hypoxanthine Actual (μM)	Found (μM)[b]
A	24.1	23.1
B	16.9	17.5
C	9.6	9.2

[a]Determination run in pH 7.0 phosphate buffer, μ=0.5 M, containing 5 mM poly(I).

[b]Average of 3 determinations.

CHAPTER III

EXPERIMENTAL

Chemicals. Polyinosinic acid (5'-potassium salt), inosine, and inosine-5'-monophosphate (disodium salt) were obtained from Sigma. Hypoxanthine was obtained from Nutritional Biochemicals.

All buffer solutions were prepared from reagent grade chemicals. Phosphate buffers (sodium salts) with an ionic strength of 0.5 M were used unless otherwise specified. Above pH 12 the supporting electrolyte utilized in the study was a sodium hydroxide solution with sodium sulfate added to obtain an ionic strength of 0.5 M.

Apparatus. Pyrolytic graphite was obtained from Pfizer Minerals, Pigments, and Metals Division. The fabrication and resurfacing of the pyrolytic graphite microelectrode have been fully described elsewhere.[35-37] A rough PGE consists of a rod of pyrolytic graphite ca. 1.5 mm x 1.5 mm x 10 mm sealed in a glass tube with epoxy resin (Epoxi-Patch, Hysol Division, Dexter Corp., Olean, NY). Resurfacing of the PGE was accomplished by grinding on 600-grit silicon carbide paper (Buehler, Inc., Evanston, IL) attached to a metallographic polishing wheel. After resurfacing, the tip of the electrode was rinsed thoroughly with doubly-distilled water. Then the body of the electrode was dried with a soft tissue paper. Excess water was

removed from the tip by dabbing gently with the soft tissue.

A Princeton Applied Research (PAR) Corporation 174A Polarographic Analyzer was used throughout this investigation. All differential pulse voltammograms at the PGE were obtained at 5 mV s^{-1} with a modulating amplitude of 25 mV and with the drop timer control set at 0.5s. An initial potential of 0.2V was applied to the electrode for 30s prior to the voltage sweep as described previously.[5] A Hewlett-Packard Model 7015 X-Y Recorder was used to record all voltammograms.

The voltammetric cell had a capacity of ca. 5 ml and was surrounded by a water-jacket for control of the temperature at 25°±0.1°C. A pool of clean mercury at the bottom of the cell served as the counter electrode. Electrical contact to the saturated calomel reference electrode (SCE) was made through a double salt bridge arrangement with a Luggin capillary positioned very close to the tip of the PGE. This arrangement prevents any significant contamination of the test solution with chloride ions from the SCE. The cell was maintained at constant temperature by using a MGW Lauda Model B-1 Water Circulation with a three liter bell jar as the water bath. The SCE was at room temperature at all times (25°±1°C) therefore all potentials are referred to the SCE at 25°C.

Controlled potential electrolysis of IMP utilized a PAR Model 373 Potentiostat/Galvanostat. A three compartment cell with a working compartment capacity of ca. 15 ml was used. All salt bridges contained agar prepared with phosphate buffer pH 7.0 with an ionic strength of 0.5 M. This agar was prepared by dissolving 4 g of agar in 90 ml of pH 7.0 phosphate buffer with heating.[38] Counter and

reference electrode compartments contained the same buffer solution. The reference electrode was a Fisher Fiber-Tip SCE and the counter electrode was platinum foil.

Solutions of any of the compounds studied were not found to be air sensitive, therefore they were not deaerated prior to differential pulse voltammetry or controlled potential electrolysis. The tendency of hypoxanthine to slowly decompose (vide supra) was not found to be a result of air oxidation.

All hypoxanthine derivatives were found to adsorb strongly to the glass surface of the voltammetric cell and very careful rinsing was necessary to prevent subsequent contamination of blank or test solutions. Therefore the cells were rinsed with doubly-distilled water ten times when changing solutions.

Procedure for Detection of Hypoxanthine in Poly(I)

The poly(I) concentration necessary for detection of trace amounts of hypoxanthine is not critically important. Typically, 3 mg of poly(I) is dissolved with gentle agitation in 1 ml of double distilled water at room temperature. This solution is transferred to the voltammetric cell and diluted 1:1 with pH 7.0 phosphate buffer with an ionic strength of 1.0 M giving a final ionic strength of 0.5 M. Dissolution of poly(I) occurred much more readily in water than in phosphate buffer, but once in solution it did not precipitate upon mixing with buffer. The solution was allowed to remain in the cell for an appropriate length of time (ca. 5 min.) to establish thermal equilibrium at 25°C. This temperature was used because no

other temperature offered better sensitivity in the determination and it has the advantage of quicker thermal equilibration between the cell and the test solution.

An initial potential of 0.2V is applied to the PGE for 30s prior to initiation of the voltage sweep. Poly(I) exhibits a single well-defined differential pulse voltammetric oxidation peak, close to the background discharge, with a peak potential (E_p) of 1.28V at 25°C. Poly(I) concentrations of ca. 1.5 mg ml^{-1} give peak currents of ca. 6 μA at a 2 mm^2 PGE. If hypoxanthine is present in the sample it will be detected by the appearance of a voltammetric oxidation peak with a peak potential of 0.94-0.95V.

Procedure for Determination of Hypoxanthine in Poly(I)

An analytical calibration curve of peak current vs. hypoxanthine concentration is prepared by obtaining voltammograms of various concentrations of hypoxanthine in a solution containing a fixed amount of poly(I) in pH 7.0 phosphate buffer with an ionic strength of 0.5 M. Approximately 3 mg of poly(I) is dissolved in 1 ml of doubly-distilled water (vide supra) and mixed 1:1 with pH 7.0 phosphate buffer, μ=1.0 M, containing the different concentrations of hypoxanthine. The concentration of hypoxanthine in the test solution ranges from 1 μM to 25 μM and the poly(I) concentration is 5 mM. Weights of poly(I) refer to the monopotassium salt and it must be emphasized that both poly(I) and hypoxanthine solutions should be freshly prepared because of the slight tendency for decomposition.

Poly(I) used for the calibration curve should be free of

hypoxanthine. Any traces of hypoxanthine can be removed by controlled potential electrolysis at 0.96V in pH 7.0 phosphate buffer, μ=0.5 M, at a PGE with a large surface area. The ionic strength of the test solutions for the differential pulse voltammetry is not critically important provided that all standards and unknowns are made up with identical buffers.

At least three voltammograms are run on each solution and the average hypoxanthine peak current used for the calibration curve.

A poly(I) sample with an unknown concentration of hypoxanthine can be analyzed by dissolving ca. 3.0 mg in 1 ml of doubly-distilled H_2O and then diluting 1:1 with pH 7.0 phosphate buffer having an ionic strength of 1.0 M. At least three voltammograms are run and the average hypoxanthine peak current determined. The hypoxanthine concentration is then determined by reference to the calibration curve obtained under identical experimental conditions.

CHAPTER IV

SUMMARY

Polyinosinic acid shows only one differential pulse voltammetric oxidation peak at the PGE close to the background discharge. Hypoxanthine, inosine, and IMP show somewhat distorted voltammograms which have the appearance of two overlapping peaks. At low concentrations hypoxanthine exhibits only a single voltammetric oxidation peak which is separated from the single peak of poly(I) by ca. 300 mV making detection and determination of trace amounts of hypoxanthine in poly(I) very easy. In the presence of a large excess of poly(I) the hypoxanthine peak current vs. concentration relationship is linear up to ca. 25 μM at a temperature of 25°C. Since the calibration curve was linear at 25°C it was not found necessary to use 10°C for linearity as reported previously for determination of xanthine in poly(X).[5]

Detection of trace amounts of IMP in poly(I) using differential pulse voltammetry was not possible because their peak potentials were practically identical at all pH values and were indistinguishable in a mixture of the two compounds. Peak I of inosine should be resolved from the oxidation peak of poly(I), however in solution with poly(I) it was not observed. This is not surprising since the peak current vs. concentration dependence for peak I of inosine indicates that it

is an adsorption peak. An adsorption peak would not appear if the electrode surface was already covered with poly(I) molecules. Therefore it does not appear that inosine is detectable in poly(I) using differential pulse voltammetry at a PGE.

The results for hypoxanthine show that it can be determined at less than 0.5% by weight in poly(I) with an accuracy of better than ±4%. Analyses at this low level have been impractical even with spectrophotometric methods because of the similarity in the u.v. spectra of poly(I) at pH 7 (λ_{max} = 247 nm) and hypoxanthine (λ_{max} = 249.5 nm).

CHAPTER V

REFERENCES

1. V. Brabec and G. Dryhurst, J. Electroanal. Chem., 89 (1978) 161.
2. V. Brabec and G. Dryhurst, J. Electroanal. Chem., 91 (1978) 219.
3. V. Brabec and G. Dryhurst, Stud. Biophys., 67 (1978) 23.
4. T. Yao, T. Wasa, and S. Musha, Bull. Chem. Soc. Japan, 51 (1978) 1235.
5. G. Dryhurst and L. G. Karber, Anal. Chim. Acta, 100 (1978) 289.
6. V. Brabec, Stud. Biophys., 82 (1981) 17.
7. D. Thiele and W. Guschlbauer, Biophysik, 9 (1973) 261.
8. G. Dryhurst, Topics Curr. Chem., 34 (1972) 47.
9. G. Dryhurst, Electrochemistry of Biological Molecules, Academic Press, New York, 1977.
10. G. Dryhurst, J. Electrochem. Soc., 119 (1972) 1659.
11. J. L. Owens, H. A. Marsh, and G. Dryhurst, J. Electroanal. Chem., 91 (1978) 213.
12. M. Z. Wrona, J. L. Owens, and G. Dryhurst, J. Electroanal. Chem., 105 (1979) 295.
13. A. C. Conway, M.S. Thesis, University of Oklahoma, 1980.
14. A. C. Conway, R. N. Goyal, and G. Dryhurst, J. Electroanal. Chem., 123 (1981) 243.
15. R. N. Goyal, A. Brajter-Toth, and G. Dryhurst, J. Electroanal. Chem., 131 (1982) 181.
16. R. N. Goyal, A. Brajter-Toth, J. S. Besca and G. Dryhurst, submitted to J. Electroanal. Chem.

17. M. T. Cleary, Ph.D. Dissertation, University of Oklahoma, 1980.

18. M. Z. Wrona and G. Dryhurst, Biochim. Biophys. Acta, 570 (1979) 371.

19. H. A. Marsh and G. Dryhurst, J. Electroanal. Chem., 95 (1979) 81.

20. A. Brajter-Toth, R. N. Goyal, M. Z. Wrona, T. Lacava, N. T. Nguyen, and G. Dryhurst, Bioelectrochem. Bioenerg., 8 (1981) 413.

21. M. Z. Wrona, R. N. Goyal, and G. Dryhurst, Bioelectrochem. Bioenerg., 7 (1980) 433.

22. M. Grunberg-Manago, P. J. Ortiz, and S. Ochoa, Science, 122 (1955) 907.

23. E. Fischer, Ber. Dtsch. Chem. Ges., 30 (1897) 558.

24. A. Albert and D. J. Brown, J. Chem. Soc., 157 (1954) 2060.

25. P. A. Levene, H. S. Simms, and L. W. Bass, J. Biol. Chem., 70 (1926) 243.

26. Calbiochem, "Properties of the Nucleic Acid Derivatives," Document No. 4955 (1976).

27. A. M. Michelson and F. Pochon, Biochim. Biophys. Acta, 114 (1966) 469.

28. R. C. Warner, J. Biol. Chem., 229 (1957) 711.

29. A. Rich, Biochim. Biophys. Acta, 29 (1958) 502.

30. S. Arnott, R. Chandrasekaran, and C. M. Martilla, Biochem. J., 141 (1974) 537.

31. J. L. Owens and G. Dryhurst, Anal. Chim. Acta, 89 (1977) 93.

32. L. G. Karber and G. Dryhurst, Anal. Chim. Acta, 108 (1979) 193.

33. D. L. Smith and P. J. Elving, Anal. Chem., 34 (1962) 930.

34. R. H. Wopschall and I. Shain, Anal. Chem., 39 (1967) 1514.

35. G. Dryhurst, Talanta, 19 (1972) 769.

36. G. Dryhurst, Anal. Chim. Acta, 57 (1971) 137.

37. G. Dryhurst and P. J. Elving, J. Electrochem. Soc., 115 (1968) 1014.

38. L. Meites, Polarographic Techniques, 2nd Ed., Interscience, New York, 1965.

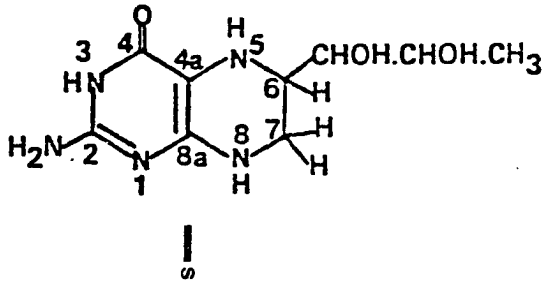
PART II

ELECTROCHEMISTRY OF 6-METHYL-5,6,7,8-TETRAHYDROPTERIN

CHAPTER I

INTRODUCTION

Tetrahydrobiopterin (I) has been shown to be the naturally occurring cofactor for a group of enzymes that introduce a hydroxyl group into phenylalanine, tyrosine, and tryptophan utilizing molecular oxygen.[1-3]

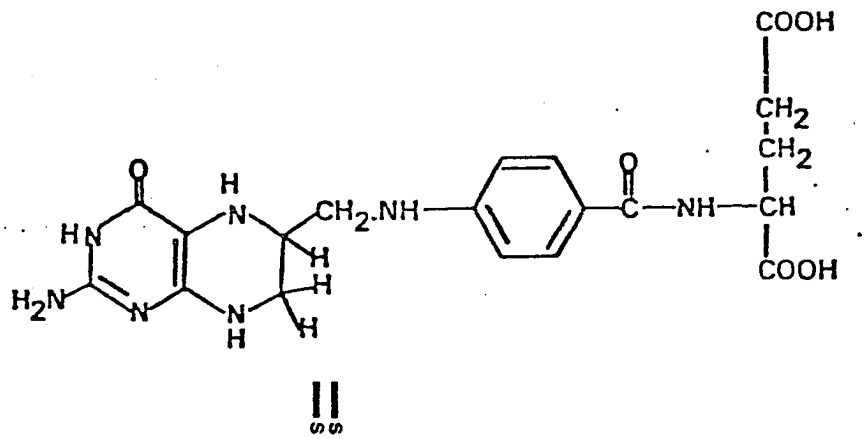


I

The hydroxylation reactions of tyrosine and tryptophan are the rate limiting steps in the biosynthesis of the neurotransmitters norepinephrine, dopamine,[4] and serotonin.[5] It is also suspected that a reduced pterin is necessary for photophosphorylation.[6,7] It has been demonstrated that a tetrahydropterin is involved in the enzymic oxidation of glyceryl ethers in the liver.[8] The same reduced pterin

cofactor is suspected of playing a role in the hydroxylation of steroids and in the formation of melanine.[9]

Another reduced pterin cofactor which occurs widely in both plants and animals is tetrahydrofolic acid (II), which may be regarded as part of the vitamin B complex.



Kaufman proposed the first mechanism to explain the involvement of tetrahydropterins in the enzymic hydroxylation of the aromatic amino acids.[1,10,11] Thus he proposed that phenylalanine is converted to tyrosine in the presence of phenylalanine hydroxylase and oxygen. Coupled to this reaction is the apparent $2\underline{e}\text{-}2H^{+}$ oxidation of the cofactor to a quinonoid-dihydropterin form (Figure 1). This quinonoid-dihydropterin is reduced to the tetrahydropterin by NADH in the presence of a second enzyme, dihydropteridine reductase. The term "pterin" is used for the moiety, 2-amino-4-hydroxypteridine.

L-erythro-tetrahydrobiopterin is the natural cofactor for the aromatic amino acid hydroxylases.[12] However there are various other tetrahydropterins which can function as so-called pseudo cofactors,[12-17] most notably 6-methyl-5,6,7,8-tetrahydropterin (6-MTHP) and 6,7-dimethyl-

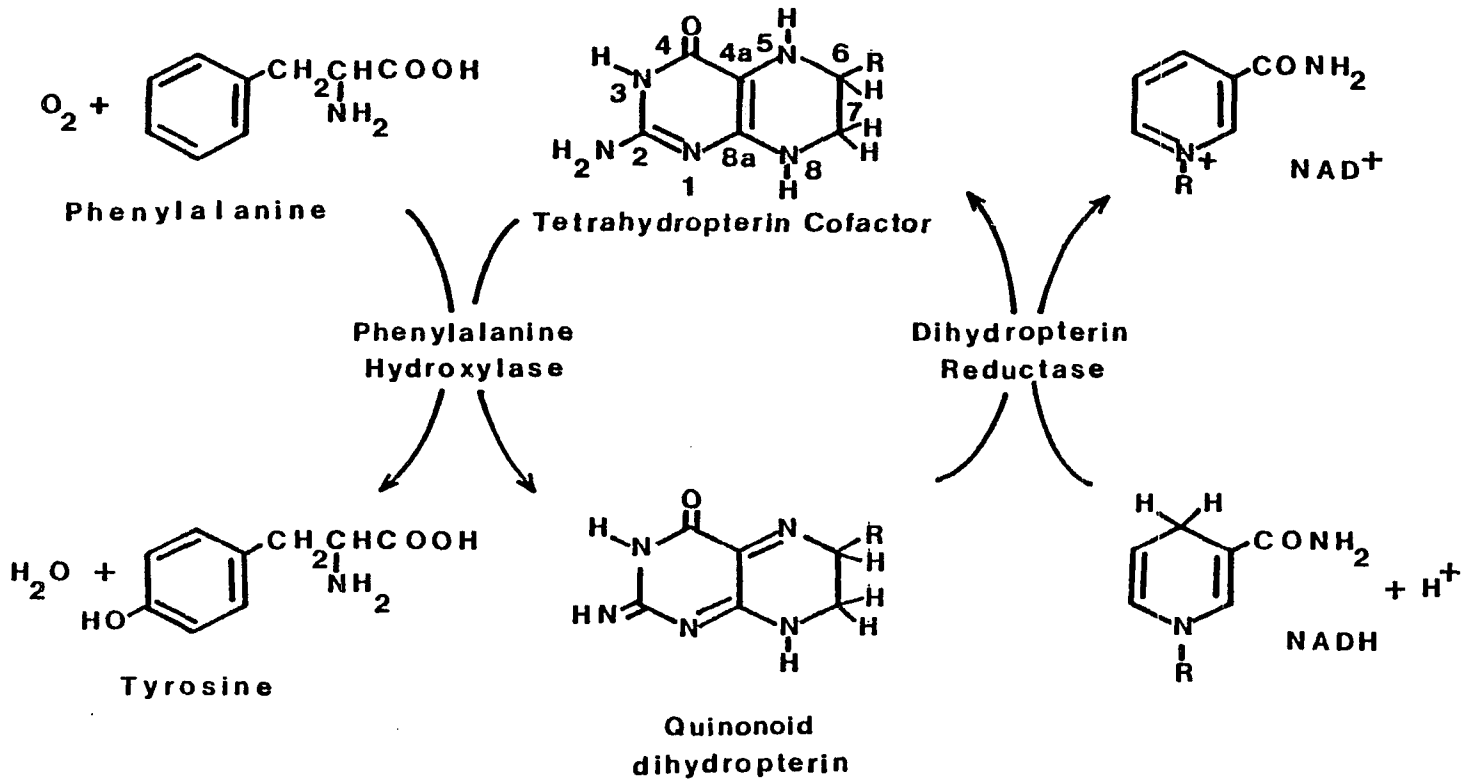


Figure 1. Original reaction scheme proposed by Kaufman for the participation of tetrahydropterin cofactors in the enzymic hydroxylation of phenylalanine.

5,6,7,8-tetrahydropterin (6,7-DMTHP). Tetrahydropterin can also function as a cofactor *in vitro*, however alkylation at the C(6)-position greatly enhances the cofactor activity.[18] When tetrahydropterin was used as the cofactor for hydroxylation of phenylalanine in the presence of phenylalanine hydroxylase and oxygen, only about one-half the amount of tyrosine was formed compared to when 6-MTHP or tetrahydrobiopterin were used.[14] Of all the synthetic cofactors 6-MTHP has been shown to have the highest activity, second only to the natural cofactor L-erthyro-tetrahydrobiopterin.[19-21] It has not been used more extensively owing to the fact that it is claimed to be less stable to air oxidation than 6,7-dimethyl-5,6,7,8-tetrahydropterin.[19] Archer and Scrimgeour[22] reported that appreciable amounts of fully oxidized 6-methylpterin and an equal amount of unoxidized 6-MTHP were detected when 6-MTHP was oxidized to the quinonoid-dihydropterin with a stoichiometric amount of $K_3Fe(CN)_6$.

The 2-amino-4-hydroxy configuration of tetrahydropterins does not appear to be an absolute requirement for cofactor activity. In fact it has been demonstrated that the 2,4-diamino compound also exhibits cofactor activity.[14] Reduced pterins in which the 2-amino and 4-hydroxy groups are reversed do not show cofactor activity.[19] Alkylation of the 2-amino group or N(8) is also sufficient to block the cofactor activity.[19]

The formation of a quinonoid-dihydropterin (II, Figure 2) when tetrahydropterins are oxidized seems to have been suggested first by Hemmerich.[23] This quinonoid intermediate is labile and rearranges to the more stable 7,8-dihydropterin (III, Figure 2).

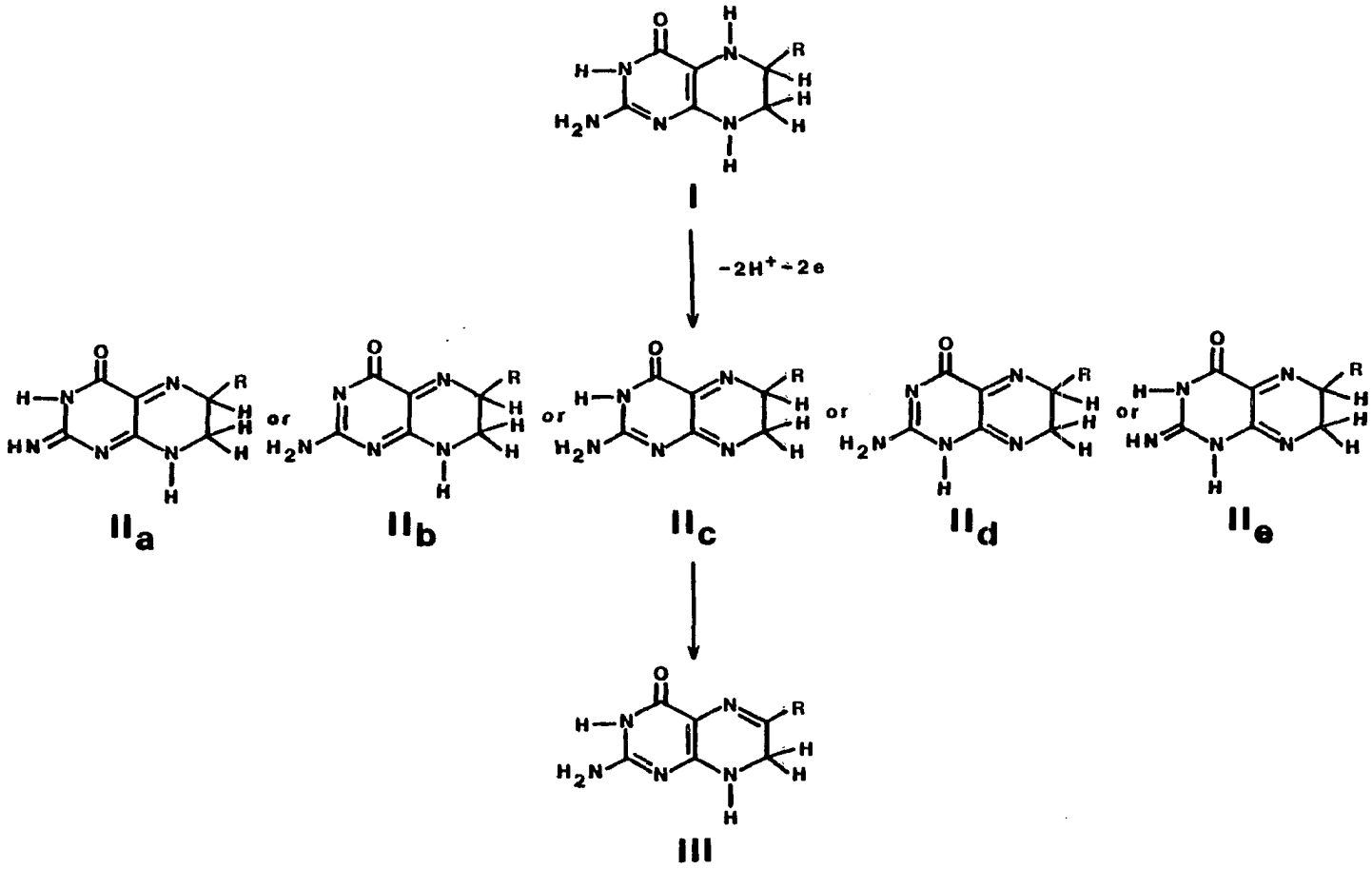


Figure 2. Reaction scheme showing the five possible quinonoid-dihydropterins which might be formed.

There are five possible structures for this quinonoid-dihydropterin species (IIa-IIe, Figure 2). Spectroscopic results[11,24] and data on the rate of oxidation of methylated tetrahydropterins[24] suggest that structure IIa is a favored structure. Electrochemical results appear to favor structure IIc, Figure 2[25] while theoretical molecular orbital calculations suggest that IIb is not a favored structure.[26] The most recent electrochemical and thin-layer spectroelectrochemical studies of 6,7-DMTHP and other methylated tetrahydropterins also favor structure IIc in Figure 2.[27] None of this evidence is conclusive for any of the five possible structures however.

In the original Kaufman scheme (Figure 1) there is no obvious role for the activation of oxygen by the tetrahydropterin cofactor. Therefore he later proposed a scheme (Figure 3) in which a 4a-hydroperoxide (II, Figure 3) is the actual hydroxylating agent.[28-30] Following the hydroxylation a 4a,5-hydrate was proposed to be formed (III, Figure 3). This was proposed to be the intermediate detected by u.v. spectroscopy (λ_{max} = 250 nm and 290 nm) during hydroxylation of phenylalanine when the tetrahydrobiopterin concentration was low and the hydroxylase concentration high. This 4a,5-hydrate decays nonenzymically or enzymically in the presence of a "stimulating" protein, to quinonoid-dihydropterin (IV, Figure 3). When the hydroxylating conditions are optimal the 4a,5-hydrate was not observed.[30] The evidence for the 4a,5-hydrate was gleaned from the similarity of its u.v. spectrum with that of a 4-hydroxy adduct of a similar compound, deazapterin (III).[31]

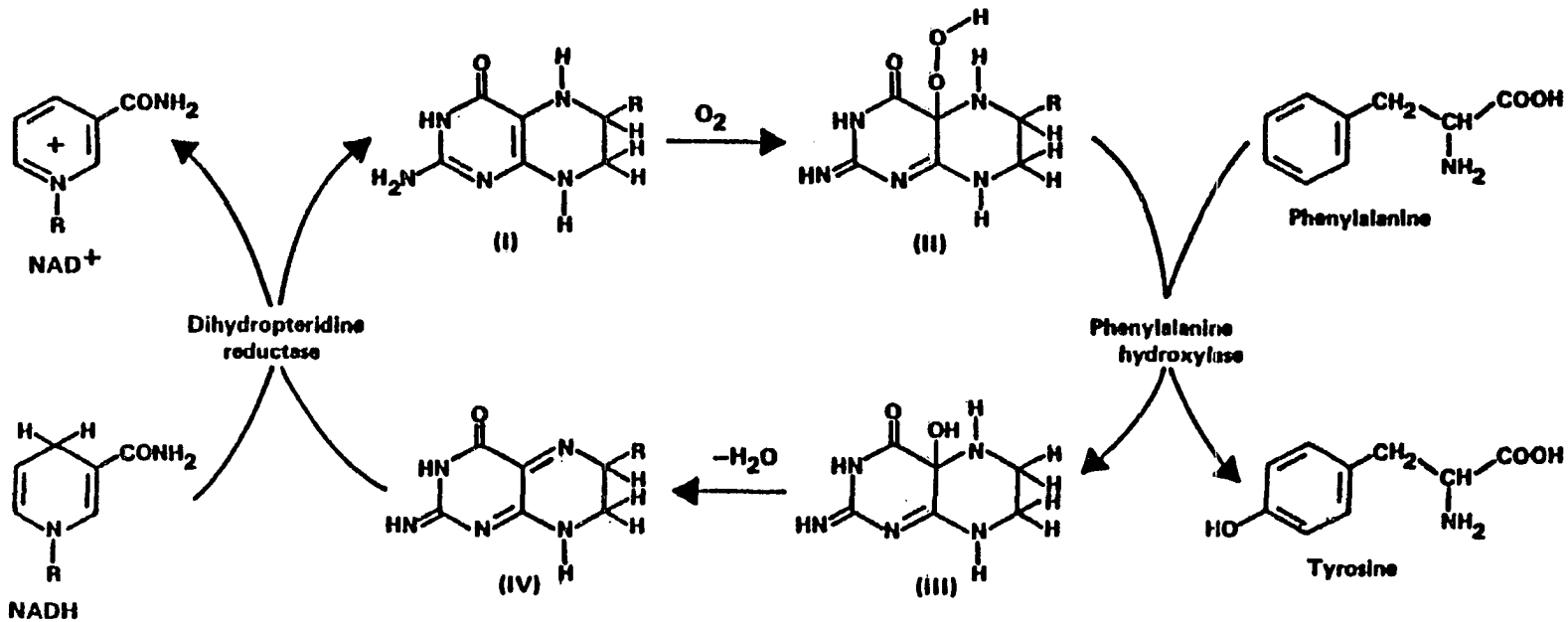
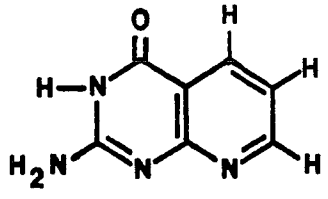


Figure 3. Later reaction scheme proposed by Kaufman to explain how molecular oxygen might be involved in the hydroxylation of phenylalanine.



III

Hamilton[32] has also proposed a hydroxylation mechanism involving hydroperoxides (Figure 4). The hydroperoxide (II, Figure 4) cleaves across the C(4a)-N(5) bond yielding a carbonyl oxide (III, Figure 4). When this reagent transfers its oxygen to the substrate it forms a pyrimidine (IV, Figure 4) which recyclizes to the quinonoid-dihydropterin (V, Figure 4). Evidence for this ring cleavage mechanism for oxygen activation is provided by the fact that several pyrimidines, 2,5,6-triamino-4-pyrimidone and 5-benzylamino-2,6-diamino-4-pyrimidone, can also function as cofactors for phenylalanine hydroxylase and both are cleaved to an oxidized pyrimidine[33] (Figure 5) and an amine. The bond cleavage occurs at the C(5)-N bond which is analogous to the C(4a)-N(5) bond in tetrahydropterins. Mager has also proposed an oxygen containing intermediate, an 8a adduct, in the autooxidation of various substituted tetrahydropterin cofactors.[34]

Further evidence for a 4a-hydroxy intermediate was thought to exist when such an intermediate was claimed to have been isolated from the oxidation of 5-methyl-6,7-diphenyl-5,6,7,8-tetrahydropterin[35] and 5-methyltetrahydrofolic acid.[36] However, the correct structure was later shown to be a pyrazino-S-triazine by Jongejan et al.[37]

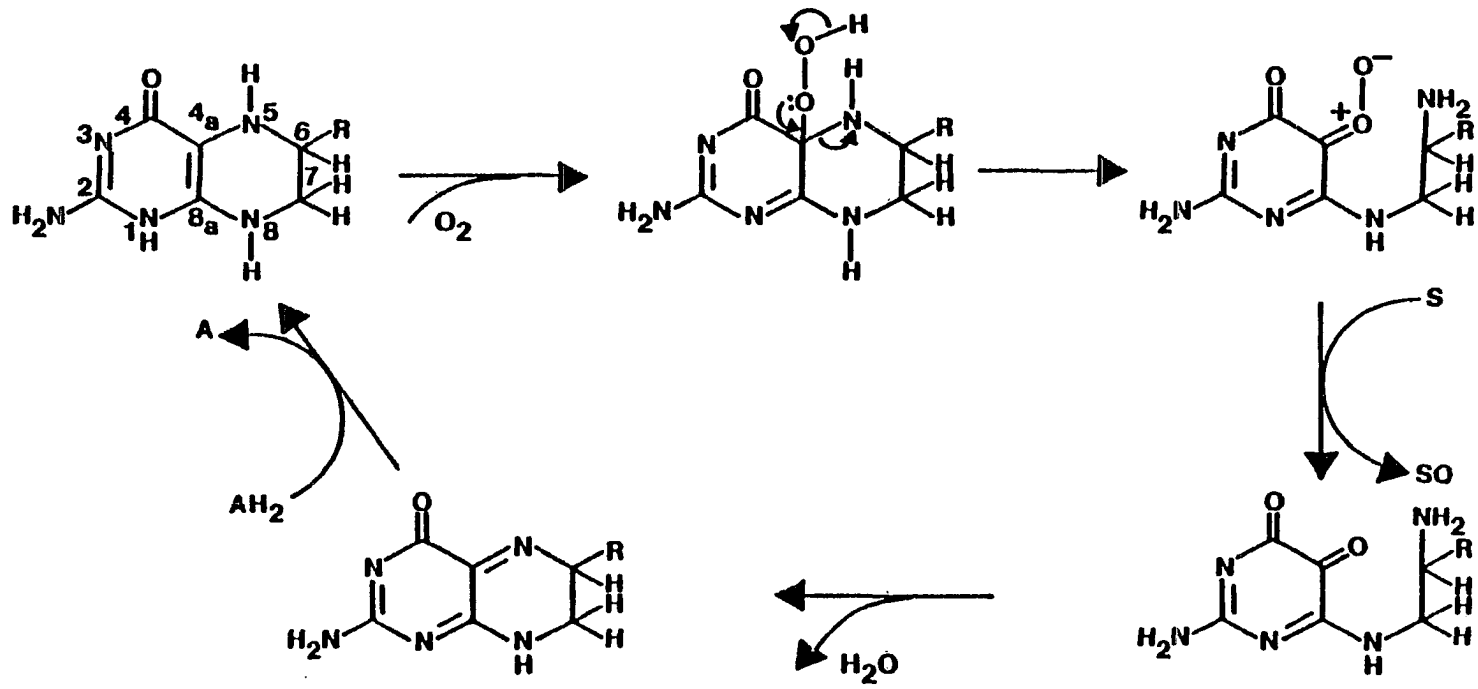


Figure 4. Hamilton's reaction scheme for enzymic hydroxylation of phenylalanine involving tetrahydropterin hydroperoxides. S is substrate, SO is hydroxylated substrate.

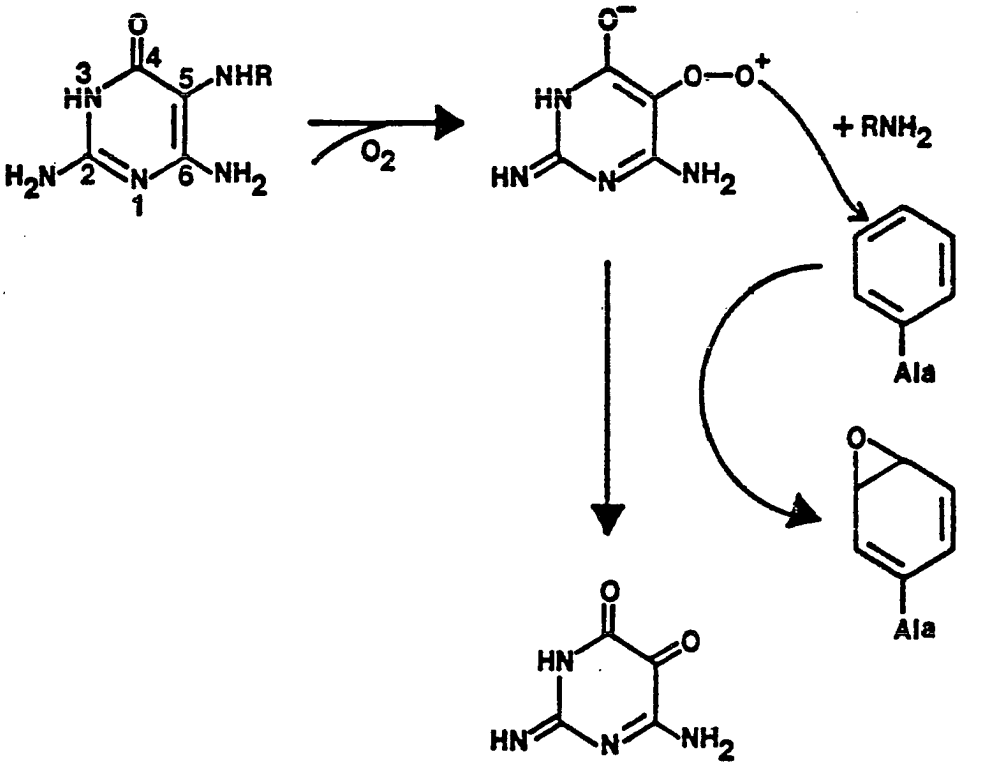


Figure 5. Bailey-Ayling reaction scheme to explain cofactor properties of pyrimidines.

Other workers have detected the existence of radical intermediates in the chemical oxidation of several tetrahydropterins.[29-31,35] Cation radicals have also been observed by EPR spectroscopy in the autooxidation of several tetrahydropterins, including tetrahydrobiopterin and tetrahydrofolic acid (THF), and a mechanism has been proposed which involves the intermediacy of radicals (Figure 6).[38-41]

Recently it has been shown that ingestion of 6-MTHP by rats can stimulate the hydroxylation of phenylalanine.[42] The evidence for this is the much higher level of phenylalanine hydroxylase activity found in liver slices from rats fed 6-MTHP as compared to rats fed a normal diet without 6-MTHP. It was speculated that it could be used for the treatment of a disease called phenylketonuria (PKU) which is characterized by an extremely low level of phenylalanine hydroxylase activity in the liver, only 0.27% of the activity found in a normal person.[43]

Persons suffering from PKU often become mentally retarded at a young age unless phenylalanine is removed from the diet. A less debilitating variation of this disease occurs in some people where about 5% of the normal level of phenylalanine hydroxylase activity is detected in the liver.[42] This variation, termed hyperphenylalaninemia, does not result in mental retardation.[44] It was proposed that perhaps a large dose of 6-MTHP or a similar pseudo cofactor could be administered to PKU patients to raise the hydroxylation rate to the point where mental retardation would not develop. Theoretical calculations indicate that this might indeed be possible as 6-MTHP had a V_{max} for hydroxylation thirteen times greater than tetrahydrobiopterin when

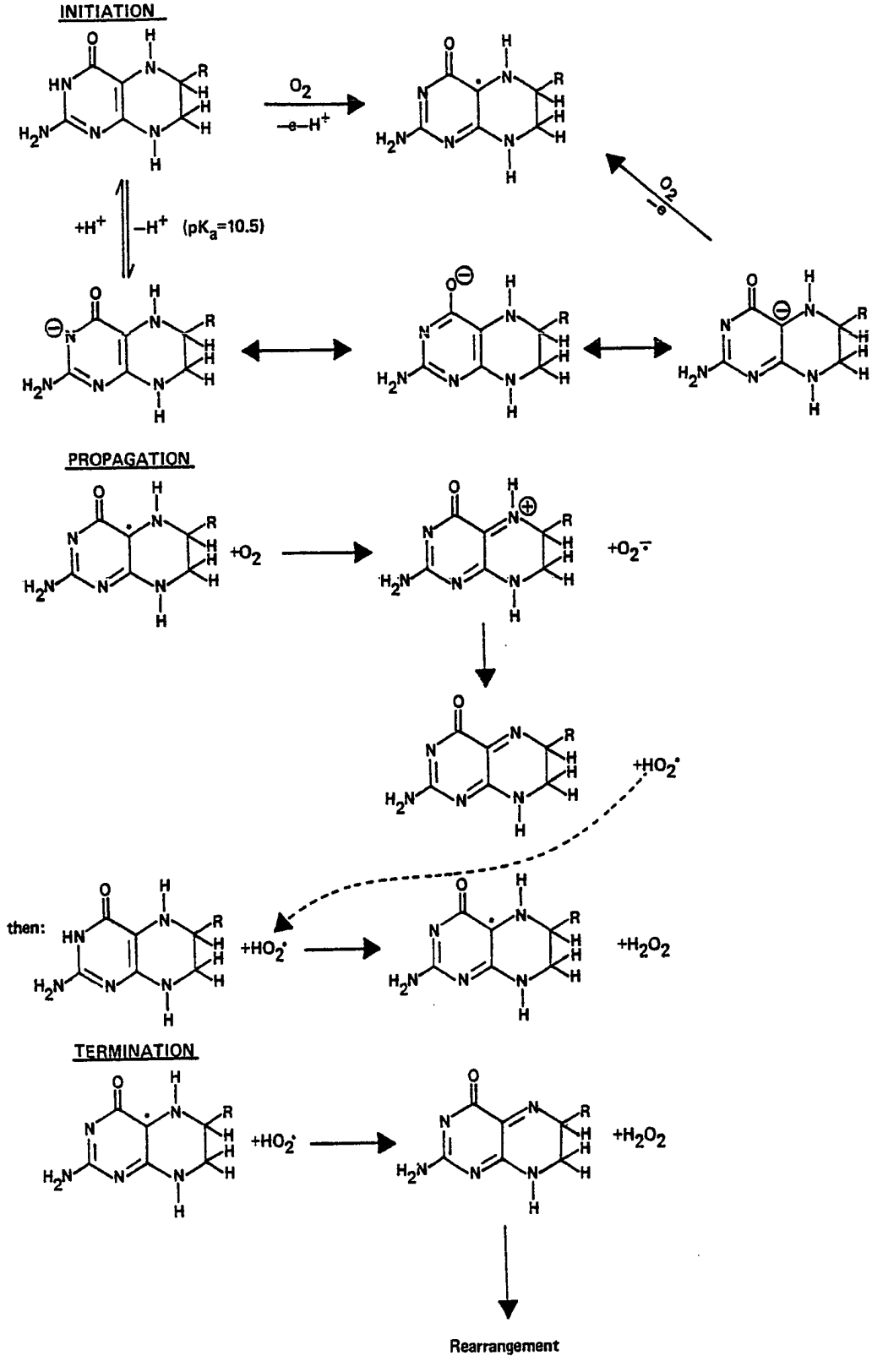


Figure 6. Proposed reaction mechanism for the intermediacy of radicals in the autoxidation of tetrahydrobiopterin and tetrahydrofolic acid.

tested on liver slices.[42]

There have been few reports of the electrochemical oxidation of tetrahydropterins. Archer and Scrimgeour[45] have reported the electrochemical oxidation of tetrahydropterin and its 6-methyl and 6,7-dimethyl derivatives at a dropping mercury electrode. Wave slope analysis of the DC polarographic wave was used to deduce that the oxidation proceeded by an ee mechanism. The first step is proposed to be a 1e oxidation and the second step is proposed to be a further 1e-$2H^+$ oxidation. However, wave slope analysis of a DC polarographic wave is subject to many complications and the results are therefore less than conclusive. Kretzschmar and Jaenicke[46,47] have likewise reported a 1e-$1H^+$ oxidation of tetrahydrofolic acid at pH 6.8. Wave slope analysis was also used to deduce this mechanism of electro-oxidation of tetrahydrofolic acid.

Pradac et al.[48] have also reported the electrooxidation of THF and 6,7-DMTHP at a platinum electrode. Kwee and Lund[25,49] have reported coulometric results for the electrooxidation of various methylated tetrahydro- and dihydropterins. They have also investigated the reduction of 6-methylpterin (6-MP) and 6-methyl-7,8-dihydropterin (6-MDHP) using cyclic voltammetry at the hanging mercury drop electrode. In the study of the reduction of folic acid it was found that 6-MDHP and 6-MTHP could be formed if the pH of the solution was low enough to protonate the folic acid.[50] Earlier Komenda[51] and Asahi[52] had also studied the reduction of 6-MP. They both reported the initial reduction product of 6-MP was an unstable 5,8-dihydropterin species

which rearranged to a more stable product, the 7,8-dihydropterin species. Several extensive reports are now appearing from this laboratory on the electrochemical behavior of various tetrahydropterins at the pyrolytic graphite electrode.[53-55]

One of these reports was concerned with the electrochemical behavior of tetrahydropterin (THP) and 7,8-dihydropterin (7,8-DHP)[54] and has opened up a completely unknown area, i.e., the reactions which can be undergone by the various 7,8-dihydro species formed upon rearrangement of the quinonoid-dihydropterins. THP is oxidized in an almost reversible process to a quinonoid of unknown structure which then rearranges to 7,8-dihydropterin. This compound appears to react with water to form a mixture of the non-hydrated and a N(5)-C(6) covalently hydrated species (Figure 7). The structure of covalently hydrated 7,8-dihydropterin is very similar to that of THP and it is therefore electrooxidized at very nearly the same potential. Another unstable quinonoid species is the product of this oxidation and it is thought to undergo rearrangement to another intermediate, a second more stable quinonoid. These quinonoids break down to give a mixture of pterin and 7,8-dihydroxanthopterin. 7,8-Dihydroxanthopterin is identified by its voltammetric oxidation peak and the oxidation peak of xanthopterin which is observed as the potential is swept farther positive (Figure 8).

Similar results are reported for the electrooxidation of 6,7-dimethyl-5,6,7,8-tetrahydropterin except that it is not possible to form 7,8-dihydroxanthopterin or xanthopterin because of the blocking methyl group at the C(6)-position.

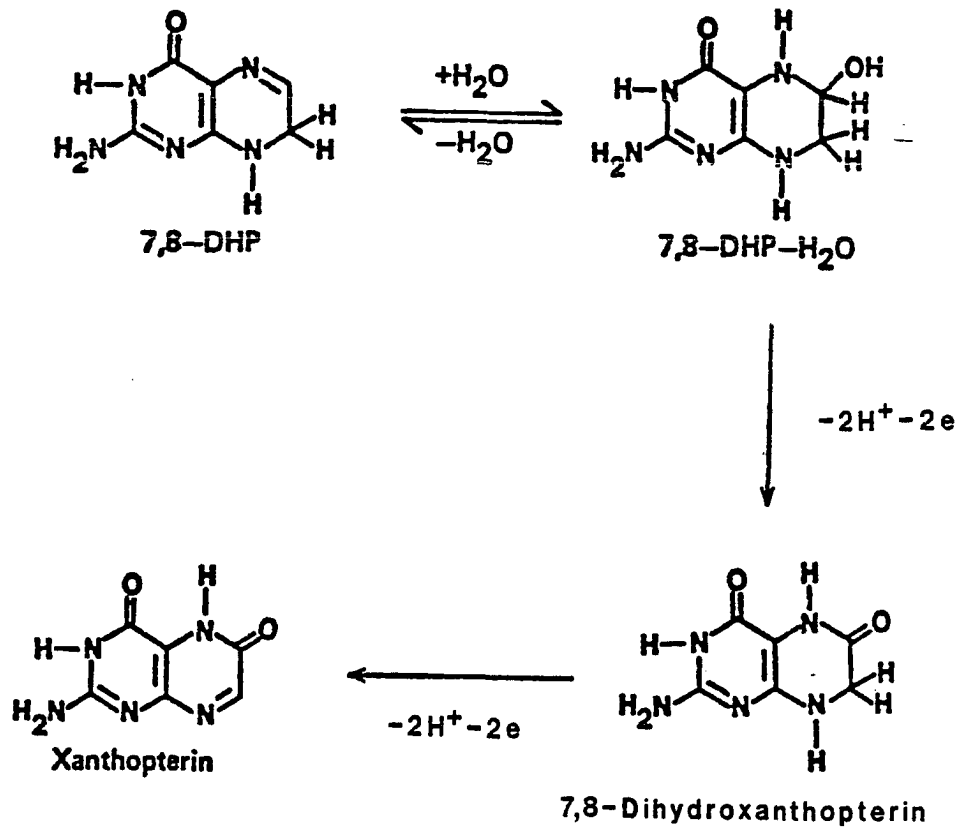


Figure 7. Simplified reaction scheme to explain the formation of 7,8-dihydroxanthopterin and xanthopterin from 7,8-dihydropterin.

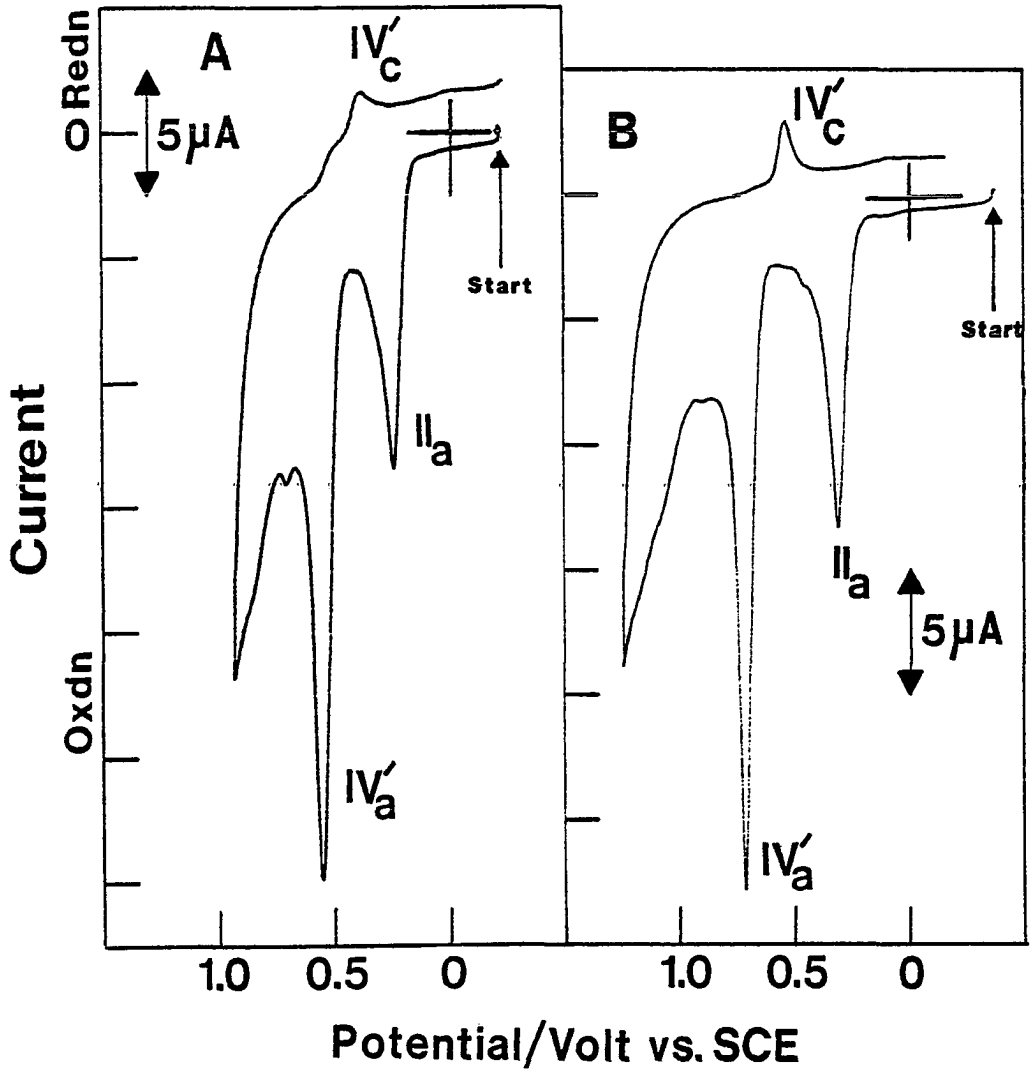
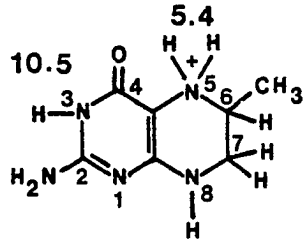


Figure 8. (A) Cyclic voltammogram of 0.5 mM 7,8-dihydroxanthopterin at the PGE in pH 6.0 phosphate buffer. Sweep rate: 200 mV s^{-1}. (B) Cyclic voltammogram of electrolysis product of 7,8-DHP in pH 6.0 phosphate buffer. Sweep rate: 200 mV s^{-1}. (Reference 7).

Past work from this laboratory has demonstrated that electrochemical studies of biologically important molecules can provide powerful insights into the biological redox reactions of such molecules. Investigations were thus continued to more clearly understand the redox properties of tetrahydropterins. This work is concerned with elucidating the redox properties of 6-MTHP which is the pseudo cofactor that has the highest activity when compared to tetrahydrobiopterin.

Physical Properties of 6-MTHP and 6-MDHP

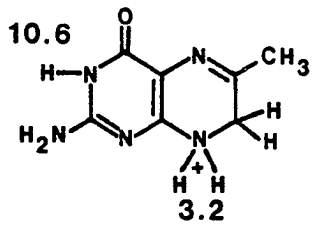
6-MTHP (IV) can exist in monocationic, neutral, or anionic forms in aqueous solution. The reported pK_a values are shown below.[56]



IV

The numbering system for pteridines which is in use currently is also shown on structure (IV). Literature values of the u.v. spectral data for 6-MTHP are given in Table 1.[56]

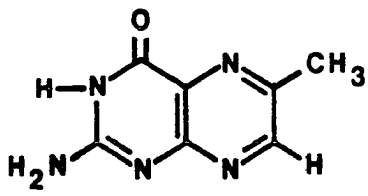
6-MDHP (V) also exists in monocationic, neutral, or anionic forms in aqueous solutions. The pK_a values reported in the literature are shown on structure (V).[56,57] There is some question about the value of the basic pK_a because of the method used for its determination. Pfleiderer and Zondler have determined the basic pK_a to be 4.17 and they do not specify which group it applies to.[57] Later Whitley and



V

Hennekens reported the basic pK_a as 3.2 (determined spectrophotometrically) and suggested that the earlier value was erroneous because it was done titrimetrically.[56] They tried to duplicate the experiment titrimetrically but always had problems with precipitation of 6-MP from the solution changing the apparent pK_a. This pK_a was tentatively assigned to the N(8)-position. Spectral data for 6-MDHP are reported in Table 2.

6-MP (VI) has pK_a values of 2,8 and 8.3 reported in the literature.[56] No assignments were made however. The values reported



VI

by Komenda[51] are in close agreement with the values above. Spectral data for 6-MP are listed in Table 3.[58,59] It is also reported that 6-MP exhibits fluorescence at 450 nm when excited by radiation at 355 nm.[60]

Table 1

U.V. Spectral Data for 6-MTHP

pH	Electrolyte	Charge on 6-MTHP	λ_{max} /nm	ε_{max} / ℓ mole^{-1} cm^{-1}
1.0	0.1 N HCl	+	265	16.0 x 10^3
7.0	0.1 M PO_4^{3-}	0	303	9.5 x 10^3
13.0	0.1 N NaOH	-	297	7.5 x 10^3

Table 2

U.V. Spectral Data for 6-MDHP[57]

pH	Electrolyte	Charge on 6-MDHP	λ_{max} /nm	ε_{max} / ℓ mole^{-1} cm^{-1}
1.0	1 N HCl	+	252	20.0 x 10^3 (Ref. 56)
1.0	--[b]	+	252	18.6 x 10^3
			(271)[a]	7.6 x 10^3
			361	5.1 x 10^3
7.0	--[b]	0	229	25.7 x 10^3
			279	10.5 x 10^3
			324	5.6 x 10^3
14.0	--[b]	-	231	14.8 x 10^3
			282	7.9 x 10^3
			322	5.8 x 10^3

[a]Parentheses indicate that an inflection rather than a peak was observed.

[b]The solution components used to maintain the pH were not reported.

Table 3

U.V. Spectral Data for 6-MP

pH	Electrolyte	Charge on 6-MP	λ_{max} /nm [a]	ε_{max} / ℓ mole^{-1} cm^{-1} [a]
1.0	0.1 N HCl	+	248 324	10.3×10^3 8.2×10^3
13.0	0.1 N NaOH	-	253 365	22.8×10^3 7.5×10^3

[a] λ_{max} and ε are estimated from published spectra.

CHAPTER II

RESULTS

It was noted that both 6-MTHP and 6-MDHP were quite stable in a continuously deaerated solution, although the susceptibility to air oxidation does increase considerably for 6-MTHP as the pH increases.

Linear and Cyclic Sweep Voltammetry

pH study. Between pH 2.0 and 11.0 6-MTHP exhibits up to four voltammetric oxidation peaks at a pyrolytic graphite electrode (PGE) (Figure 9A). Peak IV_a is very close to the background discharge and is thought to be caused by the electrooxidation of any 6-MP which is formed in the peak II_a and III_a processes and will not be considered further here. However, for the sake of completeness it must be reported that once the positive sweep in cyclic voltammetry passes through peak IVa, two additional reduction peaks are observed, peak V_c and VI_c in Figure 10. The following equations as well as Figure 11 illustrate the pH dependence of the peak potential, E_p, for the first three oxidation peaks of 6-MTHP at a sweep rate of 5 mV s^{-1}:

Peak I_a (pH 2-11): $E_p = [0.32-0.056\ pH]V$*

*The equation for the variation of the polarographic half-wave potential, $E_{1/2}$, with pH for the first oxidation process was reported by Asahi[52] to be $E_{1/2} = [0.27-0.060\ pH]V$.

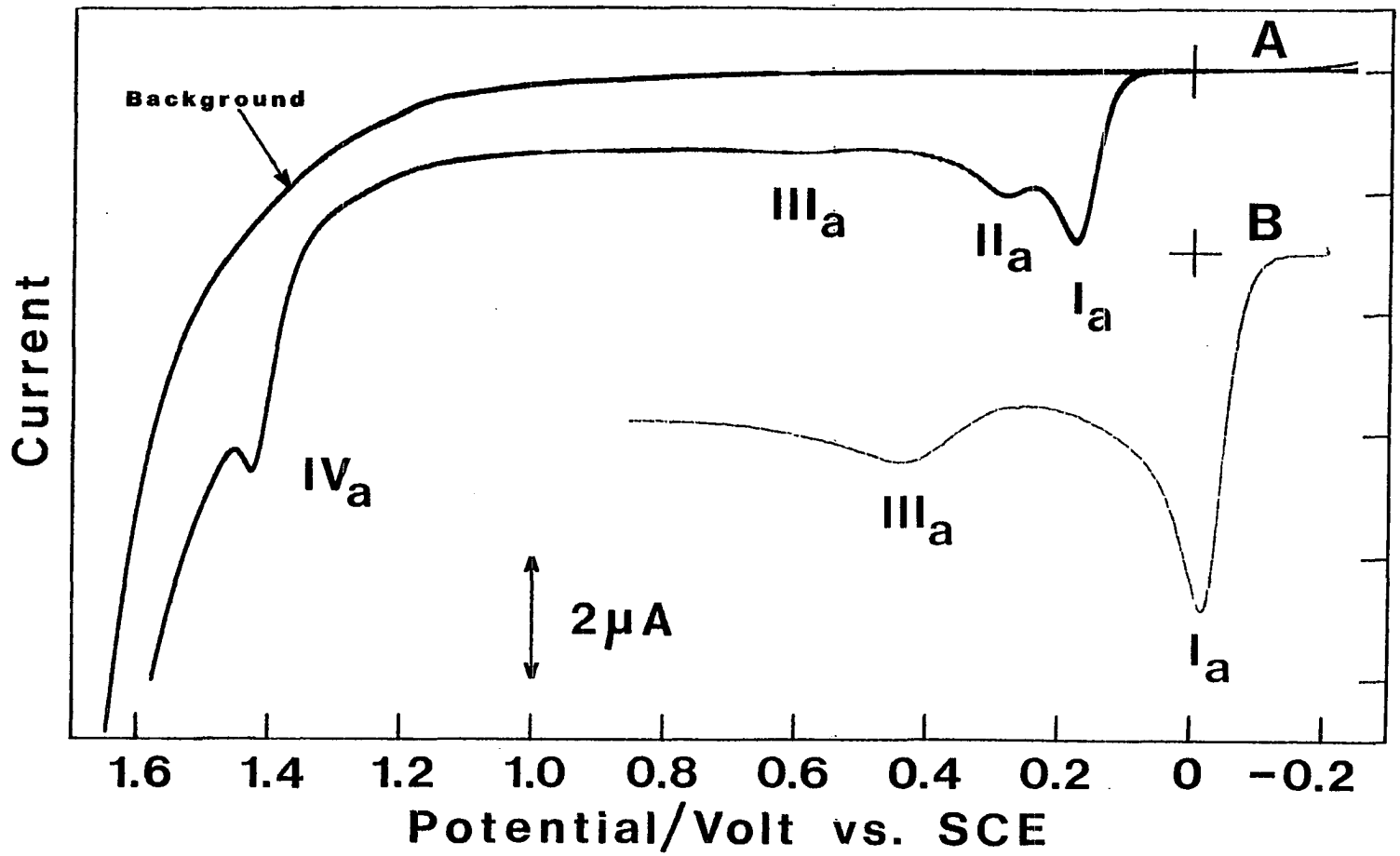


Figure 9. Linear sweep voltammograms of 1.0 mM 6-MTHP at a PGE in phosphate buffer, μ=0.5 M at a sweep rate of 5 mV s-1. (A) pH 3.0 and (B) pH 5.6.

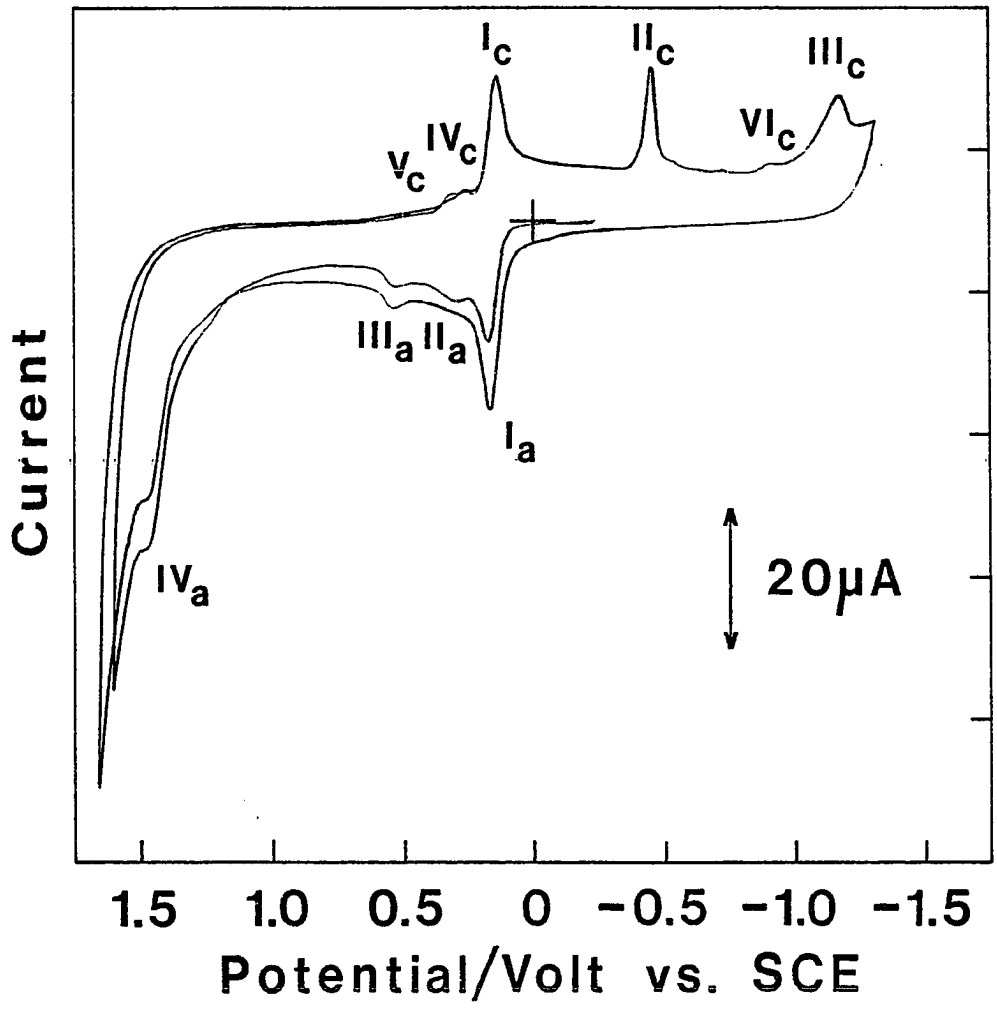


Figure 10. Cyclic voltammogram of 1.0 mM 6-MTHP in pH 3.0 phosphate buffer showing peaks V_c and VI_c. Sweep rate: 200 mV s^{-1}.

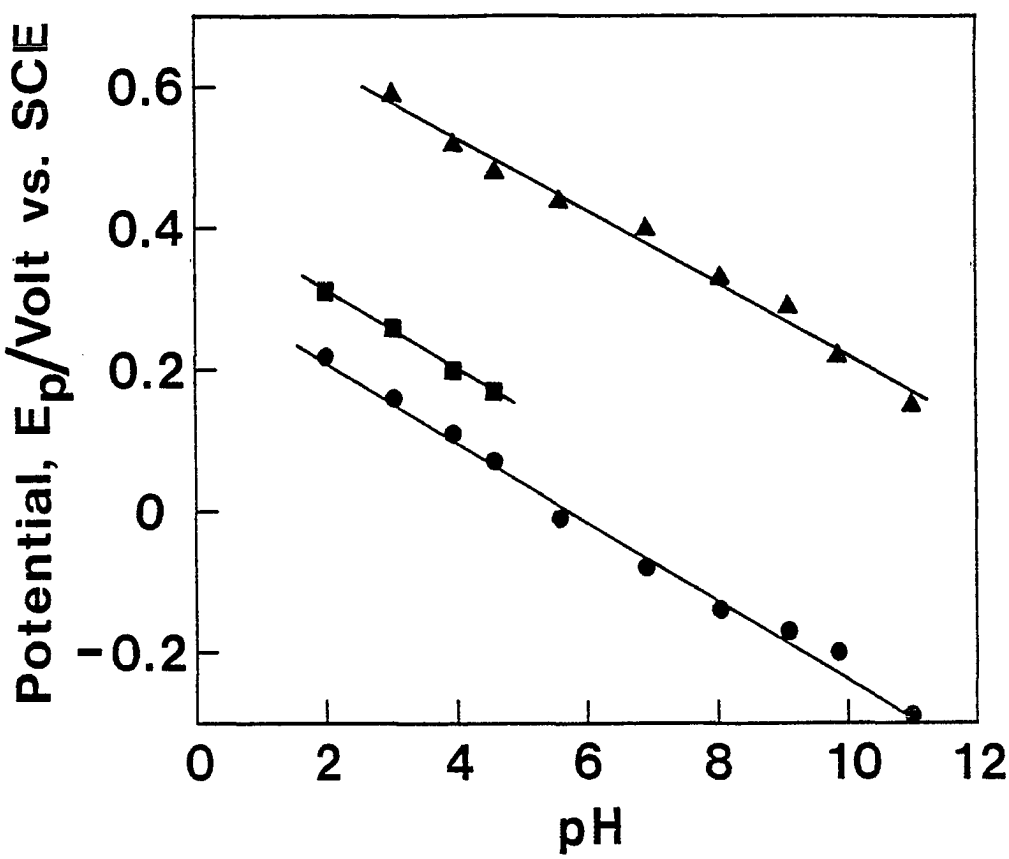


Figure 11. Variation of E_p vs. pH for the voltammetric oxidation peaks of 1.0 mM 6-MTHP observed at the PGE at a sweep rate of 5 mV s^{-1}. Peak I_a (●), Peak II_a (■), and Peak III_a (▲).

Peak II_a (pH 2-4.6): E_p = [0.42-0.055 pH]V

Peak III_a (pH 3-11): E_p = [0.73-0.051 pH]V

There are no apparent breaks in the E_p *vs.* pH plots at the PGE indicating that the oxidation process does not change drastically in the pH range investigated.

For a reversible redox reaction the slope of the E_p *vs.* pH plot is -0.059 p/n V at 25°,[61] where p is the number of protons and n is the number of electrons involved in the electrode process. If the redox reaction is irreversible the equation becomes more complex and the slope is defined by Equation (1).[61]

$$\frac{dEp}{d(pH)} = \frac{-0.059\ p}{\alpha n_a} \qquad (1)$$

Here α is the electron transfer coefficient and n_a is the number of electrons involved in the rate limiting reaction at the electrode. Thus in a reversible or quasi-reversible reaction if the slope of the E_p *vs.* pH plot is *ca.* 59 mV this indicates that the number of electrons and protons involved in the electrode process is equal.

It is clear that three voltammetric peaks are observed below pH 4.6 with peak II_a falling very close to peak I_a. Since peak II_a is so close to peak I_a it is difficult to measure the peak current, i_p. However, it is quite clear that peak II_a decreases in size relative to peak I_a and peak III_a as the pH increases. Actually peak III_a also increases in size relative to peak I_a and II_a with increasing pH. This behavior can be seen in Figures 9A and B.

At a sweep rate of 5 mV s^{-1} 6-MDHP exhibits a maximum of

three voltammetric peaks at the PGE whose peak potentials correspond very closely with peaks II_a, III_a, and IV_a of 6-MTHP (Figure 12A). The pH dependence of the peak potentials for peaks II_a and III_a is illustrated in Figure 13 and described by the equations:

$$\text{Peak } II_a \text{ (pH 2-5.6)} = [0.40\text{-}0.045\ pH]V$$
$$\text{Peak } III_a \text{ (pH 2-11)} = [0.74\text{-}0.049\ pH]V$$

Similar to the results for 6-MTHP it can be seen that with increasing pH peak II_a becomes increasingly smaller in size while peak III_a grows progressively larger (Figure 12).

Reversibility of peaks I_a and II_a. A typical cyclic voltammogram is presented in Figure 14. On the initial sweep towards positive potentials voltammetric oxidation peaks I_a, II_a, and III_a may be observed. When the potential sweep is reversed four voltammetric reduction peaks are formed. Peak I_c appears to form a quasi-reversible couple with oxidation peak I_a (ΔE_p = 37±7 mV between pH 2.0 and 5.7 at 200 mV s^{-1}). Reduction peak IV_c also forms a quasi-reversible couple with oxidation peak II_a at low pH (ΔE_p = 31±4 mV at pH 2-3 at 200 mV s^{-1}).

The criteria which is used to determine reversibility of an electrode reaction includes the separation of the peaks in the redox couple. A completely reversible system has a peak separation of 59/n mV provided adsorption is not involved in the electrode process.[62] At least at low pH the above redox systems fit this criterion. However

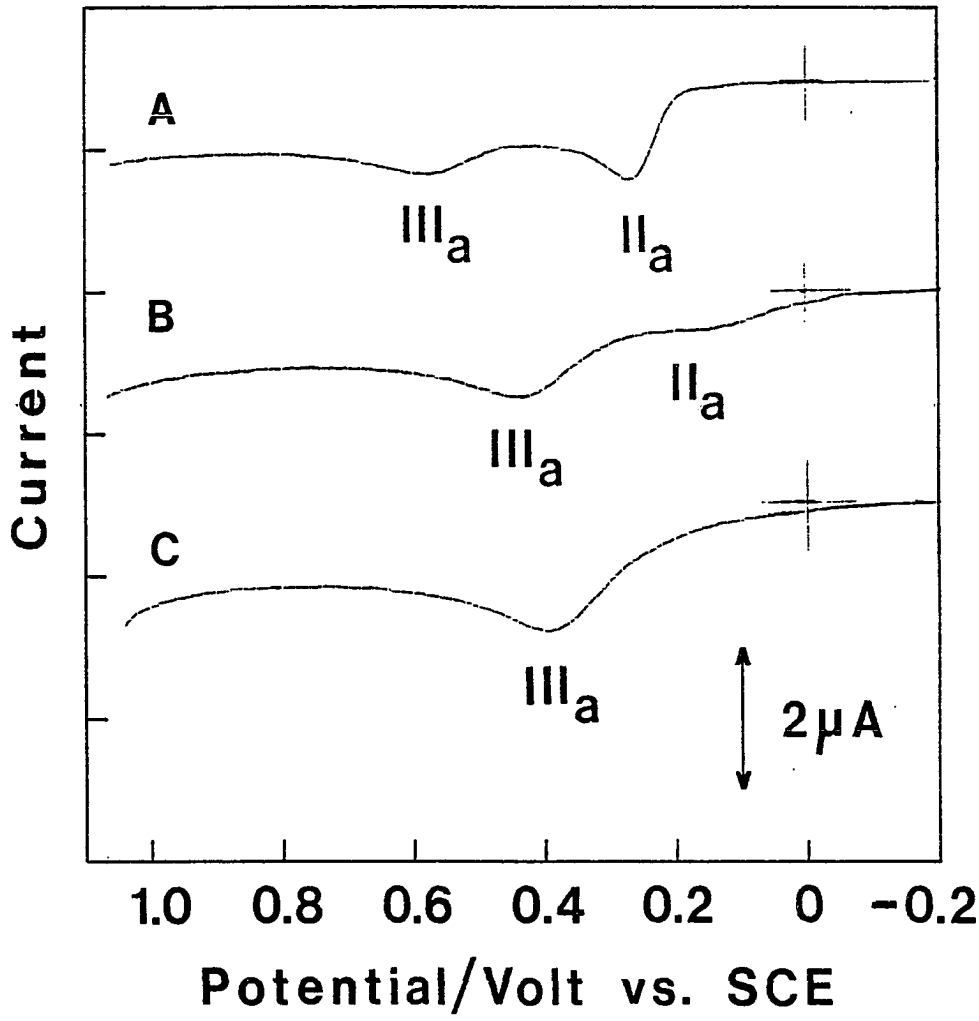


Figure 12. Linear sweep voltammograms of 0.5 mM 6-MDHP in phosphate buffers at a sweep rate of 5 mV s^{-1}. (A) pH 3.1, (B) pH 5.6, and (C) pH 6.9.

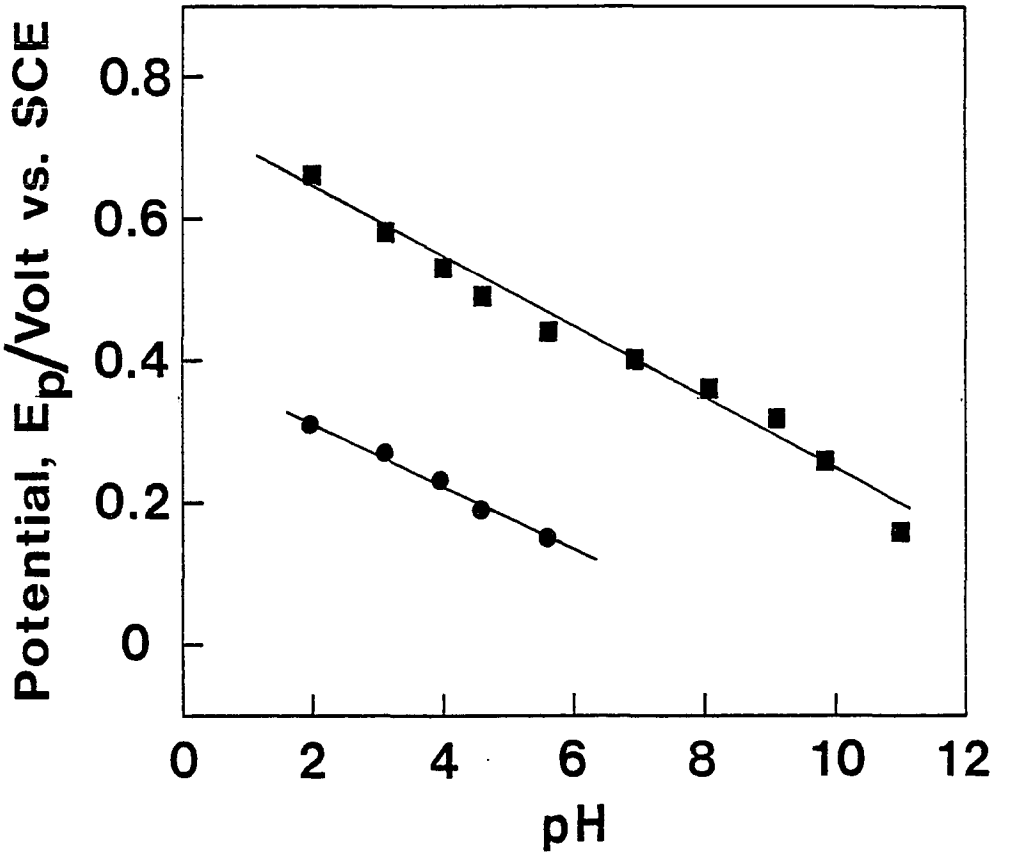


Figure 13. Variation of E_p vs. pH for the voltammetric oxidation peaks of 0.5 mM 6-MDHP observed at the PGE at a sweep rate of 5 mV s^{-1}. Peak II_a (●) and Peak III_a (■).

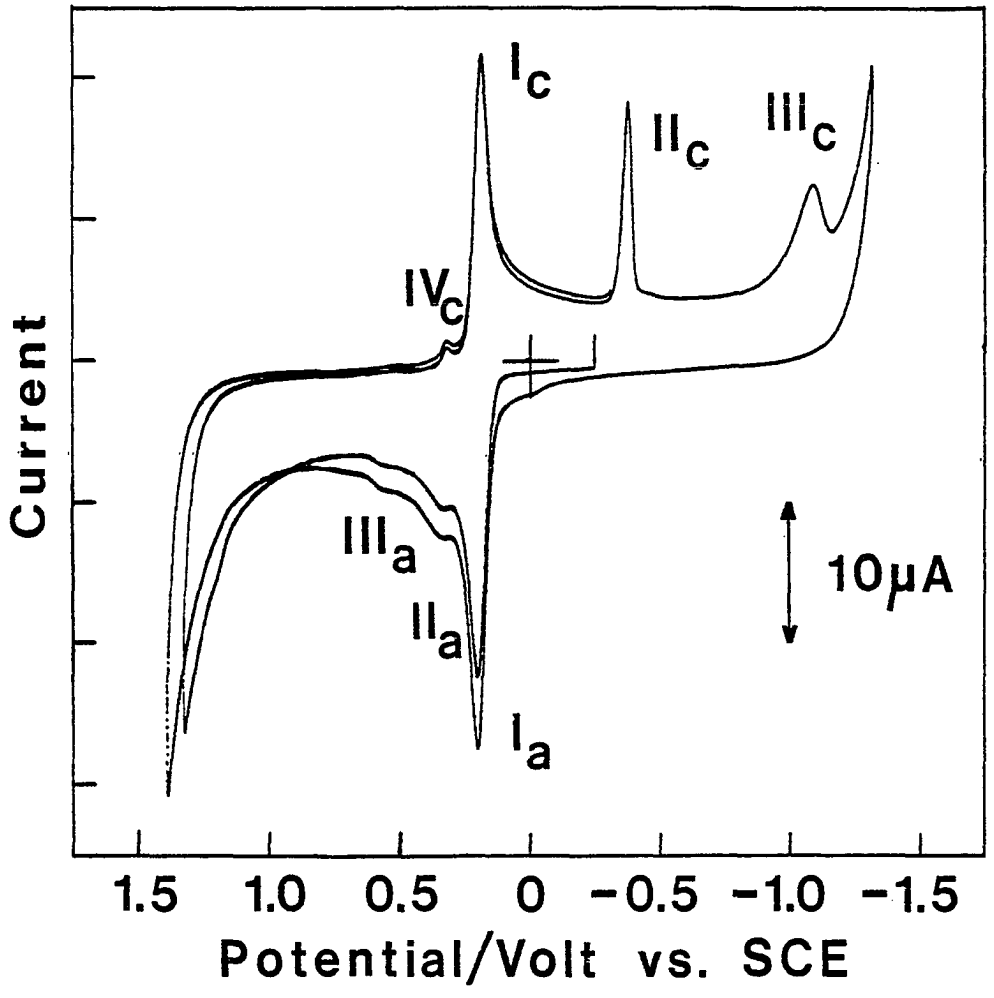


Figure 14. Cyclic voltammogram at the PGE of 1.0 mM 6-MTHP in pH 2.0 phosphate buffer. Sweep rate: 200 mV s^{-1}.

at higher pH the peak separation increases considerably from that expected for ideal reversible behavior.

Another criterion for complete chemical reversibility is that the reverse peak is the same size as the initial peak, i.e., no chemical follow-up reaction lowers the concentration of the reducible species at the electrode. Neither the peak I_a/I_c couple or the II_a/IV_c couple meet this criterion. At pH 5-6 the ratio of the peak currents for peak I_c to peak I_a is at a minimum indicating that the initial peak I_a product disappears in a chemical follow-up reaction most rapidly at this pH. Only at pH values above 7 or below 4 does the height of peak I_c approach that of peak I_a at relatively high sweep rates (0.5-1.0 V s^{-1}).

The peak II_a/IV_c couple may be observed more clearly in cyclic voltammetry of 6-MDHP (Figure 15). Its behavior appears to be somewhat different from that of the peak I_a/I_c couple. Reduction peak IV_c consists of a sharp, well defined peak followed by a broad peak at very nearly the same potential as peak I_c (Figure 15). At a sweep rate of 200 mV s^{-1} at pH 3.0 the area under both the sharp and the broad peak of IV_c is not nearly as large as the area under peak II_a (Figure 15A). However, as the sweep rate is increased to 1 V s^{-1} the combined area under both reduction peaks is approximately equal to the area under peak II_a (Figure 17B). This is not entirely the result of peak IV_c becoming larger, but rather a result of peak II_a decreasing in size. Thus it appears that electrooxidation at peak II_a also yields an unstable intermediate which can undergo chemical rearrangement.

A qualitative idea of the stability of an intermediate species

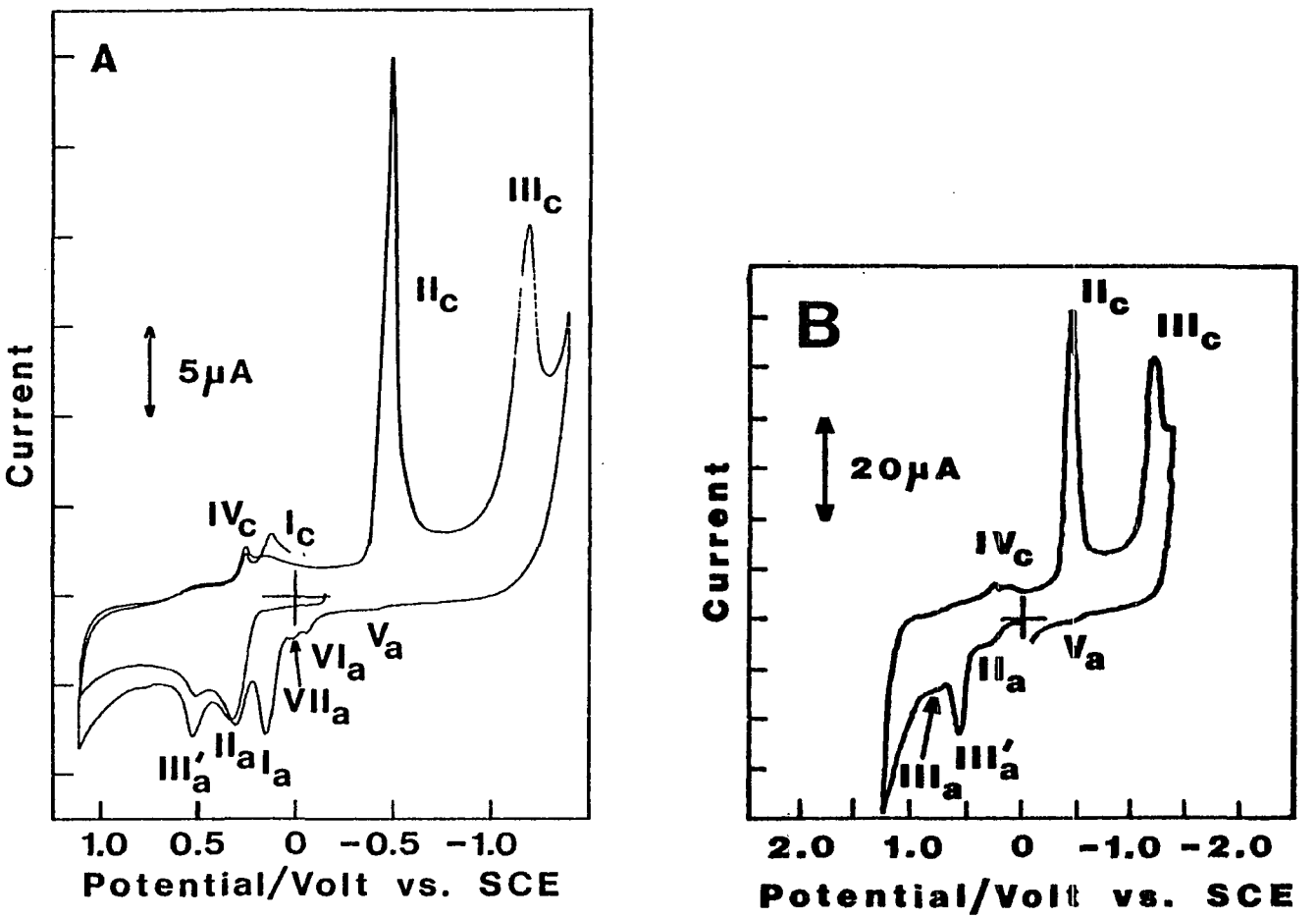


Figure 15. Cyclic voltammograms of 0.5 mM 6-MDHP at the PGE in pH 3.0 phosphate buffer. (A) 200 mV s^{-1} and (B) 1 V s^{-1}.

can be obtained from cyclic voltammetric data by changing the sweep rate. Since cyclic voltammetry is performed in a quiet, unstirred solution the product of the oxidation process should remain in the vicinity of the electrode. However, if the initial oxidation product rearranges chemically to a species which is nonreducible or reducible at a different potential the reverse peak of the couple will be smaller at slow sweep rates because more time has elapsed for the chemical process to occur. At high sweep rates less time will elapse between the positive and negative sweeps and more of the initial oxidation product will be available for reduction in the reverse process yielding a larger peak. Thus it can be deduced that the species responsible for reduction peak IV_c is not very stable.

Concentration study of 6-MTHP. A study of the peak current at the PGE vs. concentration for the oxidation peaks of 6-MTHP was done at both pH 3 and pH 7 at a sweep rate of 5 mV s^{-1}. pH 3 was chosen because oxidation peaks I_a, II_a, and III_a are all visible at this pH. At pH 7 peak II_a was no longer observed, therefore a concentration study was also done at this pH to compare the behavior with that at pH 3. This type of investigation can give insight into the type of process controlling the rate of the electrode reaction. If the electrode process is diffusion controlled the peak current is directly proportional to the bulk concentration of the electroactive species in the solution. However, if the electroactive compound is adsorbed on the electrode surface the peak current will increase in a linear fashion only at low concentration. As the concentration

of the electroactive material increases the surface coverage of the electrode will increase. When the surface of the electrode is completely covered the peak current will not increase any more because no more material can reach the electrode surface to be oxidized.

In pH 3.0 phosphate buffer peak II_a of 6-MTHP was actually larger than peak I_a at concentrations below 0.5 mM (Figure 16A). Above 0.5 mM peak I_a was the largest peak (Figure 9A) and finally completely obscured peak II_a above ca. 5 mM (Figure 16B). We believe this is a result of weak adsorption at the PGE of the species giving rise to peak II_a. Weak adsorption causes an enhancement of the peak current compared to the diffusion controlled case, particularly at low concentrations where adsorption current makes a larger contribution to the total peak current.[63] This is further substantiated by comparing the peak current vs. concentration dependence of peak II_a with peak III_a (Figure 17). At low concentrations (<ca. 1 mM) the peak current for peak II_a is ca. twice the peak current for peak III_a. However, at 5 mM 6-MTHP the peak current for peak II_a is ca. 9 μA while the peak current for peak III_a has increased to ca. 7 μA. Since the peak current vs. concentration relationship for peak III_a is perfectly linear then the peak current vs. concentration behavior for peak II_a must deviate somewhat from linearity because of adsorption.[63] The peak current vs. concentration dependence for peak III_a is perfectly linear indicating diffusion control of this electrode process.

Figure 18 illustrates the peak current vs. concentration behavior for peak I_a of 6-MTHP. It is linear to at least 10 mM indicating that 6-MTHP apparently is not adsorbed at the PGE. A

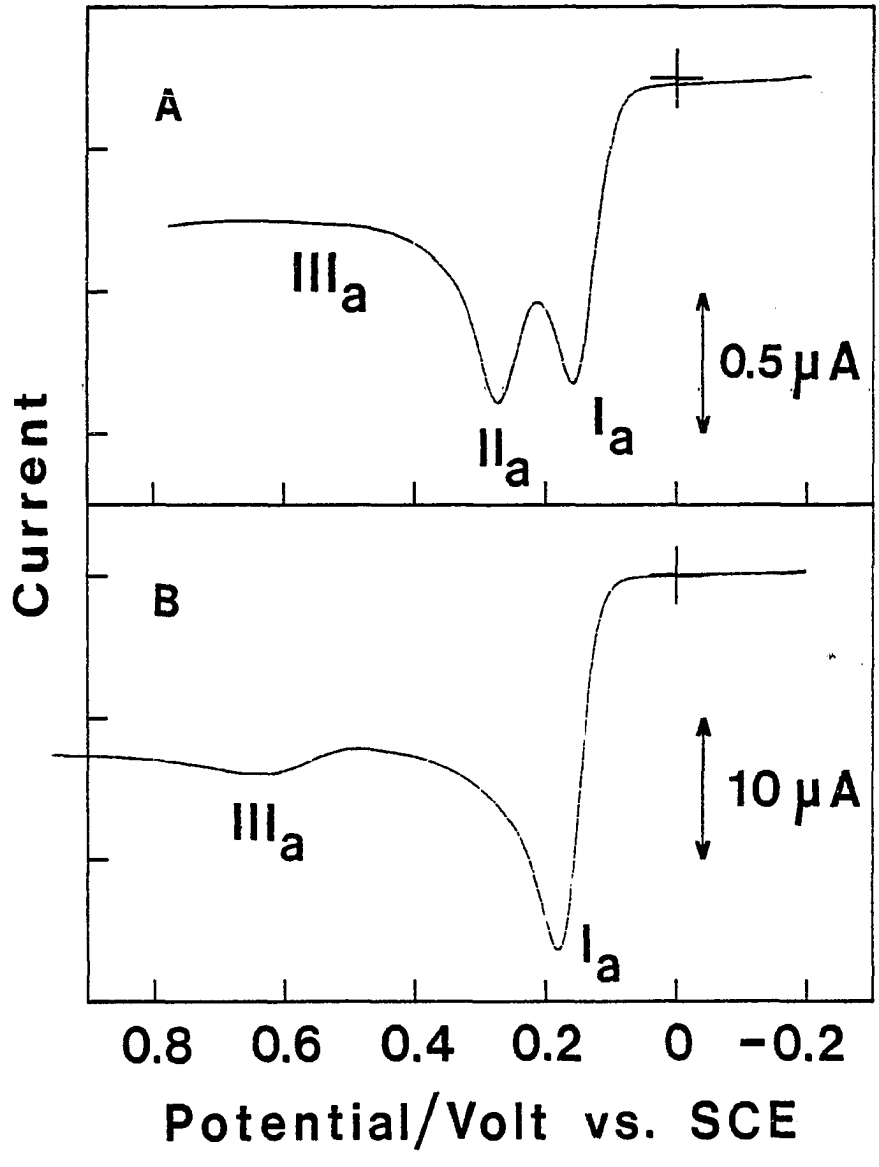


Figure 16. Linear sweep voltammograms of 6-MTHP at the PGE in pH 3.0 phosphate buffer at a 6-MTHP concentration of (A) 0.35 mM and (B) 9.7 mM.

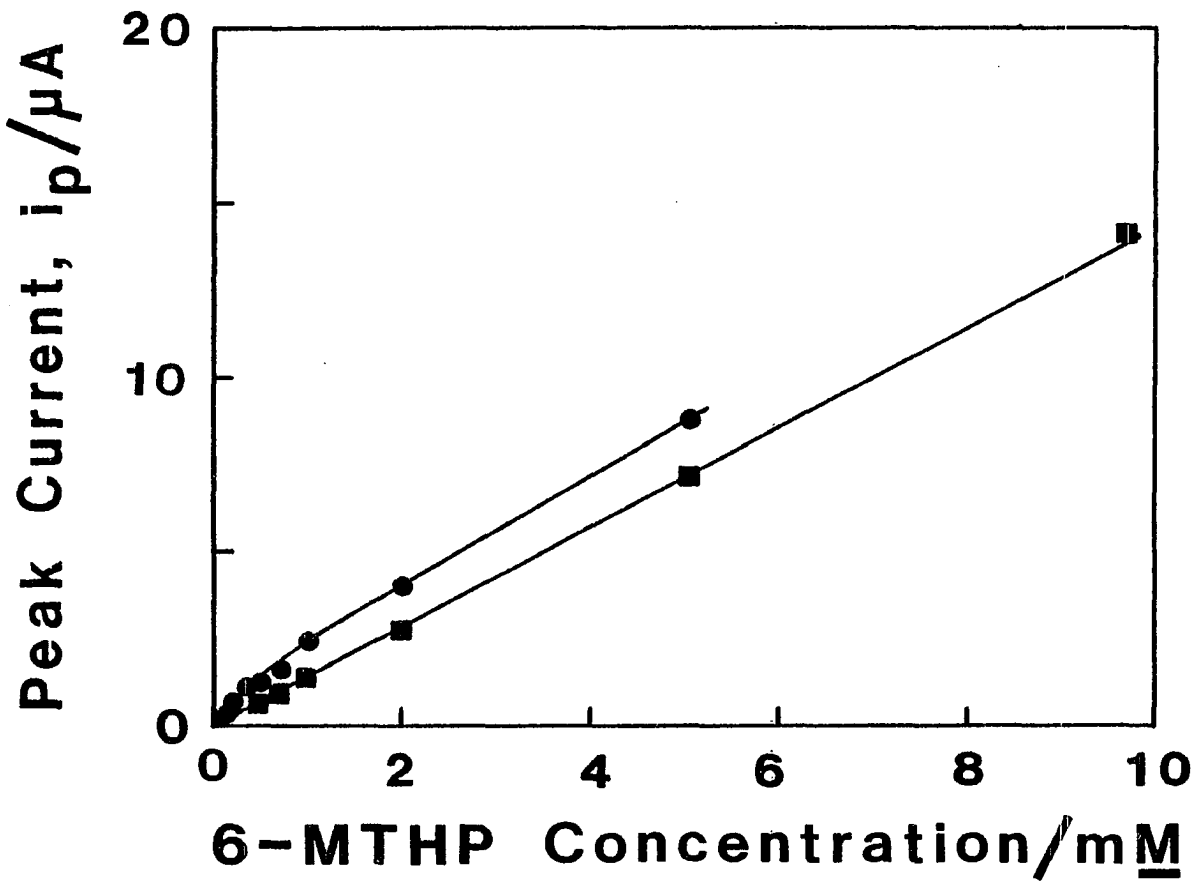


Figure 17. Peak current, i_p, vs. concentration curves for the oxidation peaks of 6-MTHP in pH 3.0 phosphate buffer. Sweep rate: 5 mV s^{-1}. Peak II_a (●) and Peak III_a (■).

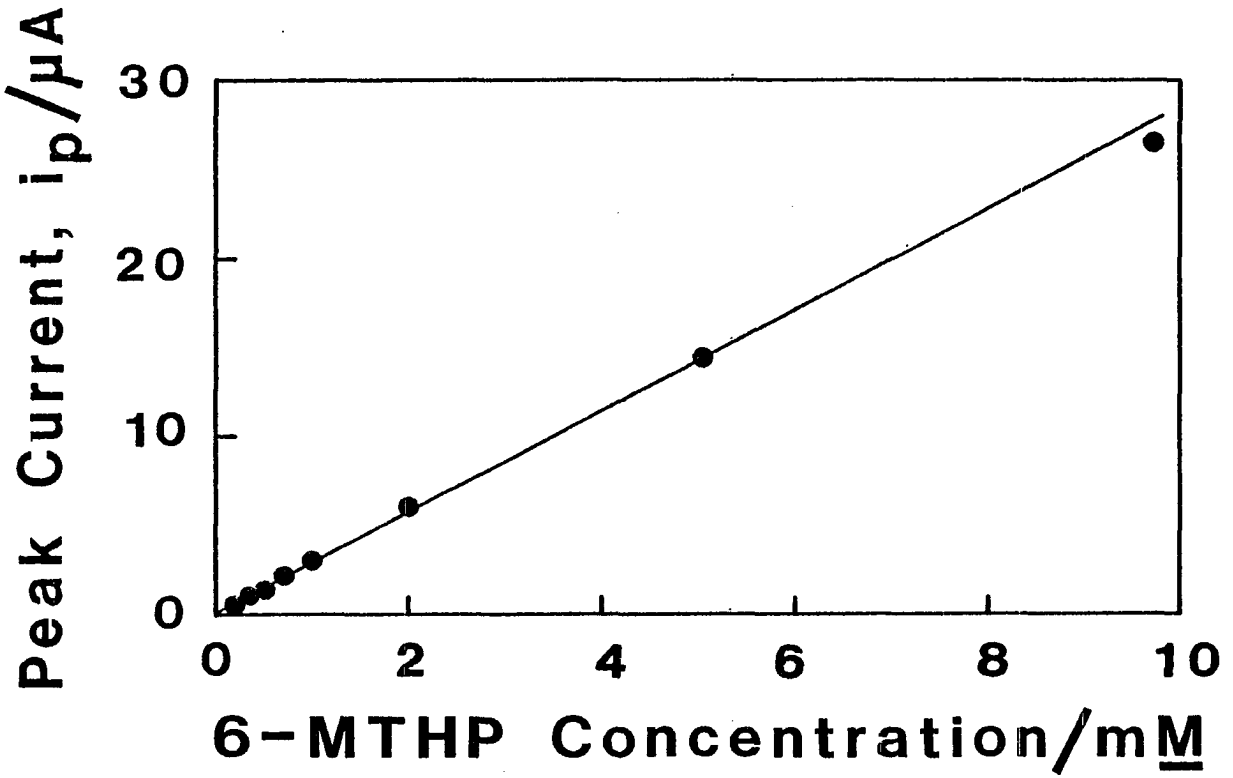


Figure 18. Peak current, i_p, vs. concentration curve for peak I_a of 6-MTHP in pH 3.0 phosphate buffer. Sweep rate: 5 mV s^{-1}.

study of the peak current vs. concentration relationship of the voltammetric oxidation peaks of 6-MTHP at pH 7 indicated that the adsorption characteristics were identical to that observed at pH 3. Peak I_a and III_a exhibited completely linear peak current vs. concentration curves to 10 mM. However, peak II_a is not observed at any concentration of 6-MTHP at pH 7.

Concentration study of 6-MDHP. The peak current vs. concentration relationship for the oxidation peaks of 6-MDHP was also investigated using a sweep rate of 5 mV s^{-1}. At pH 3 the i_p vs. concentration relationship for peak II_a rapidly approaches a limiting value at about 0.5 mM (Figure 19). It is obvious that the species responsible for the first oxidation peak of 6-MDHP is quite strongly adsorbed at a PGE. Once again the peak current for peak III_a is completely linear with increasing 6-MDHP concentration to the highest concentration investigated, 0.75 mM. The limit of solubility for 6-MDHP was found to be ca. 1.8 mM (see discussion on p.106). The 6-MDHP stock solution was made up on distilled water and diluted 1:1 with phosphate buffer, μ = 1.0 M, in the voltammetric cell. Therefore to obtain a final 6-MDHP concentration of 0.75 mM the stock solution must have a 6-MDHP concentration of 1.5 mM which is safely within the solubility limit of 6-MDHP. The linear peak current vs. concentration behavior of peak III_a supports the view that the species responsible for peak III_a is not adsorbed at a PGE. The behavior at pH 7 is completely analogous to that observed at pH 3.

Sweep rate study of 6-MTHP. Varying the sweep rate in a

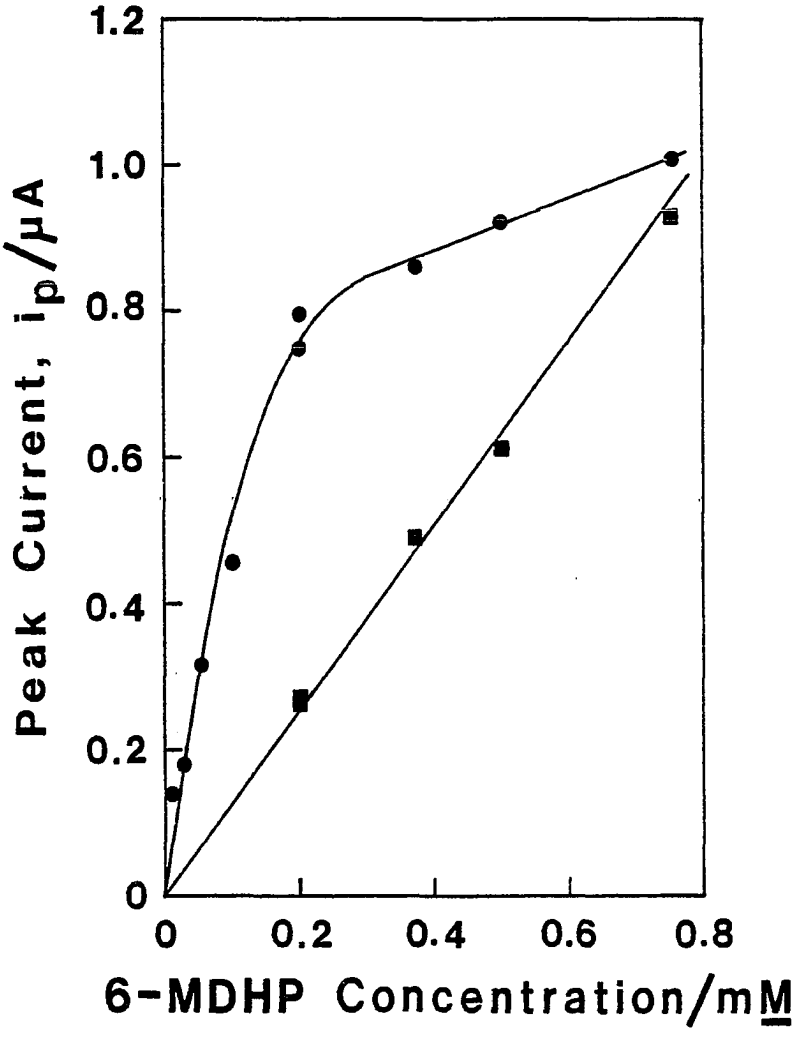


Figure 19. Peak current, i_p, vs. concentration curves for the voltammetric oxidation peaks of 6-MDHP observed at the PGE in pH 3.0 phosphate buffer. Sweep rate: 5 mV s^{-1}. Peak II_a (●) and Peak III_a (■).

cyclic voltammetric experiment can be used to obtain another piece of data for determining whether an electrooxidation process is diffusion or adsorption controlled. Once again as in a concentration study the measured experimental parameter is the peak current. From this one can calculate the peak current function, $i_p/C_o v^{1/2}$,* where i_p is the peak current in μA, C_o is the bulk solution concentration of electroactive species in mmoles/ℓ and v is the sweep rate in V s^{-1}. A peak current function which increases with increasing sweep rate is indicative of strong adsorption of the reactant.[63] If the process is under diffusion control the peak current function should remain constant as the sweep rate is varied.

In Figure 20 is illustrated the dependence of the peak current functions for the various oxidation peaks of 6-MTHP on the square root of the sweep rate. At pH 3.0 the peak current function for peak I_a is observed to increase rapidly to about 5 V s^{-1} where it remains constant. The peak current function for peak II_a decreases rapidly until peak II_a disappears above 100 mV s^{-1}. The peak current function for peak III_a increases slowly throughout the sweep rate range, but the relative change is small compared to the change in the peak current function for peak I_a with increasing sweep rate. If the initial 6-MTHP solution does not have any 6-MDHP in it, peak III_a also disappears at a sweep rate of 10 V s^{-1}. The disappearance of both peaks II_a and III_a indicates they are the result of species formed from the initial peak

---

*This is an abbreviated peak current function. The actual function is $i_p/C_o A v^{1/2}$. However A, which is the area of the electrode, must remain constant throughout the experiments.

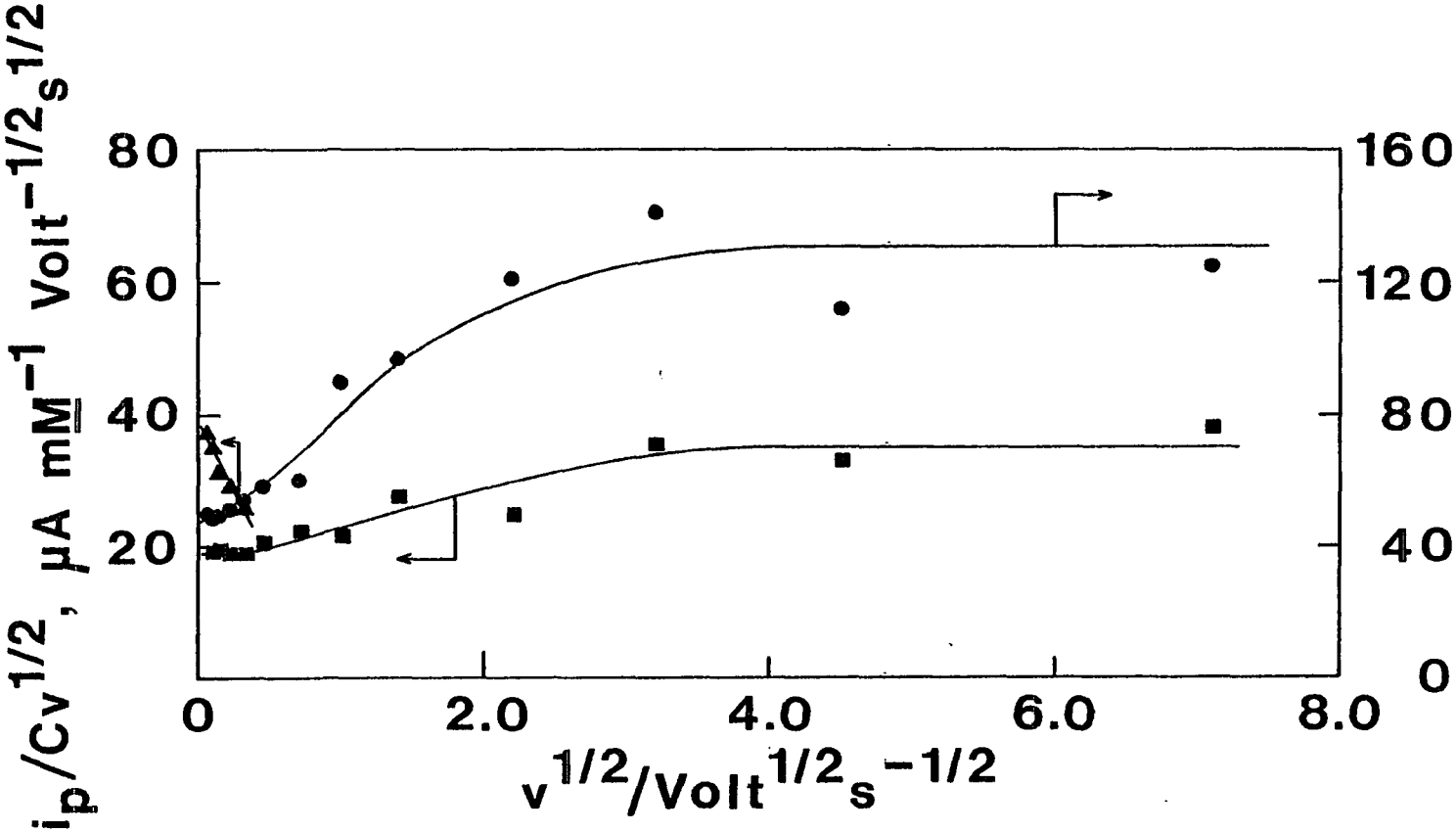


Figure 20. Peak current function vs. the square root of the sweep rate for the voltammetric oxidation peaks of 1.0 mM 6-MTHP in pH 3.0 phosphate buffer. Peak I_a (●), Peak II_a (▲), and Peak III_a (■).

I_a electrooxidation product. The fact that peak III_a appears at all sweep rates in Figure 20 is a result of the difficulty in preparing 6-MTHP solutions which do not have some small amount of 6-MDHP in them from air oxidation prior to performing the voltammetric experiment.

From these data it appears that in spite of the concentration study for 6-MTHP at pH 3 (vide supra), which indicates diffusion control, peak I_a does have a significant adsorption component. Peak II_a decreases rapidly in size with increasing sweep rate which is indicated by the decreasing peak current function. Nothing can really be stated about the adsorption of the species responsible for peak II_a from the data for 6-MTHP. However, much more information was obtained about peak II_a from the sweep rate study of 6-MDHP (vide infra). The relatively constant value of the peak current function for peak III_a indicates only a small amount of adsorption.

Sweep rate study of 6-MDHP. Very little information is gained about peak II_a in the sweep rate study of 6-MTHP, but much more information is obtained when the voltammetry of 6-MDHP is examined over a range of sweep rates. A sweep rate study was performed at pH 3.0 to compare with the sweep rate study of 6-MTHP. At sweep rates below 50 mV s^{-1} only peaks II_a and III_a are observed (Figure 21A). Between 50 and 100 mV s^{-1} another oxidation peak, peak III_a', begins to grow in at a potential between peaks II_a and III_a. With increasing sweep rate peak III_a' continues to grow and peak III_a essentially disappears (Figure 15B). The peak current function for peak III_a' increases very rapidly with sweep rate while that for peak II_a decreases

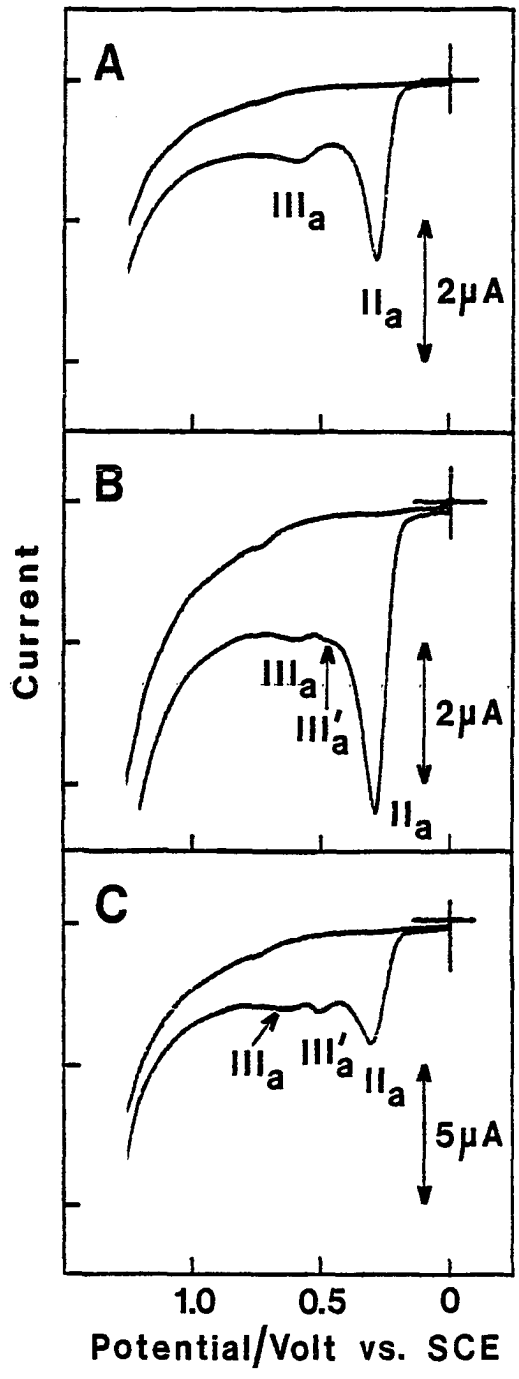


Figure 21. Linear sweep voltammograms of 0.5 mM 6-MDHP at the PGE in pH 3.0 phosphate buffer at a sweep rate of (A) 20 mV s^{-1}, (B) 50 mV s^{-1}, and (C) 100 mV s^{-1}.

(Figure 22). This behavior could be indicative of an equilibrium between the species responsible for peaks II_a and III_a'. However, it is also apparent that the peak current function for peak III_a' continues to increase after that for peak II_a has reached a constant minimum value. At sweep rates below 50 mV s^{-1} where peak III_a' cannot be observed, peak III_a also increases in height relative to peak II_a with increasing sweep rates. This suggests that peaks III_a and III_a' might be due to electrooxidation of the same species but that peak III_a' is an adsorption prepeak of peak III_a.

Further evidence that peak III_a' is an adsorption prepeak is its peak current behavior as a function of sweep rate. A diffusion controlled peak exhibits a linear relationship between peak current and the square root of the sweep rate.[64] The current for peak III_a' increases faster with sweep rate than the current does for a diffusion controlled peak. In fact the peak current for peak III_a' is directly proportional to the sweep rate (Figure 23). Thus it definitely appears that peak III_a' is indeed an adsorption peak.[64]

Reduction peaks of 6-MTHP and 6-MDHP. Reduction peaks IV_c and I_c of 6-MTHP have already been discussed above. Reduction peaks II_c and III_c are seen in Figure 14. These peaks have already been examined using cyclic voltammetry by Kwee and Lund.[25,49] Komenda[51] and Asahi[52] have independently studied the reduction peaks of 6-MP polarographically. They proposed that 6-MP is reduced in the peak II_c process to 6-methyl-5,8-dihydropterin (6-M-5,8-DHP) which is very unstable and rapidly rearranges to 6-MDHP. 6-M-5,8-DHP can be reoxidized in a quasi-reversible reaction back to 6-MP at peak V_a

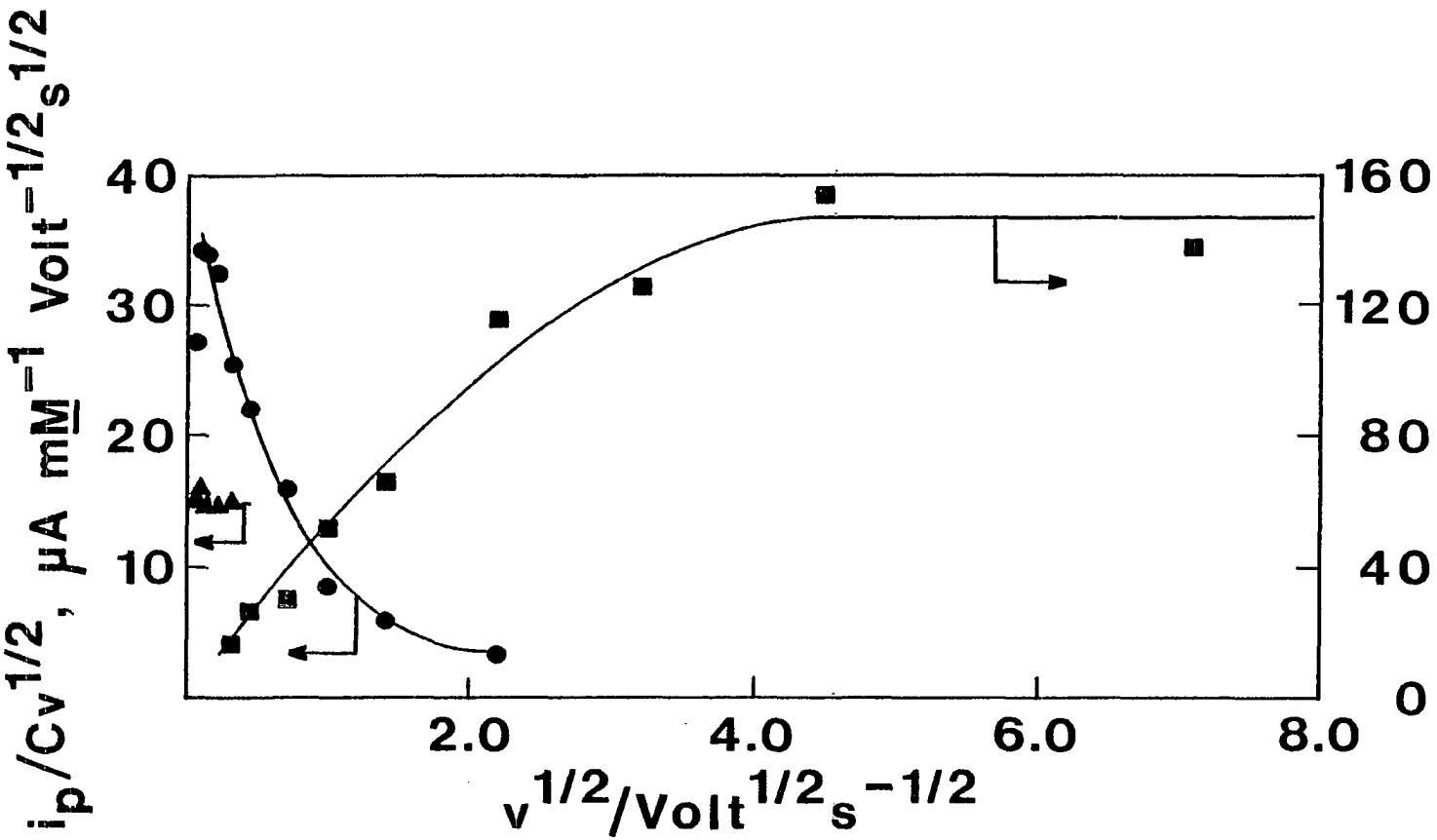


Figure 22. Peak current function vs. the square root of the sweep rate for the voltammetric oxidation peaks of 0.5 mM 6-MDHP in pH 3.0 phosphate buffer. Peak II_a (●), Peak III_a (▲), and Peak III'_a (■).

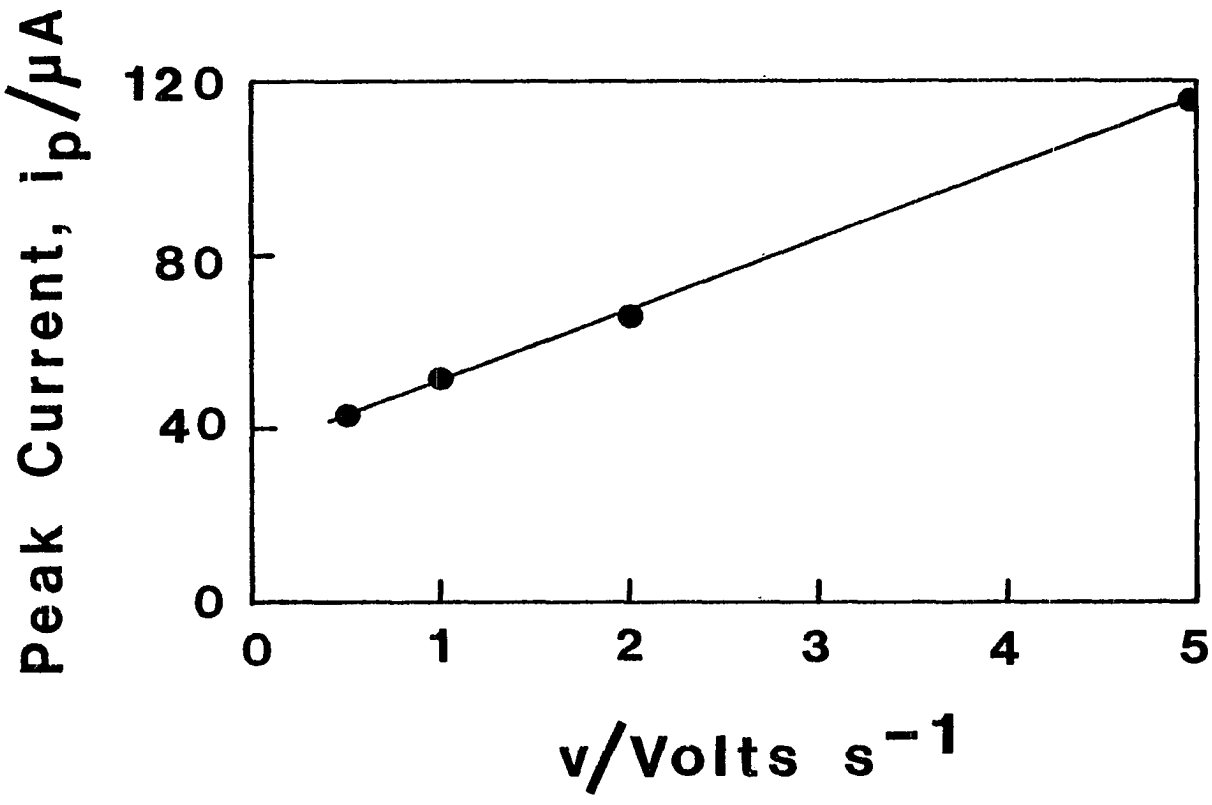


Figure 23. Peak current, i_p, vs. scan rate for peak III'_a of 0.5 mM 6-MDHP in pH 3.0 phosphate buffer.

(Figure 24). Kwee and Lund[25] reported that the 6-M-5,8-DHP was fairly stable because the reverse peak was quite large. Our work shows that in phosphate buffer reverse peak V_a is quite small even at high pH indicating that the chemical follow-up reaction is fast. The sweep rate employed (200 mV s^{-1}) was the same as that employed by Kwee and Lund.[25] Perhaps this anomaly is a result of Kwee and Lund using a different buffer, borate, compared to our work in phosphate buffers.

In order to observe reduction peak III_c in the cyclic voltammetry of 6-MTHP it is necessary to scan only oxidation peak I_a at sweep rates $\leq$2 V s^{-1}. On the reverse sweep peak I_c is observed and close to the background discharge peak III_c is observed. As the sweep rate is decreased the height of peak I_c decreases and the height of peak III_c increases. This clearly indicates that the initial peak I_a oxidation product which is responsible for peak I_c rearranges to another species which is responsible for peak III_c. Peak III_c is also observed on the first negative sweep in the cyclic voltammetry of 6-MDHP. This implies that the initial peak I_a oxidation product rearranges to 6-MDHP. Reduction peak II_c is observed only after sweeping oxidation peaks II_a, III_a', or III_a. This reduction process was observed in the polarographic investigation of 6-MP.[51,52] The implication is, therefore, that 6-MDHP is electrooxidized *via* the latter peaks (II_a, III_a', or III_a) to 6-MP.

The pH dependence of reduction peaks II_c and III_c at the PGE at a sweep rate of 5 mV s^{-1} is given by:

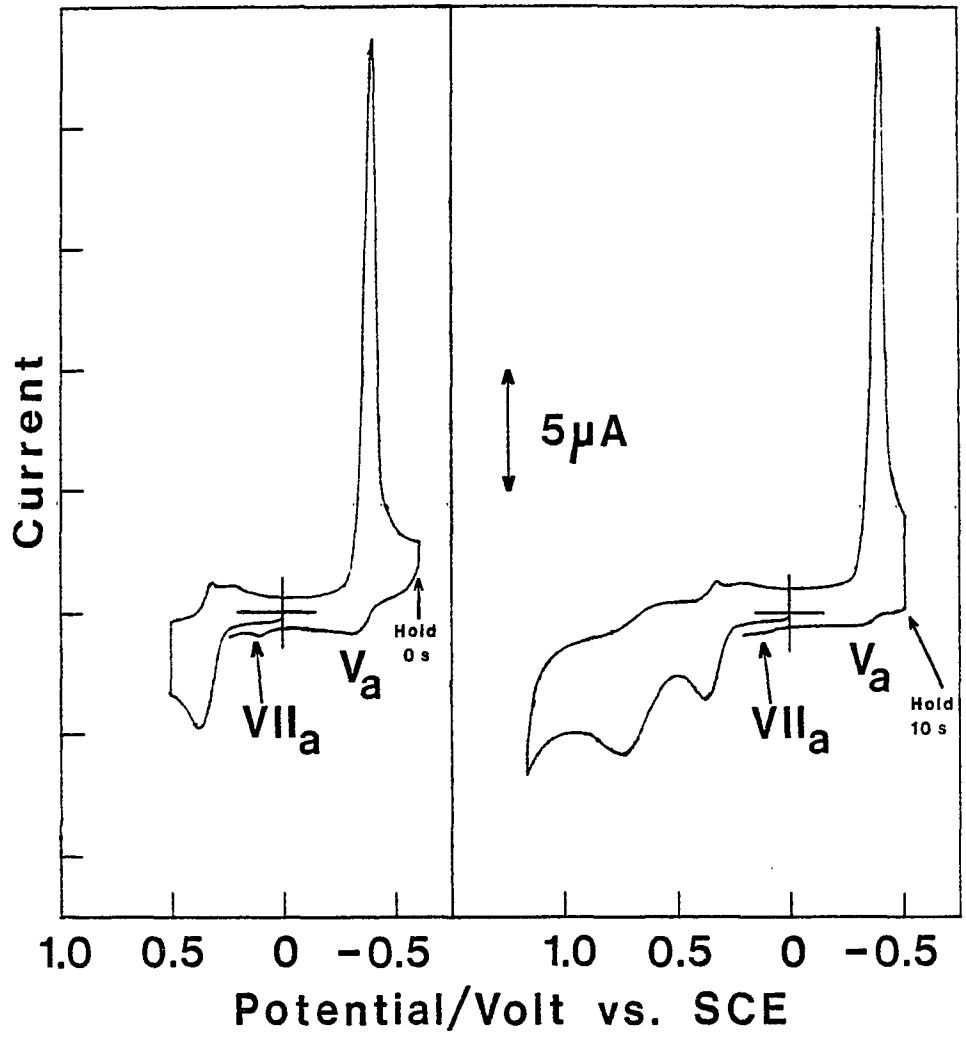


Figure 24. Cyclic voltammograms of 0.5 mM 6-MDHP in pH 2.0 phosphate buffer at a sweep rate of 200 mV s^{-1}. (A) hold 0 seconds and (B) hold 10 seconds.

*Peak II_c (pH 2.0-11.0): E_p = [-0.21-0.070 pH]V

±Peak III_c (pH 2.0-8.0): E_p = [-0.88-0.065 pH]V

Coulometric Studies

Coulometry of 6-MTHP. Most controlled potential electrolyses of 6-MTHP were carried out in a thin-layer spectroelectrochemical cell with a reticulated vitreous carbon working electrode. The thin-layer cell was sealed to prevent any oxidation of the test solution by atmospheric oxygen. For a complete description of the cell see the Experimental Chapter. n-Values for the oxidation processes were calculated by graphical integration of current vs. time curves.

Electrooxidation of 6-MTHP at peak I_a revealed that 1.9±0.1e per molecule were transferred in the pH range 3-10 (Table 4). The potentials applied in such studies were determined from linear sweep voltammograms in the RVC thin-layer cell at a sweep rate of 5 mV s^{-1}. A typical voltammogram in the thin-layer cell is presented in Figure 25A. Note the broadness of the voltammetric peaks in the thin-layer cell and the absence of peak II_a in the initial sweep. The potential of peak I_a is shifted ca. 200 mV positive of the peak potential at the same pH at the PGE microelectrode. Part of this difference

---

*Komenda[51] reported $E_{1/2}$ (pH 0-12) = [-0.15-0.075 pH]V. Asahi[52] reported $E_{1/2}$ (pH <9) = [-0.25-0.070 pH]V. These values are given for comparison only.

±Komenda's value for peak III_c was $E_{1/2}$ (pH 4-8) = [-0.90-0.063 pH]V and $E_{1/2}$ (pH >9) = [-0.82-0.032 pH]V. Asahi reported $E_{1/2}$ = [-0.93-0.064 pH]V, no pH range given.

Table 4

Coulometric n-values Observed Upon Electrolysis of 6-MTHP at Peak I_a and Peak III_a Potentials[a]

pH[b]	0.1 mM 6-MTHP		1.0 mM 6-MTHP	
	Peak I_a[c]	Peak III_a[d]	Peak I_a[c]	Peak III_a[d]
3.1	1.4	1.9	1.7	1.9
4.0	1.8	2.1	1.8	1.9
4.6	1.5	1.8	1.9	1.5
5.6	2.2	2.1	2.0	1.4
6.0	2.0	2,1	1.8	1.7
7.0	1.9	1.8	1.9	1.8
8.1	1.9	1.8	1.8	1.8
9.3	1.3	1.9	1.9	1.7
9.9	1.3	1.3	-	-

[a]Data obtained using a thin-layer cell containing a RVC electrode.

[b]Phosphate buffers with an ionic strength of 0.5 M.

[c]Potential applied corresponds to the rising portion of peak I_a to minimize interference from peak II_a.

[d]Electrolysis at peak III_a was done after exhaustive electrolysis at peak I_a.

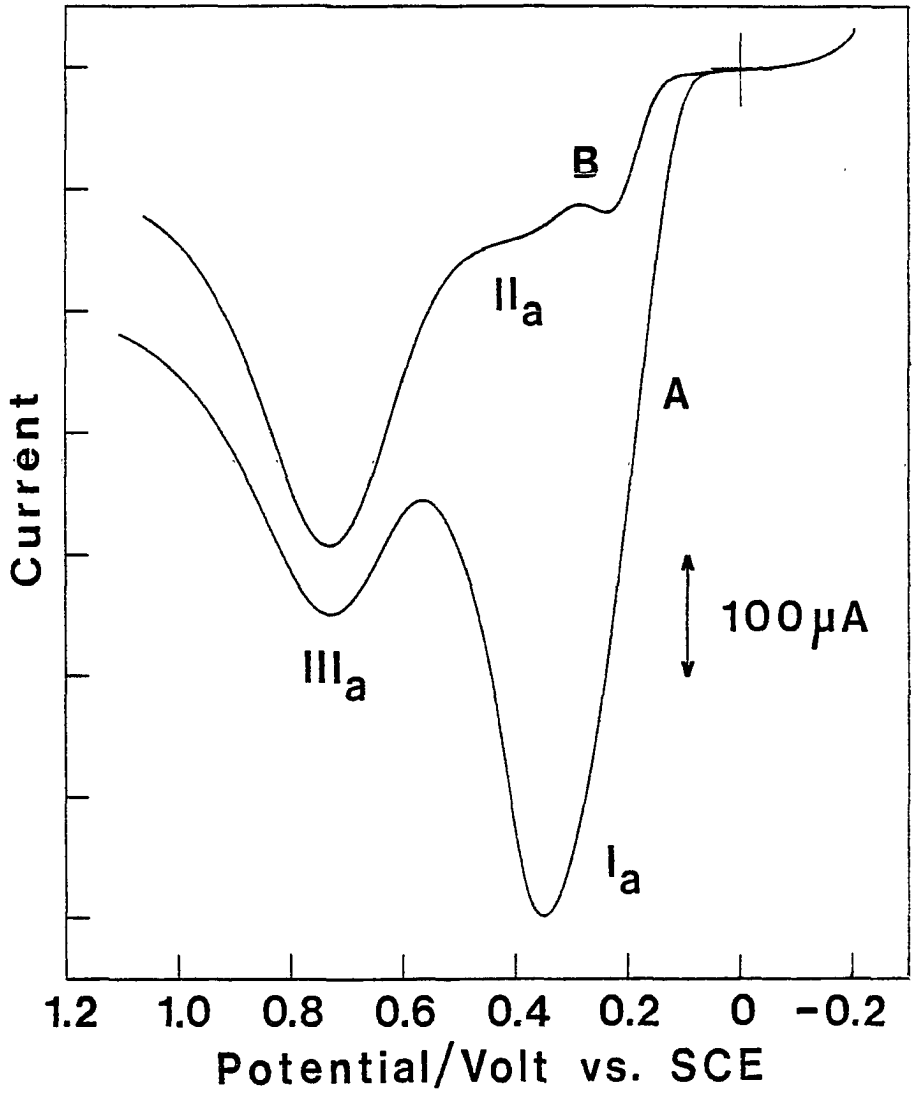


Figure 25. Linear sweep voltammogram of 1.0 mM 6-MTHP in pH 3.0 phosphate buffer in the RVC thin-layer cell. Sweep rate was 5 mV s^{-1}. (A) Fresh solution and (B) solution depleted by running one voltammogram.

is the result of using a silver-silver chloride reference electrode (SSCE) (when filled with 1 M KCl) instead of a SCE since potentials reported vs. SSCE will be 14 mV positive of those reported vs. SCE.[65] However, the bulk of this difference can be attributed to the IR drop in the cell.

Below pH 6 the potential used for the electrolysis of peak I_a is critically important because it must not be far enough positive to oxidize 6-MTHP in the peak II_a process. This was accomplished by setting the potential on the rising portion of peak I_a at ca. $E_{p/2}$, i.e., the potential where the current is one-half of the peak current. The rationale for this was determined by running a voltammogram in the thin-layer cell after partial oxidation of 6-MTHP (Figure 25B). Since the current decreases during the electrolysis the IR drop must also decrease. This is apparent in Figure 25B where it can be observed that the potential for peak I_a has shifted much more negative and that peak II_a is now observed at ca. the same peak potential as peak I_a in a fresh 6-MTHP solution. If the potential is set at $E_{p/2}$ relatively little of the peak II_a oxidation process will occur.

After complete oxidation of 6-MTHP at peak I_a potentials the potential was set at peak III_a. Oxidation at this potential resulted in the transfer of an additional 1.8±0.2e per molecule (see Table 4). Electrolysis of 6-MTHP at peak II_a potentials after electrooxidation at peak I_a also resulted in the transfer of 1.8±0.3e per molecule and linear sweep voltammetry after the electrolysis showed that peak III_a was also eliminated.

A solution containing 5 mM 6-MTHP at pH 7.0 was also oxidized

in the thin-layer cell to determine if there were any changes in the n-values as a result of increasing the 6-MTHP concentration. Oxidation at peak I_a involved the transfer of 2±0.2e_ and oxidation at peak III_a potentials involved the transfer of an additional 0.8±0.1e per molecule. This value is very low in light of the results at 0.1 mM and 1.0 mM. However, there is a reasonable explanation for this observation. 6-MDHP, which is formed when the quinonoid from oxidation at peak I_a rearranges, is quite insoluble. The limit of solubility determined from u.v. absorbance data (pH 7.0, $\varepsilon_{max}=25.7 \times 10^3$ at 229 nm) on a saturated solution of 6-MDHP was found to be ca. 1.8 mM. On close observation it could be seen that a yellow precipitate of 6-MDHP was settling out of solution, effectively removing it from the vicinity of the RVC working electrode. Therefore the amount of 6-MDHP which was oxidized was only that which remained in solution. If the amount of 6-MDHP remaining in solution had been 1.8 mM then the n-value would have been 2.2.

Coulometry of 6-MDHP. Coulometry was also performed on a 0.5 mM solution of 6-MDHP at pH 2 and 3 in a three compartment electrolysis cell using a large PGE working electrode. The working electrode compartment of the electrolysis cell was large enough to hold at least 25 ml of solution. Electrolyses were carried out at potentials corresponding to peaks II_a, III_a, and positive of peak III_a. Electrolyses were carried out in the large scale cell instead of the thin-layer cell so that aliquots could be removed for analysis by HPLC. Results are given in Table 5. In every instance it can be seen that 1.8±0.2e per molecule are transferred in the oxidation

Table 5

Coulometric n-Values Observed Upon Electrolysis of 0.5 mM 6-MDHP at Peak II_a and Peak III_a Potentials[a]

pH	Applied Potential/V vs. SCE	n-value
2.0	0.45 (peak II_a)	1.6
	0.60 (peak III_a)[c]	1.8
	0.85 (+ of peak III_a)	1.8
3.0	0.40 (peak II_a)	1.8
	0.60 (peak III_a)[c]	2.0

[a]Data obtained using a large PGE working electrode in a three compartment cell.

[b]Phosphate buffers with an ionic strength of 0.5 M.

[c]Potential corresponds to an average of peaks III_a and III_a'.

process. The fact that electrolysis of 6-MDHP at peak II_a once again causes elimination of peak III_a lends further support to the view that the species responsible for these peaks are in some sort of equilibrium.

Analysis of Starting Material and Electrolysis Products

HPLC analysis. One of the techniques used to determine the products of the electrooxidation of 6-MDHP and 6-MTHP was high performance liquid chromatography (HPLC). The reason that HPLC analysis

was so useful was the fact that Bailey and Ayling had worked out a succesful procedure for separating and analyzing a number of tetrahydropterins, dihydropterins, and pterins including 6-MTHP, 6-MDHP, and 6-MP (see the Experimental Chapter for details).[66] The HPLC analysis of the electrolysis products from peak I_a oxidations and peaks II_a or III_a oxidations of 6-MTHP displayed only peaks which could be assigned to 6-MDHP or 6-MP, respectively.

In the early HPLC experiments a number of 6-MTHP solutions at different pH values were analyzed and it was determined that as much as 30-35% of the 6-MTHP was already oxidized prior to voltammetry or coulometry. The reason these solutions were analyzed was to determine a correction factor for the observed n-values obtained in the thin-layer electrolysis cell to account for atmospheric oxidation prior to introduction into the cell. When these corrections were applied for the fraction of 6-MTHP which was already oxidized, some of the n-values calculated were close to 3. However, a later report by Bailey and Ayling[12] helped to clear up this problem. Apparently, tetrahydropterins can be oxidized on the partisil SCX column employed even if the eluant buffer is deaerated by bubbling with water-saturated nitrogen. This is true if the column has ever been used with an eluant containing oxygen. There is always some residual oxygen on the column which causes the oxidation of the tetrahydropterin species. The solution to this problem is to inject a fairly concentrated solution of a reducing agent such as sodium dithionite to reduce any oxygen trapped on the column. Some typical results of the difference in the apparent amount of oxidized components in a 6-MTHP solution

Table 6

Fraction of 6-MP and 6-MDHP Found in 6-MTHP Solutions Utilizing a High Performance Chromatographic Method[a]

pH[b]	6-MTHP conc./mM	# of inj.	6-MTHP %	6-MDHP %	6-MP %
3.0	1.05	1	97.2	2.8	trace
4.6	0.101	2	96.2(67)[c]	3.3(26)[c]	0.5(7)[c]
5.6	1.02	4	97.1	1.9	0.9
5.8	0.109	2	95.7(70)[c]	3.9(22)[c]	0.4(8)[c]
7.0	0.111	2	92.0	7.4	0.6
7.0	1.02	1	90.5	8.0	1.4
8.1	0.104	1	87.1(69)[c]	11.5(27)[c]	1.5(4)[c]
9.9	0.107	1	83.2	11.3	5.8

[a]According to Bailey and Ayling[66] except the buffer used as solvent was pH 6.1 phosphate with an ionic strength of 0.1 M. Column cleanup used sodium dithionite.[12]

[b]pH of the 6-MTHP solution, phosphate buffer μ=0.5.

[c]Values in parentheses are representative values when sodium dithionate was not used, shown for comparison.

before and after dithionite injection are seen in Figure 26A and B. Table 6 shows some representative results of analyses of a number of 6-MTHP solutions after dithionite cleanup of the column. HPLC analyses similar to these were used to determine the correction factors that were applied to observed n-values to arrive at the n-values reported in Table 4.

Peak areas on HPLC chromatograms were calculated using the method reported in Willard, Merritt and Dean.[67] Since some of the peaks were quite asymmetrical, the method used was to measure the width at 0.15 x height and 0.85 x height, taking the average of these and multiplying by the height of the peak (Figure 27). Taking into account the fact that 6-MTHP, 6-MDHP, and 6-MP all have different molar absorptivities in the pH 6.1 phosphate eluting buffer when monitored at 254 nm, another correction was applied to arrive at the percentages of each component in the test solution.

U.v. analysis. Spectra of the electrolysis products of 6-MTHP were obtained after complete electrolysis at peak I_a potentials in the RVC thin-layer cell. At pH 7, for example, the spectrum after complete electrolysis shows three peaks at wavelengths of 228 nm, 279 nm, and 324 nm. This spectrum corresponds exactly with that reported in the literature for 6-MDHP[57] and differs greatly from that of the starting material, 6-MTHP (λ_{max} = 302 nm and 218 nm at pH $\geq$7). Throughout the pH range studied, the spectrum of the electrolysis product of peak I_a oxidation of 6-MTHP corresponded to the reported spectra for the expected species of 6-MDHP at that pH.

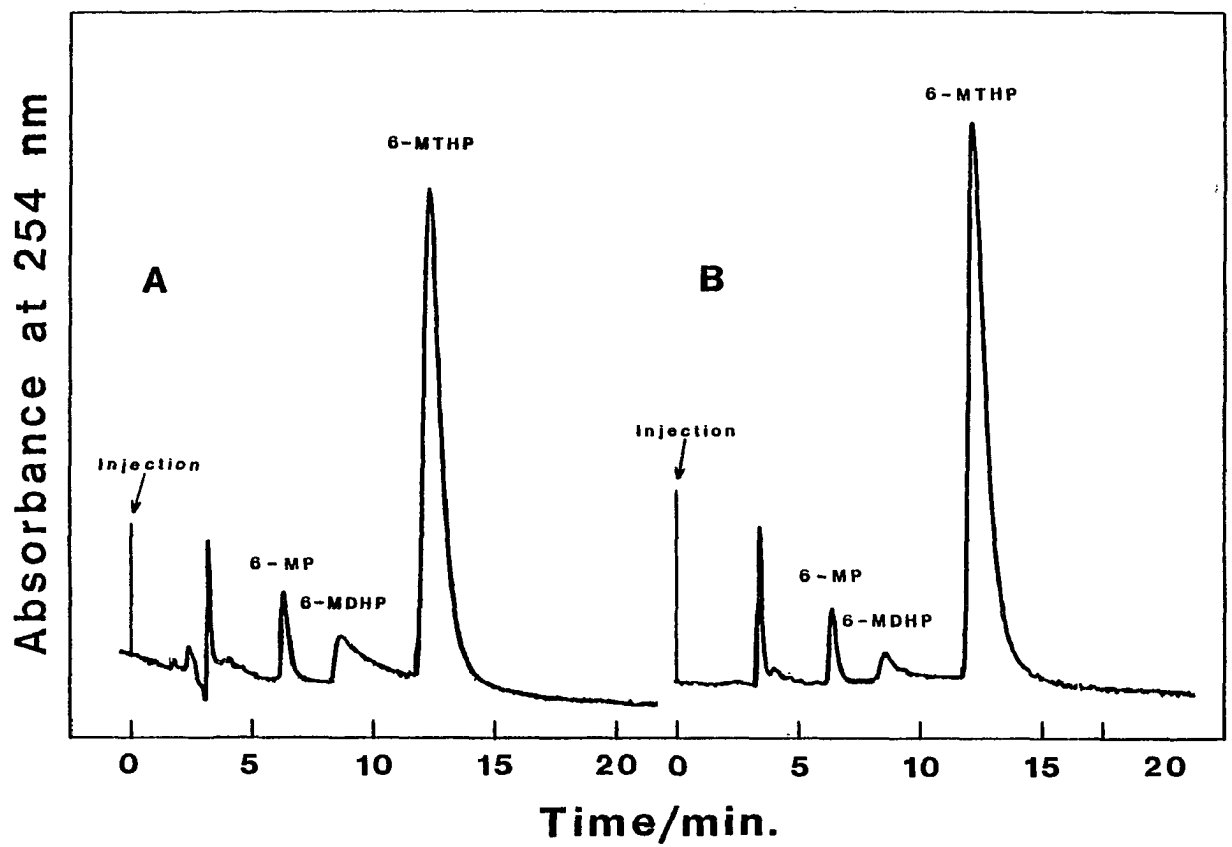


Figure 26. HPLC chromatogram of 0.1 mM 6-MTHP in pH 5.6 phosphate buffer μ=0.5 M. Eluant was pH 6.1 phosphate buffer, μ=0.1 M. Flow rate was 0.83 ml $min.^{-1}$ (A) before injection of sodium dithionite (B) after injection of 10 μl of 1.0 M sodium dithionite.

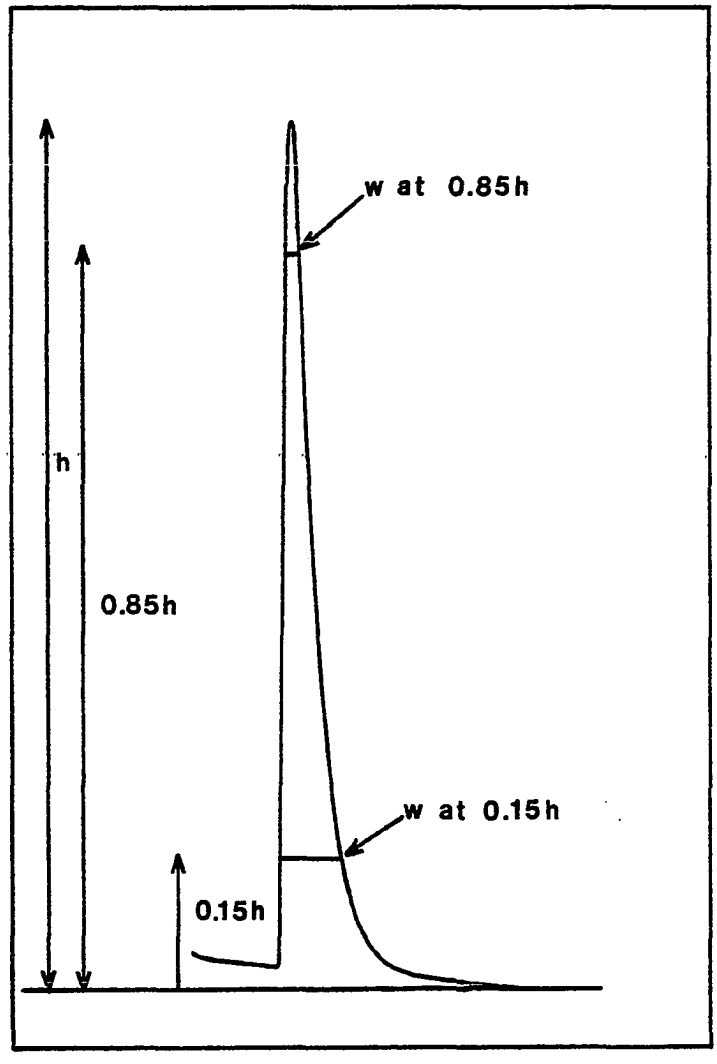


Figure 27. Method used for determining peak area.

When 6-MDHP was electrolyzed at potentials corresponding to peaks II_a, III_a, and positive of peak III_a, the u.v. spectrum of the product was found to be that of 6-MP. For example, the spectrum of 6-MDHP at pH 2.0 exhibits peaks at 207 nm, 249 nm, 270 nm, and 359 nm closely matching the reported spectrum for the cationic form of 6-MP[57] (Figure 28A,B). The product of the oxidation exhibited u.v. peaks at 210 nm, 243 nm, and 321 nm, with an inflection at 275 nm (Figure 28A,B,C), closely matching the literature λ_{max} values for 6-MP of 247 nm and 325 nm at pH 1.[59]

Thin-layer Spectroelectrochemistry of 6-MTHP

Since the cyclic voltammetry of 6-MTHP indicates that the initial peak I_a oxidation product (which is responsible for peak I_c) is unstable and appears to decompose to 6-MDHP it was felt that more information on this process could be obtained using thin-layer spectroelectrochemistry. 6-MTHP is quite air-sensitive, particularly at higher pH, therefore it was necessary to design a thin-layer cell which could exclude atmospheric oxygen. Complete details of the design and construction are given in the Experimental Chapter.

Spectral changes. The spectrum of the cationic form of 6-MTHP at pH 3.1 in the thin-layer cell is shown in curve 1 of Figure 29 and exhibits peaks at 212 nm and 264 nm. There is also a small broad band centered around 326 nm which is a result of partial air oxidation of 6-MTHP prior to introduction into the thin-layer cell. The potential for oxidation of peak I_a was once again deter-

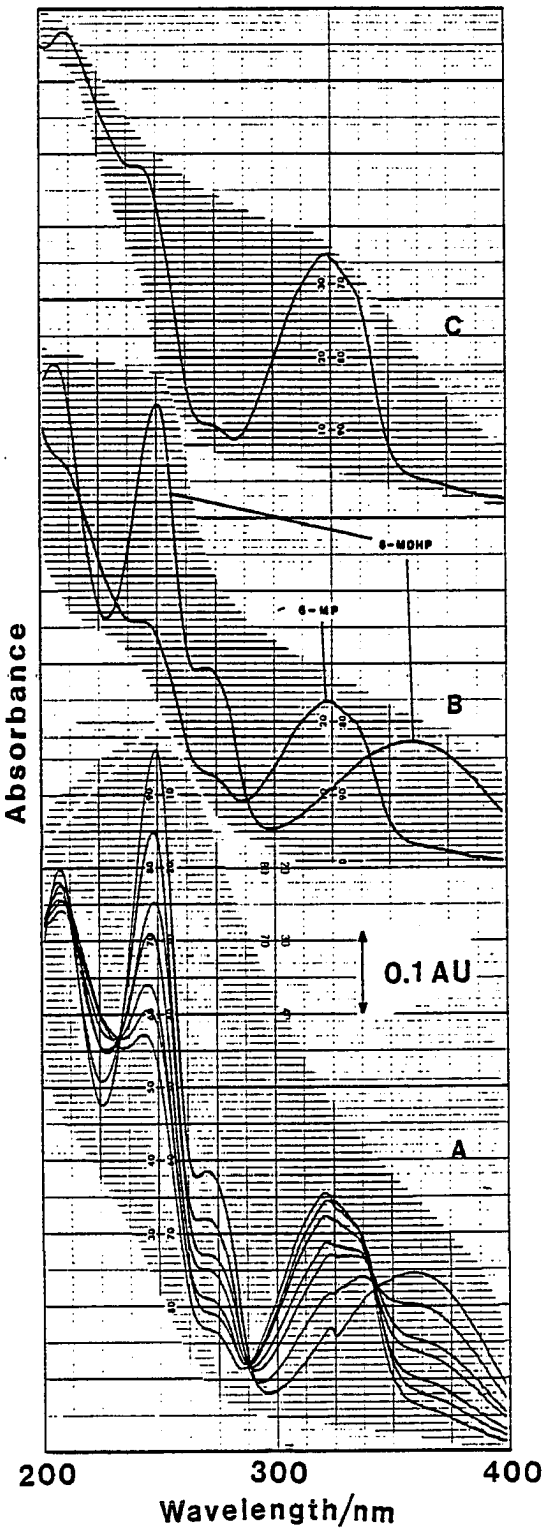


Figure 28. U.v. spectra of 0.5 mM 6-MDHP in pH 2.0 phosphate buffer in 1 mm quartz cells. (A) during electrolysis at peak II_a potentials (0.35V), (B) before and after electrolysis at peak III_a potentials (0.60V), and (C) after electrolysis at a potential positive of peak III_a (0.85V).

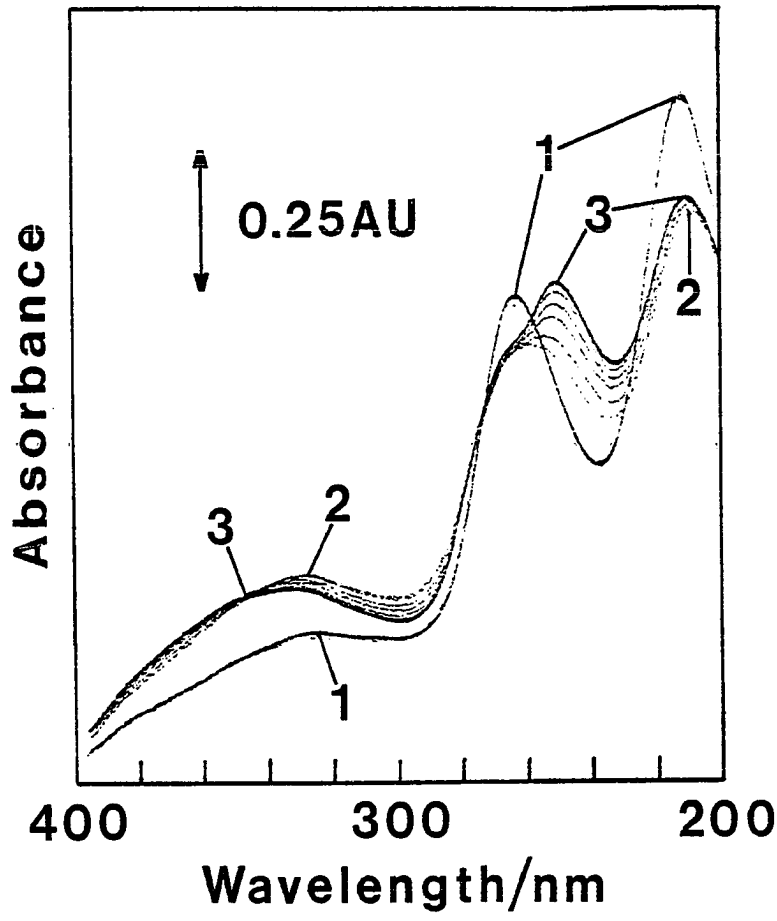


Figure 29. Spectrum of 0.5 mM 6-MTHP electrolyzing at 0.37V at a RVC electrode in a thin-layer cell in phosphate buffer pH 3.1. Curve 1 is the spectrum of 6-MTHP before electrolysis. Curve 2 is the spectrum after 20s electrolysis. The potenwas turned off immediately prior to curve 2. Curve 3 is the spectrum after complete decay of the intermediate. Repetitive scans between curves 2 and 3 are 19s in duration.

mined by running a linear sweep voltammogram in the thin-layer cell. Immediately after electrooxidation, at a potential corresponding to ca. $E_{p/2}$ of peak I_a, for 20s the working electrode was open-circuited and the spectrum of curve 2 in Figure 29 was recorded. A decrease is seen in both u.v. peaks of the spectrum for 6-MTHP and a substantial increase is noted in the wavelength region greater than 300 nm with a peak maximum near 328 nm. The spectrum continues to change for a considerable period of time after termination of the electrolysis (ca. 15 min.) with the most noticeable difference being the growth of a peak at 250 nm. Other changes noted were a small increase in the absorbance of the peak at 212 nm and a shift in the long wavelength peak to ca. 340 nm. Curve 3 of Figure 29 is the spectrum after complete decay of the intermediate species. It has absorbance maxima at 212 nm, 250 nm, and 340 nm, with an inflection at 268 nm. This compares favorably with the literature values reported for the cationic species of 6-MDHP with λ_{max} = 250 nm, 271 nm (inflection), and 361 nm.[57] The difference in the long wavelength peak (340 nm observed, 361 nm reported) of 6-MDHP is probably a result of the fact that the pH of the solution is 3.1 which is very close to the pK_a (3.2) for 6-MDHP. Neutral 6-MDHP has a long wavelength peak at 324 nm. Thus near the pK_a there is nearly equal quantities of protonated and non-protonated species yielding a composite spectrum with a maximum somewhere between 361 nm and 325 nm. The peak observed in curve 2 of Figure 20 at 328 nm must be largely characteristic of the intermediate species.

Above about pH 4 the spectral changes observed upon electro-

oxidation of 6-MTHP were somewhat different because the final product, 6-MDHP, now exists as a neutral species. For example, at pH 4.6 the spectral changes can be seen in Figure 30. Curve 1 in Figure 30 is the spectrum of the cation of 6-MTHP and is identical to curve 1 of Figure 29. Curve 2 of Figure 30 is after virtually complete electrolysis of 6-MTHP at peak I_a and exhibits bands at λ_{max} = 218 nm, 268 nm, and 325 nm. After the working RVC electrode was open-circuited at curve 2 the spectrum continued to change as the intermediate rearranged. The absorbance increased in the range from 220 nm to 260 nm as well as in the wavelength region above 330 nm. Especially characteristic was the peak growing in at 274 nm. The final product exhibited u.v. peaks at 226 nm, 274 nm, and 324 nm (curve 3, Figure 20) which compared well with the literature values for 6-MDHP of 229 nm, 279 nm, and 324 nm.[57] There is no feature of the spectrum shown in curve 2 which can be directly attributed to the intermediate species.

Above pH 7 the species oxidized at peak I_a is neutral 6-MTHP which has u.v. bands at 218 nm and 302 nm (curve 1, Figure 31). Since the observed spectral changes are the same throughout the range from pH 7 to 10 a typical example at pH 9.1 is shown. A shoulder at ca. 280 nm is observed in some spectra of 6-MTHP which is actually due to partial air oxidation to 6-MDHP. Upon initiating the electrolysis at peak I_a potentials, both u.v. peaks of 6-MTHP decrease and the absorbance above 320 nm increased. After 80s electrooxidation the spectrum shown in curve 2 in Figure 31 was recorded. This spectrum is probably a fairly good representation of the spectrum for the quinonoid-dihydropterin and has one major peak centered at 300 nm.

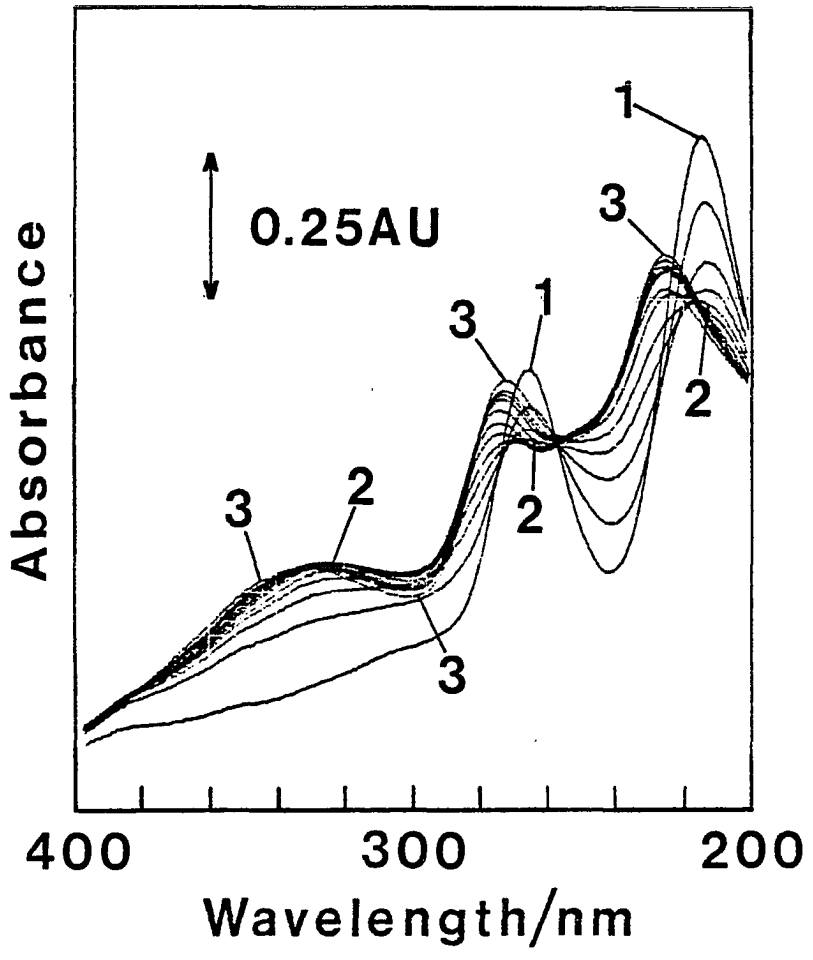


Figure 30. Spectra of 0.51 mM 6-MTHP electrolyzing at 0.27V at a RVC electrode in a thin-layer cell in pH 4.7 phosphate buffer. Curve 1 is the spectrum of 6-MTHP. Curve 2 is the spectrum after ca. 120s at peak I_a potentials. Prior to scanning curve 2 the RVC working electrode was open-circuited. Curve 3 is the spectrum after complete decay of the intermediate species and corresponds to 6-MDHP. Repetitive spectral scans between curves 2 and 3 are 38s in duration.

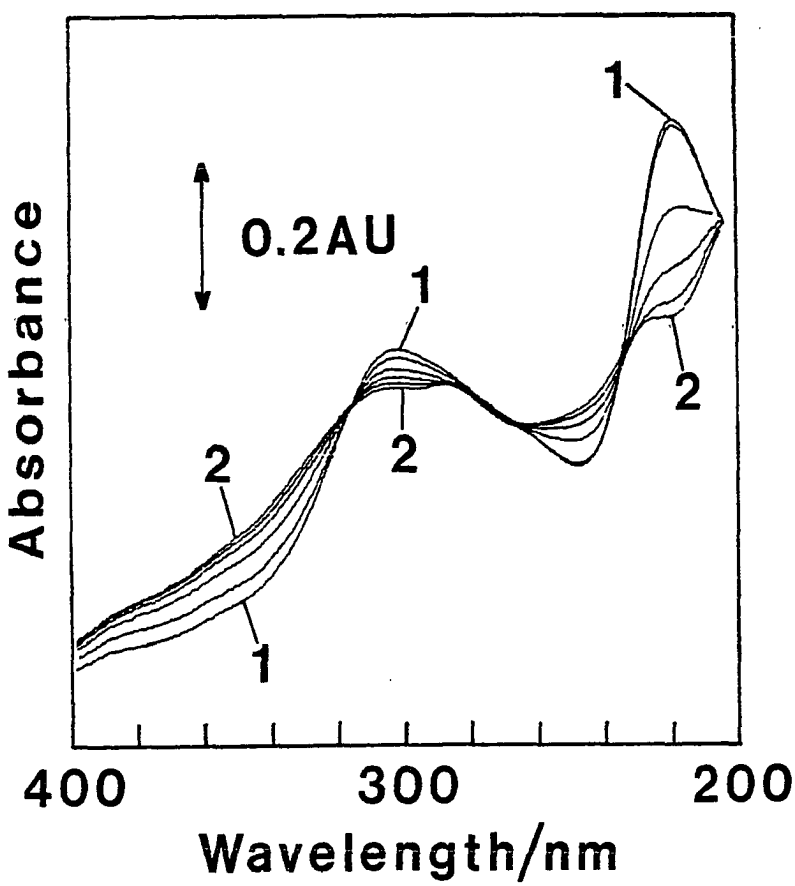


Figure 31. Spectra of 0.52 mM 6-MTHP electrolyzing at 0.08V at a RVC electrode in a thin-layer cell in pH 9.1 phosphate buffer. Curve 1 is the spectrum of 6-MTHP. Curve 2 is the spectrum after ca. 80s electrolysis, but before the intermediate species has had time to decay. Repetitive sweeps of 19s are shown.

Two small peaks at 226 nm and 280 nm are also observed in curve 2, however they are a result of the rearrangement of a fraction of the quinonoid-dihydropterin to 6-MDHP. If the species characterized by curve 2 in Figure 31 is allowed to decompose, the final spectrum exhibits peaks at 226-228 nm, 279 nm, and 324 nm indicating that the final product of peak I_a oxidation of 6-MTHP is 6-MDHP.

Kinetics of the rearrangement reaction. Spectroelectrochemical results as well as the data from cyclic voltammetry clearly indicate that the initial product of peak I_a electrolysis of 6-MTHP is unstable and rearranges in a chemical follow-up reaction to 6-MDHP. The rate of this follow-up reaction was studied using thin-layer spectroelectrochemical techniques by monitoring the decrease in the absorbance of the intermediate or the increase in the u.v. absorbance of 6-MDHP, the reaction product.

Rate constants were obtained at three concentrations of 6-MTHP, 0.1 mM, 0.5 mM, and 1.0 mM. The u.v. peaks which were monitored to obtain the rate constants were the short wavelength peak of 6-MDHP at 220-226 nm, the peak of 6-MDHP at 252 nm (pH $<pK_a$ of 6-MDHP), the peak of 6-MDHP at 270-278 nm (pH $>pK_a$ of 6-MDHP), or the u.v. peak of the intermediate at 300-304 nm.

The largest absorbance change after the RVC working electrode was open-circuited occurred at the short wavelength peak. A typical absorbance vs. time curve is shown in Figure 32A for the growth of the low wavelength peak of 6-MDHP after partial electrolysis at peak I_a of a 1.0 mM 6-MTHP solution. Plotting $\ln|A-A_\infty|$ vs. time for

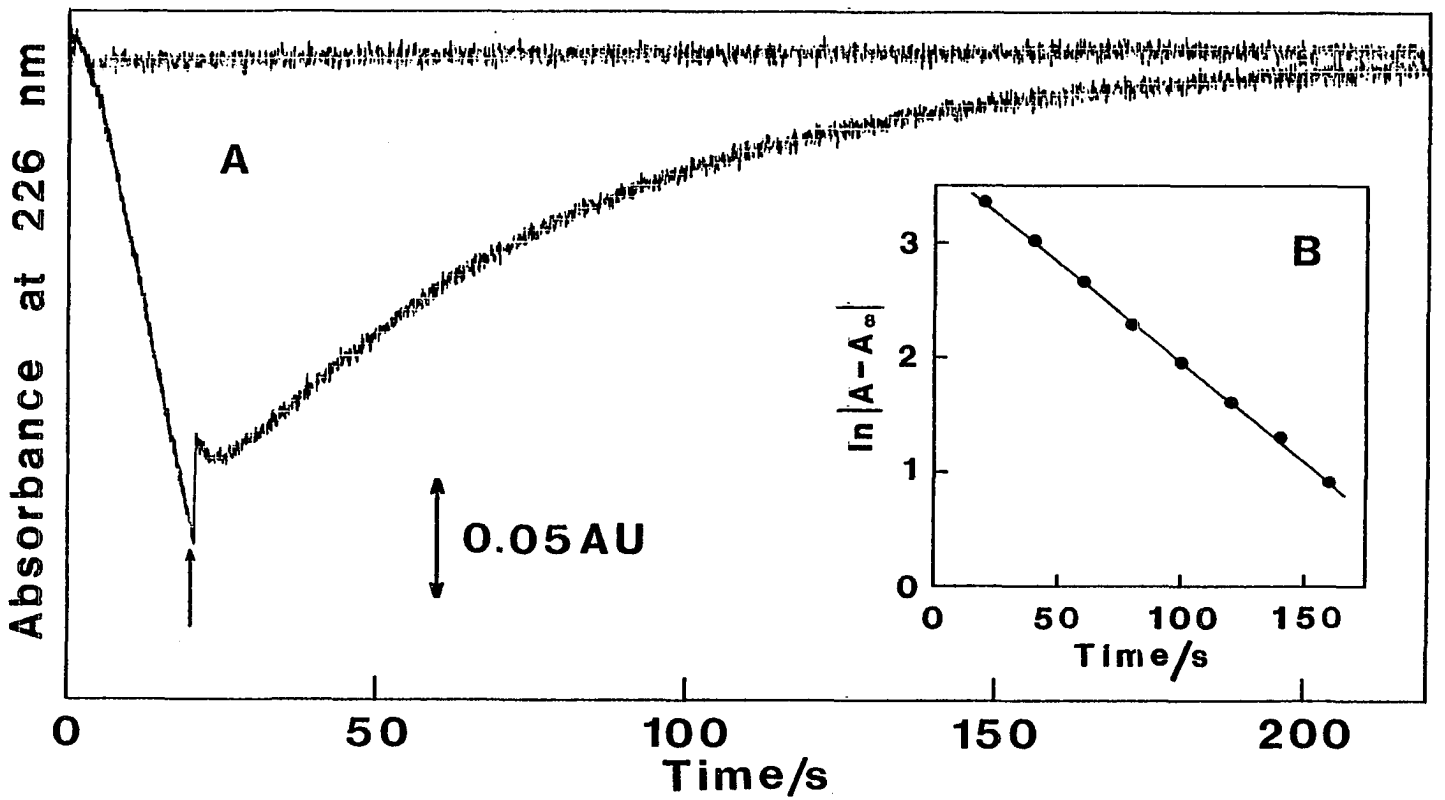


Figure 32. (A) Absorbance vs. time curve for the decay of the intermediate species generated upon electrolysis of 1.0 mM 6-MTHP at 0.32V for 20s in pH 4.0 phosphate buffer. Arrow indicates time where electrode was open-circuited. (B) Ln $|A-A_\infty|$ vs. time for the decay curve in A.

Table 7

Observed First Order Rate Constants for Chemical Reaction of the Intermediate Generated Upon Peak I_a Oxidation of 1.0 mM 6-MTHP as a Function of pH[a]

pH[b]	$k_1 \times 10^2/s^{-1}$ measured at			
	220-226 nm	252nm	278 nm	304 nm
2.0		1.1±0.18		0.83±0.06
3.1	1.2±0.06	2.1±0.1		
4.0	1.7±0.08		1.8±0.17	
4.6	1.5±0.09		1.7±0.29	
5.6	3.5±0.24		3.5±0.57	
6.0	2.9±0.22		3.4±0.07	3.2±0.17
7.0	1.2±0.05			1.2±0.03
8.1	0.31±0.01			0.41±0.03
9.3	0.38±0.01			0.27±0.02
9.9	0.23±0.02			c

[a]Data obtained by a thin-layer spectroelectrochemical method using an optically transparent RVC electrode.

[b]Phosphate buffers with an ionic strength 0.5 M.

[c]Two rate constants were observed. Fast step: 0.45±0.13. Slow step: 0.074±0.001.

Table 8

Observed First Order Rate Constants for Chemical Reaction of the Intermediate Generated Upon Peak I_a Oxidation of 0.5 mM 6-MTHP as a Function of pH[a]

pH[b]	$k_1 \times 10^2/s^{-1}$			
	214-226 nm	252 nm	272-287 nm	300-304 nm
3.1	1.3±0.12	1.6±0.04		
4.0	2.5±0.31		1.7±0.26	
4.6	2.1±0.04		2.0±0.01	
5.6	2.6±0.12		2.7±0.09	
6.0	3.1±0.12		3.3±0.19	2.3±0.12
7.0	1.0±0.16			0.88±0.07
8.1	0.29±0.04			0.43±0.04
9.3	0.26±0.02			0.27±0.08
9.9	0.27±0.03			0.26±0.07[c]

[a]Data obtained by a thin-layer spectroelectrochemical method using an optically transparent RVC electrode.

[b]Phosphate buffers with an ionic strength of 0.5 M.

[c]At times two rate constants were observed. Fast step: 0.36±0.09. Slow step: 0.068±0.02.

Table 9

Observed First Order Rate Constants for Chemical Reaction of the Intermediate Generated Upon Peak I_a Oxidation of 0.1 mM 6-MTHP as a Function of pH[a]

pH[b]	$k_1 x 10^2/s^{-1}$ measured at			
	220-228 nm	245-252 nm	270-278 nm	300-304 nm
3.1		2.5±0.16		
4.0		2.6±0.53	1.4±0.09	
4.6	2.0±0.33		1.0±0.08[c]	
5.6	2.3±0.23		2.7±0.05	
6.0	2.9±0.05		2.3±0.18	1.6±0.03
7.0	1.0±0.05			0.5±0.01
8.1	0.24±0.03			0.26±0.03
9.1	0.27±0.03			0.21±0.01
9.9	0.46±0.03			0.21±0.02

[a]Data obtained by a thin-layer spectroelectrochemical method using an optically transparent RVC electrode.

[b]Phosphate buffers with an ionic strength of 0.5 M.

[c]Often two rate constants were observed. Fast step: 3.7±0.8. Slow step: 0.56±0.14.

this curve yielded linear plots indicating that the reaction is first order (Figure 32B). Rate constants throughout the pH range 2-10 are given for 1.0 mM 6-MTHP in Table 7. The only unusual results were observed at pH 9.9 while monitoring at 304 nm (Figure 33A). $Ln|A-A_\infty|$ vs. time curves at this pH were not linear indicating the possibility of two first order chemical processes occurring simultaneously or sequentially (Figure 33B).

At a 6-MTHP concentration of 0.5 mM the behavior of the intermediate generated upon electrooxidation at peak I_a was almost identical to the behavior at a 6-MTHP concentration of 1.0 mM. The experimental results are shown in Table 8. Again the results at pH 9.9 are unusual in that two rate constants are observed. However, at a concentration level of 0.1 mM 6-MTHP no unusual results were observed at pH 9.9. Instead, two rate constants were observed at pH 4.6. Results for 0.1 mM 6-MTHP are given in Table 9. A typical absorbance vs. time curve for 0.1 mM 6-MTHP can be seen in Figure 34 and illustrates the difficulty of measuring the small absorbance changes at this low concentration because of the noise in the signal from the RSS.

The magnitude of the rate constants as a function of pH is illustrated in Figure 35. From this figure it can be seen that there is a maximum in the rate of the follow-up reaction at ca. pH 5.6-6.0. These results suggested that perhaps the rearrangement of the intermediate was catalyzed by one or more of the buffer components. This was suspected because the maximum rate occurred at a pH where $H_2PO_4^-$ is the main phosphate species present in solution.

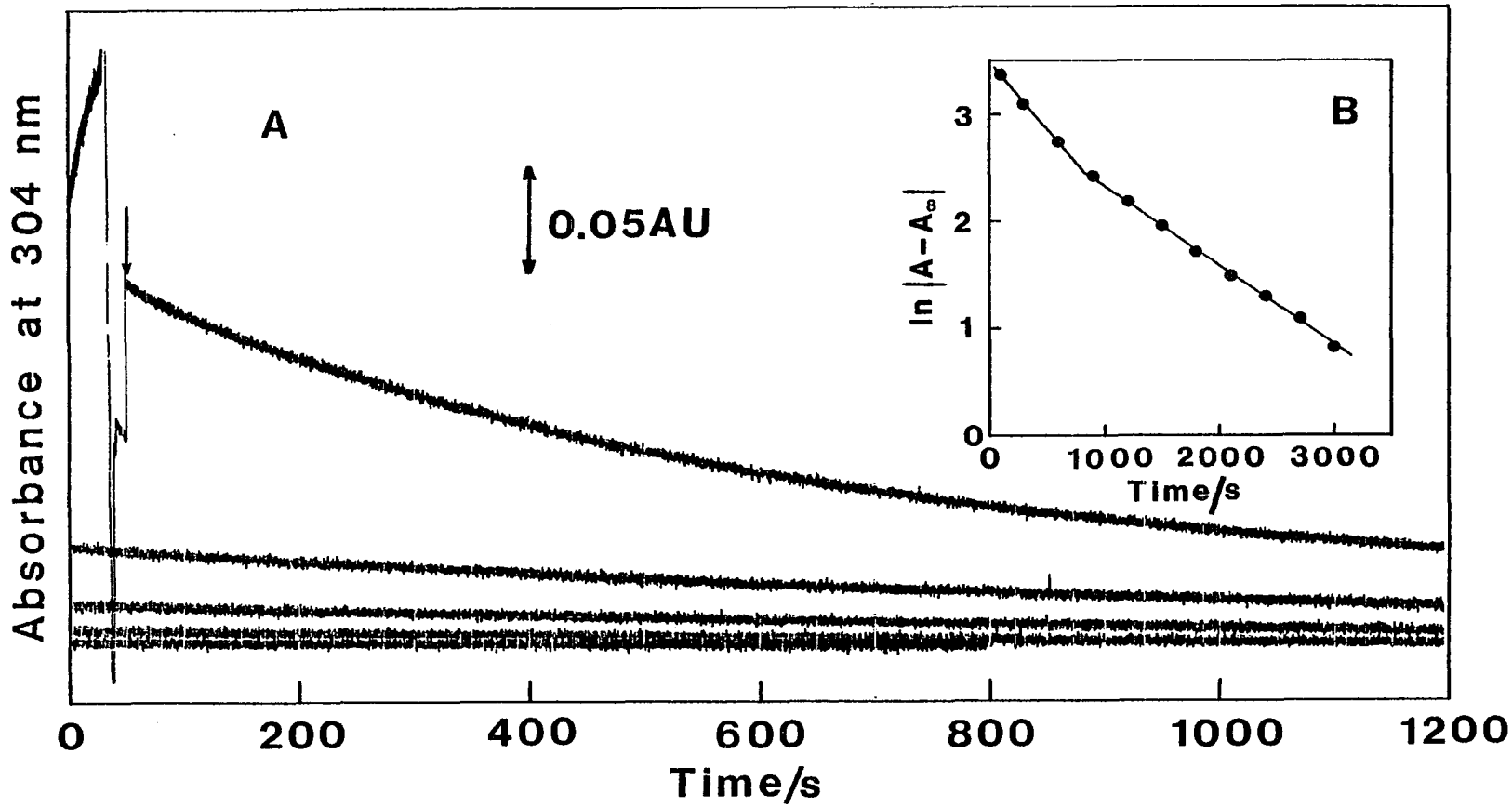


Figure 33. (A) Absorbance vs. time curve for the decay of the intermediate generated upon electrolysis of 1.0 mM 6-MTHP at 0.01V for 50s in pH 9.9 phosphate buffer, μ=0.5 M. (B) Ln $|A-A_\infty|$ vs. time for the decay curve in A.

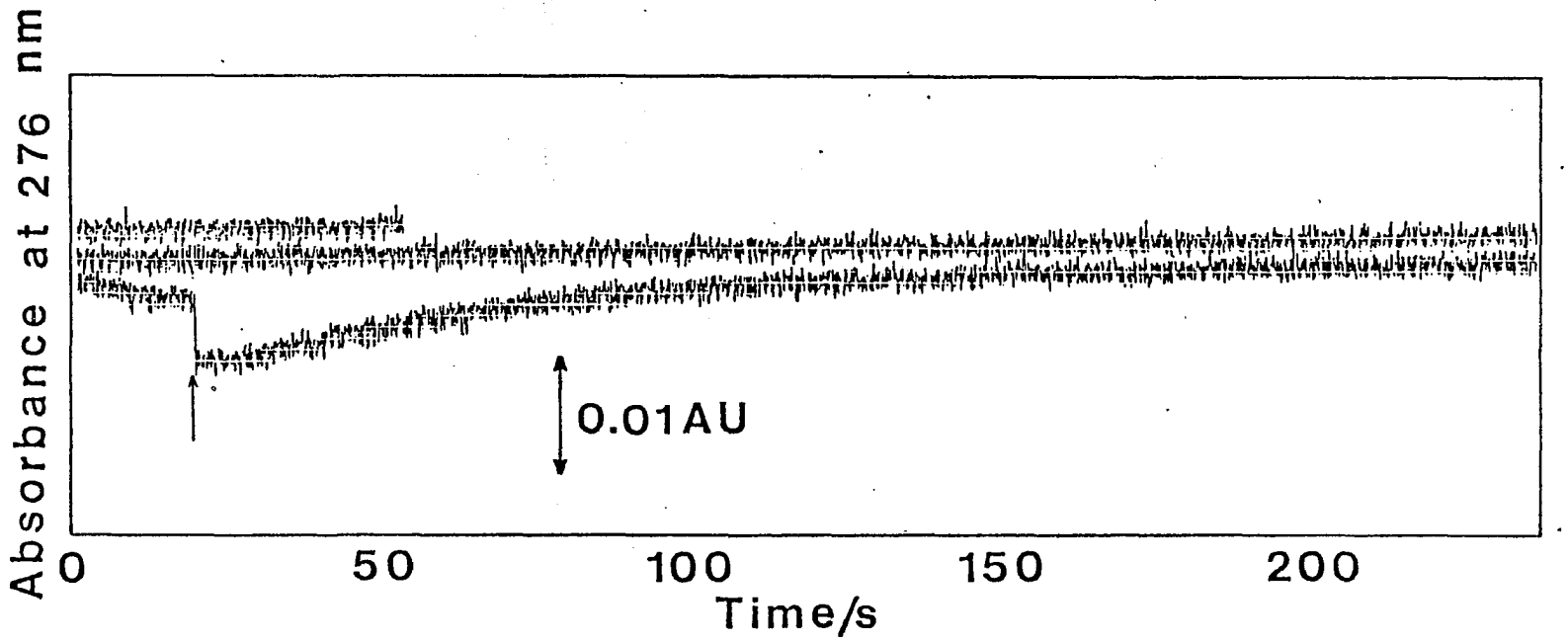


Figure 34. Absorbance vs. time curve for the decay of the intermediate species generated upon electrolysis of 0.1 mM 6-MTHP at 0.28V for 20s in pH 4.6 phosphate buffer, μ=0.5 M. Arrow indicates time where the electrode was open-circuited.

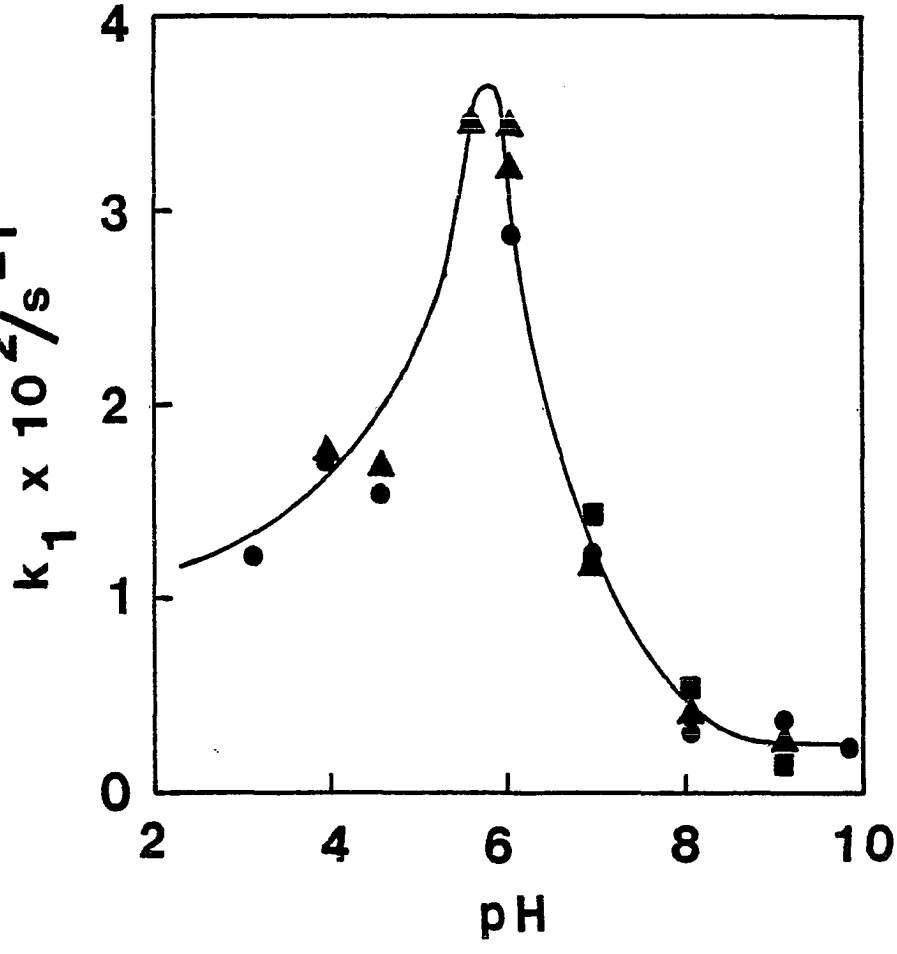


Figure 35. Variation of rate constant vs. pH for the rearrangement of the intermediate generated upon peak I_a electrooxidation of 1.0 mM 6-MTHP. 220-226 nm (●), 277-278 nm (▲), and 304 nm (■).

The rate of the rearrangement of the intermediate falls off very rapidly at lower or higher pH where the concentration of $H_2PO_4^-$ decreases.

Dependence of reaction rate on buffer concentration. A spectroelectrochemical study was consequently done to determine if the concentration of phosphate affects the rate of the chemical reaction of the intermediate generated by peak I_a electrooxidation of 6-MTHP. This investigation was done at pH 2.0 because of the increased stability of 6-MTHP at low pH removing any complications as a result of air oxidation. Results are shown in Table 10 and Figure 36.

Potentiostatic study. As a further confirmation of the rate constant a potentiostatic study on 1.0 mM 6-MTHP in pH 5.6 phosphate buffer with an ionic strength of 0.5 M was completed according to the method of Alberts and Shain.[68] A pH of 5.6 was chosen because the rate constant for the chemical rearrangement is at its maximum at this pH. For the potentiostatic method to be applicable it is necessary for the electrode reaction to occur under diffusion control at the electrode surface. At pH 5.6 there should be little complication from the equilibrium between hydrated 6-MDHP and non-hydrated 6-MDHP (see later discussion).

The potential was set at a point where both the peak I_a process, electrooxidation of 6-MTHP, and the peak III_a process, electrooxidation of non-hydrated 6-MDHP formed from the rearrangement of the primary peak I_a product, could occur. Under such conditions it was anticipated that an ece reaction depicted in Equation 2 would

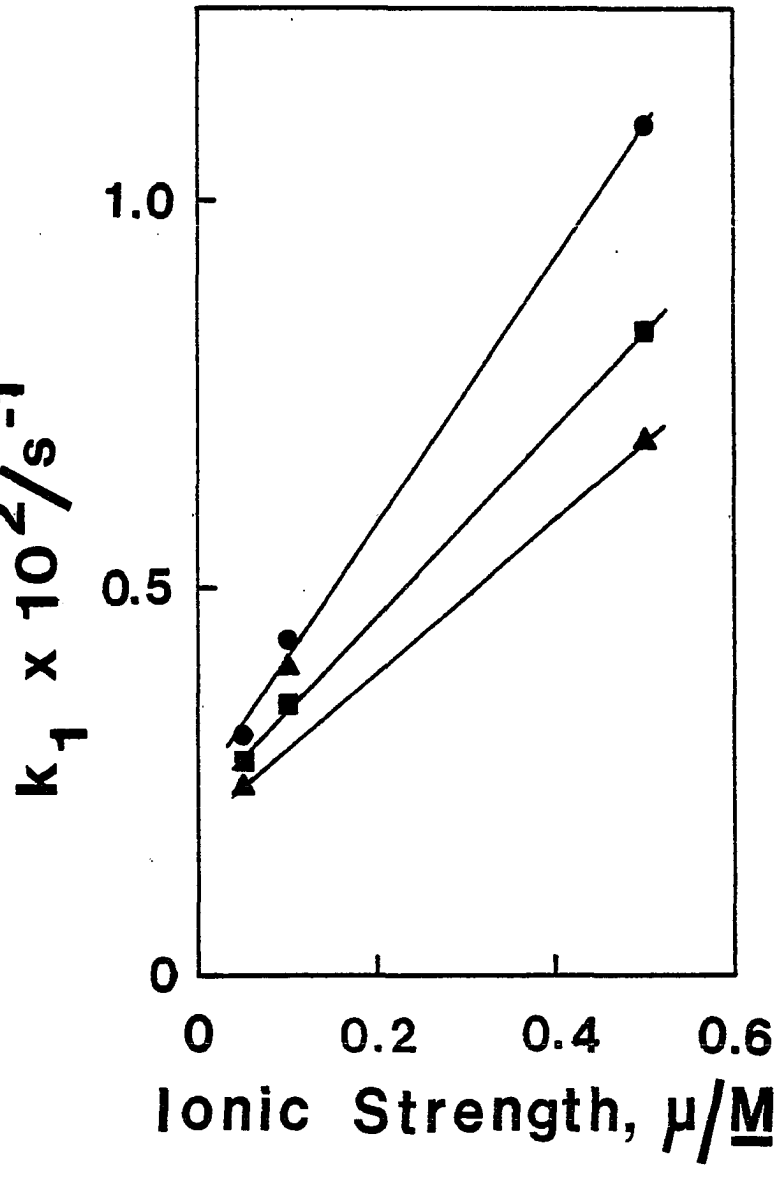


Figure 36. Variation of the rate constant for the rearrangement of the intermediate generated upon peak I_a electrooxidation of 1.0 mM 6-MTHP *vs.* the ionic strength of the pH 7 phosphate buffer. 254 nm (●), 306 nm (■), and 336 nm (▲).

Table 10

Observed Pseudo-first Order Rate Constants for Chemical Reaction of the Intermediate Generated Upon Peak I_a Oxidation of 6-MTHP[a] as a Function of Buffer Ionic Strength at pH 7.0

Buffer Ionic Strength[b]	$kx10^2/s^{-1}$ 254 nm	306 nm	336 nm
0.05	0.31±0.03	0.28±0.03	0.24[c]
0.10	0.43±0.04	0.35±0.06	0.41±0.05
0.50	1.1±0.18	0.83±0.06	0.69±0.13

[a]The concentration of 6-MTHP was 1.0 mM.

[b]Ionic strength of the phosphate buffer.

[c]Only one run was made.

occur.

$$\text{6-MTHP} \xrightarrow[\underline{e}]{-2H^+-2e} \text{Intermediate} \xrightarrow[\underline{c}]{k_1} \text{6-MDHP} \xrightarrow[\underline{e}]{-2H^+-2e} \text{6-MP} \qquad (2)$$

At short times the current observed should be that predicted for a 2e process and at longer times it should approach that for a 4e process. The equation relating current to time for an ece mechanism is given by Equation 3.[68]

$$i_t = \frac{FAD^{1/2}C[n_1+n_2(1-e^{-kft})]}{t^{1/2}\pi^{1/2}} \qquad (3)$$

i_t = instantaneous current at time t in μA

n_1 = number of electrons involved in the first charge transfer step

n_2 = number of electrons involved in the second charge transfer step

t = elapsed time from the application of the potential in s

A = area of the electrode in cm^2

D = diffusion coefficient, $cm^2\ s^{-1}$

C = concentration of the electroactive species in mmoles/ℓ

F = 96,500 coulombs

Equation 3 can be rearranged as follows:

$$i_t = \frac{FAD^{1/2}C\,[n_1+n_2(1-e^{-k_f t})]}{\pi^{1/2}t^{1/2}}$$

$$\frac{i_t\pi^{1/2}t^{1/2}}{FAD^{1/2}C} - n_1 = n_2\,(1-e^{-k_f t}) \qquad \text{since } n_1=n_2$$

$$\frac{i_t\pi^{1/2}t^{1/2}}{n_2FAD^{1/2}C} - \frac{n_1}{n_2} = 1-e^{-k_f t}$$

$$\frac{i_t\pi^{1/2}t^{1/2}}{n_2FAD^{1/2}C} - 2 = -e^{-k_f t}$$

$$\ln\left[\frac{-i_t\,^{1/2}t^{1/2}}{n_2FAD^{1/2}C} + 2\right] = -k_f t$$

$$\frac{-\ln\left[\dfrac{-i_t\pi^{1/2}t^{1/2}}{n_2FAD^{1/2}C} + 2\right]}{t} = k_f \qquad (4)$$

In order to measure the homogeneous rate constant, k_f, the diffusion coefficient for 6-MTHP and the area of the PGE were first

determined. The area of the PGE used in this study was determined by monitoring the current vs. time curve for electrooxidation of 4.0 mM potassium ferrocyanide with a supporting electrolyte of 2.0 M KCl. The diffusion coefficient for ferrocyanide under these conditions is $6.29 \times 10^{-6} cm^2 s^{-1}$.[69] Oxidation of ferrocyanide is diffusion controlled and hence the area of the electrode could be calculated using the Cottrell equation (Equation 5):[70, 71]

$$it = \frac{nFAD^{1/2}C}{t^{1/2}\pi^{1/2}} \tag{5}$$

rearranges to

$$A = \frac{it^{1/2}\pi^{1/2}}{nFD^{1/2}C} \tag{6}$$

where all terms have been previously defined. The electrode area determined in this manner was $2.90 \times 10^{-2} cm^2 s$.

Using this value for the electrode area, the diffusion coefficient for 6-MTHP was determined assuming that the peak I_a electrooxidation was diffusion controlled. This was proved to be true because the product of $i \times t^{\frac{1}{2}}$ was constant for times as long as ca. 8s. Rearranging the Cottrell equation again gives Equation 7,

$$D = \left[\frac{it^{1/2}\pi^{1/2}}{nFAC} \right]^2 \tag{7}$$

which was used to give a diffusion coefficient of $6.32 \times 10^{-6} cm^2 s^{-1}$ for 6-MTHP.

The homogeneous solution rate constant for rearrangement of the primary quinonoid-dihydropterin to 6-MDHP was obtained by using

Equation 9 and values for D of $6.32 \times 10^{-6} cm^2 s^{-1}$ and A of $2.90 \times 10^{-2} cm^2$. The value of i used in the equation was the experimental value measured from current vs. time curves at time t. An average of these rate constants over a range of times gave a value of $3.1 \pm 0.1 \times 10^{-2} s^{-1}$ compared to $3.5 \pm 0.4 \times 10^{-2} s^{-1}$ obtained spectroelectrochemically.

Chemical oxidation of 6-MTHP. The rate constant for the rearrangement of the intermediate obtained by chemical oxidation of 6-MTHP was also determined and compared to the spectroelectrochemical results. One of the biggest problems with chemical oxidation is finding a suitable oxidant, one that is mild, quick, and which does not possess a significant u.v. absorbance in the wavelength region of interest. The oxidant chosen was iodine in an iodide solution buffered with phosphate to pH 7.0. In an iodide solution the actual oxidizing agent is I_3^-. The redox potential of I_3^- is great enough to oxidize both 6-MTHP and 6-MDHP. Consequently, a stoichiometric amount of I_2 was used so that only 6-MTHP would be oxidized to the putative quinonoid-dihydropterin. Spectral data was obtained using the same rapid scanning spectrometer used in spectroelectrochemical studies. One of the main problems with using iodine is that it is reduced to iodide which is colorless, but still exhibits a strong u.v. peak centered at 228 nm. This peak obscures the short wavelength band of both 6-MTHP and 6-MDHP. In fact with iodide solution in the reference beam of the RSS there is little useful spectral data in the region below ca. 240 nm.

Since iodine is a mild oxidizing agent[65] it was also felt that a good spectrum of the quinonoid intermediate could be obtained. Curve 1 of Figure 37A is the spectrum of 6-MTHP with iodide solution in both

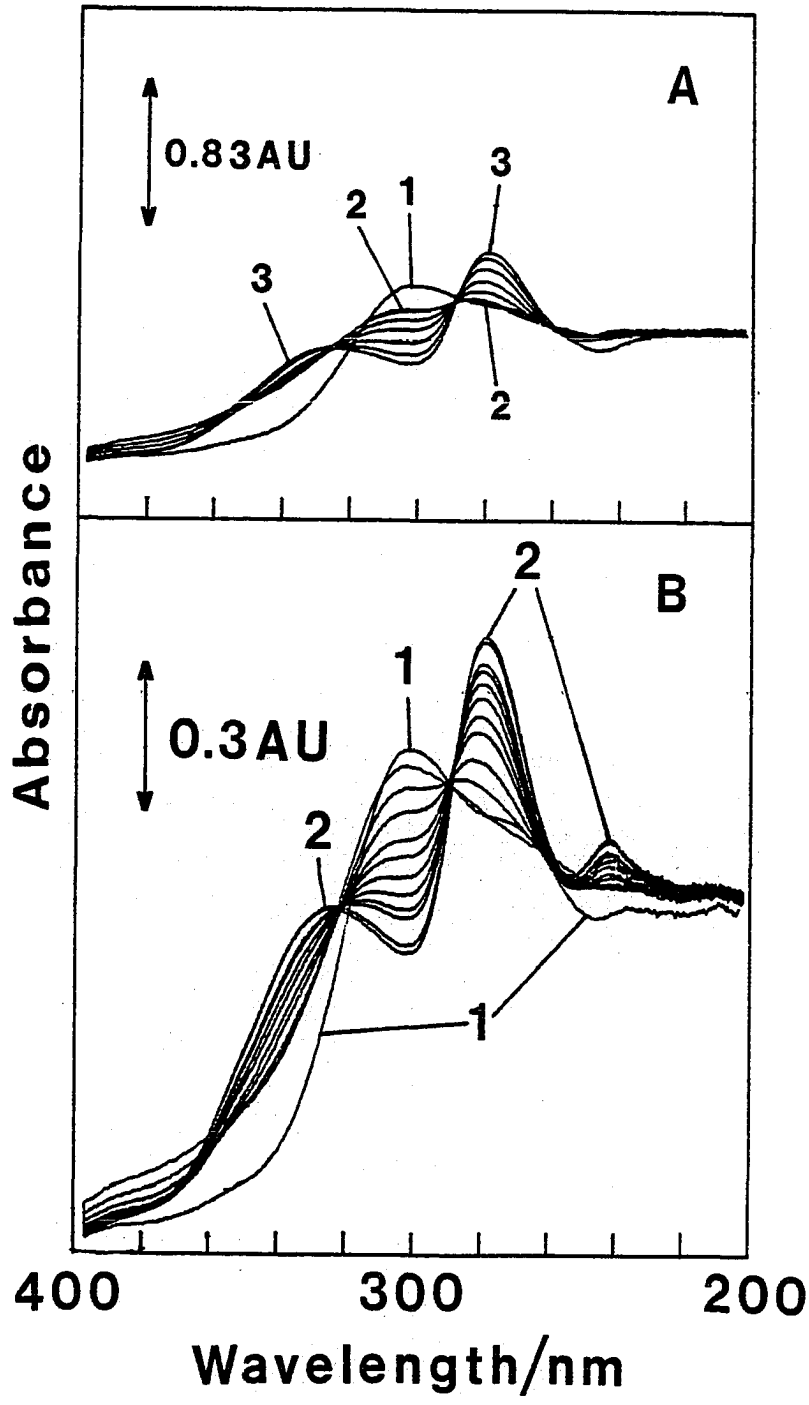


Figure 37. (A) Spectra of 0.054 mM 6-MTHP oxidizing in a solution of 0.039 mM I_2/0.2 mM iodide buffered to pH 7 with phosphate in a 1 cm quartz cuvette. Curve 1 is the spectrum immediately before oxidation. Curve 2 is the spectrum immediately after the addition of I_2. Curve 3 is the spectrum after complete decay of the intermediate and corresponds to the spectrum of 6-MDHP. Repetitive scans are 19s. (B) Same conditions as A except now a peak is observed at 242 nm.

the sample and reference cuvettes. Curve 2 is the spectrum after the introduction of iodine into the sample cell. This spectrum should be a good approximation of the spectrum for the quinonoid-dihydropterin (compare curve 2 of Figure 31). Curve 3 is the spectrum after complete decay of the intermediate species and exhibits u.v. maxima at 279 nm and 324 nm which corresponds to 6-MDHP. All spectral changes observed upon chemical oxidation of 6-MTHP are completely analogous to those observed upon electrochemical oxidation.

One cm quartz cuvettes were used in the spectrochemical study of 6-MTHP. As a result of the increased pathlength, compared to the thin-layer cell, the 6-MTHP concentration used was ca. 0.05 mM to keep the absorbance within the limits of the RSS. The rate constant for the chemical rearrangement of the intermediate generated from iodine oxidation of 6-MTHP was $0.0026\pm0.0003\,s^{-1}$. This compares with a value of $0.005\pm0.001\,s^{-1}$ for 0.1 mM 6-MTHP determined spectroelectrochemically.

Kaufman observed an u.v. peak around 240 nm in the enzymic oxidation of tetrahydropterins which he claimed as evidence for a hydroperoxy intermediate.[28,29] Occasionally, we have observed a similar u.v. peak at 242-243 nm in the chemical oxidation of 6-MTHP (Figure 37B). This peak was also observed when a 6-MTHP/iodide solution at pH 7 was allowed to air oxidize. However, this peak was observed only after complete oxidation of 6-MTHP. If the u.v. peak at 242 nm was characteristic of a hydroperoxy intermediate it should have been observed immediately after initiating the oxidation with iodine, not in the spectrum of the final product (curve 2, Figure 37B). 6-MDHP, the final product, has a short wavelength u.v. peak at 228 nm which has a high

molar absorptivity. It is possible that the increase in absorbance observed at 242 nm, which appears to be a peak, was really the beginning of the 6-MDHP u.v. peak at λ_{max} = 228 nm. The remaining part of this peak (λ_{max} = 228 nm) was probably obscured by the short wavelength iodide absorption.

Spectroelectrochemical Studies of 6-MDHP

Thin-layer spectroelectrochemical studies were also carried out on the intermediate generated when 6-MDHP is electrooxidized at peak II_a potentials. These studies were limited to solutions with pH values less than 5.6 because peak II_a is not observed in voltammetry at higher pH values. Cyclic voltammetry reveals that an intermediate is also generated by electrooxidation of 6-MDHP at peak II_a. This intermediate is responsible for reduction peak IV_c (see Figure 15A). Peaks III_a or III_a' do not have reversible peaks associated with them.

Curve 1 of Figure 38A is the spectrum of 0.5 M 6-MDHP at pH 2.0 (λ_{max} = 360, 274 (shoulder), and 250 nm) in the RVC thin-layer cell. Initiating the electrolysis at peak II_a potentials causes a decrease in absorbance throughout the wavelength range scanned except between 290-340 nm where an increase in absorbance was noted. The RVC working electrode was open-circuited immediately prior to recording curve 2 of Figure 38A. The spectrum continues to change in the manner described, but the change was extremely small. Curve 3 is the spectrum after the absorbance has stopped changing, i.e., the rearrangement of the intermediate has been completed. The only difference from the initial spectrum is the peak at 336 nm. If the potential is allowed to remain

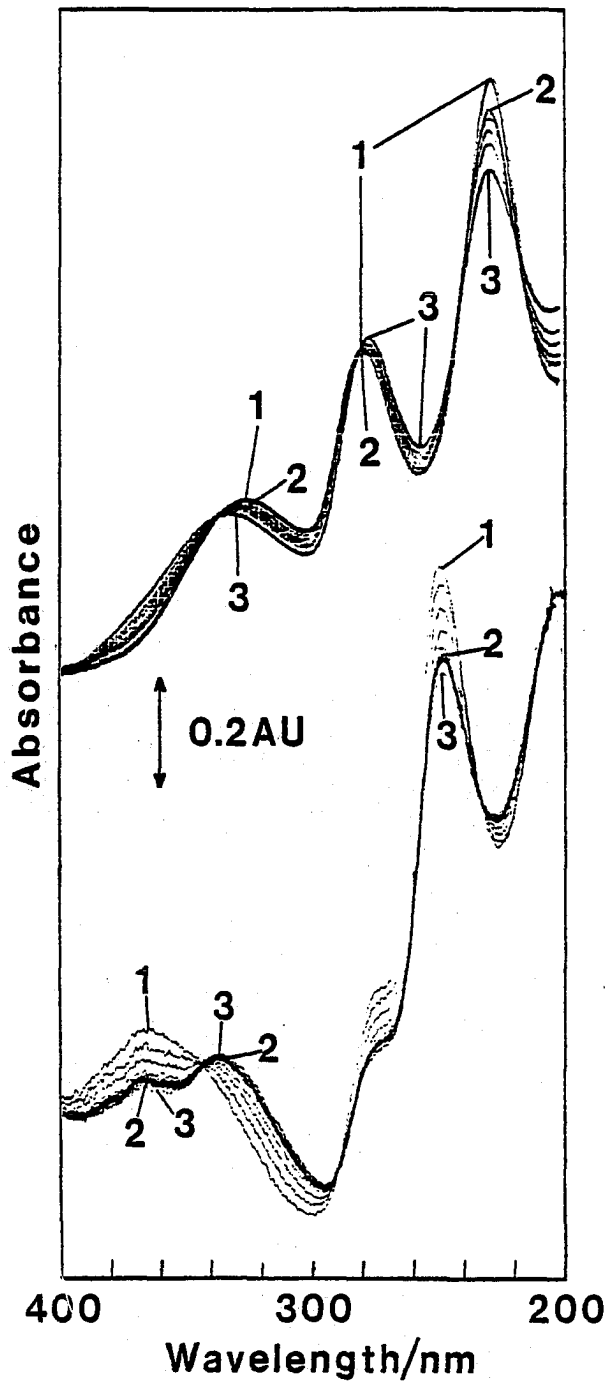


Figure 38. Spectra of 0.5 mM 6-MDHP electrolyzing at peak II_a potentials at a RVC electrode in several different phosphate buffers in a thin-layer cell. Curve 1 is the spectrum of 6-MDHP. Curve 2 is the spectrum immediately after open-circuiting the working electrode. Curve 3 is the spectrum after complete decay of the intermediate species. Repetitive scans are 19s in duration. (A) pH 2.0 and (B) pH 5.6.

on, this u.v. peak continues to shift to shorter wavelengths corresponding to the spectrum of 6-MP at pH 1 (λ_{max} = 324 nm).[59] Curve 3 in Figure 38A actually corresponds to a spectrum expected for a mixture of 6-MDHP and 6-MP. Similar results were obtained at this pH when the solution was electrooxidized at peak III_a potentials.

At pH 5.6 the basic pK_a of 6-MDHP has been exceeded thus the spectrum of 6-MDHP now exhibits u.v. maxima at 229 nm, 279 nm, and 325 nm (curve 1, Figure 38B). Upon application of the potential at peak II_a the absorbance of the two short wavelength peaks decreases somewhat. Curve 2 is the spectrum immediately after the working electrode is open-circuited after electrolyzing for 60s. The peak at 229 nm continues to decrease while the peak at ca. 279 nm begins to increase and shift to slightly shorter wavelengths. The long wavelength peak decreases and shifts to even longer wavelengths. The same changes in the spectra occur after electrooxidation of 6-MDHP at peak III_a potentials.

Kinetic studies. Absorbance vs. time curves observed immediately following electrooxidation of 6-MDHP in a thin-layer cell indicate that the behavior is not as simple as it appears in the above spectra. This is especially apparent when the A vs. t curves actually change directions long after the working electrode is open-circuited (Figure 39A). Plots of ln $|A-A_\infty|$ vs. time are not straight lines therefore the rearrangement of the intermediate cannot be a simple single first order process (Figure 39B). Analysis of A vs. t curves using a non-linear least squares program[72] shows that two first order processes occur with different rate constants. However it was not possible to determine

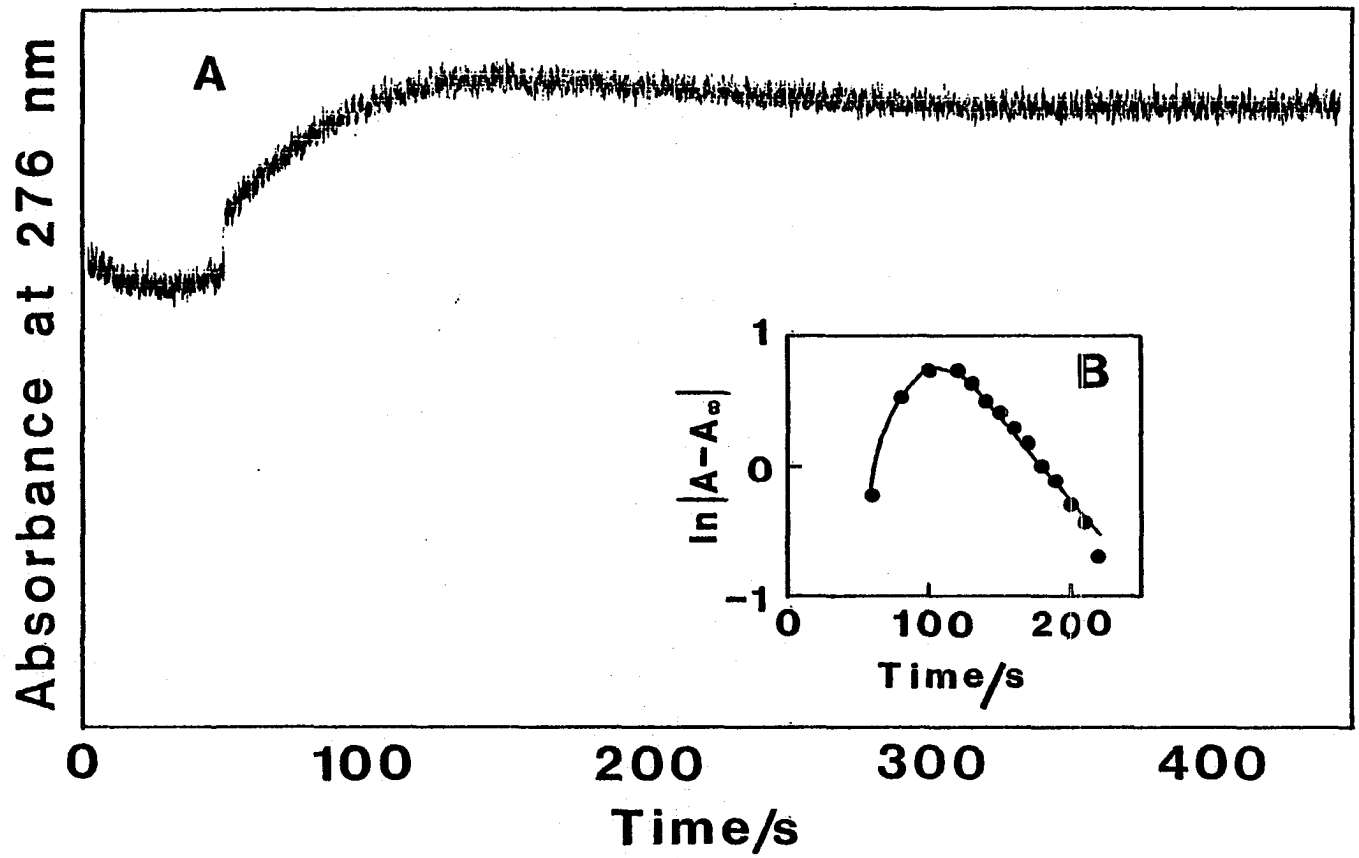
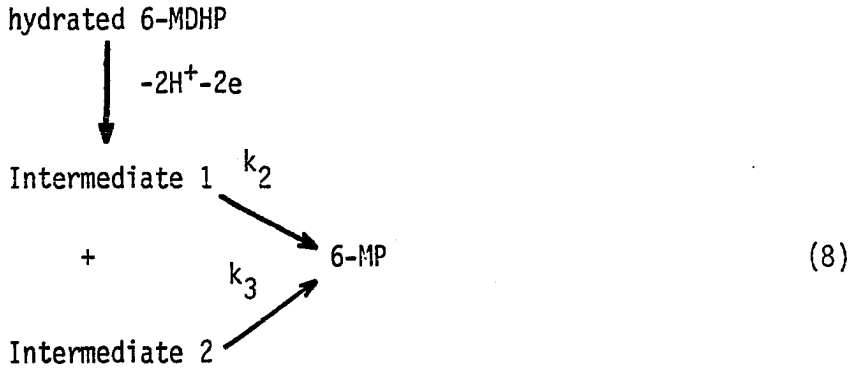


Figure 39. (A) Absorbance vs. time curve for the decay of the intermediate generated upon electrolysis of 0.5 mM 6-MDHP at 0.40V for 50s in pH 4.5 phosphate buffer, μ=0.5 M. (B) Plot of $\ln|A-A_\infty|$ vs. time for the decay curve in (A).

whether the two intermediates are both formed simultaneously in the electrooxidation (Equation 8) or the first intermediate rearranges to a second intermediate which rearranges to the product, 6-MP (Equation 9).



(8)

hydrated 6-MDHP $\xrightarrow{-2H^+-2e}$ Inter. 1 $\xrightarrow{k_2}$ Inter. 2 $\xrightarrow{k_3}$ 6-MP (9)

Unfortunately total absorbance changes were very small (often less than 0.08 absorbance units) and determination of the faster, first order rate constant, k_2, was quite unreliable because of the considerable noise present in the A vs. t curves. Values for the rate constant, k_3, of the slower reaction are reported in Table 11.

Table 11

Observed First Order Rate Constants for Chemical Reaction of the Intermediate Formed Upon Peak II_a and Peak III_a Electrooxidation of 6-MDHP[a]

pH[b]	λ/nm[c]	k_3^dobs/s^{-1}
	Electrooxidation at peak II_a potentials	
3.0	252	0.0028±0.0006
4.5	231	0.0027±0.001
5.6	304	0.021±0.003
	Electrooxidation at peak III_a potentials	
3.0	252	0.0013±0.003
4.1	276	0.0091±0.0005
4.5	276	0.0035±0.0003
5.6	304	0.010±0.001

[a]Data obtained by thin-layer spectroelectrochemistry using an optically-transparent RVC electrode.

[b]Phosphate buffers having an ionic strength of 0.5 M.

[c]Wavelength employed to measure A vs. t curves.

[d]Value of the second, or smaller, rate constant. Reliable values of k_2 could not be obtained.

CHAPTER III

DISCUSSION

Reaction Scheme

6-MTHP exhibits up to four voltammetric oxidation peaks at a PGE of which the first three were studied in detail. Peak I_a is a $2\underline{e}$-$2H^+$ quasi-reversible redox reaction of 6-MTHP giving an unstable product which may be detected as cyclic voltammetric peak I_c or by its spectrum in thin-layer spectroelectrochemical experiments. This intermediate rearranges in a first order chemical follow-up reaction yielding 6-MDHP as the final product. The intermediate generated upon electrooxidation of 6-MTHP (I, Figure 40) at peak I_a is proposed to be an unstable quinonoid-dihydropterin. There are in fact five possible structures for such a quinonoid intermediate (II_a-II_e, Figure 40) and there is little or no evidence to exclusively favor any one of these structures. Peak I_c is the $2\underline{e}$-$2H^+$ reduction of this intermediate back to 6-MTHP.

The quinonoid-dihydropterin (II_a-II_e, Figure 40) rearranges to 6-MDHP (III, Figure 40) in a first order process characterized by rate constant k_1 (Tables 7, 8, and 9). Experiments with 6-MDHP reveal that it is responsible for oxidation peaks II_a, III_a, and adsorption peak III'_a.

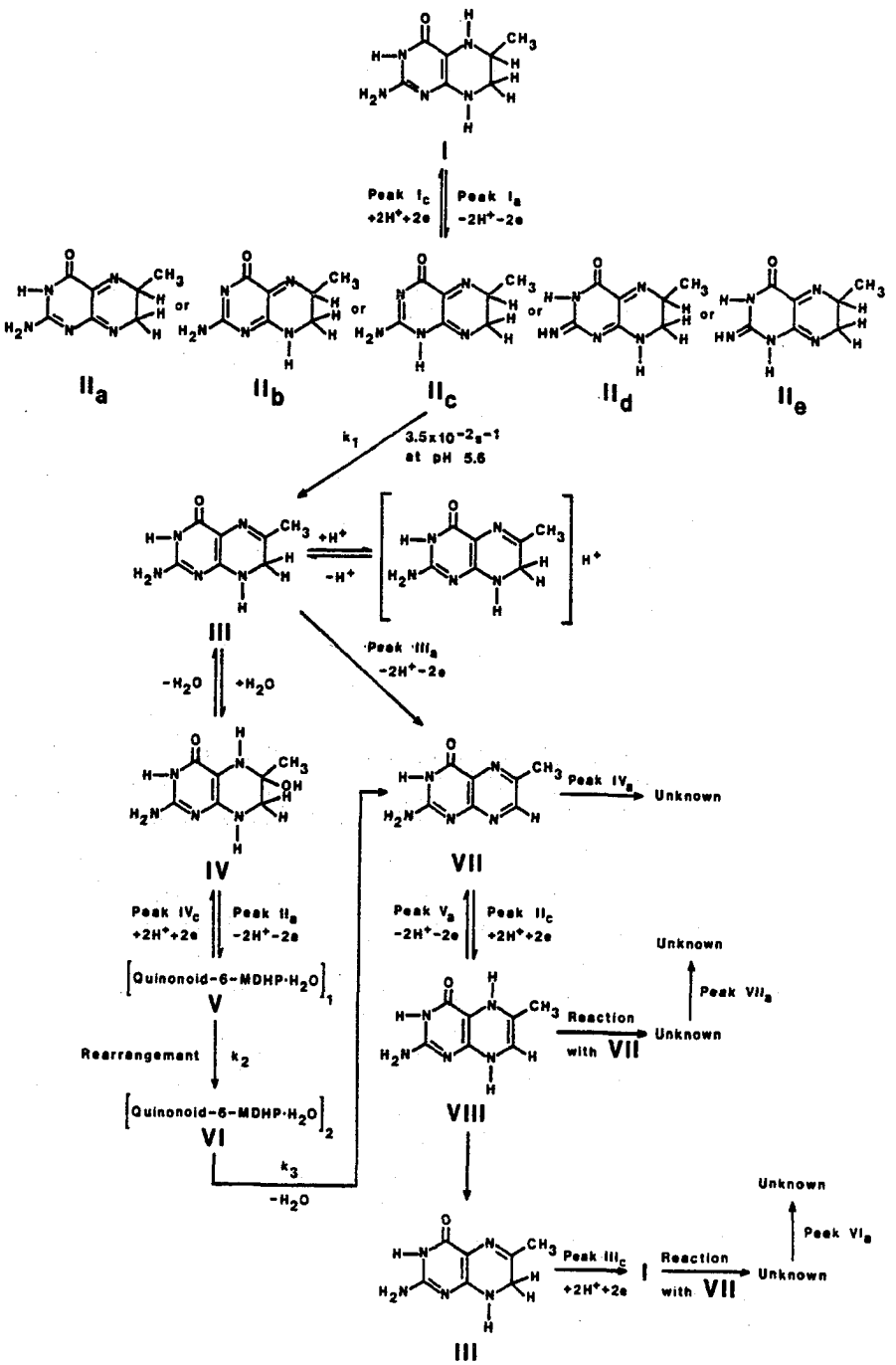
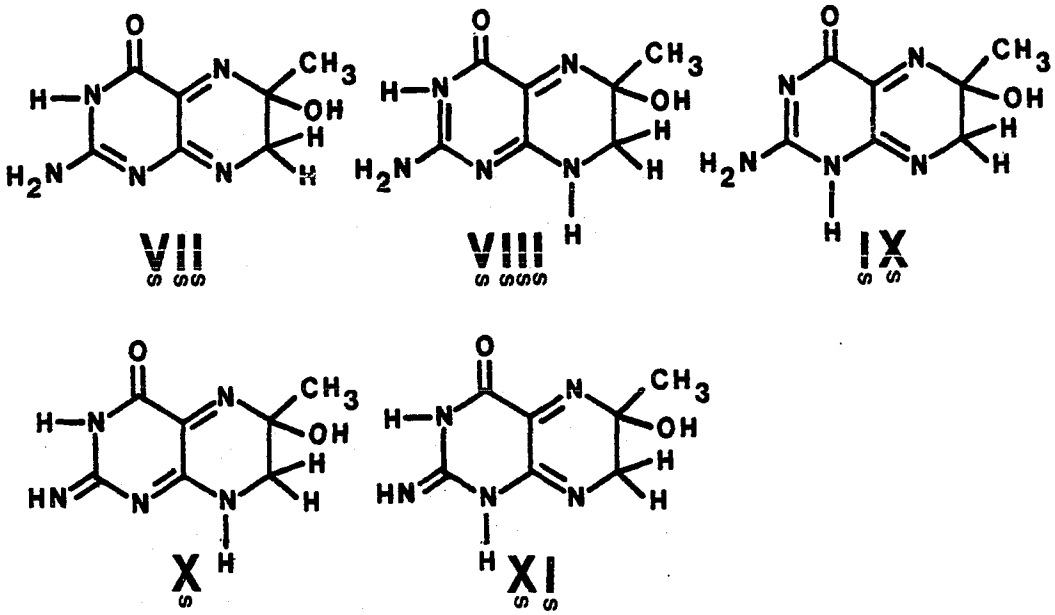


Figure 40. Reaction scheme proposed to explain the oxidation and reduction peaks observed upon cyclic voltammetry of 6-MTHP at the PGE.

Oxidation peak II_a of 6-MDHP appears below pH 5.6 and electrolysis at these potentials also causes peak III_a to disappear. Sweep rate studies also reveal that peak II_a decreases with increasing sweep rate while peak III_a (and at sweep rates above ca. 100 mV s^{-1} peak III_a') increase. When 6-MDHP is electrooxidized at either peak II_a or III_a potentials the ultimate product is 6-MP (VII, Figure 40). These results suggest that there are two electrochemically oxidizable species which are in equilibrium.

A clue as to the identity of the two species responsible for peaks II_a and III_a comes from the investigation of 7,8-DHP which was discussed in the Introduction.[54] This compound exhibited voltametric oxidation peaks and electrolysis products which could only be a result of covalent hydration of the N(5)-C(6) bond. It is proposed that 6-MDHP (III, Figure 40) undergoes a similar hydration forming hydrated 6-MDHP (IV, Figure 40). Voltammetry indicates that this hydration is acid catalyzed and that at any pH below 5.6 the covalently hydrated species exists in equilibrium with non-hydrated 6-MDHP (III, Figure 40). Hydrated 6-MDHP has a structure very similar to 6-MTHP, thus it should be oxidized at potentials very close to those for 6-MTHP. Since the structure and the oxidation potential for hydrated 6-MDHP are similar to 6-MTHP, it might be expected that the mechanism would be similar. Consequently peak II_a is proposed to be a $2e^-2H^+$ electrooxidation of covalently hydrated 6-MDHP to an unstable quinonoid intermediate ([Quinonoid-6-MDHP$\cdot H_2O$], V, Figure 40). This quinonoid can once again exist as one of five possible structures (VII-XI). A vs. t curves reveal that the intermediate formed by electrooxidation of covalently hydrated



6-MDHP rearranges via two first order processes to 6-MP. It is not possible to determine from the experimental evidence whether two quinonoids are formed simultaneously, a single quinonoid is formed which subsequently rearranges to a more stable form, or some other intermediate is involved. It seems more plausible that a single quinonoid is formed (V, Figure 40) which rearranges to a more stable form (VI, Figure 40) characterized by rate constant k_2. This second quinonoid rearranges and dehydrates to 6-MP in a slower process characterized by rate constant k_3. Cyclic voltammetry of 6-MDHP at low pH provides additional support for this mechanism. After scanning peak II_a and reversing the sweep direction peak IV_c appears to be

composed of two peaks, a normal peak followed by a broad peak at more negative potentials (Figure 15A,B). It is possible that the first peak is due to reduction of V (Figure 40) and the broad peak due to reduction of VI (Figure 40).

Peak III_a for 6-MDHP is observed throughout the pH range and must be due to the irreversible $2\underline{e}$-$2H^+$ electrooxidation of the non-hydrated form of 6-MDHP (III, Figure 40) to 6-MP.

The reduction peaks observed in the cyclic voltammetry of 6-MTHP have been studied previously by Kwee and Lund[25,49] and Komenda.[51] Peak III_c (Figure 14) is due to the reduction of 6-MDHP (III, Figure 40) in a $2\underline{e}$-$2H^+$ process to 6-MTHP (I, Figure 40). 6-MP (VII, Figure 40) is also reduced in a $2\underline{e}$-$2H^+$ process at peak II_c (Figure 14) to an unstable 6-methyl-5, 8-dihydropterin (VIII, Figure 40) which rapidly rearranges to 6-MDHP (III, Figure 40). Oxidation peak V_a (Figure 24A) is the quasi-reversible oxidation of VIII back to 6-MP (VII, Figure 40).

After sweeping through reduction peaks II_c and III_c of 6-MTHP or 6-MDHP two minor oxidation peaks are observed on the subsequent positive sweep (peaks VI_a and VII_a). These peaks are clearly visible in Figure 15. Peak VII_a may be observed if the potential is switched immediately after passing through reduction peak II_c (Figure 24A). In order to observe oxidation peak VI_a it is necessary that the negative sweep also passes through peak III_c. The size of both peaks VI_a and VII_a decrease relative to reduction peaks II_c and III_c if the sweep rate is decreased. This leads to the conclusion that the species responsible for these oxidation peaks are unstable. Figure 24B also illustrates this by holding the potential just negative of peak II_c for

10s then sweeping in a positive direction. Peak VII_a is barely visible under these conditions indicating that the species responsible for it has disappeared.

If a 6-MDHP solution is allowed to partially air oxidize, cyclic voltammetry reveals that peaks VI_a and VII_a are considerably larger. This leads us to suggest that perhaps peak VII_a is due to a reaction product formed between 6-MP and the unstable peak II_c reduction product 6-methyl-5, 8-dihydropterin (VIII, Figure 40). It is also possible that peak VI_a may be due to the electrooxidation of a reaction product of 6-MP and 6-MTHP (the peak III_c reduction product).

The intermediate generated from peak I_a electrooxidation of 6-MTHP and peak II_a electrooxidation of 6-MDHP have been studied using primarily thin-layer spectroelectrochemistry. Rate constants for these reactions have been determined and the intermediate from 6-MTHP has been found to be most reactive between pH 5.5-6.0. However there does not seem to be a general trend for the stability of the intermediate from peak II_a oxidation of 6-MDHP.

CHAPTER IV

EXPERIMENTAL

Chemicals. 6-MTHP as the dihydrochloride salt was obtained from Calbiochem and Sigma. 6-MDHP as the monohydrochloride was obtained from Calbiochem. 6-MTHP was generally contaminated with small amounts of 6-MP and 6-MDHP. 6-MDHP was likewise contaminated with a small amount of 6-MP. This contamination could be easily detected voltammetrically and could be quantitated using high performance liquid chromatography (HPLC).

When large amounts of 6-MDHP and 6-MP were detected in 6-MTHP solutions prior to electrolysis, such solutions were preelectrolyzed at a large pyrolytic graphite electrode at a potential sufficiently negative to reduce both 6-MP and 6-MDHP to 6-MTHP. On occasion, test solutions were not preelectrolyzed. Under these circumstances a correction was applied to observed n-values corresponding to the fraction of oxidized species present as determined by HPLC.

Phosphate buffers were used throughout which had an ionic strength of 1.0 M before 1:1 dilution with the appropriate pterin stock solution yielding a final ionic strength of 0.5 M.[73] Nitrogen used for deaeration of all solutions was equilibrated with water in a bubbling chamber. Mercury used was triply distilled (Bethlehem Apparatus, Hellertown, PA).

Apparatus. A thin-layer cell using an optically transparent reticulated vitreous carbon electrode was constructed similar to the design of Norvell and Mamantov.[74] Modification of the cell to exclude atmospheric oxygen was done similar to the design of Norris, et al.[75] as well as Hawkridge and Kuwana.[76] This particular cell has already been used for several earlier spectroelectrochemical investigations.[54,55]

Figure 41 shows the cell design as it was eventually utilized for spectroelectrochemical studies. For work in the ultraviolet region it was necessary to use quartz microscope slides (A) 2"x1"x1/16" (Esco Optics Products, Oak Ridge, NJ). A thin slice of reticulated vitreous carbon (RVC) of 100 ppi porosity (Fluorocarbon Co., Anaheim, CA) 12 mm x 30 mm x 0.7 mm (B) as well as a piece of platinum foil 18 mm x 23 mm (C) were sandwiched between the slides and the edges of the slides were sealed with epoxy cement (Epoxi-Patch, Hysol Division, The Dexter Corp., Olean, NY). The platinum foil acted as a counter electrode and the close proximity to the RVC working electrode was necessary to reduce IR drop. Openings were left at the top, side, and bottom of the cell for attachment of other cell components. Connections to the cell for valves were made using 4 mm I.D. soft glass tubing (D) with a female luer taper on one end (7602-35, Ace Glass Co., Vineland, NJ). Dimensions for the top and side connections were kept as short and compact as possible. The valves (E) for filling the cell and for opening it to the reference electrode were miniature inert valves (86725, HV1-1, Hamilton Co., Reno, NV). The Ag/AgCl reference electrode compartment (F) was fashioned from a female luer taper and a shortened (ca. 7 mm) 10/30 ȿ inner ground glass joint. A silver wire coated with silver chloride[76] was epoxied into a shortened

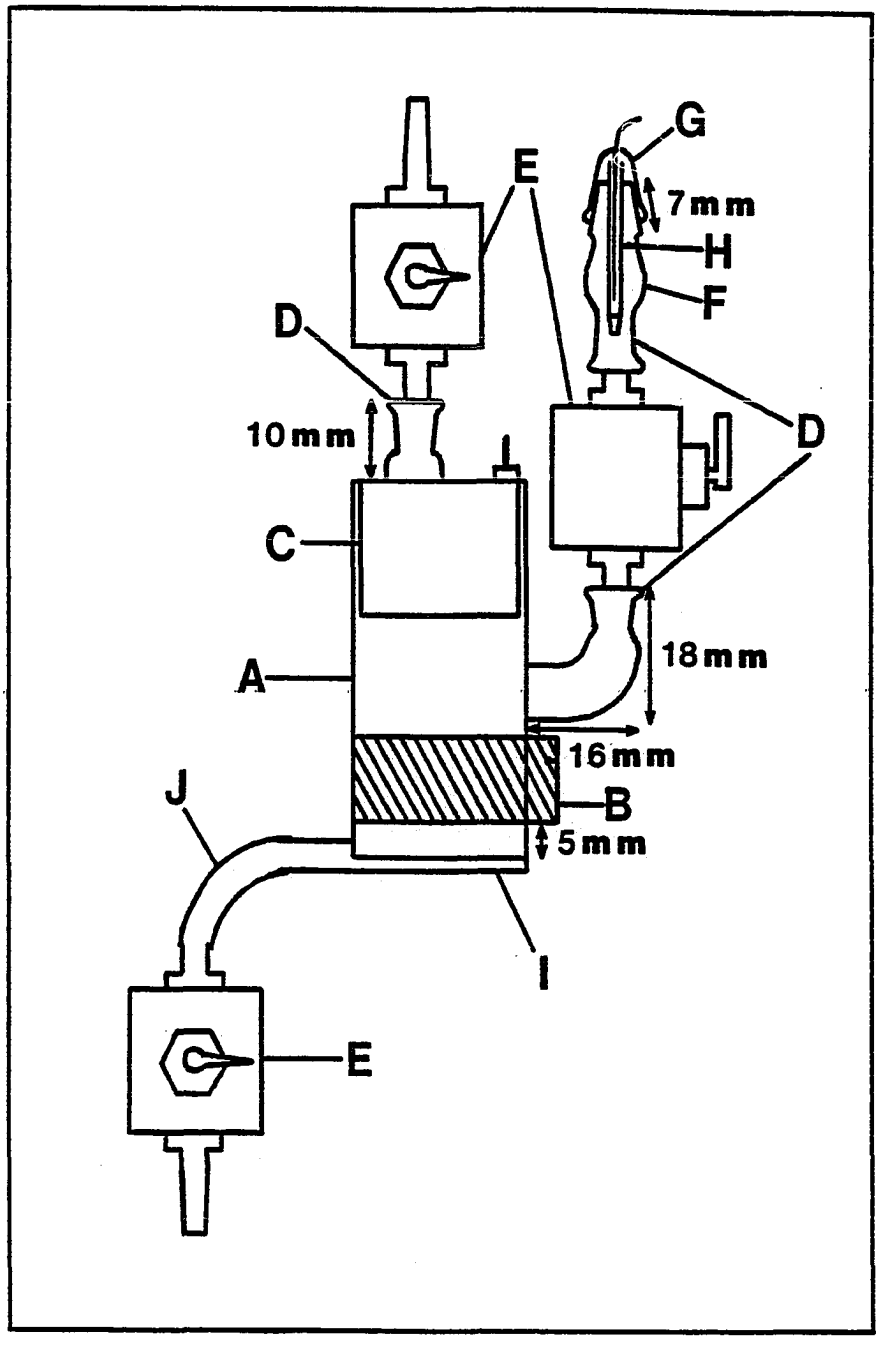


Figure 41. Design of RVC thin-layer cell for spectroelectrochemical studies in the absence of atmospheric oxygen. (A) quartz microscope slides (2" x 1" x 1/16"). (B) RVC electrode (100 ppi, 12 mm x 30 mm x 0.7 mm). (C) Platinum foil (18 mm x 23 mm). (D) 4 mm i.d. glass tubing. (E) Valves. (F) Ag/AgCl reference electrode compartment. (G) Cap. (H) Reference tube. (I) Glass tubing. (J) Surgical rubber tubing.

10/30 ₹ outer ground glass joint (G) and suspended in the reference tube (H). Reference tube (H) (117147 Leeds and Northrup, North Wales, PA) had a small glass frit at the tip and was filled with a 1.0 M KCl solution. The bottom of the cell was closed off with a piece of glass tubing (I) cut in half and epoxied to the bottom. Attached to the glass tubing was a short length of surgical rubber tubing (J) and sealing was accomplished either by the use of another valve or a pinch clamp.

Filling of the cell was accomplished by attaching an aspirator to the top valve and drawing a N_2-bubbled solution into the cell through the surgical rubber tubing. The side arm and reference electrode compartment (F) were filled by closing off the tubing and forcing the solution out of the sidearm into the reference electrode compartment by attaching low pressure nitrogen to the top valve. When the thin-layer cell was placed in a spectrophotometer it was important to make sure that the valve to the reference electrode was opened to provide electrical contact.

Initial removal of air bubbles from the RVC working electrode before filling with the test solution was accomplished by alternately aspirating distilled water and air through the cell. The blast of water which follows when the inlet to the cell is reinserted in the water clears the air bubbles from the RVC.

Optical measurements were performed on a Harrick Rapid Scanning Spectrometer and signal processing module (Harrick Scientific Co., Ossining, NY). Repetitive scans were recorded on a Hewlett-Packard 7001A X-Y recorder or a Houston Instruments 2000 X-Y recorder.

Construction of the pyrolytic graphite microelectrodes has been described in the Experimental Chapter of Part I. Linear and cyclic sweep voltammetry were carried out with an instrument based on conventional operational amplifier design.[77] Cyclic voltammograms at very high sweep rates (>500 mVs^{-1}) were recorded on a Tektronix Model 5031 dual beam storage oscilloscope equipped with a Tektronix Model 70 camera. The cell used for the voltammetric experiments contained a mercury pool counter electrode and electrical connection to a saturated calomel reference electrode (SCE) was made through a Luggin capillary. All potentials are referred to the SCE at 25°C except in the thin-layer experiments. The potentials in the thin-layer experiments are referred to the SSCE (silver-silver chloride reference electrode). Controlled potential electrolysis and coulometry were performed either with a three compartment cell containing an SCE reference electrode and a platinum gauze counter electrode, or with the thin-layer RVC cell discussed above. Potential was controlled with a Princeton Applied Research (PAR) Model 173 or a Wenking Model LT 73 potentiostat in the large electrolysis cell. In the thin-layer cell potential control was achieved using a PAR 174A Polarographic Analyzer or the cyclic voltammetry unit referred to above. Current integration was accomplished with a Koslow Scientific Model 541 Coulometer or a PAR 379 Digital Coulometer. Current integration for electrolysis in the thin-layer RVC cell was done by calculating the area under a current-time curve.

Analysis of 6-MTHP for 6-MDHP and 6-MP utilized a high performance chromatographic method.[12,66] The HPLC unit consisted of a Milton

Roy Instrument mini pump (St. Petersburg, FL), a Waters Associates (Milford, MA) Model U6K injector, and a Waters Associates Model 440 u.v. absorbance dectector. The column was a Partisil strong cation exchanger with a particle diameter of 10μ. Eluants used were continuously deaerated by N_2-bubbling. Any trapped oxygen on the column (from using non-deaerated buffers) could be reduced by injecting 10 ul of 1.0 M sodium dithionite ($Na_2S_2O_4$) periodically. The eluant buffer was pH 6.1 phosphate of ionic strength 0.1 M. The buffer was prepared by dissolving 9.33 g of $NaH_2PO_4 \cdot H_2O$ and 1.53 g of Na_2HPO_4 in a small amount of distilled water and then filling to the mark with distilled water in a 1 ℓ volumetric flask.

CHAPTER V

SUMMARY

The electrochemical oxidation of 6-MTHP and 6-MDHP was studied using a variety of electrochemical techniques. It was found that 6-MTHP is electrooxidized in a $2\underline{e}$-$2H^+$ quasi-reversible process to an unstable quinonoid-dihydropterin which was studied primarily using thin-layer spectroelectrochemistry. A new thin-layer cell for the study of air-sensitive compounds was developed during the course of these investigations and was used to study the kinetics of the rearrangement of the intermediate. Rearrangement of the intermediate generated 6-MDHP, which was found to exist in two forms, a non-hydrated species and a covalently hydrated species. Covalently hydrated 6-MDHP is oxidixed in a $2\underline{e}$-$2H^+$ quasi-reversible process to another quinonoid type species which subsequently rearranges to a more stable form before rearranging and dehydrating to 6-MP. Non-hydrated 6-MDHP is also electrolyzed in a $2\underline{e}$-$2H^+$ process directly to 6-MP. Several other rather minor processes were detected, but were not studied in greater detail.

CHAPTER VI

REFERENCES

1. S. Kaufman, Proc. Nat. Acad. Sci. U.S.A., 50 (1963) 1085.

2. A. R. Brenneman and S. Kaufman, Biochem. Biophys. Res. Commun., 17 (1964) 177.

3. W. Lovenberg, E. Jequier, and A. Sjoerdsma, Science, 155 (1967) 217.

4. T. Nagatsu, M. Levitt, and S. Udenfriend, J. Biol. Chem., 239 (1964) 2910.

5. R. Shiman, M. Akino, and S. Kaufman, J. Biol. Chem., 246 (1971) 1330.

6. F. J. Maclean, I. Fujita, H. S. Forrest, and J. Myers, Science, 149 (1965) 636.

7. F. J. Maclean, I. Fujita, H. S. Forrest, and J. Myers, Plant Physiol., 41 (1966) 774.

8. A. Tietz, M. Lindberg, and E. P. Kennedy, J. Biol. Chem., 239 (1964) 4081.

9. A. Albert in Chemistry and Biology of Pteridines, W. Pfleiderer (Ed.), W. de Gruyter, Berlin, 1975, p. 1.

10. S. Kaufman, J. Biol. Chem., 234 (1959) 2677.

11. S. Kaufman, J. Biol. Chem., 239 (1964) 332.

12. S. W. Bailey and J. E. Ayling, J. Biol. Chem., 253 (1978) 1598.

13. M. Osanai and H. Rembold, Z. Physiol. Chem., 352 (1971) 1359.

14. J. E. Ayling, G. R. Boehm, S. C. Textor, and R. A. Pirson, Biochemistry, 12 (1973) 2045.

15. Y. Numata, T. Kato, T. Nagatsu, T. Sugimoto, and S. Matsuura, Biochim. Biophys. Acta, 480 (1977) 104.

16. T. Nagatsu, K. Mizutani, I. Nagatsu, S. Matsuura, and T. Sugimoto, Biochem. Pharmacol., 21 (1972) 1945.

17. S. Kaufman, J. Biol. Chem., 245 (1970) 4751.

18. S. Kaufman, Biochim. Biophys. Acta, 27 (1958) 428.

19. S. Kaufman and B. Levenberg, J. Biol. Chem., 234 (1959) 2683.

20. S. Kaufman in Pteridine Chemistry, W. Pfleiderer and E. C. Taylor (Eds.) Pergammon, London, 1964, p. 309.

21. N. N. Osborne, P. B. Guthrie, and V. Neuhoff, Biochem. Pharmacol., 25 (1976) 925.

22. M. C. Archer and K. G. Scrimgeour, Can. J. Biochem., 48 (1970) 278.

23. P. Hemmerich in Pteridine Chemistry, W. Pfleiderer and E. C. Taylor (Eds.), Pergammon, London, 1964, p. 163, 323.

24. M. Viscontini and A. Bobst, Helv. Chim. Acta, 48 (1965) 816.

25. S. Kwee and H. Lund, Biochim. Biophys. Acta, 297 (1973) 285.

26. A. Bobst, Helv. Chim. Acta, 50 (1967) 1480.

27. D. Ege-Serpkenci, Ph.D. Dissertation, University of Oklahoma, 1982.

28. S. Kaufman in Chemistry and Biology of Pteridines, W. Pfleiderer (Ed.), W. de Gruyter, Berlin, 1975, p. 291.

29. C. Huang, E. E. Max, and S. Kaufman, J. Biol. Chem., 248 (1973) 4233.

30. S. Kaufman, Adv. Exp. Med. Biol., 74 (1976) 91.

31. G. Moad, C. L. Luthy, and S. J. Benkovic, J. Am. Chem. Soc., 101 (1979) 6068.

32. G. A. Hamilton in Progress in Bioorganic Chemistry, E. T. Kaiser and F. J. Kezdy (Eds.), Vol. 1, Wiley-Interscience, New York, 1971, p. 141.

33. S. W. Bailey and J. E. Ayling, J. Biol. Chem., 255 (1980) 7774.

34. H. I. X. Mager in Chemistry and Biology of Pteridines, W. Pfleiderer (Ed.), W. de Gruyter, Berlin, 1975, p. 753.

35. M. Viscontini and T. Okada, Helv. Chim. Acta, 50 (1967) 1492.

36. G. R. Gapski, J. M. Whiteley, and F. M. Huennekens, Biochemistry, 10 (1971) 2930.

37. J. A. Jongejan, H. I. X. Mager, and W. Berends in Chemistry and Biology of Pteridines, R. L. Kisliuk and G. M. Brown (Eds.), Elsevier, New York, 1979, p. 241.

38. J. A. Blair and A. J. Pearson, J. Chem. Soc. Perkin II, (1974) 80.

39. A. J. Pearson, Chem. Ind., (1974), 233.

40. J. A. Blair, A. J. Pearson, and A. J. Robb, J. Chem. Soc. Perkin II, (1975) 18.

41. J. A. Blair and A. J. Pearson, J. Chem. Soc. Perkin II, (1975) 245.

42. S. Milstein and S. Kaufman, J. Biol. Chem., 250 (1975) 4777.

43. P. A. Friedman, D. B. Fisher, E. S. Kang, and S. Kaufman, Proc. Nat. Acad. Sci. U.S.A., 70 (1973) 552.

44. S. Kaufman and E. E. Max in Phenylketonuria, H. Bickel, F. P. Hudson, and L. I. Wolf (Eds.), G. Thieme, Stuttgart, (1971) p. 12.

45. M. C. Archer and K. G. Scrimgeour, Can. J. Biochem., 48 (1970) 526.

46. K. Kretzschmar and W. Jaenicke, Z. Naturforsch, Teil B, 26 (1971) 225.

47. K. Kretzschmar and W. Jaenicke, Z. Naturforsch, Teil B, 26 (1971) 999.

48. J. Pradáč, J. Pradácová, D. Homolka, J. Koryta, J. Weber, K. Slavík, and R. Cihar, J. Electroanal. Chem., 74 (1976) 205.

49. H. Lund in Chemistry and Biology of Pteridines, W. Pfleiderer (Ed.), W. de Gruyter, Berlin, (1975) 645.

50. S. Kwee and H. Lund, Bioelectrochem. Bioenerg., 6 (1979) 441.

51. J. Komenda, Collect. Czech. Chem. Commun., 24 (1959) 903.

52. Y. Asahi, Yakugaku Zasshi, 79 (1959) 1554.

53. L. G. Karber and G. Dryhurst, J. Electroanal. Chem., 136 (1982) 271.

54. R. Raghavan and G. Dryhurst, J. Electroanal. Chem., 129 (1981) 189.

55. D. Ege-Serpkenci and G. Dryhurst, Bioelectrochem. Bioenerg., 9 (1982) 175.

56. J. M. Whiteley and F. M. Huennekens, Biochemistry, 6 (1967) 2620.

57. W. Pfleiderer and H. Zondler, Chem. Ber., 99 (1966) 3008.

58. R. L. Blakely in The Biochemistry of Folic Acid and Related Pteridines, A. Neuberger and E. L. Tatum (Eds.), North-Holland Pub. Co., Amsterdam, 1969, p. 62, 67.

59. J. H. Mowat, J. H. Booth, B. L. Hutchings, E. L. R. Stokstad, C. W. Waller, R. B. Angier, J. Semb, D. B. Cosulich, and Y. Subba Row, J. Am. Chem. Soc., 70 (1948) 14.

60. K. Uyeda and J. C. Rabinowitz, Anal. Biochem., 6 (1963) 100.

61. G. Dryhurst, Electrochemistry of Biological Molecules, Academic Press, New York, 1977.

62. R. S. Nicholson, Anal. Chem., 37 (1965) 1315.

63. R. H. Wopschall and I. Shain, Anal. Chem., 39 (1967) 1514.

64. A. J. Bard and L. R. Faulkner, Electrochemical Methods: Fundamentals and Applications, John Wiley & Sons, New York, 1980, Chapter 12.

65. D. A. Skoog and D. M. West, Fundamentals of Analytical Chemistry, 2nd Edition, Holt, Rinehart, and Winston, New York, 1969, p. 814.

66. S. W. Bailey and J. E. Ayling in Chemistry and Biology of Pteridines, W. Pfleiderer (Ed.), W. de Gruyter, Berlin, 1975, p. 633.

67. H. H. Willard, L. L. Merritt, Jr., and J. A. Dean, Instrumental Methods of Analysis, 5th Edition, D. Van Nostrand, New York, 1974, p. 533.

68. G. S. Alberts and I. Shain, Anal. Chem., 35 (1963) 1859.

69. R. N. Adams, Electrochemistry at Solid Electrodes, Marcel Dekker, New York, 1969, p. 219.

70. ibid., p. 50.

71. F. G. Cottrell, Z. Physik. Chem., 42 (1902) 385.

72. Non-linear least squares program employs an optimizing routine written by Dr. E. Enwall incorporating an algorithm by Dr. W. Marquardt, J. Soc. Indust. Appl. Math., II (1963) 431.

73. G. D. Christian and W. C. Purdy, J. Electroanal. Chem., 3 (1962) 363.

74. V. E. Norvell and G. Mamantov, Anal. Chem., 49 (1977) 1470.

75. B. J. Norris, M. L. Meckstroth, and W. R. Heineman, Anal. Chem., 48 (1976) 630.

76. F. M. Hawkridge and T. Kuwana, Anal. Chem., 45 (1973) 1021.

77. G. Dryhurst, M. Rosen, and P. J. Elving, Anal. Chim. Acta, 42 (1968) 143.

PART III

ELECTROCHEMISTRY OF 5-METHYL-5,6,7,8-TETRHYDROPTERIN

CHAPTER I

INTRODUCTION

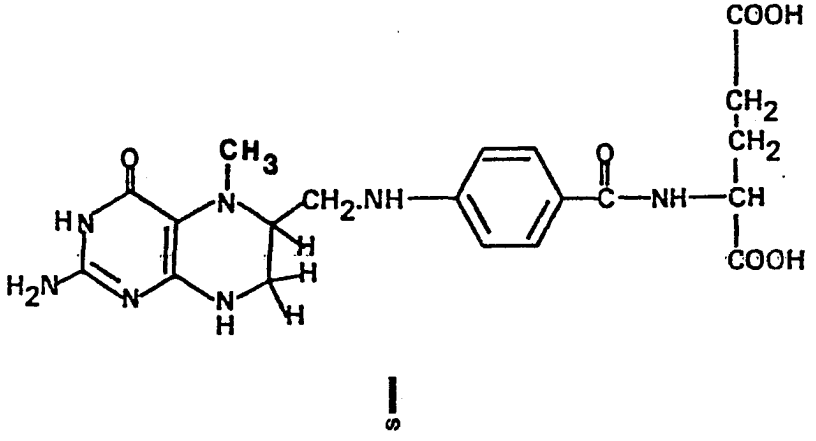
Reduced or unconjugated pterins have been known for years to be cofactors for a number of biologically important enzymic hydroxylation reactions[1-3] as well as other enzymic reactions *in vivo*[4-6] (see more detailed discussion in Introduction of Part II). Recently several detailed reports of the electrochemical oxidation of various methylated tetrahydropterins have been published.[7-10] These studies have helped give a greater understanding of the redox properties of reduced pterin compounds.

So-called pseudo cofactors with the highest activity compared to the natural cofactor, tetrahydrobiopterin, are those which have a substituent at the C(6)-position.[11] Tetrahydropterins with substituents at N(8) do not show any cofactor activity.[12] However, they do not inhibit the hydroxylation reaction in the presence of an active cofactor either.[13]

Nagatsu, *et al.* have reported however that all tetrahydropterins with a substituent in the N(5)-position are potent inhibitors when 6,7-DMTHP is used as the active cofactor.[13] The inhibitor activity

decreases in the following order: 5-methyl-6,7-diphenyltetrahydropterin > 5-benzyltetrahydropterin > 5-benzyl-6,7-dimethyltetrahydropterin >5-methyltetrahydropterin ≈ 5,6,7-trimethyltetrahydropterin.

Studies of various N(5)-methylated tetrahydropterins have been done because these compounds are model compounds for 5-methyltetrahydrofolic acid (I) (5-MTHF).[14,15] 5-MTHF is

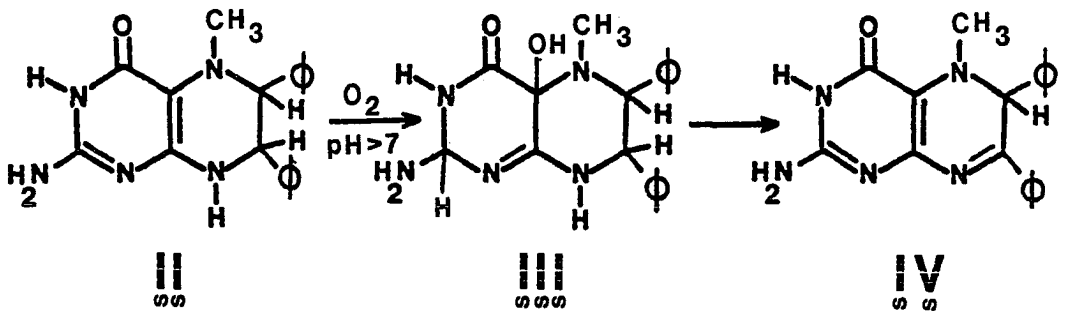


I

often the source of a methyl group in biological methylation reactions.[15-18] 5-MTHF is directly involved in the synthesis of methionine and indirectly in the synthesis of choline.[16,17] In chemotherapy 5-MTHF is the active metabolite of leucovorin which is used for the prevention of methotrexate (also known as amethopterin) toxicity.[19-22]

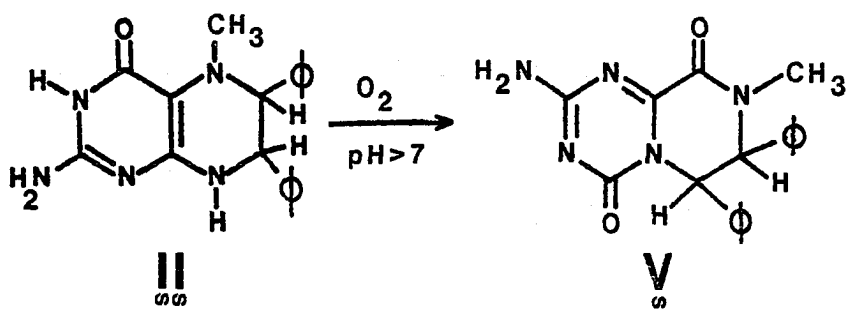
The most extensively studied of the synthetic 5-MTHF analogues is 5-methyl-6,7-diphenyltetrahydropterin (5-M-6,7-DPTHP).[23-28] The chemical oxidation and air oxidation of 5-M-6,7-DPTHP (II, Equation 1) have been studied and a mechanism was proposed which involved the intermediacy of a 4a-hydroxy compound (III, Equation 1).[23-26] The final product of the oxidation was proposed to be 5-methyl-6,7-diphenyl-5,6-

dihydropterin (5-M-6,7-DPDHP) (IV, Equation 1).



ESR studies have also shown the existence of radicals in the air oxidation.[24,27]

These findings were later disputed by Jongejan, et al.[28,29] who have shown that the actual product for air oxidation of 5-M-6,7-DPTHP was 2-amino-8-methyl-4,9-dioxo-cis-6,7-diphenyl-6,7,8,9-tetrahydro-4H-pyrazino (1,2-a)-s-triazine (V, Equation 2) shown in Equation 2:



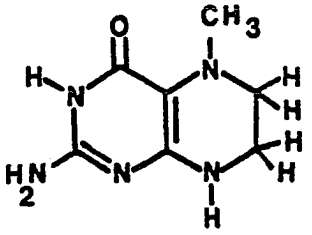
The structure of the pyrazino-s-triazine (V, Equation 2) was determined by X-ray crystallography of the acylated product.[30] This reaction was shown to proceed through a hydroxyperoxy intermediate. The 4a-hydroxy adduct of 5-MTHF reported by Gapski, et al.[31] in the H_2O_2 oxidation of

5-MTHF was also proposed to be a pyrazino-s-triazine by Jongejan, et al.[28]

A methyl group at N(5) has been shown to stabilize tetrahydropterins to air oxidation.[32] 5-MTHF has also been shown to be ca. 10 times more stable to air oxidation than tetrahydrofolic acid.[33,34] However, 5-methyl-5,6-dihydrofolic acid (5-M-5, 6-DHF) decomposes rapidly in acidic solution yielding p-aminobenzoylglutamate and an undetermined tetrahydropterin.[34,35]

Loss of the N(5)-methyl group has been demonstrated for 1,3, 5,6-tetramethyltetrahydropterin during elution from Dowex 50W with 3 N aqueous ammonia.[15] N(5)-demethylation of 5-M-6,7-DPTHP and 5-M-6,7-DPDHP during the air oxidation has also been demonstrated by Viscontini, et al.[36]

5-Methyltetrahydropterin has also been shown to form the pyrazino-s-triazine compound when air oxidized above pH 7 in the presence of oxygen.[28] If 5-MTHP is oxidized to the 5-methyl-5,6-dihydropterin at low pH it may be unstable, analogous to the instability of 5-M-5,6-DHF. Thus the study of the electrochemical oxidation of 5-MTHP may aid in the understanding of its inhibitor properties. Elucidation of the reaction pathway for electrooxidation of 5-MTHP may also help to understand the methyl transferring ability of 5-methyltetrahydrofolic acid in vivo. A preliminary report of the electrochemical properties of 5-MTHP has already appeared.[37] However none of the electrooxidation products were identified. This report continues the investigation of the electrooxidation of 5-MTHP, particularly from the viewpoint of identifying the electrolysis products.



5-MTHP

CHAPTER II

RESULTS AND DISCUSSION

Linear and Cyclic Sweep Voltammetry

pH study of 5-MTHP. At low pH 5-MTHP exhibits one major oxidation peak identified as peak I_a at a sweep rate of 5 mV s^{-1} at a pyrolytic graphite electrode (PGE) (Figure 1). The pH dependence of the peak potential (E_p) of peak I_a is given by Equation 3 and is illustrated in Figure 2.

$$\text{Peak } I_a: \quad E_p(\text{pH } 1.4\text{-}11) = [0.43\text{-}0.047\ \text{pH}]\text{V} \qquad (3)$$

Below pH 3 there are three other very small peaks visible in the linear sweep voltammetry, peaks II_a, III_a, and IV_a (Figure 1). Peaks II_a and III_a appear as shoulders on peak I_a and their peak potential is fairly difficult to determine. Peak IV_a is considerably more positive and is well defined although it has a very small peak current. The variation of the peak potential with pH is given by Equations 4-6 and is illustrated graphically in Figure 2.

$$\text{Peak } II_a: \quad E_p(\text{pH } 1.4\text{-}7) = [0.51\text{-}0.049\ \text{pH}]\ \text{V} \qquad (4)$$

$$\text{Peak } III_a: \quad E_p(\text{pH } 1.4\text{-}9) = [0.63\text{-}0.053\ \text{pH}]\ \text{V} \qquad (5)$$

$$\text{Peak } IV_a: \quad E_p(\text{pH } 1.4\text{-}8) = [0.83\text{-}0.054\ \text{pH}]\ \text{V} \qquad (6)$$

In the pH range 7-9 peaks II_a, III_a, and IV_a become too poorly

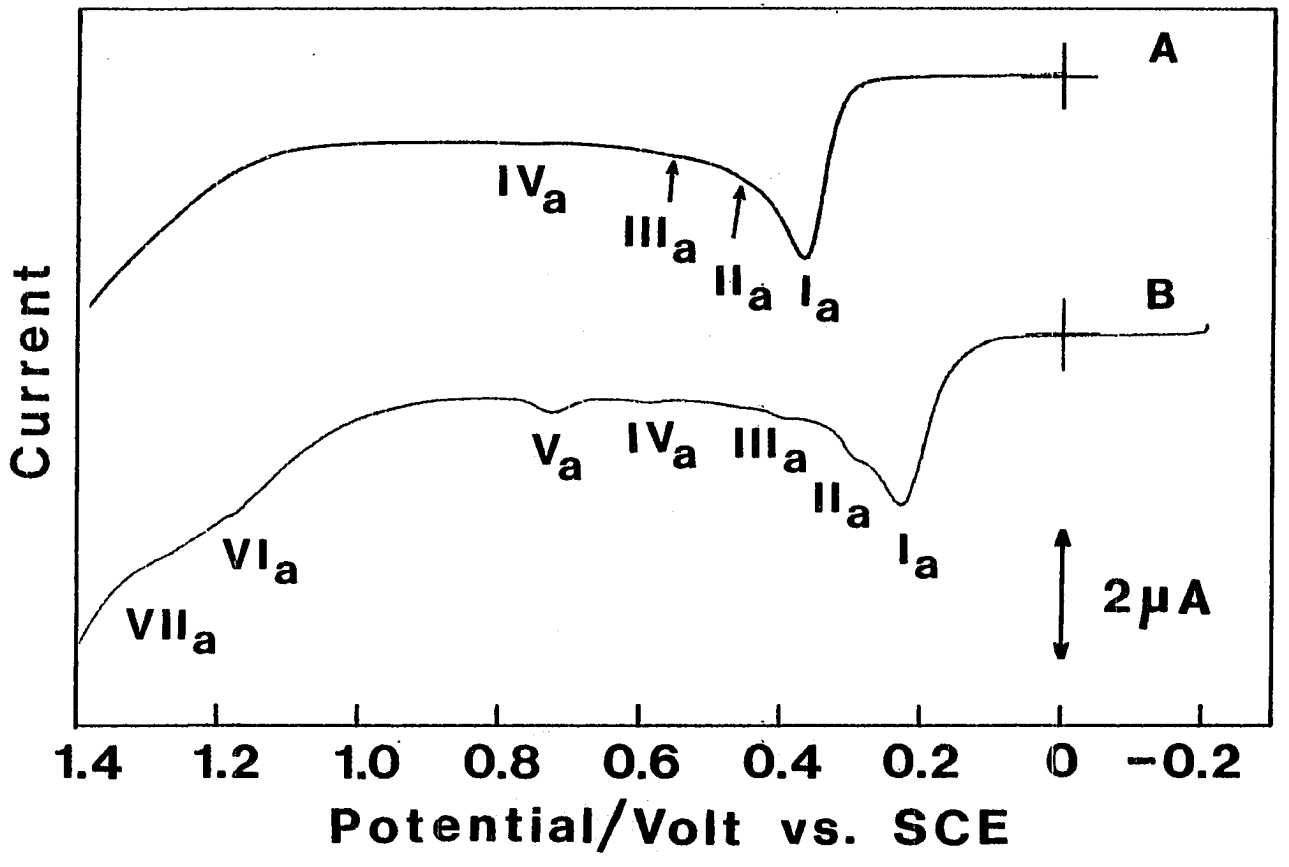


Figure 1. Linear sweep voltammograms of 1.0 mM 5-MTHP in phosphate buffers of ionic strength 0.5 M. Sweep rate: 5 mV s^{-1}. (A) pH 1.4 and (B) pH 4.6.

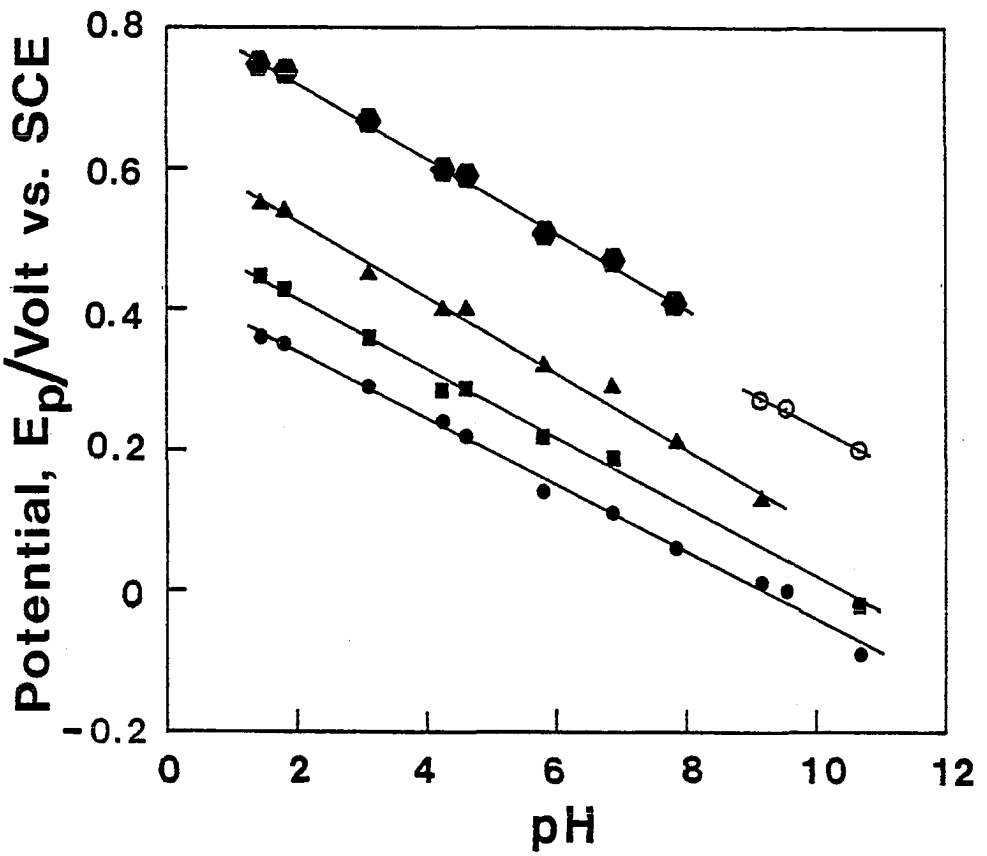


Figure 2. Variation of E_p vs. pH for the voltammetric oxidation peaks of 1.0 mM 5-MTHP observed at a PGE at a sweep rate of 5 mV s^{-1}. (●) Peak I_a, (■) Peak II_a, (▲) Peak III_a, (⬢) Peak IV_a, and (○) Peak IV'_a.

defined to determine the peak potential accurately. At pH 9, a new small oxidation peak designated peak IV'_a appears and is visible to pH 11. Over this range the pH dependence is given by Equation 7 and is illustrated in Figure 2:

$$\text{Peak } IV'_a: \quad E_p(\text{pH 9-11}) = [0.71-0.048\ \text{pH}]\ \text{V} \qquad (7)$$

Peak V_a appears at pH 4.2 and is never very large. Peaks VI_a and VII_a also begin to appear in this pH region. They appear as a very broad peak which is only partially resolved. At pH 6 peak VII_a can no longer be seen as an identifiable shoulder on peak VI_a. However peak VI_a becomes larger as the pH increases and is observed to the upper limit of the pH range investigated. The pH dependence of these voltammetric oxidation peaks is summarized by Equations 8-10 and Figure 3.

$$\text{Peak } V_a: \quad E_p(\text{pH 4-10}) = [0.92-0.047\ \text{pH}]\ \text{V} \qquad (8)$$

$$\text{Peak } VI_a: \quad E_p(\text{pH 6-11}) = [1.43-0.072\ \text{pH}]\ \text{V} \qquad (9)$$

$$\text{Peak } VII_a: \quad E_p(\text{pH 4-6}) = [1.47-0.051\ \text{pH}]\ \text{V} \qquad (10)$$

Under cyclic voltammetric conditions several new oxidation peaks appear on the second positive sweep. Particularly at low pH the peak current of peak I'_a approaches the value of the peak current for peak I_a (Figure 4A). At pH 1.4 oxidation peaks I_a, I'_a, and II'_a all exhibit reverse peaks designated I_c, I'_c, and II'_c respectively. The only other oxidation peak observed at pH 1.4 is peak V_a at a sweep rate of 200 mV s^{-1}. Reduction peaks II_c and III_c are also observed at this low pH. As the pH is increased to 4.7 several differences are observed, most notably oxidation peak II'_a is absent (Figure 4B). Peak II'_c appears

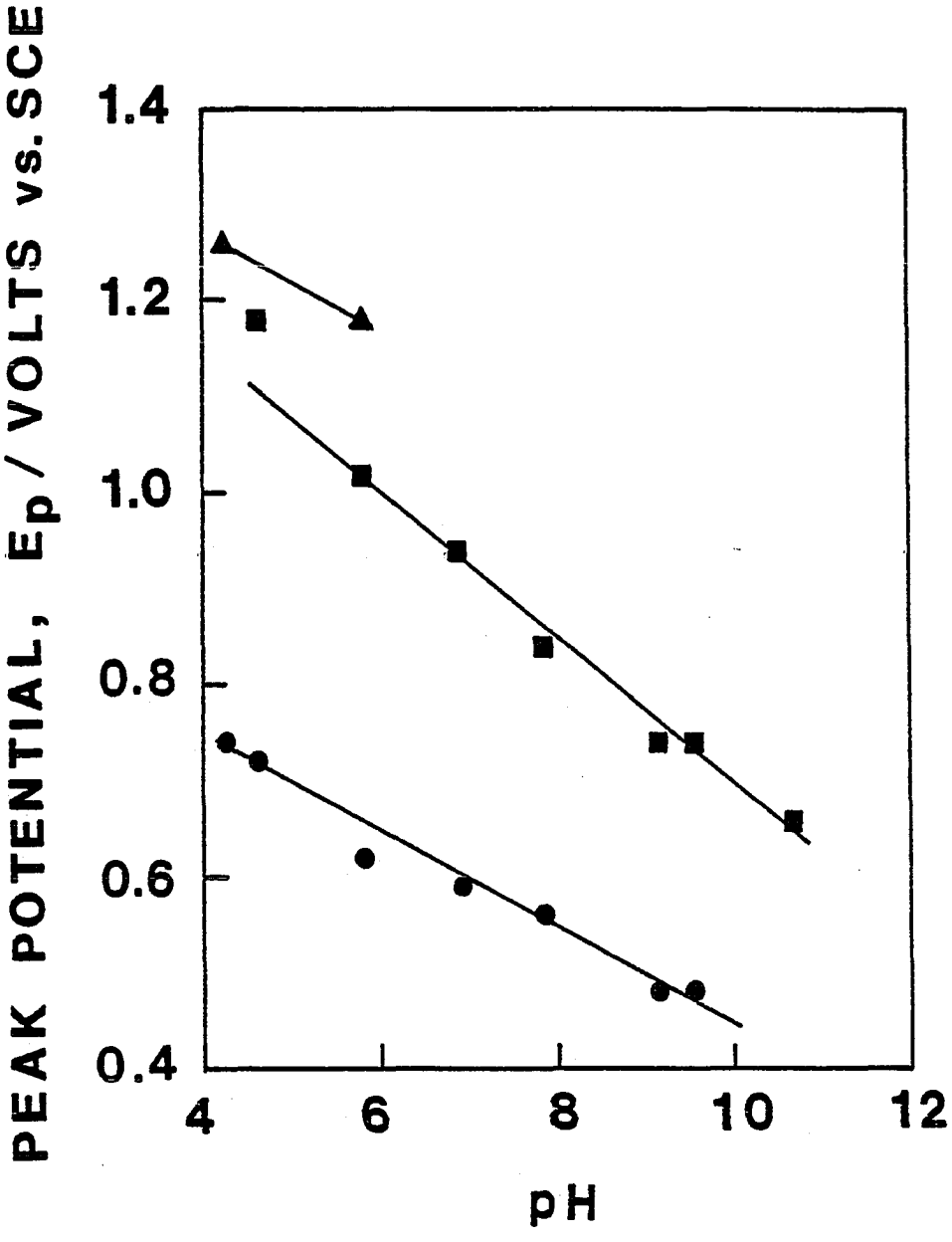


Figure 3. Variation of E_p vs. pH for voltammetric oxidation peaks V_a, VI_a, and VII_a of 1.0 mM 5-MTHP observed at the PGE at a sweep rate of 5 $mV^a s^{-1}$. (●) Peak V_a, (■) Peak VI_a, and (▲) Peak VII_a.

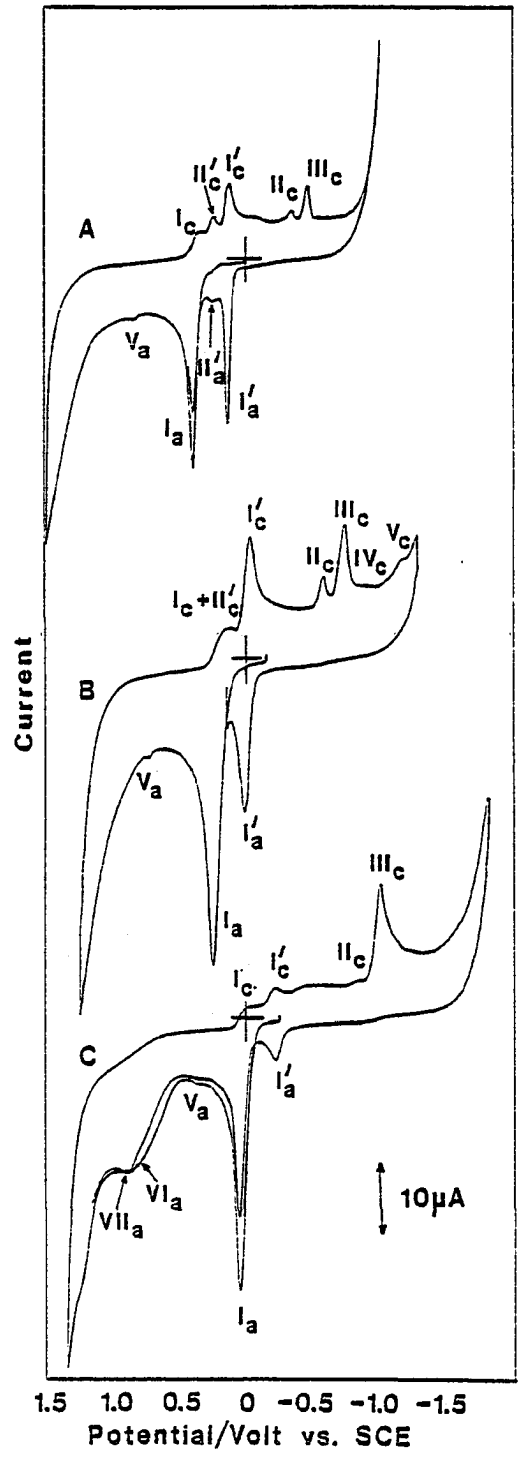


Figure 4. Cyclic voltammograms of 1.0 mM 5-MTHP at the PGE in phosphate buffers, μ=0.5 M. Sweep rate: 200 mV s^{-1}. (A) pH 1.4, (B) pH 4.7, and (C) pH 9.2.

to be merged together with peak I_c. Several other reduction reaks are observed however, peaks IV_c and V_c increase in size.

As the pH is increased above pH 7 the partially resolved peaks VI_a and VII_a have increased in size to the point where they are now larger than peak V_a (Figure 4C). It is also apparent that reduction peaks I_c, I'_c, and II_c are much smaller at pH 9.15 than at lower pH. The ratio of peak I'_a to I_a is much lower at higher pH indicating that the initial oxidation product of peak I_a which is reduced at peak I'_c is present at a smaller percentage of the total products.

If the positive potential sweep is reversed before the peak potential of peak VI_a is reached, reduction peak III_c is observed to be very small in the subsequent negative sweep (Figure 5). Oxidation peaks VI_a and VII_a are resolved into definable peaks only in the narrow pH range, 4-6, at a sweep rate of 5 mV s^{-1}. However, at a sweep rate of 200 mV s^{-1} peak VI_a is much more clearly defined above pH 6.

Further investigation of the peak I'_a/I'_c reversible couple reveals that the peak separation, ΔE_p, is 29±5 mV from pH 1.4 to 8 at a sweep rate of 200 mV s^{-1}. This is characteristic for an electrochemically reversible reaction where $\Delta E_p = \frac{59}{n}$ mV. The variation of the peak potential of peak I'_a with pH is given by Equations 11 and 12:

$$E_p(\text{pH } 1.4\text{-}7) = [0.18\text{-}0.038 \text{ pH}] \text{ V} \quad (11)$$

$$E_p(\text{pH } 7\text{-}11) = [0.40\text{-}0.069 \text{ pH}] \text{ V} \quad (12)$$

The reversible behavior and the pH equations are very similar to that reported for the peak I_a/I_c reversible couple of tetrahydropterin.[7] The reversible couple peak II'_a/II'_c also exhibits similar behavior to

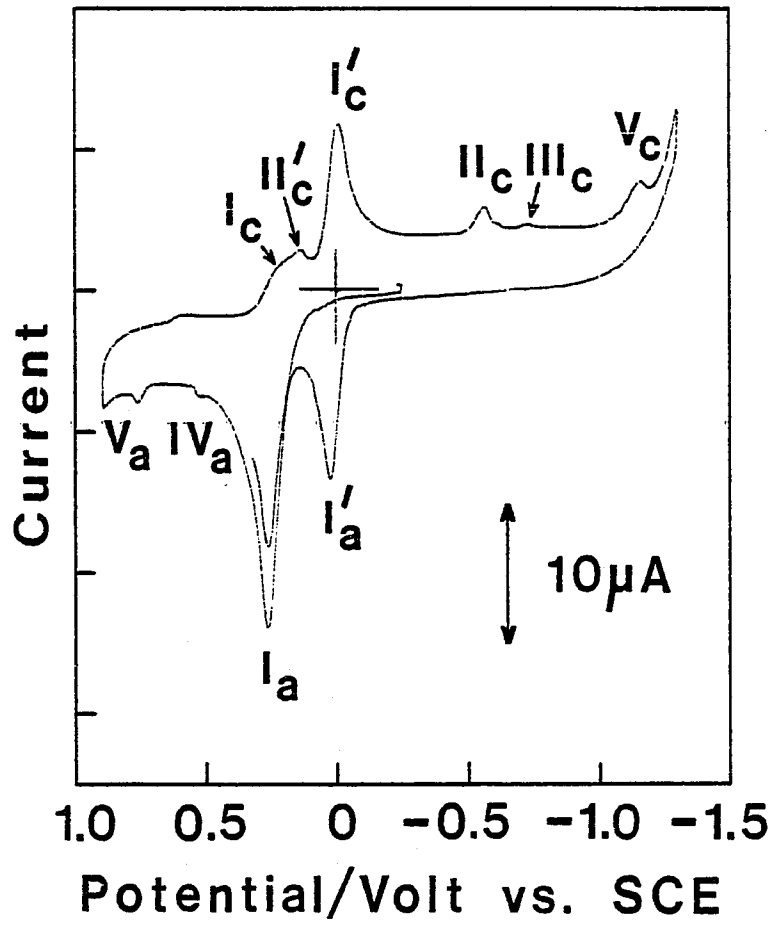


Figure 5. Cyclic voltammogram of 0.9 mM 5-MTHP in pH 4.6 phosphate buffer, μ=0.5 M. Switching potential was negative of peaks VI_a and VII_a. Sweep rate: 200 mV s^{-1} at a PGE.

that reported for the peak I'_a/I'_c reversible couple of 7,8-dihydropterin.[7] It is only observed at pH values below pH 3 however. For example, the peak potential for peak II'_a at pH 1.43 (Figure 4A) is 0.25 V/SCE. The peak potential for peak I'_a of 7,8-dihydropterin is calculated from the equation for the pH dependence as 0.27 V/SCE.[7] Apparently both the quinonoid species of tetrahydropterin and 7,8-dihydropterin respectively are generated in the peak I_a oxidation process of 5-MTHP.

Similarly reduction peaks II_c and V_c (Figure 4B) can be compared to the reduction peaks observed in cyclic voltammetry of an authentic pterin sample (see Figure 47B below). The potential of peak V_c is identical with the peak potential of the second reduction peak of pterin, however the peak potential of peak II_c (0.58V in Figure 4B) is somewhat different from that of the first reduction peak of pterin (0.62V in Figure 47B). It is reported that the first reduction peak (also identified as peak II_c in reference 7) of pterin has a very large adsorption component. Adsorption has been shown to cause a shift in peak potential with change in concentration.[38] This could certainly explain the shift in the peak potential observed for peak II_c. From the peak current observed for peak II_c of 5-MTHP in Figure 4B and the peak current for peak II_c of authentic pterin in Figure 47B it can be ascertained that the concentration of pterin is much higher in the solution containing authentic pterin.

Concentration study. A peak current, ip, vs. concentration study on 5-MTHP was carried out in pH 4.7 phosphate buffer of ionic strength 0.5 M. pH 4.7 was chosen for this investigation because the predominant buffer species is $H_2PO_4^-$ at this pH. Earlier electrochemical

investigations of other tetrahydropterins have shown that phosphate buffers catalyze the rearrangement of intermediates generated in the peak I_a oxidation processes.[7,8,10] Therefore it was felt that the complexity of this process could be reduced by having $H_2PO_4^-$ as the predominant species present in the buffer solution. Also at this pH 5-MTHP is present almost entirely as the monocation (ca. 95%) since the pH is ca. 1.3 units lower than the pK_a of 5.99.[39] The voltammetry indicates that the peak VI_a-VII_a process does not occur to any great extent at pH 4.7.

The peak current, ip, behavior as a function of 5-MTHP concentration is illustrated in Figure 6 for peak I_a. It is ca. linear up to 2.4 mM 5-MTHP indicating that adsorption of 5-MTHP does not make an important contribution to the peak current of peak I_a.

In the cyclic voltammetry of 5-MTHP at a sweep rate of 20 mV s^{-1} several additional reduction peaks are observed which were not observed at a sweep rate of 200 mV s^{-1}. One of these, peak IV'_c, increases in size as the concentration decreases (Figure 7A,B). The other peak, III'_c, is observed simply because the sweep rate is slower than the sweep rate of the cyclic voltammograms discussed in the pH study (vide supra). This behavior will be discussed further in the sweep rate study. At a sweep rate of 200 mV s^{-1} the peak current for peak I'_a increases relative to the peak current for peak I_a as the concentration decreases (Figure 8A,B,C).

Sweep rate study at pH 4.7. A sweep rate study of 1.0 mM 5-MTHP was carried out in pH 4.7 phosphate buffer over the sweep rate range of 10 mV s^{-1} to 50 V s^{-1}. The peak current increases in an ca.

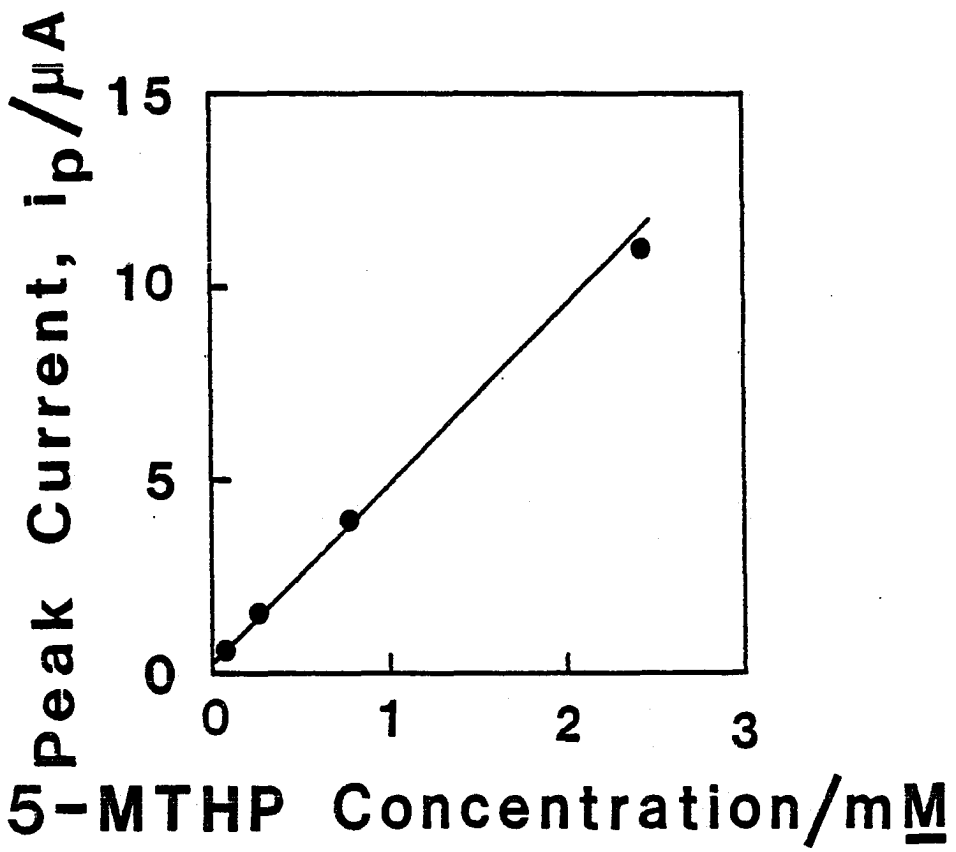


Figure 6. Variation of peak current, i_p, vs. concentration for peak I_a of 5-MTHP in pH 4.7 phosphate buffer. Sweep rate: 5 mV s^{-1}.

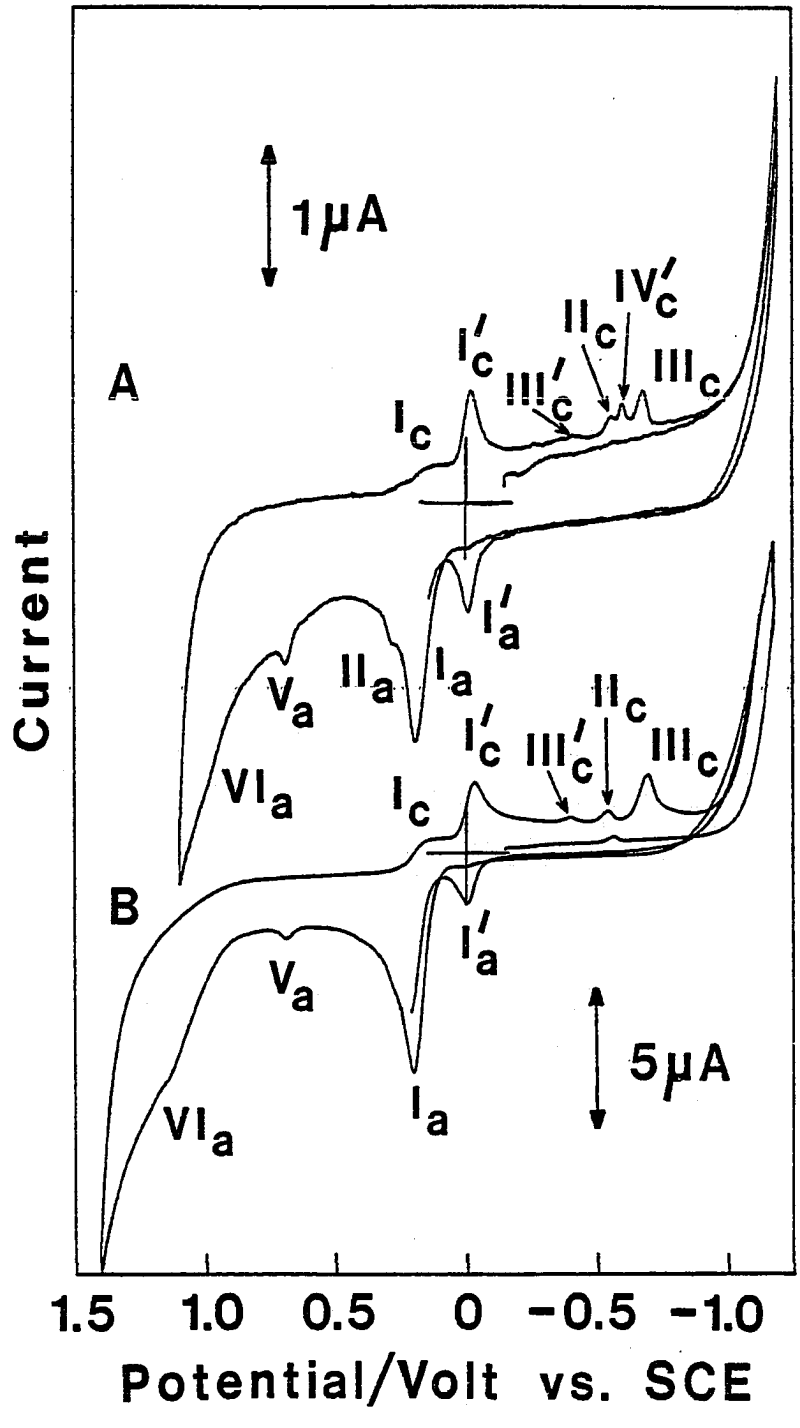


Figure 7. Cyclic voltammograms of 5-MTHP at the PGE in pH 4.7 phosphate buffer. Sweep rate: 20 mV s^{-1}. 5-MTHP concentration (A) 0.075 mM, (B) 0.77 mM.

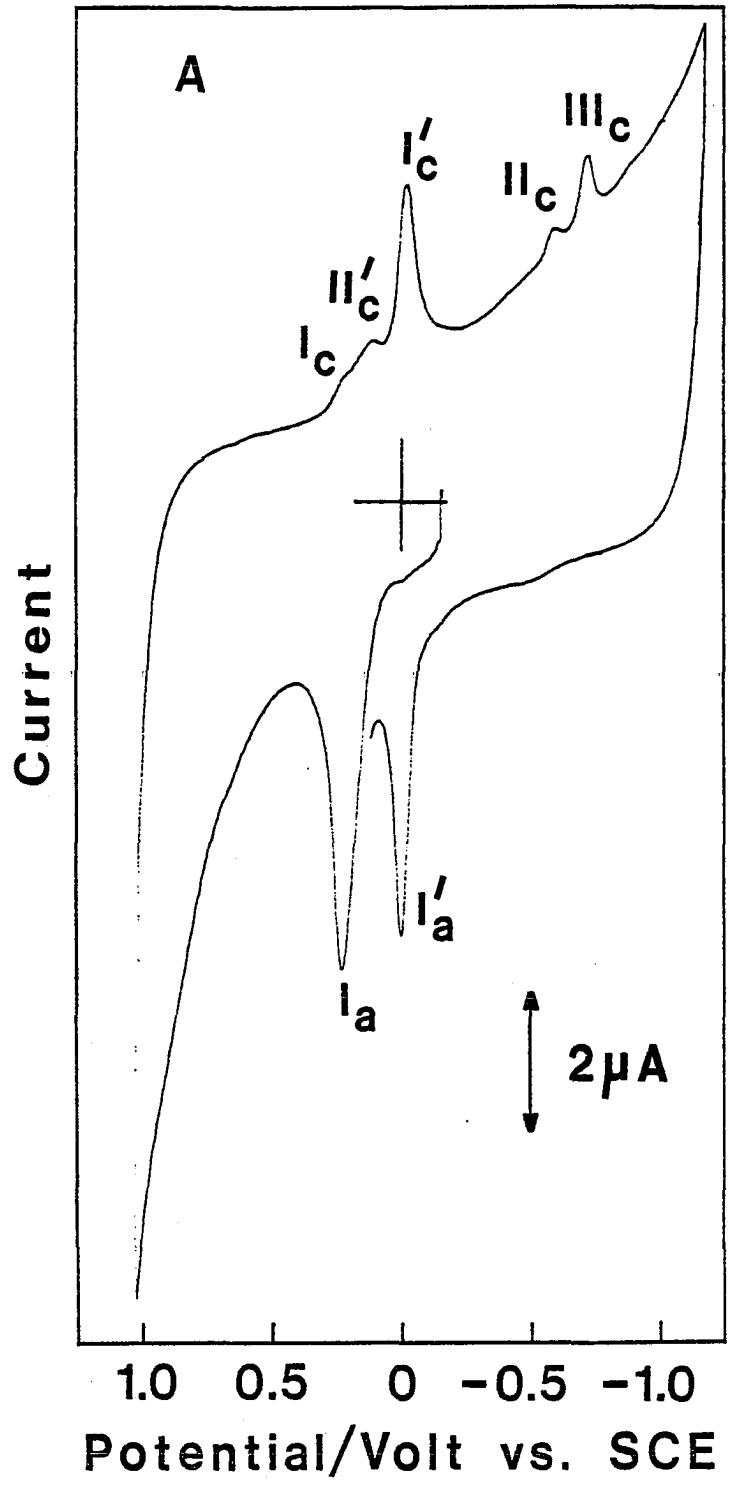


Figure 8. (A) Cyclic voltammogram of 0.075 mM 5-MTHP at the PGE in pH 4.7 phosphate buffer. Sweep rate: 200 mV s^{-1}.

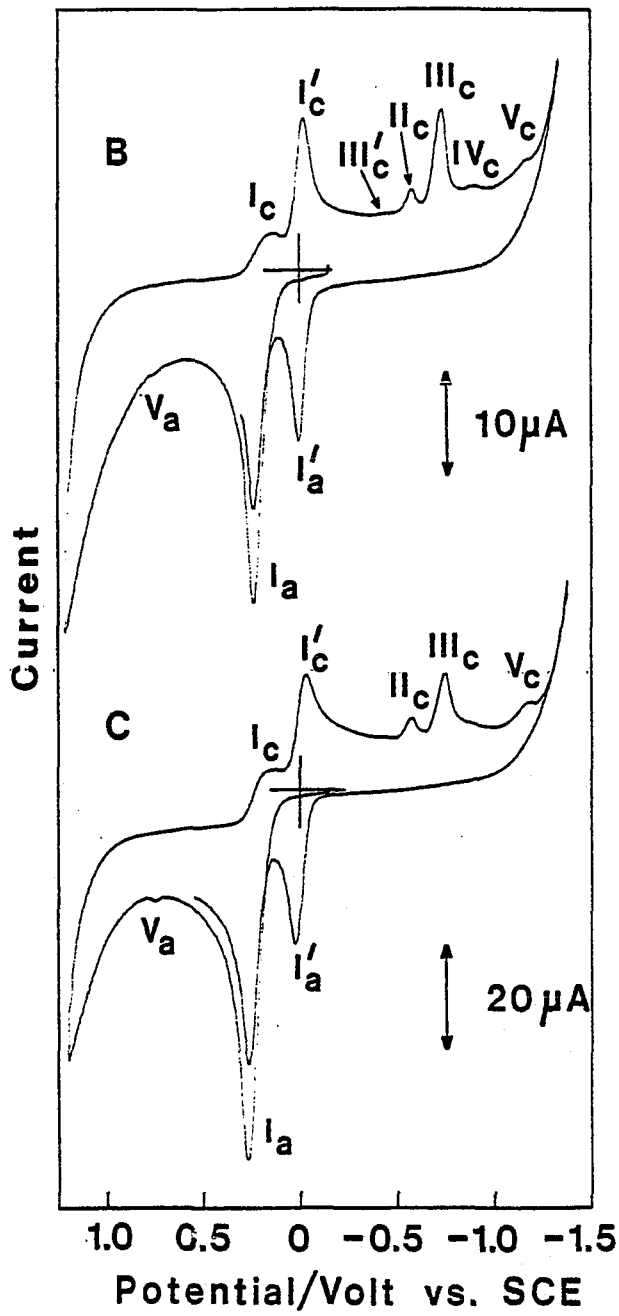


Figure 8. Cyclic voltammograms of 5-MTHP at the PGE in pH 4.7 phosphate. Sweep rate: 200 mV s^{-1}. 5-MTHP concentration (B) 0.77 mM, and (C) 2.4 mM.

linear fashion up to 50 V s^{-1} as a function of the square root of the sweep rate (Figure 9A). This supports the evidence presented in the concentration study that adsorption does not play a significant role in the peak I_a process. The peak current function, $i_p/v^{\frac{1}{2}}$, increases slightly with the square root of the sweep rate as illustrated in Figure 9B indicative of a small amount of adsorption. Actually the complete peak current function is $i_p/ACv^{\frac{1}{2}}$, however A (the area of the electrode) and C (the 5-MTHP concentration) do not change significantly during the course of the study.

As mentioned above peak III_c' increases in size as the sweep rate is decreased (Figures 4B, 10A,B). It can be seen in Figure 10A,B that peak IV_c' also increases in size as the sweep rate is decreased. However peak IV_c' does not become as large at slow sweep rates as it does at low concentrations (see Figure 7A). Increasing the sweep rate reveals that reduction peak IV_c, which is first observed at 500 mV s^{-1} (Figure 11A), increases in size (Figure 11B). At a sweep rate of 20 V s^{-1} a new oxidation peak is observed at ca. -0.6V/SCE which will be designated peak III_a' (Figure 11C). This peak is the same peak which is identified as peak IV_a in the cyclic voltammetry of pterin.[7] It is not observed at slower sweep rates because of the instability of the 5, 8-dihydropterin generated in the peak II_c process.

The fact that oxidation peaks II_a-V_a all disappear as the sweep rate is increased indicates they are due to the electrooxidation of products formed from the rearrangement of intermediates generated in the peak I_a process. It was also observed that several reduction peaks increase as the sweep rate decreases while other reduction peaks are

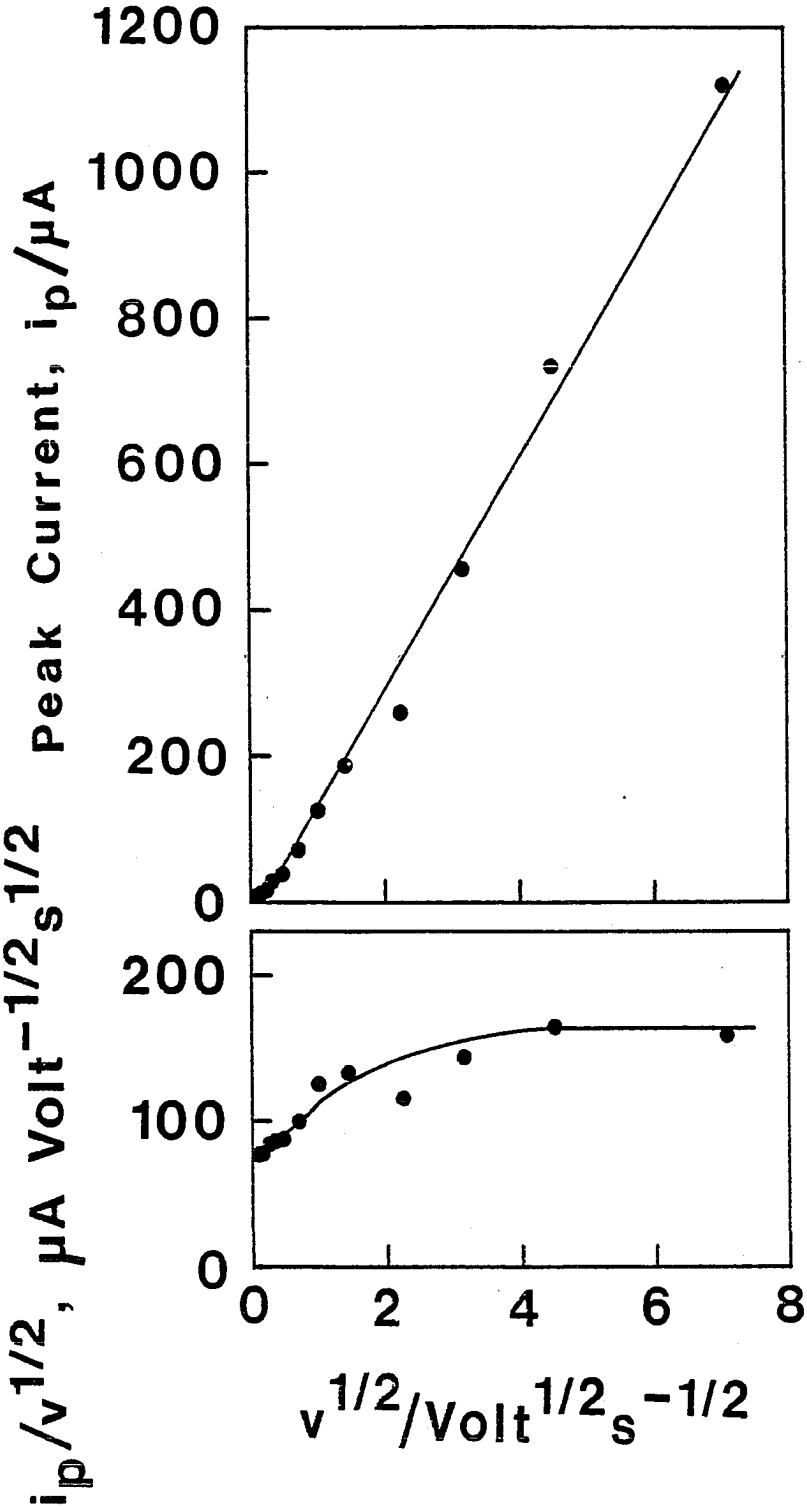


Figure 9. (A) Peak current for peak I_a of 1.0 mM 5-MTHP vs. the square root of the sweep rate at pH 4.7. (B) Peak current function for peak I_a of 1.0 mM 5-MTHP vs. the square root of the sweep at pH 4.7.

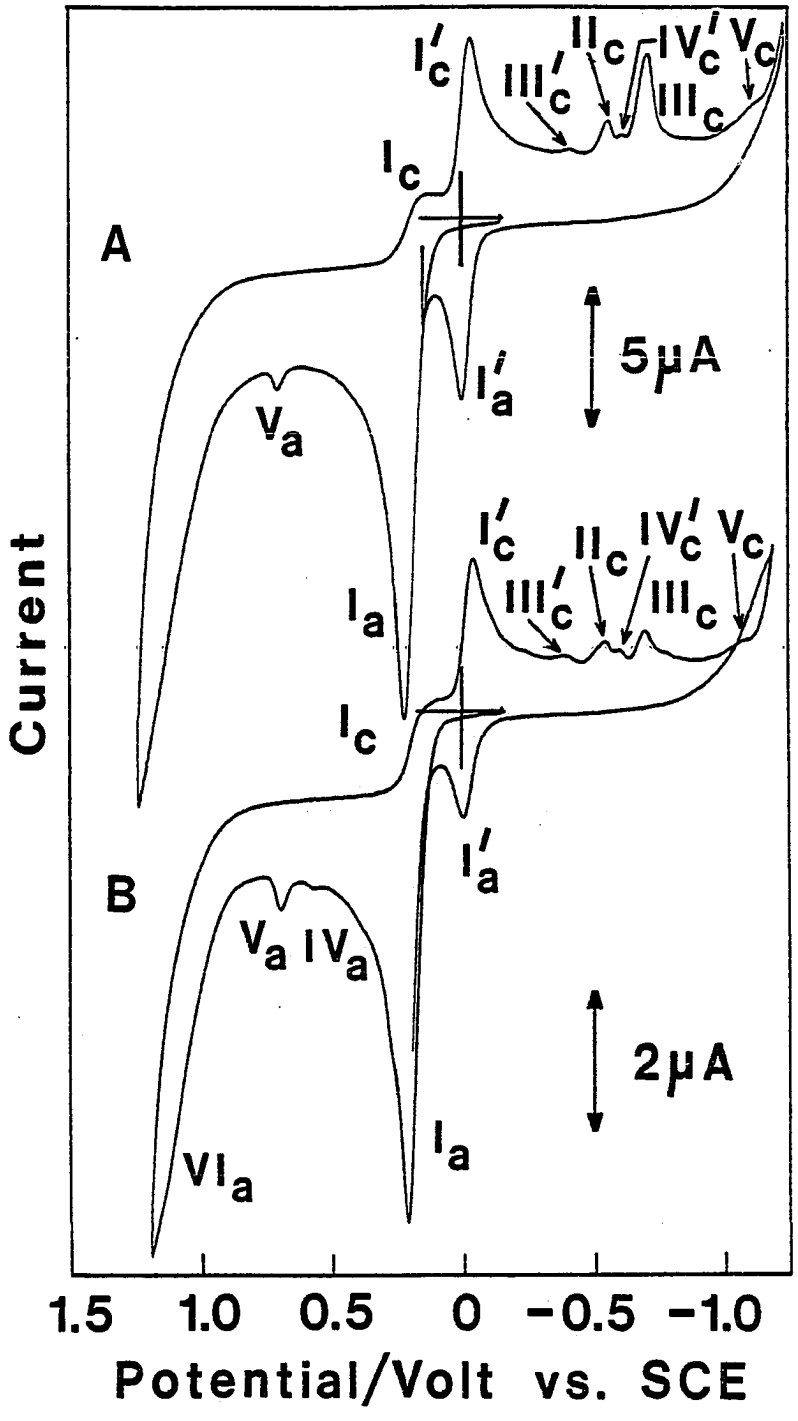


Figure 10. Cyclic voltammograms of 1.0 mM 5-MTHP at the PGE in pH 4.7 phosphate buffer. Sweep rate: (A) 50 mV s^{-1} and (B) 10 mV s^{-1}.

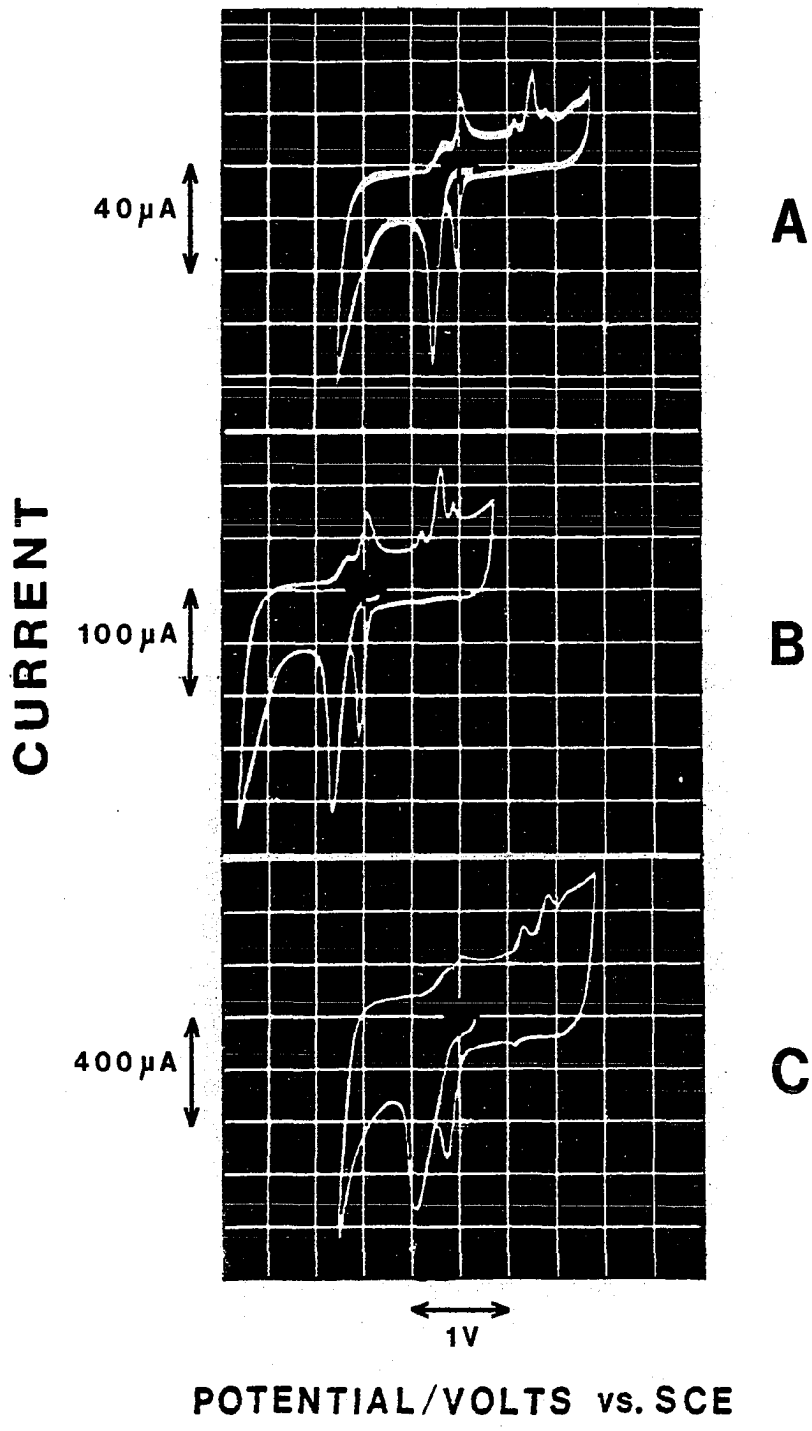


Figure 11. Cyclic voltammograms of 1.0 mM 5-MTHP at the PGE in pH 4.7 phosphate buffer. Sweep rate: (A) 500 mV s^{-1}, (B) 2 V s^{-1}, and (C) 20 V s^{-1}.

observed only at high sweep rates. This fact together with the observation that both reduction peaks I_c and I_c' decrease with increasing sweep rate suggests that more than one intermediate is generated in the peak I_a oxidation process. It was not possible to determine whether both intermediates are generated simultaneously or whether one intermediate is generated which rearranges to a second intermediate. This second intermediate would then rearrange to the final product.

Bulk Electrolyses of 5-MTHP

Large scale electrolyses of 5-MTHP were performed in pH 4.7 phosphate buffer with an ionic strength of 0.5 M or in 0.5 M NaCl pH 4.7±0.1. It is apparent from the voltammetry that there are several oxidation peaks very close to peak I_a, therefore electrolyses were carried out at the half-peak potential, 0.20V vs. SCE in pH 4.7 phosphate. After electrooxidation at 0.20V/SCE a number of oxidation and reduction peaks are observed (Figure 12A,B). Figure 13 shows that peaks III_a and IV_a both exhibit quasi-reversible reduction peaks.

5-MTHP was also electrolyzed at peak I_a potentials in a solution containing 0.5 M NaCl maintained at pH 4.7±0.1 by monitoring the pH during the electrolysis and adding microliter quantities of ca. 1 N NaOH. Figure 14A shows a cyclic voltammogram of 5-MTHP before the electrolysis. After the electrolysis a number of new oxidation and reduction peaks are observed (Figure 14B). Because of the change in pH at the electrode surface as a result of the release or consumption of protons during the redox processes a shift in peak potentials is observed relative to the peaks in phosphate buffer. The peaks are also

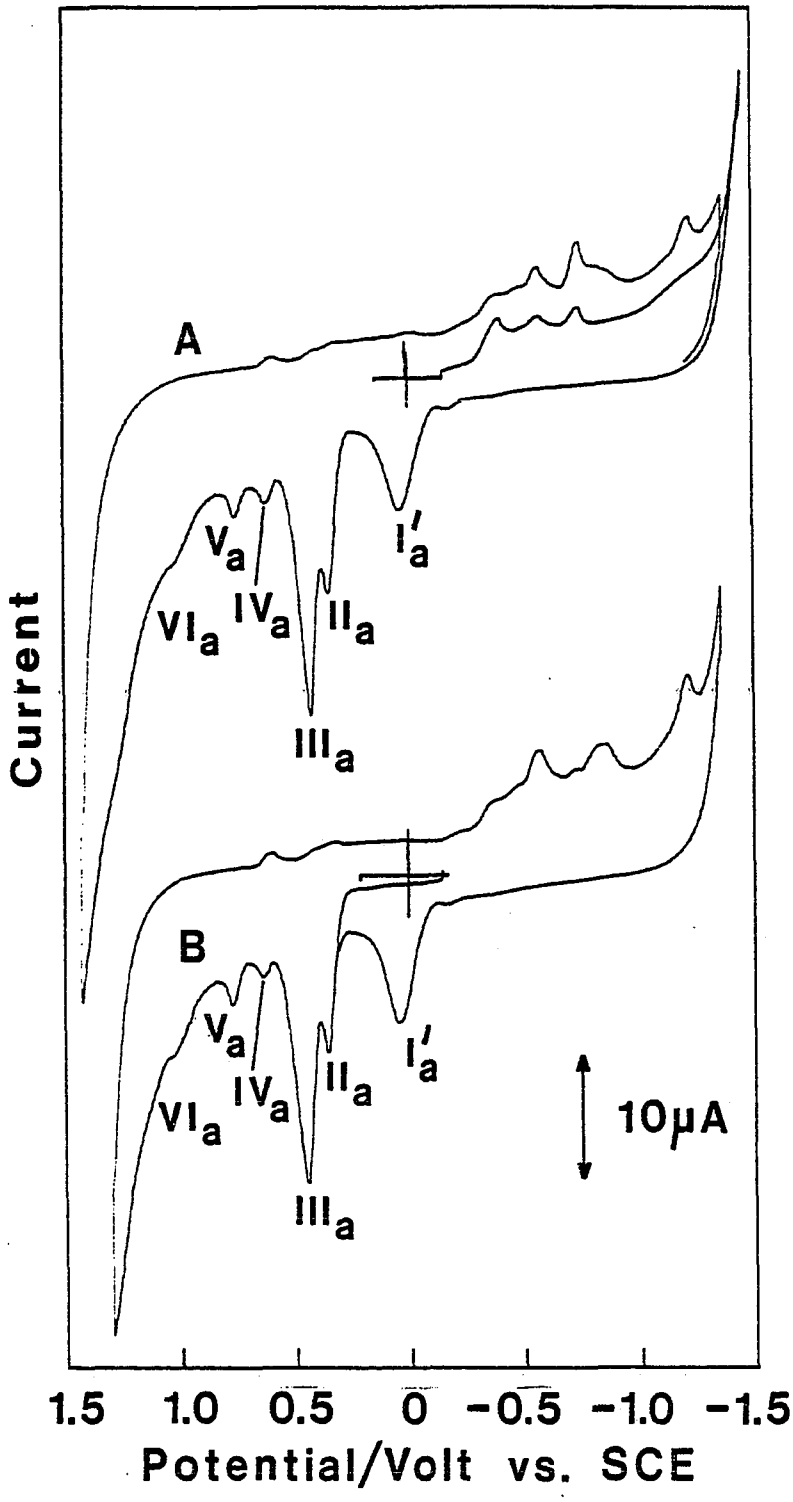


Figure 12. Cyclic voltammogram of 0.75 mM 5-MTHP at the PGE in pH 4.7 phosphate buffer, μ=0.5 M after electrooxidation at 0.20V. Sweep rate: 200 mV s^{-1}. (A) Initial sweep negative and (B) initial sweep positive.

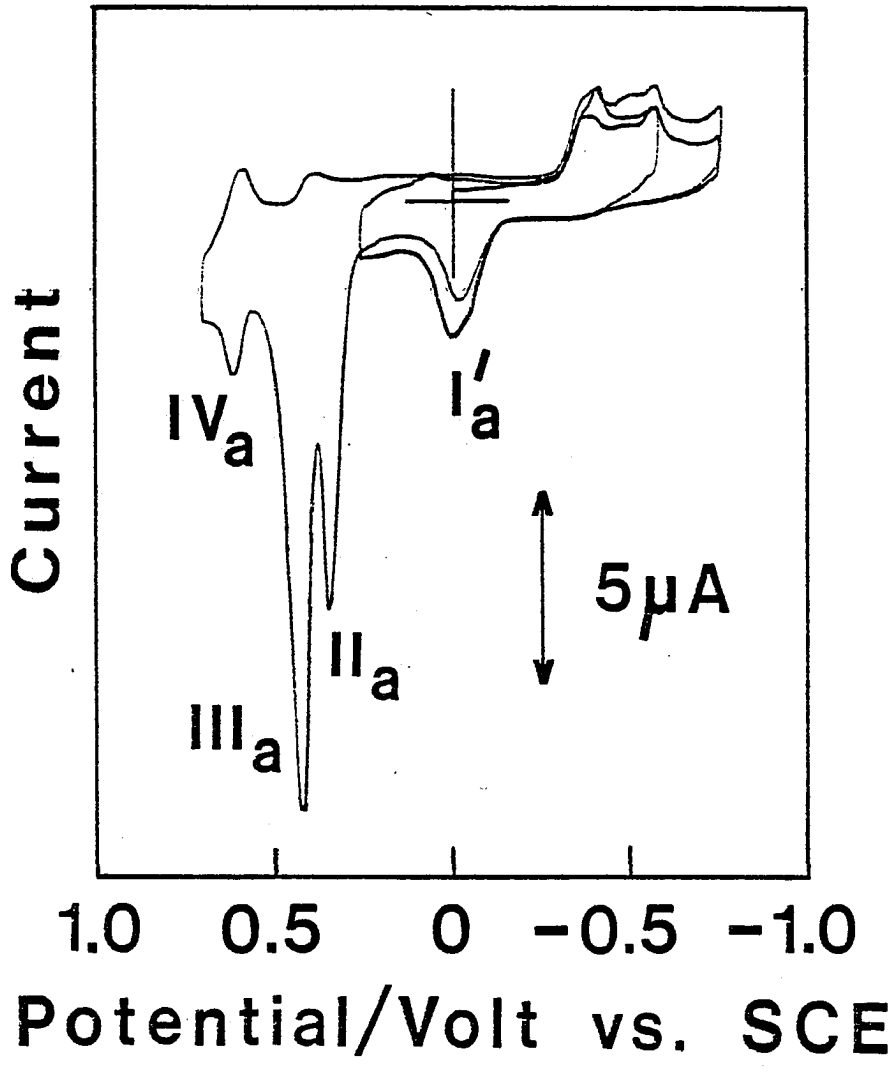


Figure 13. Cyclic voltammogram of 0.75 mM 5-MTHP at the PGE in pH 4.7 phosphate buffer, μ=0.5 M after electroxidation at 0.20V/SCE. Sweep rate: 200 mV s^{-1}. Illustrates the reversibility of peaks III_a and IV_a.

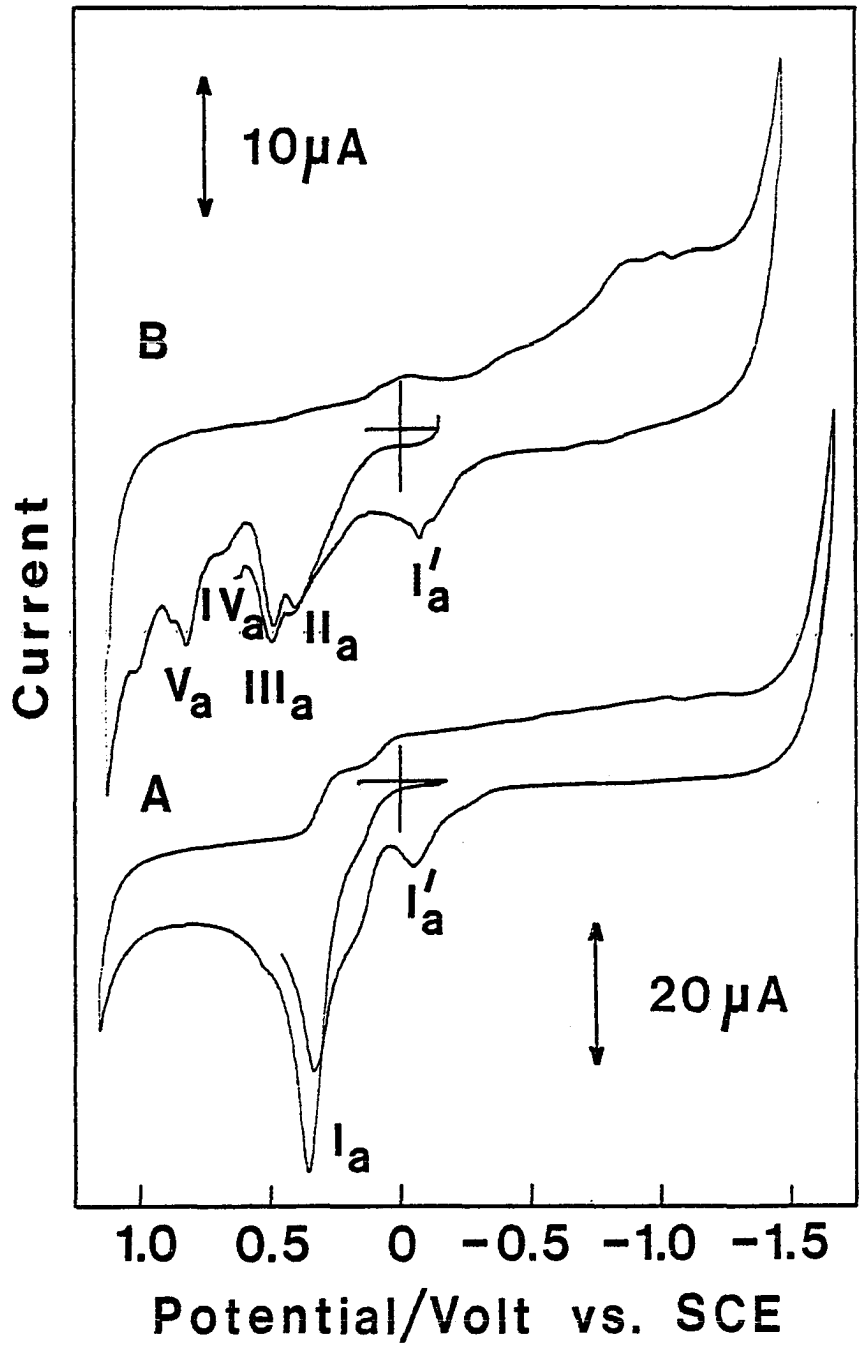


Figure 14. Cyclic voltammograms of 2.3 mM 5-MTHP at the PGE in pH 4.7, 0.5 M NaCl. Sweep rate: 200 mV s^{-1}. (A) Before electrolysis and (B) after electrolysis at 0.26V/SCE ($E_p/2$).

broadened for the same reason. However it appears that the oxidation yields similar products.

Several differences were noted between electrolyses performed in pH 4.7 phosphate buffer and those performed in 0.5 M NaCl solutions. Electrolyses in 0.5 M NaCl were found to proceed much faster and were usually completed in several hours. This was determined from cyclic voltammetry. In contrast, electrolyses carried out in phosphate buffer usually required application of potential for 12-18 hours to proceed to completion. Another difference noted was the much more intense yellow color generated during electrolysis in the phosphate buffer. This has been attributed to the formation of a greater percentage of xanthopterin (see section on product identification below).

n-Values for Large-Scale Electrolysis

Electrolyses were carried out in pH 4.7 phosphate at potentials necessary to oxidize fresh solutions of 5-MTHP at peaks I_a-V_a as well as at several more positive potentials. Results are shown in Table 1. It can be seen in Table 1 that electrolysis at peak I_a appears to give slightly more than 2 electrons per molecule. It is also observed that electrolyses at successive peaks yield n-values which are only fractionally larger. This indicates that they are probably oxidation of only a part of the products formed in the peak I_a process. In fact it is possible that some of the products from peak I_a electrolysis of 5-MTHP are not electroactive.

Electrolyses in thin-layer cell. Further electrolyses were carried out in phosphate buffers in a RVC thin-layer cell. The potential

TABLE 1

n-Values for Electrolysis of Fresh Solutions of 0.75 mM 5-MTHP in pH 4.7 Phosphate[a]

Potential/V vs. SCE	Peak	n-Value
0.20	I_a	2.4±0.2
0.32	II_a	2.8±0.1
0.40	III_a	3.0±0.1
0.60	IV_a	3.1[b]
0.80	V_a	3.1[b]
0.95		3.4[b]
1.30		4.8[b]

[a]Electrolyses were carried out in a three compartment cell at a large PGE.

[b]Only a single experiment was performed at these potentials.

for electrolysis was determined by running a linear sweep voltammogram in the RVC thin-layer cell (Figure 15). Electrolyses were carried out at the peak potential of the first peak. The number of electrons transferred under these conditions is reported in Table 2. After electro-oxidation of the solution at peak I_a, the potential was set at the peak potential of the last oxidation peak in the linear sweep voltammogram (ca. 0.73V/SSCE in Figure 15). The number of electrons transferred under these conditions in also reported in Table 2.

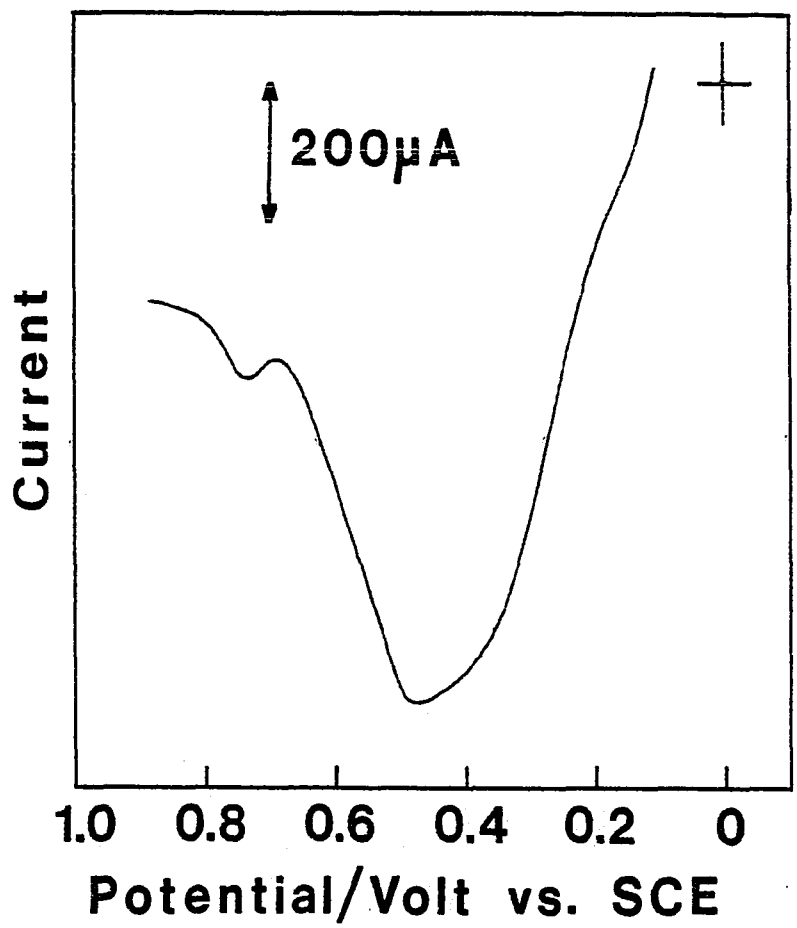


Figure 15. Linear sweep voltammogram of 0.99 mM 5-MTHP in pH 4.2 phosphate at a RVC electrode in a thin-layer cell. Sweep rate: 5 mV s^{-1}.

TABLE 2

Coulometric n-Values Observed Upon Electrooxidation of 1.0 mM 5-MTHP in Phosphate Buffers[a]

pH	Potential V/SSCE[b]	n-Value	Potential V/SSCE[c]	n-Value	Total n-Value
1.8	0.56	2.7	0.85	2.4	5.1
3.1	0.55	3.4	0.80	1.5	4.9
4.2	0.50	3.3	0.73	0.7	4.0
4.7	0.64	3.5	0.98	1.5	5.0
5.8	0.46	2.3	0.90	1.7	4.0
6.9	0.48	4.1	0.90	1.7	5.8
7.8	0.40	3.8	0.80	3.7	7.5
9.6	0.32	3.0	0.80	2.1	5.1
10.3	0.26	2.4	0.75	2.4	4.8
10.7	0.23	1.9	0.73	2.6	4.5

[a]Electrolyses were carried out in phosphate buffers of ionic strength 0.5 M at a RVC working electrode in a thin-layer cell.

[b]Applied potential corresponds to the peak potential of peak I_a determined by running a voltammogram in the thin-layer cell. This potential also oxidizes the peak corresponding to peak II_a at a PGE microelectrode.

[c]Applied potential was the peak potential of the last voltammetric oxidation peak observed in the thin-layer cell. Electrolysis at this potential was carried out after exhaustive electrolysis at peak I_a potentials.

Electrolysis at peak I_a potentials was also found to electrolyze the species which is responsible for peak II_a. The number of electrons transferred under these conditions was 3.0±0.7e per molecule. This compares with the value of 2.8e for peak II_a electrolysis in pH 4.7 phosphate buffer in the large-scale electrolysis cell. The number of electrons transferred for complete electrolysis in the thin-layer cell is 4.8±0.6e per molecule compared to 3.1 in the bulk electrolysis at peak V_a. This suggests the possibility that some of the products generated (in the oxidation processes which occur at more negative potentials) during bulk electrolysis are decomposing to electroinactive compounds before they can be electrolyzed further. Since the electrolyses in the thin-layer cell are usually completed in less than 25 minutes there is not nearly as much time for the decomposition to take place.

Thin Layer Spectroelectrochemistry

Because the cyclic voltammetry indicates that several intermediates are generated in the peak I_a electrolysis of 5-MTHP it was decided to study these intermediates using thin-layer spectroelectrochemistry. A number of electrolyses were also carried to completion to study the u.v. spectrum of the products.

The first pH studied was 4.7 because many of the other investigations had been carried out at this pH. In pH 4.7 phosphate buffer, μ=0.5, the peak potential of peak I_a was 0.57V/SSCE in the RVC thin-layer cell. Electrolyses were then carried out at potentials somewhat negative of the peak I_a potential to minimize interference by

other oxidation processes. Electrolyses of 1.0 mM 5-MTHP were carried out at 0.39 V (ca. $E_p/2$) for 100s and 0.49V (E_p-80 mV) for 50s to generate an appreciable concentration of the intermediates. The results are presented in Figure 16. No significant differences are noted for the two different potentials. Curve 1 in Figures 16A and B is the spectrum of 5-MTHP at pH 4.7 and exhibits maxima at 215 nm and 266 nm. Upon initiation of the oxidation the peak at 215 nm began to decrease and the peak at 266 nm increased. After a short time the RVC working electrode was open-circuited and the spectra in curve 2 were recorded. U.v. peaks are at λ_{max}=219 nm and 269 nm in curve 2 of Figure 16A,B. As the intermediate species decays, the absorbance of the short wavelength peak increased and the absorbance of the peak at 269 nm decreased. A general increase in absorbance was noted in the region above ca. 320 nm. Curve 3 (Figure 16A,B) is the spectrum after complete decay of the intermediate and peaks are now observed at λ_{max}=216 nm, 264 nm, 316 nm, and 387 nm. The largest absorbance change occurred at ca. 264 nm.

When the electrolyses at these two potentials were carried to completion several differences were observed. After electrolysis at 0.39V/SSCE the spectrum shown in curve 2 of Figure 17A is observed with λ_{max}=216 nm, (276) nm, (305) nm, and 390 nm. The peak at 216 nm is very broad and the inflection at 305 nm is quite pronounced. When the electrolysis potential was 0.49V/SSCE the spectrum of the electrolysis product (curve 2, Figure 17B) had λ_{max}=205 nm, (231) nm, (278) nm, (305) nm, and 388 nm. The peak at 388 nm was observed to be considerably larger when electrooxidation was carried out at the more positive potential and the inflection at 305 nm is considerably smaller. 7,8-

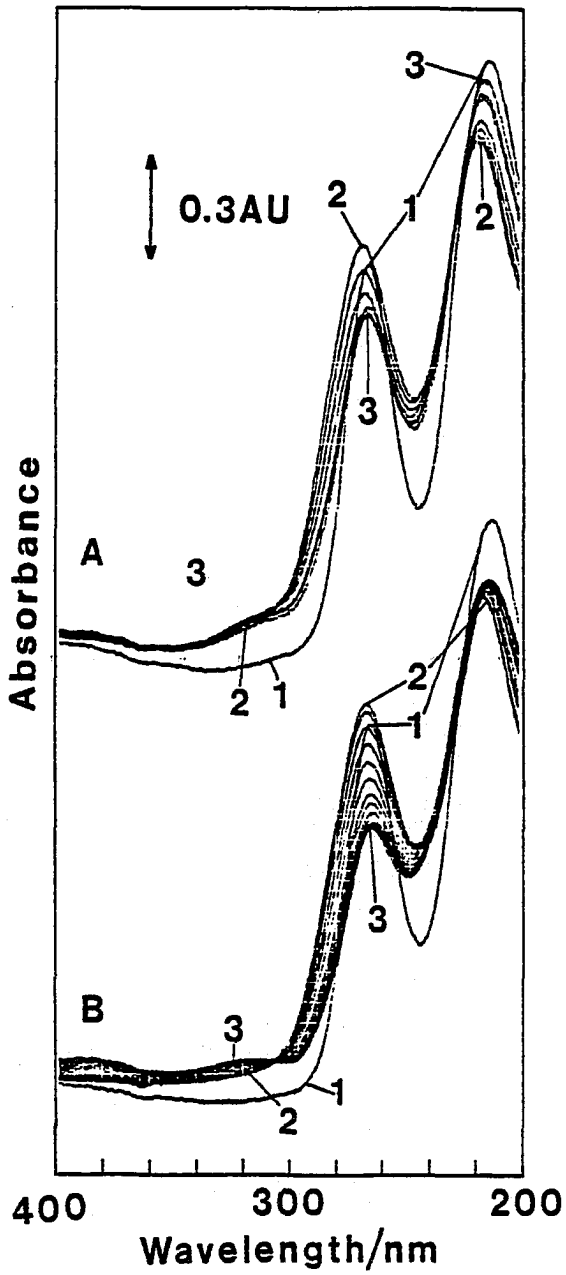


Figure 16. Spectra observed during Peak I_a electrolysis of 1.0 mM 5-MTHP and decay of the intermediate species generated at a RVC electrode in a thin-layer cell. Repetitive scans are 19s. Buffer was pH 4.7 phosphate, μ=0.5 M. Curve 1 is the spectrum of 5-MTHP. Curve 2 is the spectrum immediately upon open-circuiting the RVC working electrode after (A) 100s electrolysis at 0.39V/SSCE ($E_p/2$) and (B) 50s electrolysis at 0.49V/SSCE (E_p - 80 mV). Curve 3 is the spectrum after decay of the intermediate.

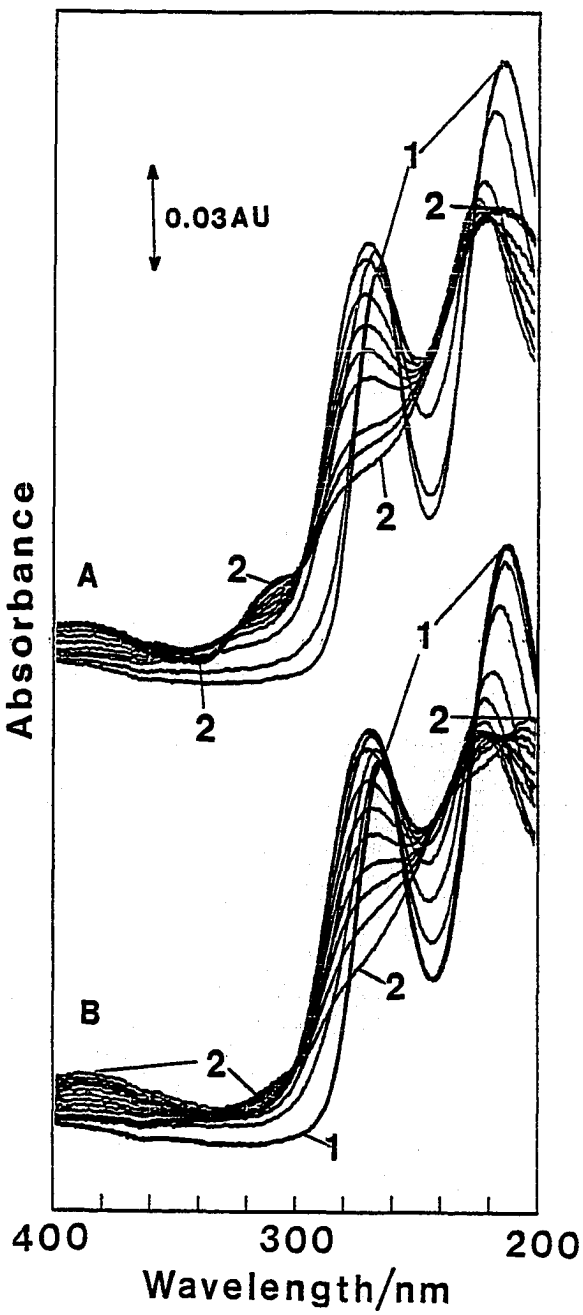


Figure 17. Spectra observed during complete electrolysis of 1.0 mM 5-MTHP in pH 4.7 phosphate buffer, μ=0.5 M at a RVC electrode in a thin-layer cell. Curve 1 is the spectrum of 5-MTHP before electrolysis. Curve 2 is the spectrum after complete electrolysis at (A) 0.39V/SSCE ($E_p/2$) and (B) 0.49V/SSCE (E_p - 80 mV). Consecutive scans are 19s.

dihydroxanthopterins have an absorption maximum at ca. 305 nm and xanthopterin has an u.v. peak at 388 nm.[40] Therefore electrolysis at the more positive potential apparently produces more xanthopterin.

In Figure 16 (pH 4.7) the peak which is observed in curve 3 at ca. 316 nm is characteristic for 7,8-dihydropterin (7,8-DHP). The reported spectrum for 7,8-DHP has u.v. maxima at λ=280 nm and 320 nm at pH 6.8.[40] The peak at ca. 316 nm was not observed when the potential was applied until electrolysis was complete (curve 3, Figure 17A,B). 7,8-DHP is the rearrangement product of quinonoid-dihydropterin and was oxidized as quickly as it was produced. However, if the working electrode was open-circuited after a significant quantity of the quinonoid was generated, u.v. peaks characteristic of 7,8-DHP were observed in the spectrum illustrated by curve 3 in Figure 16.

Above the pK_a (5.99) of 5-MTHP the initial spectrum of 1.0 mM 5-MTHP exhibits u.v. peaks at λ_{max}=218 nm and 288 nm (Figure 18, curve 1). At pH 7.83 the peak potential of peak I_a is 0.38 V/SSCE in the RVC thin-layer cell. Since there is no apparent difference between the behavior when a partial electrolysis is carried out at $E_p/2$ or at 80 mV negative of the peak potential, further electrolyses to generate the intermediate were done at E_p - 80 mV so a higher concentration of the intermediate could be obtained. After electrolysis at 0.30V/SSCE for 50s, the RVC working electrode was open-circuited and the spectrum in curve 2 of Figure 18 was recorded. The peak at 218 nm is no longer observed, instead a new peak at 246 nm is observed. The peak at 288 nm only exhibits a decrease in absorbance during the partial electrolysis. Since the peak at 246 nm is not observed in either the spectrum of 5-MTHP

(curve 1, Figure 18) or in the spectrum of the final product (curve 3, Figure 18) it must be characteristic of the intermediate. Curve 3 of Figure 18 is the spectrum of the final product with u.v. peaks at 226 nm and 284 nm and an inflection at ca. 332 nm. This compares almost exactly with the reported spectrum of 7,8-DHP at pH 7 (λ_{max}=230 nm, 280 nm, and 330 nm).[7]

The spectral changes which occur between curves 2 and 3 (Figure 18) are quite unusual. For example, the absorbance of the peak at 287 nm first decreases and then increases again. Similar behavior is exhibited in the wavelength region above 320 nm. When the electrolysis was carried to completion the spectrum in curve 2 of Figure 19 is observed with λ_{max}=209 nm, (234) nm, (260) nm, (301) nm, and 398 nm. The peak at 398 nm is ca. the wavelength of the long wavelength peak of xanthopterin. None of the peaks of 7,8-DHP were observed when the electrolysis was carried to completion.

Kinetic study. Depending on the wavelength which was monitored, either one or two first order rate constants are observed. An absorbance vs. time curve at pH 6.9 for rearrangement of the intermediates from peak I_a electrooxidation of 5-MTHP is shown in Figure 20A. This A vs. t curve illustrates the type of behavior which yielded two rate constants. The method for calculating the two rate constants is reported in the 6-MDHP section of Part II. The fact that there are two rate constants is immediately obvious when a plot of ln A vs. t is prepared (Figure 20B). One first order rate constant gives a straight line when ln A vs. t is plotted. Table 3 lists the rate constants obtained for rearrangement of peak I_a electrooxidation generated intermediates. Two rate constants

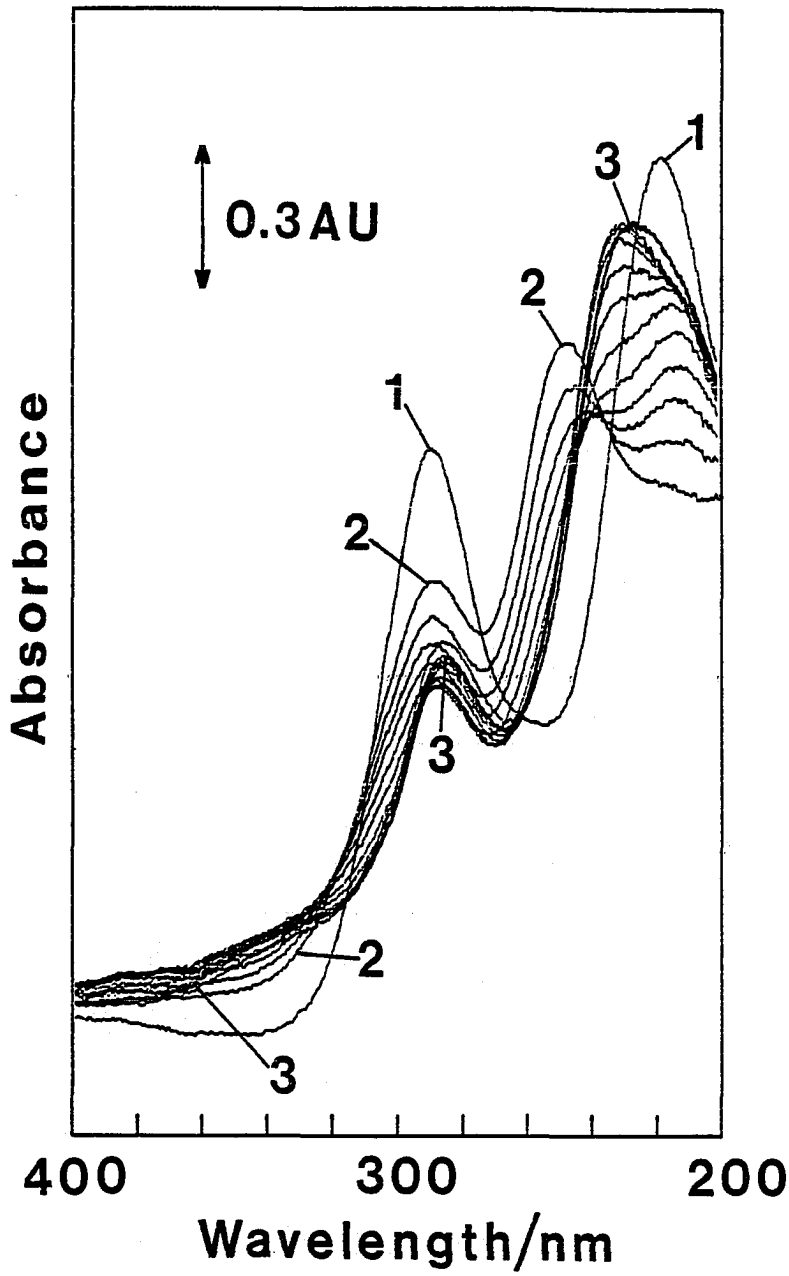


Figure 18. Spectra observed during Peak I_a electrolysis of 1.0 mM 5-MTHP and subsequent decay of the intermediate generated in pH 7.8 phosphate buffer at a RVC electrode in a thin-layer cell. Curve 1 is the spectrum of 5-MTHP. Curve 2 is the spectrum immediately upon open-circuiting the RVC electrode after 50s electrolysis at 0.30V/SSCE (E_p - 80 mV). Curve 3 is the spectrum after complete decay of the intermediate. Repetitive scans are 19s.

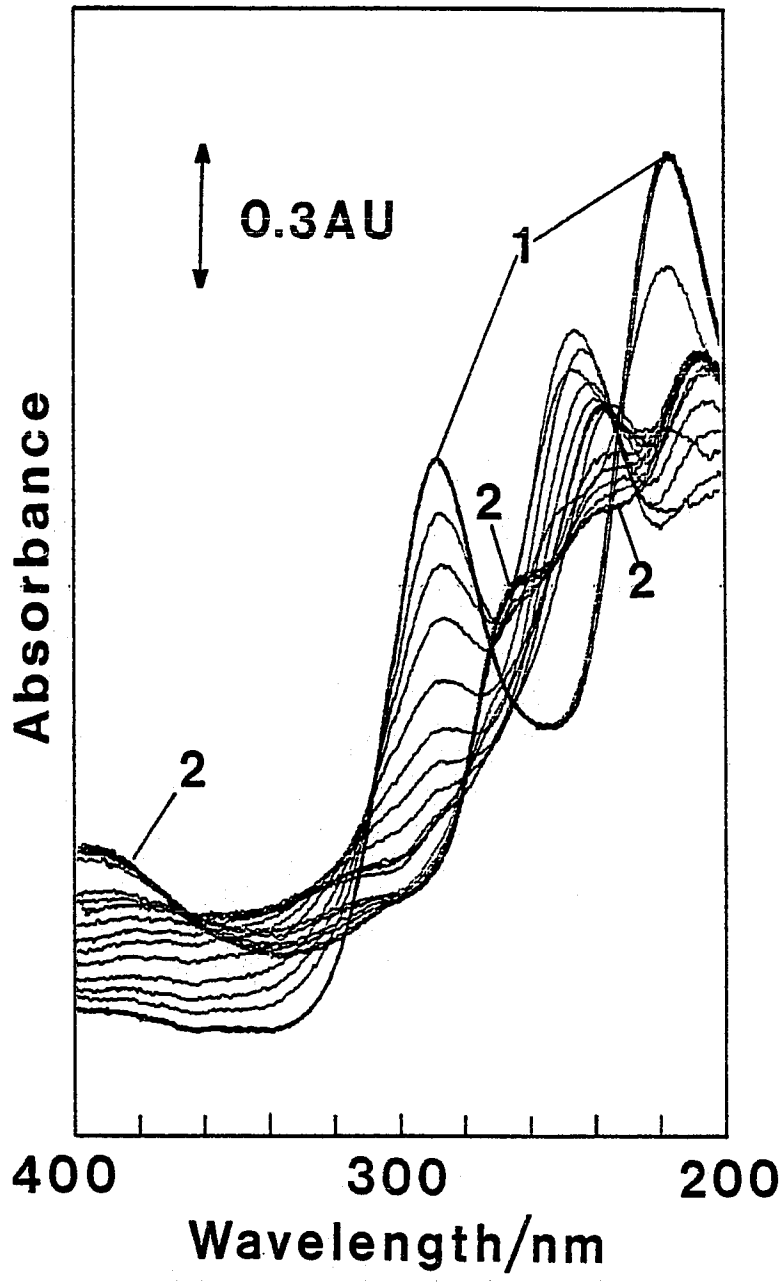


Figure 19. Spectra observed during complete electrolysis of 1.0 mM 5-MTHP in pH 7.8 phosphate buffer, μ=0.5 M at a RVC electrode in a thin-layer cell. Curve 1 is the spectrum of 5-MTHP. Curve 2 is the spectrum after complete electrolysis at 0.30V/SSCE (E_p - 80 mV). Repetitive scans are 19s.

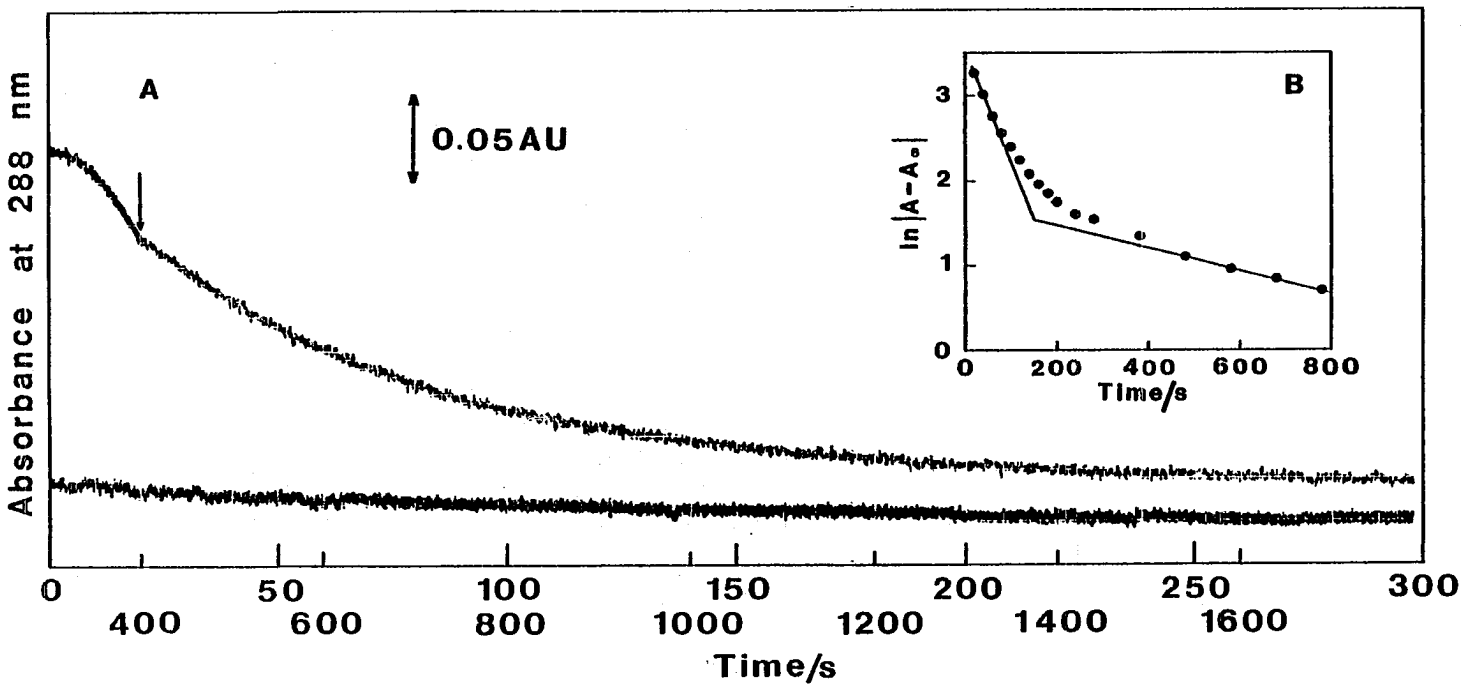


Figure 20. (A) Absorbance vs. time curve observed after electrooxidation of 1.0 mM 5-MTHP in pH 6.9 phosphate buffer, μ=0.5 M at peak I_a potentials (0.24V/SSCE, $E_p/2$). Arrow indicates time at which the working electrode was open-circuited. (B) Ln $|A-A_\infty|$ vs. t plot for the decay curve in A

are not always observed because sometimes the slow rate constant could not be determined due to diffusion of the starting material into the RVC working electrode.

At pH 6.9 and 7.8 the rate constants for the fast step compare quite well with those reported for the chemical rearrangement of the quinonoid-dihydropterin generated from tetrahydropterin.[7] As the pH is decreased further the rate constant does not increase, but instead is observed to become much smaller. This slower step could be rearrangement of 5-methyl-5,8-dihydropterin because none of the intermediates generated in the electrooxidation of 7,8-DHP and tetrahydropterin absorb at 246 nm.

Identification of Peak I_a Electrolysis Products of 5-MTHP

Products from electrolyses in pH 4.7 PO_4^{3-}, μ=0.5 M. Silylation of the separated products from electrolyses carried out in pH 4.7 phosphate buffer was rather unsuccessful. BSA, BSTFA, and MTBSTFA were all tried as silylating reagents and pyridine and acetonitrile were tried as solvents. The temperature and time of the silylation reaction were varied in an attempt to obtain a derivatized product. All the components which elute near the phosphate peaks in the liquid chromatography were so contaminated with phosphate that the only GC peak observed was that of silylated phosphate.

MTBSTFA was used as the silylating reagent at a temperature of 140°C. The total ion current chromatogram in the GC-MS always exhibited the same peaks regardless of the compound which was silylated. These

TABLE 3

First Order Rate Constants Obtained for the Chemical Rearrangement of Intermediates Generated Upon Electrooxidation of 1.0 mM 5-MTHP at Peak I_a[a]

pH[b]	$k_1 \times 10^2/s^{-1}$	k[e]	$k_2 \times 10^2/s^{-1}$
4.7		0.23±0.03	
5.8	2.5±0.7[f]	1.1±0.1	0.9±0.1
6.9	1.7±0.3	1.7±0.4	0.20±0.09
7.8	1.7±0.2	1.4±0.3	0.80±0.07

[a]Potentials applied correspond to $E_p/2$ and E_p-80 mV. Electrolysis was at a RVC working electrode in a thin-layer cell.

[b]Phosphate buffers having an ionic strength of 0.5 M.

[c]Rate constant obtained by subtracting the contribution to the total absorbance contributed by the slow step.

[d]Rate constant for slow step. Both rate constants were determined at several wavelengths.

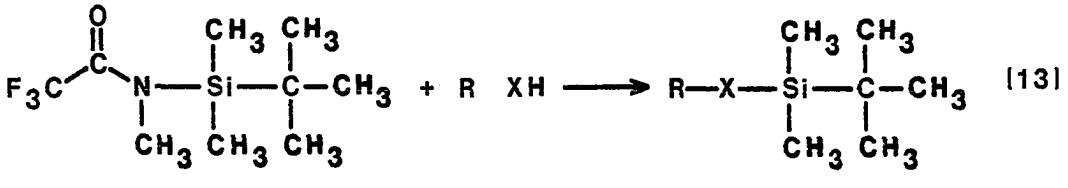
[e]Only one rate constant was observed in some instances because slow step was obscured by diffusion of starting material into the RVC working electrode.

[f]One rate constant was observed when electrolysis was at E_p-80 mV. Two when electrolysis was at $E_p/2$.

peaks were determined to be reaction, degradation, or rearrangement products of the silylating reagent by running a GC-MS (gas chromatography-mass spectrometry) analysis on a blank containing only MTBSTFA and pyridine. It was later found that in several instances the product was successfully silylated, but the size of the product peak was so much smaller than the peaks characteristic of MTBSTFA that it appeared insignificant.

Phosphate silylates very easily with MTBSTFA even at room temperature exhibiting a large peak in the total ion current chromatogram at a retention time (R_t) of ca. 29-30 minutes (Figure 21). The mass spectrum of triply silylated phosphate is shown in tabular form in Figure 22. It almost always has a base peak at a mass of 383 (M-57) and a prominent peak at mass 425 (M-15). Often the molecular ion (M^+) is also observed at mass 440 if the total counts for that peak are above ca. 10,000.

However it is not necessary to observe the molecular ion when interpreting mass spectra of MTBSTFA silylated derivatives because of the intensity of the M-57 peak. Thus the mass of the molecular ion can be obtained by simply adding 57. Mass spectra of compounds silylated with MTBSTFA will almost always show the clearly recognizable pattern of M-57 and M-15 peaks even if the sample is dilute. The reason for this is the structure of the t-butyldimethylsilyl (TBDMS) group which is transferred to the sample from MTBSTFA by the reaction shown in Equation 13:



[13]

MTBSTFA

X = O, N, S, etc.

In the mass spectrometer the easiest fragment to lose is the tertiary butyl carbonium ion because of its stability, hence the intense M-57

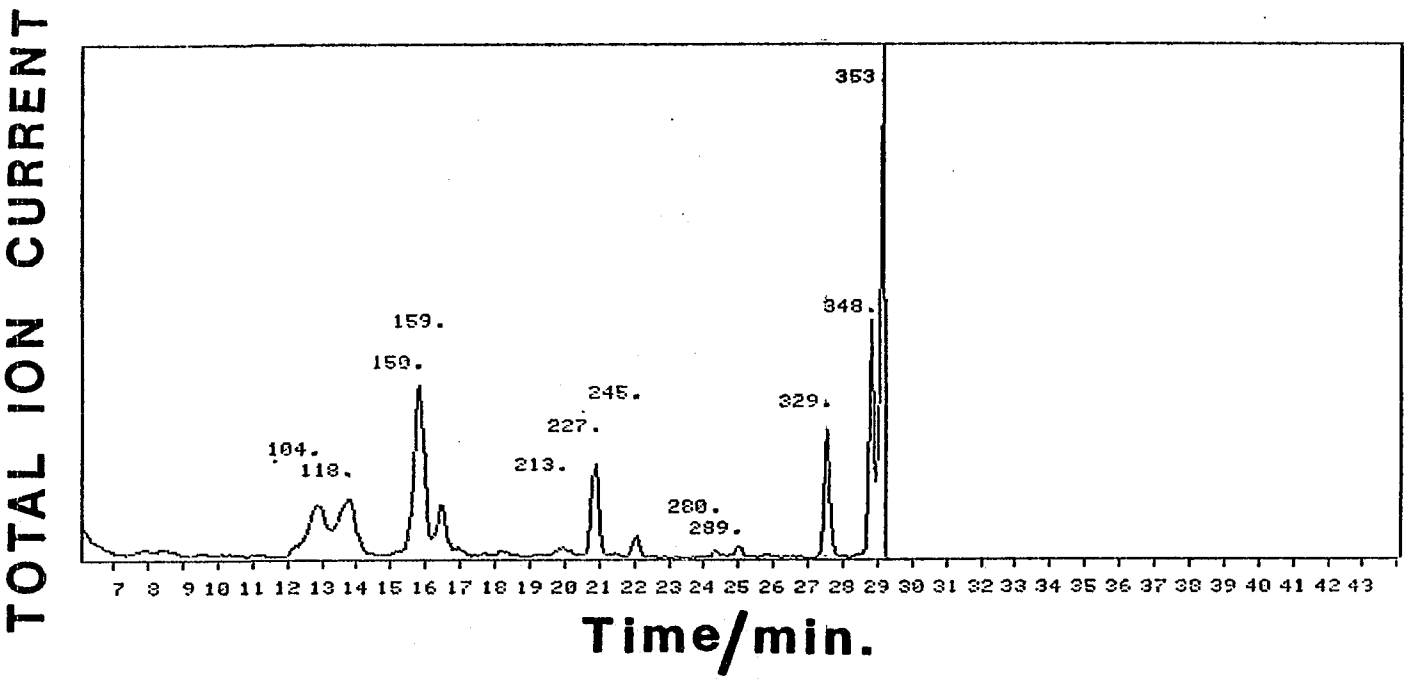


Figure 21. Typical ion current chromatogram of a MTBSTFA silylated product only partially separated from phosphate buffer showing the phosphate peak at 29 minutes.

MASS	%	MASS	%	MASS	%	MASS	%	MASS	%	MASS	%	MASS	%	MASS	%
97.0	.3	179.0	1.6	243.0	.2	328.1	2.0								
99.0	.8	180.9	4.0	251.1	.6	328.9	.6								
103.1	.5	182.0	.6	253.0	1.2	330.1	.2								
104.9	.4	183.0	1.2	255.0	8.1	341.0	1.8								
107.1	.2	189.0	.7	256.0	2.5	342.0	.5								
115.0	1.5	191.0	4.0	256.9	1.8	343.0	.3								
116.1	.2	192.9	11.2	257.9	.5	351.1	.4								
117.0	.4	193.9	2.2	266.9	.3	353.1	.4								
119.0	.6	195.0	2.6	269.0	14.1	367.2	1.0								
121.0	.8	195.9	.4	270.0	15.9	368.2	.4								
123.0	.4	196.9	2.4	270.9	4.9	369.0	.4								
130.9	.6	198.0	.3	272.0	4.9	383.2	100.0								
132.9	8.5	198.9	.3	273.0	1.2	384.1	32.8								
134.0	1.3	205.0	.6	273.9	.6	385.0	19.3								
135.0	2.9	207.0	7.9	280.8	.2	386.0	3.9								
136.0	.4	208.0	1.6	283.0	.3	387.0	.8								
136.9	1.6	209.0	1.2	284.0	.4	409.0	.3								
137.9	.2	211.0	15.7	285.1	.2	425.1	5.2								
139.0	.2	212.0	2.5	286.0	.2	426.1	2.0								
147.0	2.2	213.0	1.9	294.9	.9	427.1	.8								
148.0	.5	214.0	.2	297.0	.5	428.1	.2								
148.9	.6	221.1	.4	297.9	.3	439.2	.2								
150.9	.4	223.1	.2	299.0	.3										
152.9	.5	224.9	.3	309.0	.8										
154.8	.2	227.1	.3	311.1	1.0										
163.0	.3	235.0	.3	312.0	.5										
165.0	.8	237.0	1.2	312.9	.3										
166.2	.2	238.0	.2	322.9	.2										
167.0	.9	239.0	.3	325.0	.6										
177.0	.9	241.0	1.4	326.0	.9										
177.9	.3	241.9	.3	327.1	1.4										

Figure 22. Mass spectrum of phosphate triply silylated with MTBSTFA. R_t=30 minutes.

peak. Loss of a single methyl group is responsible for the M-15 peak. Replacement of an active hydrogen by a TBDMS group increases the molecular weight by increments of 114 g/mole for each group transferred.

One problem associated with the analysis of samples containing significant amounts of phosphate is contamination of the GC column packing material. In samples containing phosphate some of the phosphate was observed to dissolve in the reagent/solvent mixture and remain in the underivatized state. This was subsequently injected into the GC column. After the solvent was boiled off in the GC column a deposit of phosphate remained at the head of the column. Subsequent injections of samples which did not contain phosphate were observed to yield chromatograms exhibiting a large phosphate peak because excess MTBSTFA in the sample silylated the underivatized phosphate remaining on the column from previous injections.

Silylation of products from low phosphate buffer. Because of the very limited success with the silylation of the products from peak I_a electrooxidation of 5-MTHP in pH 4.7 PO_4^{3-} of ionic strength 0.5 M, it was decided to lower the phosphate concentration of the buffer. A "buffer" was subsequently prepared which had a sodium dihydrogen phosphate concentration of 10 mM. This buffer also contained 0.5 M NaCl as a supporting electrolyte. The pH was adjusted to 4.7 by adding microliter quantities of ca. 0.1 N HCl or 1 N NaOH.

The potential for the electrolysis was determined by running a voltammogram directly in the electrolysis cell and setting the potential at $E_p/2$ (usually 0.20V/SCE). The close proximity of peak II_a to peak I_a prevents electrooxidation at potentials more positive if the peak

II_a process is to be minimized. During the electrolysis the pH was continuously monitored and was maintained at 4.7±0.1 by adding microliter quantities of ca. 1 N NaOH. Samples of the electrolysis solution were taken at the beginning and at intervals throughout the electrolysis. These were lyophilized and silylated with MTBSTFA in pyridine at 100°C for 15 minutes. Of course these samples contained large amounts of chloride and a small amount of phosphate.

Aliquots removed early in the electrolysis showed the presence of primarily phosphate at R_t=28.9 minutes, singly silylated 5-MTHP (MW=295) at 33.2 minutes and doubly silylated 5-MTHP (MW=409) at 36.8 minutes (Figure 23). The peaks at R_t=33.2 and 36.8 minutes were identified by comparison to the total ion current chromatogram (Figure 24) and mass spectrum of a solid sample (no Cl^-) of 5-MTHP (MW=181) starting material silylated in a similar manner with MTBSTFA. This chromatogram shows peaks corresponding to silylation at one position (MS=295, R_t=33.1 min.), two positions (MW=409, R_t=37.2 min.), and three positions (MW=523, R_t=40.3 min.). The mass spectra of these peaks are presented in Figures 25-27. Later during the electrolysis the only peak observed in the total ion current chromatogram has a R_t=29.3 minutes and corresponds to triply silylated phosphate (MW=440). No other peaks were observed to increase as the electrolysis proceeded. Apparently phosphate is much more easily silylated than the electrolysis products of 5-MTHP.

Silylation of products from a solution containing only NaCl as the supporting electrolyte. It was decided to eliminate phosphate altogether from the electrolysis solution and use only 0.5 M NaCl as

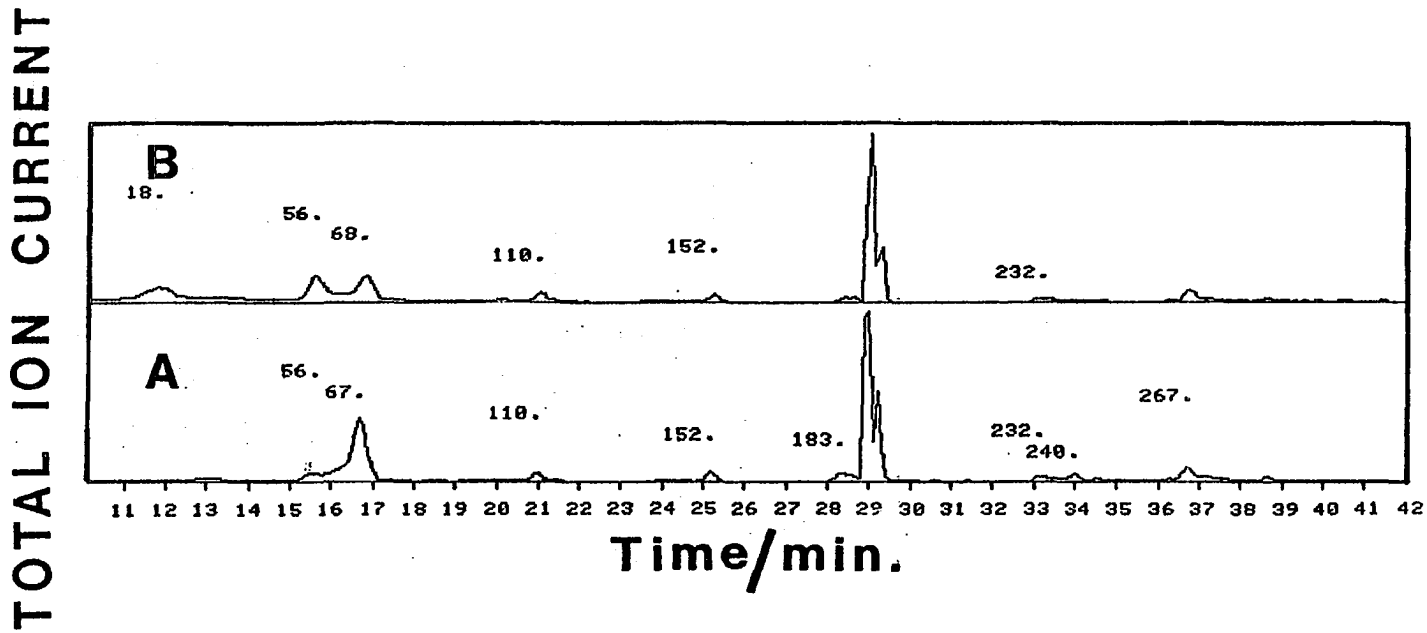


Figure 23. Total ion current chromatogram of aliquots of 5-MTHP electrolyzed at Peak I_a in a low phosphate buffer and silylated with MTBSTFA. (A) Chromatogram of solution before electrolysis. (B) Chromatogram of solution with ca 10% of 5-MTHP oxidized.

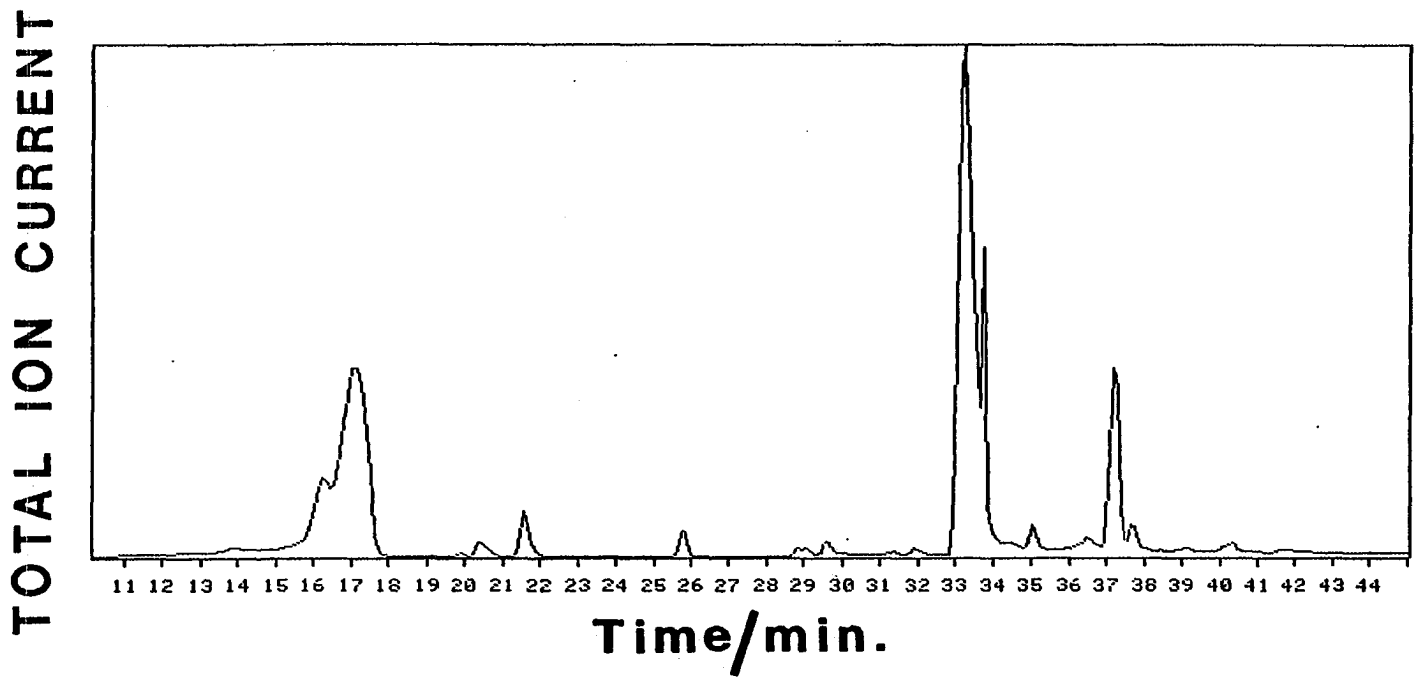


Figure 24. Total ion current chromatogram of 5-MTHP starting material silylated with MTBSTFA in pyridine at room temperature for 75 minutes.

MASS	%	MASS	%	MASS	%	MASS	%	MASS	%	MASS	%	MASS	%	MASS	%
90.5	.2	127.1	.4	160.0	.0	196.9	.6	240.1	2.4	293.1	.3				
92.1	.2	128.1	.2	161.0	.1	198.1	.1	241.0	.3	299.2	.3				
93.1	.5	128.9	.2	162.0	.4	199.2	.0	242.1	.0	300.2	.1				
94.1	.9	130.1	.0	163.0	.5	202.0	.1	246.1	.0	301.3	.0				
95.1	.8	131.0	.1	164.0	1.0	203.0	.0	247.2	.0	307.2	.0				
96.1	.8	133.0	.1	165.0	1.0	204.0	.5	248.1	.1	309.0	.0				
97.1	1.0	134.1	.3	166.0	2.1	205.0	.2	249.1	.4	310.1	.0				
98.1	1.1	135.0	.6	167.0	1.0	206.0	.5	250.1	.4	334.1	.1				
99.1	4.6	136.0	.4	168.0	1.1	207.0	.7	251.1	.2	335.2	.0				
100.1	2.7	137.0	1.0	169.0	.5	208.0	3.1	252.1	.1	336.1	.0				
101.1	.9	138.0	1.6	170.1	.1	209.0	1.4	253.1	.2	337.1	.0				
102.1	.6	139.0	1.0	171.0	.0	210.0	1.2	254.1	.0	352.2	.3				
104.2	.4	140.0	.5	173.1	.0	211.0	.2	262.0	.2	353.2	.1				
106.2	.3	141.0	.5	176.0	.0	212.0	.1	263.0	.2	354.2	.0				
107.1	.5	142.0	.2	177.0	.1	213.0	.0	264.1	.4	355.1	.0				
108.2	.5	143.1	.1	178.0	.4	218.1	.0	265.0	1.6	409.3	.1				
109.0	.6	144.1	.0	179.1	.5	220.0	1.5	266.1	.4	410.3	.0				
110.2	1.6	145.0	.0	180.1	2.0	221.0	3.7	267.1	.1						
111.2	2.2	146.1	.1	181.0	1.6	222.1	11.0	277.0	.0						
113.1	.4	147.0	.3	182.0	1.7	223.1	100.0	278.1	.6						
114.1	.2	148.0	1.3	183.0	.6	224.1	18.9	279.1	.5						
115.2	.2	148.9	.8	184.1	.2	225.0	5.1	280.1	4.8						
116.2	.1	150.0	.5	185.0	.0	226.1	.7	281.1	1.2						
117.2	.2	151.1	.5	189.0	.0	227.1	.0	282.1	.3						
118.7	11.1	152.0	1.2	190.0	.2	232.0	.0	283.1	.0						
121.1	.5	153.1	.7	191.1	.3	233.1	.0	292.1	.0						
122.1	.8	154.1	.9	192.0	.6	234.0	.1	293.1	.1						
123.1	.5	155.0	.5	193.0	3.9	235.1	.2	294.1	2.6						
124.1	1.1	156.1	.1	194.0	1.1	236.1	.7	295.2	47.9						
125.1	1.5	157.0	.1	195.0	2.4	238.1	53.9	296.2	9.8						
126.1	.6	157.9	.0	196.0	2.1	239.1	9.4	297.1	2.7						

Figure 25. Mass spectrum of 5-MTHP silylated in one position with MTBSTFA. R_t=33.1 minutes.

MASS	%	MASS	%	MASS	%	MASS	%	MASS	%	MASS	%	MASS	%	MASS	%
91.1	.2	122.1	.6	158.0	3.1	189.1	.1	220.1	2.0	261.0	.1	306.1	.6	353.2	29.7
92.2	.2	123.1	.6	159.0	.9	190.0	.3	221.0	1.2	262.0	.4	307.2	.3	354.2	10.3
93.0	.7	124.1	1.2	160.1	.4	191.0	.4	222.0	5.5	263.0	.3	308.2	.3	355.2	2.0
94.1	.5	125.1	2.7	161.0	.1	192.0	.4	223.1	4.5	264.0	.8	309.1	.2	356.1	.4
95.1	1.1	126.1	1.4	162.0	.5	193.0	1.1	224.1	1.4	265.0	.5	310.1	.4	357.0	.1
96.1	.8	127.1	1.1	163.1	.5	194.0	1.0	225.0	.7	266.0	2.0	311.1	.1	359.2	.1
97.1	.9	128.1	.6	164.1	.4	195.1	.9	226.1	.3	267.0	.7	312.1	.1	364.3	.1
98.1	2.1	129.0	.7	165.1	.7	196.1	2.6	227.2	.2	268.1	.3	313.1	.1	366.2	.1
99.1	10.3	130.0	1.4	166.0	1.3	197.0	1.3	231.0	.1	269.0	.1	320.1	.4	367.2	.1
100.1	6.0	131.1	2.3	167.1	1.5	197.9	1.0	232.0	.1	271.3	.1	321.1	.4	368.2	.1
101.1	1.4	132.8	2.7	168.1	9.2	199.1	.4	233.0	.1	276.0	.2	322.1	1.7	369.2	.1
102.1	.6	133.8	.7	169.0	2.1	200.1	.1	234.0	.2	277.0	.4	323.1	.6	376.2	.1
103.1	.3	135.0	.5	170.0	.6	201.0	.1	235.0	.3	278.0	1.3	324.1	.6	378.3	.2
104.2	.2	136.0	.3	171.1	3.6	201.9	.2	236.1	2.2	279.1	1.8	325.0	.2	379.3	.2
105.2	.3	137.1	.9	172.1	1.1	203.0	.1	237.1	3.7	280.0	17.7	326.1	.1	380.2	.1
106.2	.2	138.1	2.6	173.0	1.7	204.0	.4	238.1	2.2	281.0	6.7	327.1	.1	381.3	.1
107.1	.3	139.1	4.8	174.1	.3	205.0	.3	239.1	1.0	282.0	2.4	334.1	1.5	391.2	.1
108.2	.3	140.1	16.2	175.1	.2	206.0	1.0	240.1	.4	283.0	.5	335.1	.9	392.1	.2
109.1	.7	142.1	1.1	176.1	.7	207.0	1.9	241.1	.2	284.0	.1	336.1	2.3	393.2	.2
110.1	1.9	143.0	.9	177.0	.4	208.0	1.2	242.1	.1	290.0	.1	337.1	7.8	394.2	7.1
111.2	1.7	144.0	.4	178.1	.4	209.0	.8	246.1	.1	291.1	.1	338.1	2.7	395.2	2.2
112.2	1.2	145.1	.2	179.1	1.0	210.0	.6	247.1	.1	292.1	.3	339.2	1.3	396.1	.8
113.1	3.2	147.6	10.5	180.1	1.7	211.0	.4	248.0	.2	293.1	.2	340.1	.3	397.2	.2
114.1	1.1	150.0	.5	181.0	1.4	212.0	.1	249.1	.3	294.1	2.2	341.2	.2	408.2	2.6
115.2	1.3	151.1	.6	182.0	1.4	213.0	1.4	250.1	1.4	295.1	2.1	342.1	.1	409.2	62.1
116.2	.7	152.1	1.1	183.0	1.4	214.1	.4	251.1	.9	296.1	2.5	347.1	.1	410.2	20.1
117.1	.9	153.1	1.0	184.0	.6	215.0	.2	252.1	.6	297.1	.8	348.1	.2	411.3	7.0
118.1	.4	154.1	.9	185.1	.3	216.1	.1	253.0	.9	298.1	.3	349.1	.1	412.2	1.4
119.1	.9	155.0	.9	186.0	.1	217.0	.1	254.1	.3	299.2	.1	350.0	.4	413.2	.3
120.0	.4	156.0	.7	187.1	.1	218.0	.1	255.1	.1	304.1	.1	351.2	2.2		
121.1	.4	157.0	2.7	187.9	.1	219.1	.2	260.0	.1	305.0	.1	352.2	100.0		

Figure 26. Mass spectrum of 5-MTHP silylated in two positions with MTBSTFA. R_t=37.2 minutes.

MASS	%	MASS	%	MASS	%	MASS	%	MASS	%	MASS	%	MASS	%	MASS	%
91.2	9.1	128.1	4.0	161.0	9.1	199.0	1.7	251.2	3.0	335.2	2.0				
93.0	26.9	129.1	10.6	162.2	3.5	202.1	2.0	253.0	3.7	337.1	3.0				
94.1	3.5	130.0	3.5	163.0	8.1	203.1	4.2	255.2	2.0	339.1	1.5				
95.1	11.6	131.1	7.7	165.0	4.7	204.9	8.4	262.0	1.8	341.0	6.1				
96.1	16.5	132.1	4.2	165.8	1.8	207.0	100.0	263.1	1.7	342.1	1.7				
97.0	8.9	132.9	18.2	167.0	2.4	208.0	23.7	264.9	3.9	342.9	1.8				
98.1	1.8	133.9	6.7	168.1	3.0	208.9	16.1	265.8	1.7	350.2	2.9				
99.1	10.4	135.0	13.9	169.1	3.7	210.0	4.4	266.9	4.4	352.2	2.9				
100.1	14.6	136.1	2.5	170.9	3.9	213.0	2.2	269.0	2.0	353.2	2.5				
101.1	3.2	137.0	3.0	173.1	3.9	215.0	2.0	277.0	2.7	355.1	6.7				
102.1	1.7	138.2	1.8	175.1	23.4	217.0	3.4	278.0	1.7	356.1	2.5				
103.0	5.7	139.0	2.9	176.1	5.0	218.2	1.7	279.0	2.0	357.1	2.2				
104.1	2.7	140.2	2.5	177.0	28.1	219.1	6.9	280.1	2.2	367.1	2.5				
105.1	9.6	141.0	3.9	178.1	6.9	220.1	19.5	280.9	19.7	369.2	18.0				
107.2	2.9	141.9	2.4	179.1	12.4	221.0	26.4	282.0	5.5	370.3	5.4				
109.2	3.2	143.0	2.9	180.1	3.0	222.1	7.1	283.0	4.4	371.3	1.8				
110.2	2.9	144.0	1.7	181.0	2.7	223.1	16.8	284.0	1.5	409.3	2.2				
111.2	4.7	145.0	6.1	182.1	1.8	224.0	4.4	292.2	46.4	429.0	2.4				
112.2	2.4	147.1	34.1	183.0	3.7	225.0	4.2	293.1	13.8	466.3	6.1				
113.1	3.0	148.1	6.4	184.0	3.0	226.0	1.7	294.2	4.9	467.4	2.7				
115.2	8.9	148.9	16.5	185.2	2.9	231.2	2.2	295.1	11.1	482.4	6.1				
116.2	4.9	150.0	5.0	187.0	1.7	233.0	3.4	296.1	3.2	483.3	2.2				
117.2	14.5	151.2	4.2	189.1	7.7	234.2	2.9	297.0	2.4	523.4	8.2				
119.1	17.6	152.1	3.5	190.0	4.0	235.1	28.4	299.1	2.2	524.3	4.5				
120.1	2.4	152.9	2.2	191.1	23.4	236.2	7.7	311.3	2.7	525.3	2.5				
121.0	4.4	153.9	3.2	192.1	5.4	237.1	4.9	313.1	85.0						
123.2	3.5	155.1	4.2	193.0	11.3	238.1	8.2	314.1	21.8						
124.1	1.7	156.1	2.0	194.0	2.9	239.2	2.2	315.1	6.1						
125.1	2.7	157.0	3.9	195.0	2.5	247.1	1.8	325.0	2.2						
126.1	1.7	158.0	3.4	196.1	2.9	249.0	3.9	327.0	2.9						
127.1	3.9	159.1	4.0	197.1	12.1	250.1	2.4	334.1	3.0						

Figure 27. Mass spectrum of 5-MTHP silylated in three positions with MTBSTFA. R_t=40.3 minutes.

the electrolyte. Again the pH was maintained at 4.7±0.1 by adding small quantities of 1 N NaOH. Initially 5 mg of 5-MTHP was electrolyzed in 25 ml of 0.5 M NaCl. The 5-MTHP concentration is about 0.75 mM under these conditions. Comparison of the total ion current chromatograms of samples taken at intervals throughout the electrolysis and silylated with MTBSTFA is shown in Figure 28. The peaks at R_t=33.2 minutes and 37.2 minutes corresponding to 5-MTHP silylated in one and two positions respectively are observed to decrease as the electrolysis proceeds. It appears that a peak at a retention time of 16.5 minutes increases as the electrolysis proceeds. However repetition of this experiment and later experiments failed to reproduce these results, i.e., the size of the peak at R_t=16.5 minutes was not related to the progress of the electrolysis. Since it also appeared in all other chromatograms of silylated products when MTBSTFA was used it must be a by-product of the silylation reagent.

Since no product peaks were observed, the concentration of starting material was doubled to 10 mg. (ca. 1.5 mM). It has been observed by other workers that when attempting to silylate unisolated products the concentration of the starting material must be at least 1 mM. The complete procedure for taking aliquots of the electrolysis solution and silylating them will be detailed in the Experimental Chapter. As can be seen in Figure 29 a peak is observed to increase in size during the course of the electrolysis at a retention time of 36.9 minutes. The mass spectrum of this peak can be seen in Figure 30 and exhibits a base peak of mass 334 (M-57). It also exhibits peaks at mass 376 and 391 which are the M-15 and M^+ peak respectively. This was

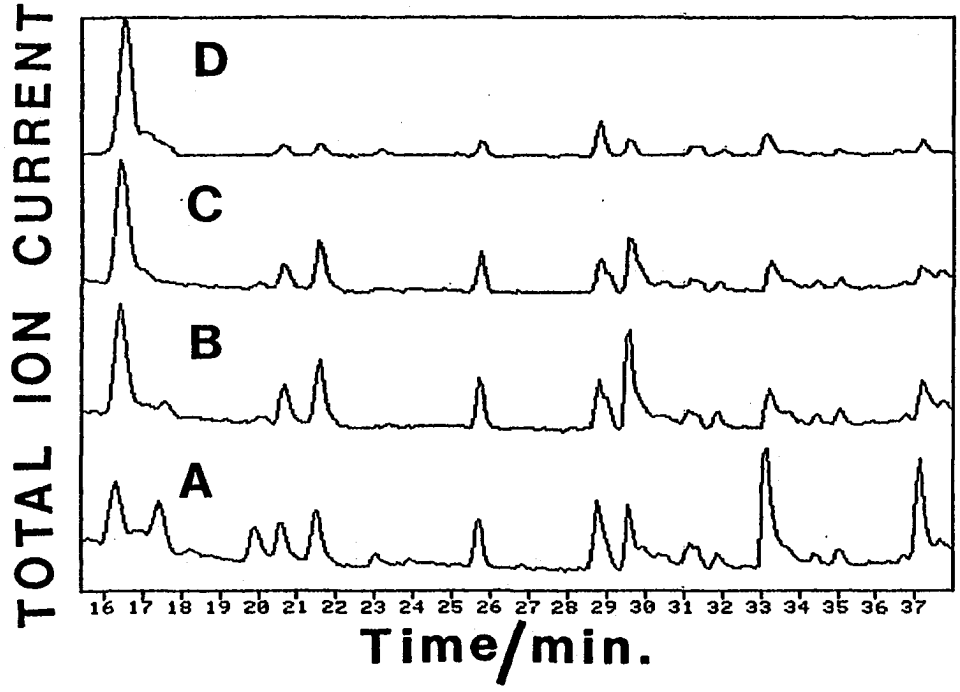


Figure 28. Comparison of total ion current chromatograms of samples taken during Peak I_a electrolysis of 5 mg of 5-MTHP in pH 4.7 NaCl and silylated with MTBSTFA. Percent 5-MTHP electrolyzed: (A) 0%, (B) 12%, (C) 23%, and (D) 31%.

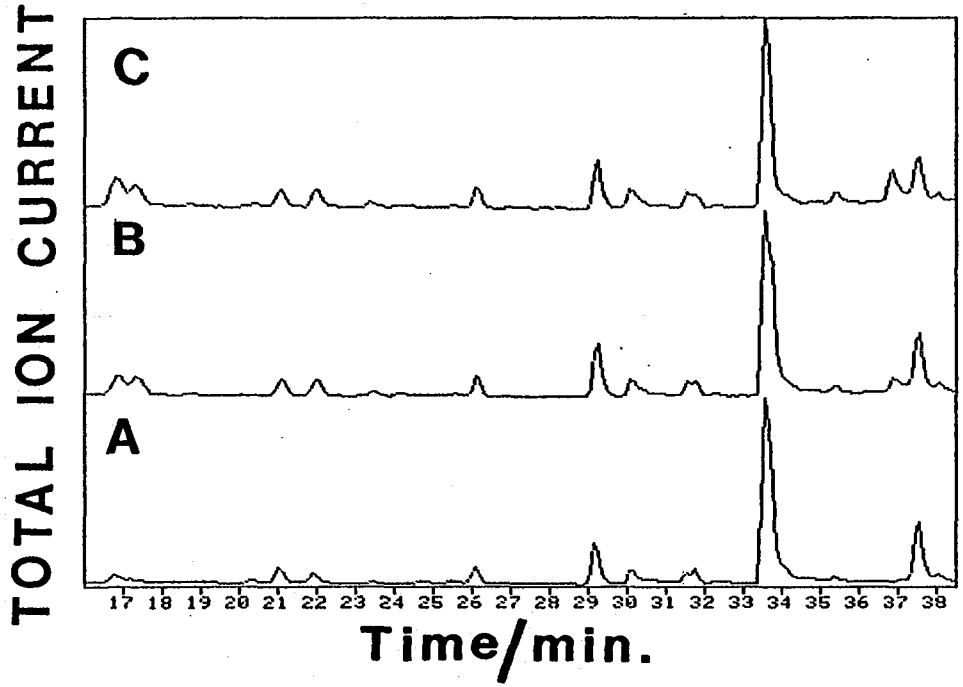


Figure 29. Comparison of total ion current chromatograms of samples taken during Peak I_a electrolysis of 10 mg of 5-MTHP in pH 4.7 NaCl and silylated with MTBSTFA. Percent 5-MTHP electrolyzed: (A) 0%, (B) 32%, and (C) 58%.

MASS	%	MASS	%	MASS	%	MASS	%	MASS	%	MASS	%	MASS	%	MASS	%
91.0	.9	122.1	.2	157.0	2.5	189.1	.2	235.0	3.0	284.1	.1	339.1	.2		
92.0	.4	123.1	1.0	158.0	1.9	190.0	.4	236.1	.8	292.1	.4	341.1	.3		
93.0	2.5	124.1	.7	159.1	.6	191.0	.6	237.0	.6	293.0	.2	351.3	.2		
94.0	.5	125.1	.6	160.0	.2	192.0	.6	238.1	1.0	294.1	.2	352.1	2.1		
95.0	1.4	126.1	.4	160.9	.4	192.9	.6	239.1	.3	295.1	.7	353.2	1.0		
96.0	.9	126.9	.8	162.0	.2	194.0	.4	240.1	.1	296.1	.2	354.2	.4		
97.0	.8	128.0	.8	163.0	.3	195.0	.3	244.9	.1	297.1	.2	355.1	.3		
98.0	1.1	129.0	.5	164.0	.2	196.0	.2	246.0	.2	304.1	.3	356.1	.1		
99.1	5.1	130.9	2.7	165.0	.4	197.0	.3	246.9	.5	305.0	.1	376.2	3.1		
100.1	3.8	131.9	1.6	166.0	.2	198.0	.8	248.1	.4	310.1	.1	377.2	.9		
101.1	.8	133.0	2.1	167.1	.3	199.0	.2	249.0	.4	312.0	.2	378.2	.4		
102.0	.5	134.0	2.5	168.1	.4	202.0	2.5	250.1	.3	313.1	.2	379.3	.3		
103.1	.5	134.9	.7	169.0	.4	203.0	.6	251.1	1.4	315.2	.8	383.2	.3		
104.3	.5	135.9	.4	170.0	.2	204.1	.8	252.1	.4	316.2	.2	390.2	.2		
105.0	.5	137.0	.3	171.0	1.6	205.1	.6	253.1	.3	317.1	.2	391.2	2.2		
106.0	.1	138.6	6.2	172.0	.4	206.1	1.6	260.1	.4	318.0	.3	392.1	1.0		
107.0	.2	141.0	.7	173.0	.9	207.0	4.8	261.0	.3	319.1	.4	393.1	.3		
107.9	.2	142.0	1.2	174.1	.3	208.0	1.6	262.0	.6	320.1	.3	394.3	.2		
109.0	.4	143.0	.9	175.0	.2	209.0	1.9	263.0	.4	321.1	.2	395.2	.1		
110.1	.6	144.1	.3	176.1	.5	210.1	.5	264.0	.3	322.1	1.6	409.2	1.2		
111.2	.6	144.9	.2	177.0	1.5	211.0	.3	265.0	.4	323.1	.7	410.2	.5		
112.1	.3	146.0	.6	178.0	1.0	213.0	.7	266.0	.2	324.1	.2	411.2	.2		
113.0	.5	147.0	3.6	179.1	.5	214.1	.2	267.0	.3	325.1	.2	413.3	.1		
114.0	.2	148.0	.9	180.0	.5	218.0	.2	276.1	1.0	327.2	1.0	429.2	.1		
115.0	1.0	148.9	1.0	181.1	.5	220.0	13.8	277.0	5.9	328.2	.3	469.2	.2		
116.2	.4	150.0	1.3	182.0	.5	221.0	3.1	278.0	5.0	329.0	.1				
117.1	2.0	150.9	.5	183.0	.4	222.0	1.3	279.0	2.3	334.1	100.0				
118.0	.8	152.0	.5	184.0	1.5	223.0	1.4	280.0	1.0	335.1	38.5				
119.0	1.1	153.1	.3	185.0	.4	224.0	.4	281.0	1.3	336.1	13.1				
120.1	.4	154.0	.3	186.0	.2	225.0	.2	281.9	.4	337.1	3.8				
121.1	.3	155.1	.5	188.0	.2	234.1	.6	283.0	.3	338.1	.7				

Figure 30. Mass spectrum of peak at R_t=36.9 minutes from chromatogram of Figure 29C.

determined from the characteristic pattern shown by MTBSTFA silylated derivatives. The sample from the electrolysis of 10 mg 5-MTHP at 58% completion (Figure 29C) also exhibits peaks at R_t=39.6 minutes and 41.0 minutes which have molecular ions of mass 423 and 553 respectively.

To determine the number of positions which are silylated in a particular derivative it is necessary to silylate it with a different silylation reagent. Since MTBSTFA was used, either BSA or BSTFA (which transfer a trimethylsilyl group) were used to determine the number of silylated positions using the following equation:

$$MI_{MTBSTFA} - MI_B = 42(n) \qquad (14)$$

$MI_{MTBSTFA}$ is the molecular weight of the molecular ion when silylated with MTBSTFA. MI_B is the molecular ion when silylated with BSA or BSTFA. n is the number of silylatable sites. This equation applies however only if the compound can be silylated by both reagents.

Samples from another 10 mg electrolysis of 5-MTHP at peak I_a potentials in pH 4.7±0.1 NaCl, 0.5 M were silylated with BSA in pyridine at 100°C for 15 minutes. The sample at 77% completion shows a number of peaks not observed in the sample taken before the electrolysis was begun. All the peaks after 32 minutes are not observed in the first sample taken before the electrolysis (Figure 31). However only the peak at R_t=35.1 minutes (M^+=339) appears to have a counterpart in a similar sample silylated with MTBSTFA. This is the peak at 39.6 minutes in Figure 29C which exhibits M^+=423. The number of silylated positions was determined using Equation 14.

$$423 - 339 = 84 = 42(n)$$
$$n = 2$$

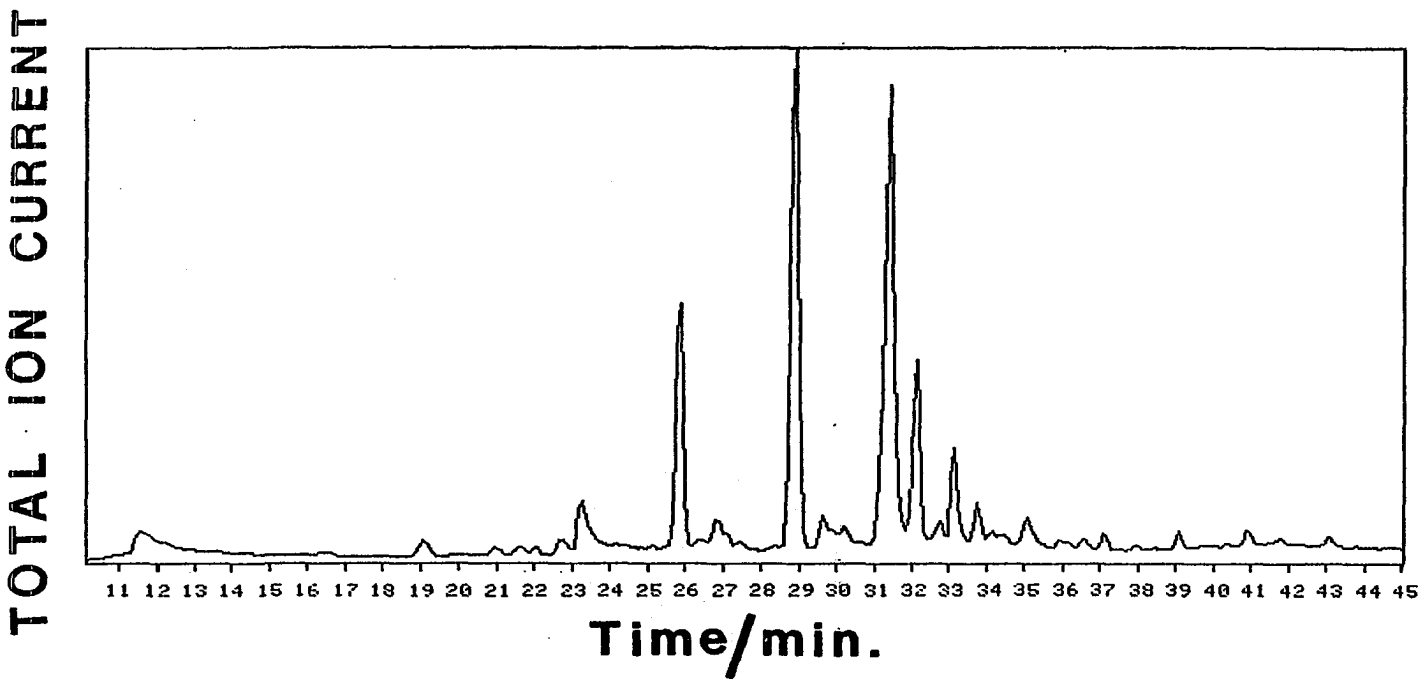


Figure 31. Total ion current chromatogram of a sample from Peak I_a electrolysis of 10 mg of 5-MTHP in pH 4.7 NaCl silylated with MTBSTFA. Electrolysis was 77% complete.

The molecular weight of the non-silylated compound is 195 g/mole. No peak was observed in the total ion current chromatogram which corresponds to the peak with molecular ion of mass 391 observed in the MTBSTFA silylation.

By far the most significant information was obtained by silylation of samples taken during the peak I_a electrolysis of 15 mg 5-MTHP in pH 4.7±0.1 NaCl, 0.5 M. Comparison of the total ion current chromatograms for the four samples silylated with MTBSTFA at 100°C for 15 minutes is shown in Figure 32. There are a number of peaks which increase in size as the electrolysis proceeds. These peaks are summarized in Table 4. From Table 4 it can be seen that several components of the electrolysis solution are present in higher concentration during the electrolysis than at the completion of the electrolyses. Once again the peak at a retention time of 36.7 minutes (M^+=391) is one of the largest peaks, particularly early in the electrolysis.

Another fully electrolyzed sample from the same electrolysis was silylated with MTBSTFA in pyridine. This time the silylation was done at room temperature for ca. 45 minutes. Silylation at room temperature with MTBSTFA revealed some differences from silylation at 100°C (Figure 33). These differences are summarized in Table 5. It is possible that those peaks which are only observed at high temperature are due to the degradation and/or rearrangement of the MTBSTFA.

At this point a number of possibilities appeared reasonable to account for the products of peak I_a electrolyses of 5-MTHP when silylated with MTBSTFA. Unfortunately BSA or BSTFA did not silylate nearly as many products, therefore the number of silylated positions could not be

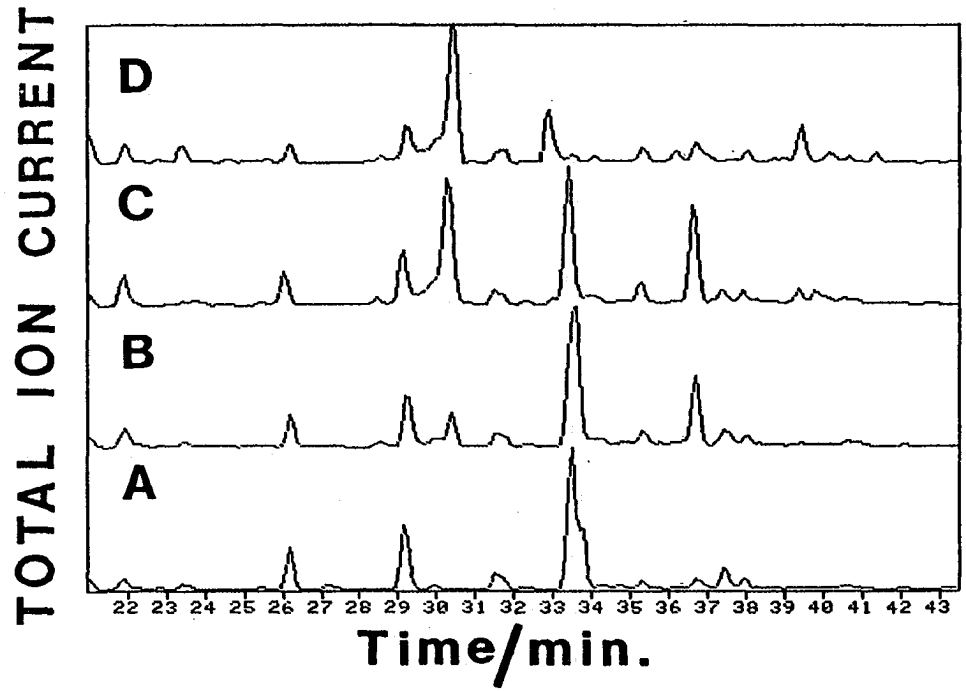


Figure 32. Comparison of total ion current chromatograms of samples taken during Peak I_a electrolysis of 15 mg 5-MTHP in pH 4.7 NaCl and silylated with MTBSTFA. Percent 5-MTHP electrolyzed: (A) 0%, (B) 30%, (C) 67%, and (D) 100%.

TABLE 4

Molecular Ions for GC-MS Peaks[a] Which Increase During Peak I_a

Electrolysis of 15 mg 5-MTHP in pH 4.7 NaCl, 0.5 M

R_t/min.	Counts[b]	M^+	Counts[c]
24.4	3,298	288	
30.3	51,980	401	
31.8	5,198	518	
32.9	55,470	266	
36.2	6,525	516	
36.7	14,387	391	59,190[e]
38.8	1,116	407	
39.3	21,150	423	
39.8	----[d]	432	4,664
40.2	3,838	421	
41.4	6,814	437	
42.8	870	521	1,069
43.6	1,057	537	

[a]Sample was silylated with MTBSTFA/Pyridine at 100°C for 15 minutes.

[b]Counts are from the sample which was taken from the fully electrolyzed solution.

[c]Counts are from the sample which was 67% electrolyzed. Only those counts are listed in which the peak was larger than in the fully electrolyzed solution.

[d]No peak with this R_t was observed in the fully electrolyzed sample.

[e]The peak at R_t = 36.7 minutes was actually even larger in the sample which was only 30% electrolyzed.

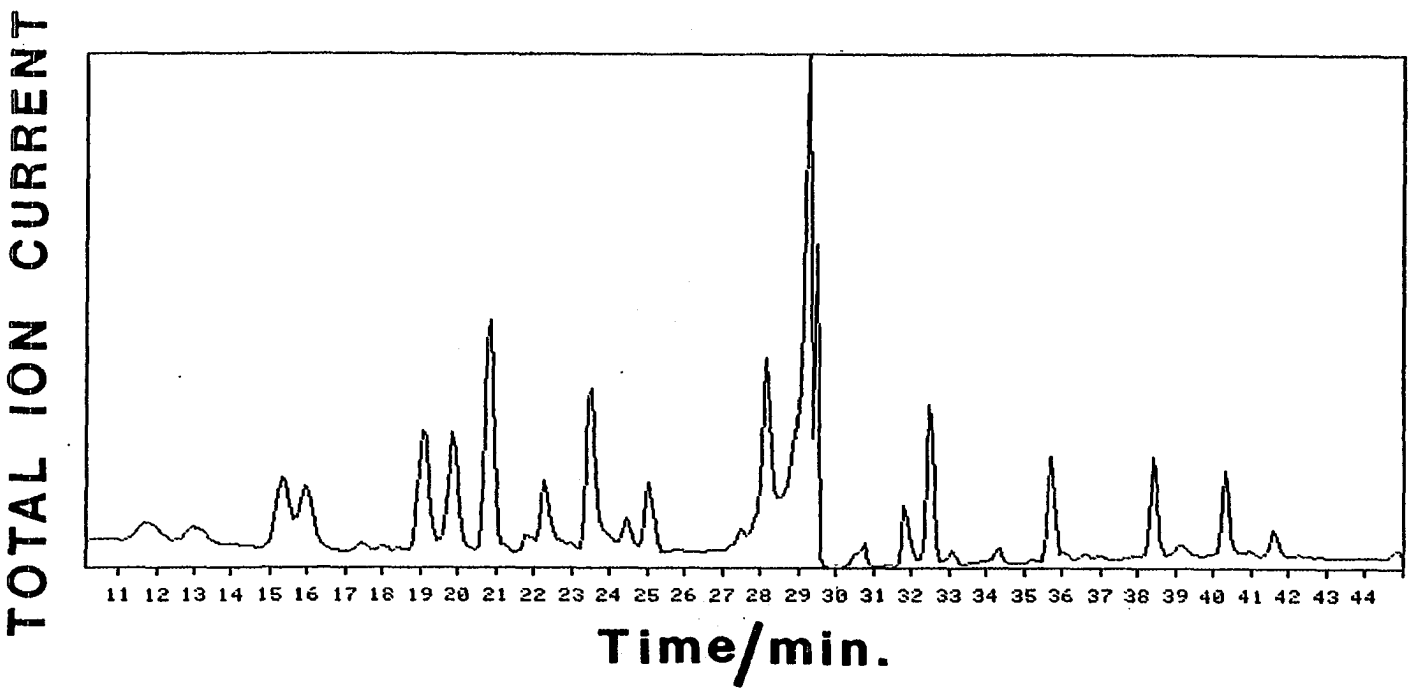


Figure 33. Total ion current chromatogram of a fully electrolyzed sample from peak I_a electrolysis of 15 mg of 5-MTHP in pH 4.7 NaCl. Silylation was carried out with MTBSTFA at room temperature for ca. 30 minutes.

TABLE 5

Comparison of Fully Electrolyzed Samples at Different Silylation Temperatures from Electrolysis of 15 mg 5-MTHP in pH 4.7 NaCl[a]

M^+	Sample 1[b] R_t/min.	Counts	Sample 2[c] R_t/min.[d]	Counts
236	*	*	19.0	10,509
288	24.6	3,298	23.5	7,539
401	30.4	51,980	29.3	21,712
518	31.8	5,198	30.9	173
471	*	*	32.5	4,418
516	36.2	6,525	*	*
391	36.7	14,387	35.7	6,049
407	38.8	1,116	*	*
423	39.5	21,150	38.5	2,488
421	40.2	3,838	39.1	390
437	41.4	6,814	40.3	5,792
521	42.8	870	41.6	1,299
537	43.6	1,057	*	*
551	*	*	44.8	642

*Peaks are not observed for this molecular ion.

[a]Samples were silylated with MTBSTFA/pyridine.

[b]Silylation was carried out at 100°C, 15 minutes. Total counts were 3.31×10^5.

[c]Silylation was carried out at room temperature for ca. 45 minutes. Total counts were 9.50×10^4.

[d]The observed retention time is somewhat different than for sample 1 because of a change in the carrier gas flow rate.

determined unequivocally. Table 6 contains all the possible molecular weights for nonderivatized molecules which could give the molecular ions listed in Table 5 when using MTBSTFA as the silylating reagent. An increment of 114 g/mole is subtracted for each TBDMS group. The

TABLE 6

Possible Molecular Weights Which Could Yield the Observed Molecular Ions When Silylated with MTBSTFA

M^+	Number of Possible Silylation Sites			
	1	2	3	4
236	122			
288	174	60		
401	287	173	59	
518	404	290	176	62
471	357	243	129	
516	402	288	174	60
391	277	163	49	
407	293	179	65	
423	309	195	81	
421	307	193	79	
437	323	209	95	
521	407	293	179	65
537	423	309	195	81
551	437	323	209	95
553	439	325	211	97

most likely possibilities for electrooxidation products are those which have molecular weights relatively close to that of the starting material, 5-MTHP (181 g/mole).

A number of peaks were observed in the linear sweep voltammetry at 5 mV s^{-1} which had very similar peak potentials to the electrooxidation peaks of tetrahydropterin (vide supra). A redox couple was also observed near 0V in the cyclic voltammetry of 5-MTHP which exhibited behavior the same as the reversible couple formed by tetrahydropterin and its quinonoid-dihydropterin. Therefore the possibility of finding pterin (MW=163) in the electrolysis solution of 5-MTHP is raised. Indeed the silylated derivative which exhibits a molecular ion of mass 391 (see Table 6) could be pterin substituted with 2 TBDMS groups.

A second set of samples from peak I_a electrolysis of 15 mg 5-MTHP in pH 4.7 NaCl was available for silylation with BSA in pyridine at 100°C for 15 minutes. Fortunately a counterpart was observed for the peak exhibiting mass 391 when silylated with MTBSTFA. Comparison of the total ion current chromatograms of BSA silylated samples obtained at intervals during the electrolysis revealed several peaks that increased as the electrolysis progressed (Figure 34). The peak at a retention time of 30.1 minutes has a molecular ion of 307 and a base peak of 292 (M-15) (Figure 35). Therefore Equation 14 was used to obtain the molecular weight of the underivatized compound:

$$391 - 307 = 84 = 42(n)$$

$$n = 2$$

Therefore the compound must have a mass of 391-(114)2=307-(72)2=163 g/mole.

To further investigate the possibility that pterin is the compound of MW=163, an authentic sample of pterin (VI) was silylated with MTBSTFA

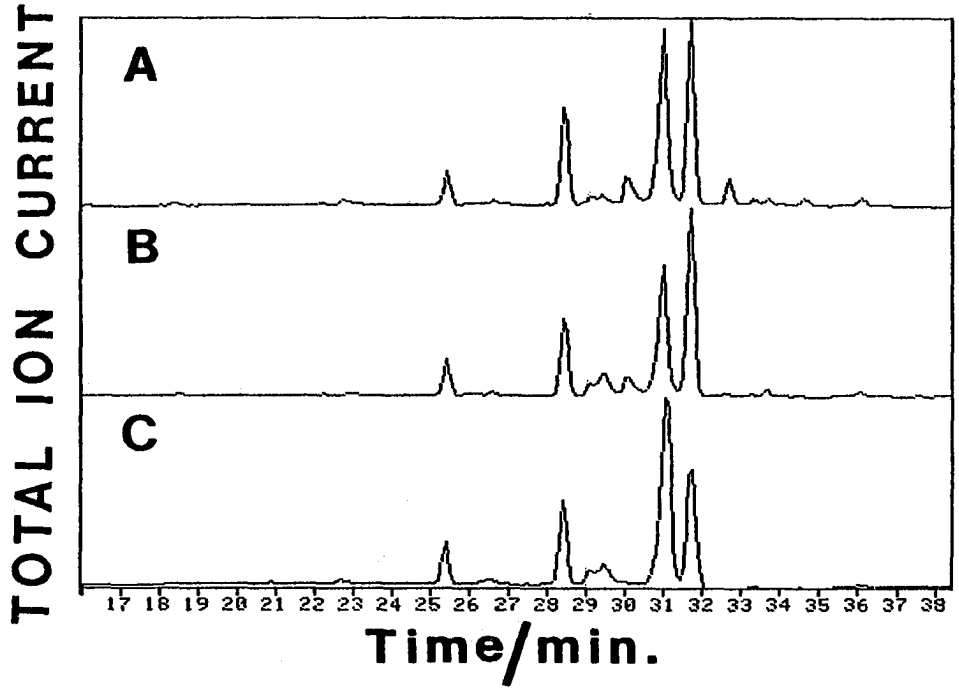
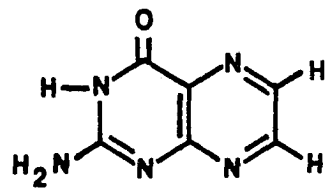


Figure 34. Comparison of total ion current chromatograms of samples taken during Peak I_a electrolysis of 15 mg 5-MTHP in pH 4.7 NaCl and silylated with BSA. Percent 5-MTHP electrolyzed: (A) 0%, (B) 30%, and (C) 67%.

MASS	%	MASS	%	MASS	%	MASS	%	MASS	%	MASS	%	MASS	%	MASS	%
91.1	1.8	126.1	2.3	178.0	2.6	237.1	2.8								
92.1	8.5	128.1	1.3	179.0	1.1	238.1	3.0								
93.0	5.0	128.9	1.7	180.1	1.1	253.2	4.0								
94.0	2.7	131.0	13.2	181.0	1.3	254.2	1.1								
95.1	4.2	132.0	4.7	182.1	1.1	263.1	1.3								
96.1	1.3	133.0	4.4	183.0	1.2	277.0	1.3								
97.1	2.3	134.0	1.9	191.2	1.3	281.0	2.9								
98.1	3.7	135.1	6.7	193.0	2.9	291.2	3.7								
99.1	19.7	136.0	1.8	194.0	1.8	292.1	100.0								
100.1	20.5	138.5	33.5	195.1	1.1	293.1	27.8								
101.0	4.2	141.0	1.9	197.0	3.6	294.2	11.2								
102.0	2.3	142.0	2.2	198.1	2.2	295.1	2.4								
103.1	3.0	142.9	1.1	202.1	2.9	296.1	1.1								
104.1	6.7	144.8	1.1	203.2	1.1	306.1	3.0								
104.9	2.4	147.1	46.3	204.0	3.6	307.2	58.2								
109.0	2.4	148.0	8.5	205.0	1.4	308.1	17.0								
110.1	2.7	149.1	8.6	207.0	5.9	309.1	6.5								
111.0	2.3	150.0	2.9	208.2	1.3	310.1	2.6								
111.9	1.2	151.0	1.9	209.2	3.9	325.2	3.1								
113.0	2.3	152.0	1.9	210.1	1.3	326.2	1.4								
114.2	1.3	155.1	1.8	217.1	1.2	355.3	1.6								
115.2	3.0	156.0	1.1	218.1	2.8										
116.1	2.9	157.0	4.7	219.1	1.9										
117.1	4.9	158.0	3.1	220.1	5.1										
118.1	2.8	159.0	1.1	221.1	6.2										
119.1	6.8	165.1	1.7	222.1	2.7										
120.0	2.3	168.1	1.2	223.1	2.6										
121.9	1.3	171.1	9.8	224.2	2.4										
123.1	4.6	172.1	2.2	234.1	3.8										
124.1	4.2	172.9	2.1	235.1	5.3										
125.0	3.2	177.1	3.2	236.1	1.3										

Figure 35. Mass spectrum of peak at 30.1 minutes from chromatogram of Figure 34C.



VI

in pyridine at 100°C for 15 minutes. A single large peak is observed in the total ion current chromatogram at a retention time of 36.0 minutes that exhibits a molecular ion of mass 391 (Figure 36). The mass spectrum of the peak with R_t = 36.0 minutes is presented in Figure 37. Comparing the authentic pterin mass spectrum in Figure 37 with the mass spectrum in Figure 30 shows that the fragmentation pattern is identical. The peak retention times are not exactly the same because of small changes in the carrier gas flow rate in the GC-MS. This information together with the voltammetric data is strong evidence of the presence of pterin in the peak I_a electrolysis product solution of 5-MTHP.

Finding pterin as one of the products of the peak I_a electrolysis of 5-MTHP was rather surprising because it indicates that the methyl group on N-(5) is lost during the electrooxidation. Since pterin is in the product solution it is reasonable to expect that it is generated from 7,8-dihydropterin.[7] Electrooxidation of covalently hydrated 7,8-dihydropterin was shown by Raghavan and Dryhurst to yield approximately equal molar quantities of pterin and 7,8-dihydroxanthopterin. At pH 4.7 covalently hydrated 7,8-dihydropterin has a peak potential for electrooxidation of 0.13V/SCE. This was calculated from the pH dependence of peak I_a' of 7,8-dihydropterin: E_p(pH 2-10)=[0.33-0.042 pH].[7] Thus it

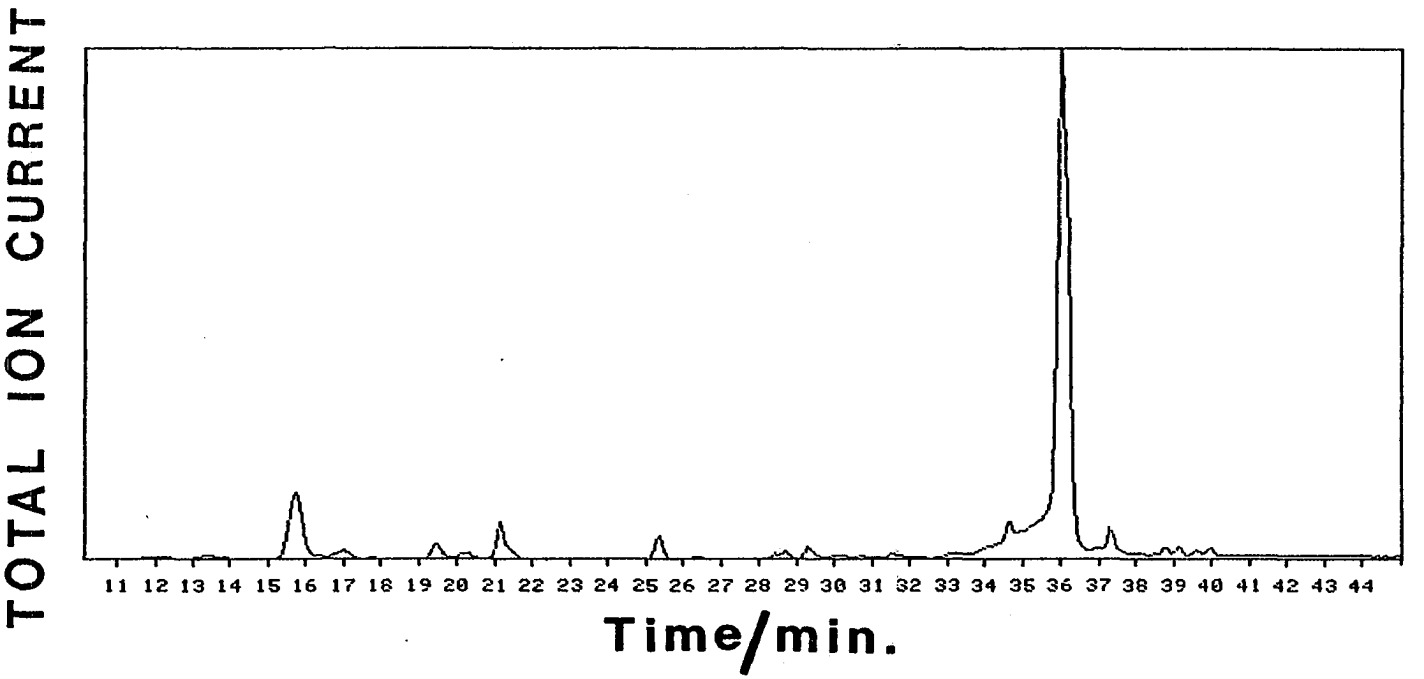
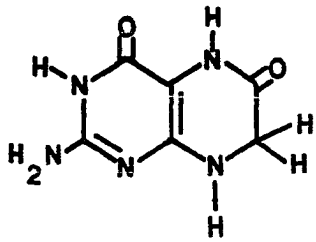


Figure 36. Total ion current chromatogram of an authentic sample of pterin silylated with MTBSTFA in pyridine at 100°C for 15 minutes.

MASS	%	MASS	%	MASS	%	MASS	%	MASS	%	MASS	%	MASS	%	MASS	%
91.1	.3	122.1	.2	155.0	.3	186.1	.0	222.0	.8	267.0	.0	327.1	.0		
92.1	.5	123.1	1.1	156.0	.5	187.1	.0	223.1	.2	274.1	.0	332.0	.0		
93.1	.3	124.0	.6	157.0	3.1	188.1	.2	224.1	.1	275.1	.0	334.1	100.0		
94.1	.3	125.1	.4	158.0	2.1	189.1	.1	225.1	.0	276.1	1.2	335.2	39.8		
95.1	.5	126.0	.4	159.1	.6	190.1	.3	226.1	.0	277.0	7.7	336.1	13.0		
96.1	.2	127.1	.2	160.1	.2	191.0	.2	230.1	.0	278.1	6.3	337.1	3.1		
97.1	.3	128.1	.4	161.0	.3	192.1	.3	231.1	.0	279.1	2.5	338.1	.5		
98.1	1.2	129.0	.2	162.0	.1	193.0	.2	232.0	.1	280.1	.7	339.2	.1		
99.1	5.0	130.1	1.1	162.9	.2	194.0	.2	233.0	.1	281.1	.2	357.0	.0		
100.1	1.8	131.0	2.8	164.0	.1	195.0	.1	235.1	4.5	282.0	.0	360.2	.1		
101.0	.7	132.0	1.7	165.1	.2	196.0	.1	236.1	1.0	288.1	.0	361.2	.0		
102.0	.4	133.0	1.7	166.1	.1	198.0	.9	237.1	.6	291.0	.0	362.2	.0		
103.1	.4	134.0	.5	167.0	.1	199.0	.1	238.0	.1	292.1	.2	374.1	.0		
104.1	.6	135.0	.2	168.0	.2	200.0	.1	244.2	.1	293.0	.1	376.2	3.1		
105.0	.3	136.0	.4	168.9	.2	202.0	2.8	245.1	.0	294.1	.0	377.2	1.0		
106.0	.0	137.0	.1	170.1	.1	203.1	.8	246.0	.2	302.1	.1	378.2	.3		
107.1	.1	138.5	3.8	171.2	.9	204.1	1.1	247.0	.5	303.2	.0	379.2	.0		
108.1	.1	141.0	.4	172.2	.2	205.0	.6	248.0	.4	304.1	.2	390.1	.2		
109.1	.3	142.0	1.5	173.0	1.2	206.0	.2	249.1	.3	305.1	.1	391.1	2.6		
110.1	.3	143.0	.8	174.0	.2	207.1	.4	250.1	.2	306.1	.0	392.1	.9		
111.1	.3	144.0	.3	175.1	.1	208.1	.3	251.1	1.9	307.0	.0	393.1	.3		
112.1	.1	145.0	.1	176.1	.4	208.9	.2	252.1	.4	308.9	.0	394.1	.1		
113.1	.2	146.0	.5	177.0	1.8	210.1	.2	253.1	.2	315.2	.0				
114.1	.1	147.0	2.7	178.0	1.1	211.1	.0	254.1	.0	316.2	.0				
115.1	.8	148.1	.6	179.1	.4	213.1	.0	259.0	.0	317.1	.1				
116.2	.4	149.0	.4	180.1	.5	214.0	.0	260.1	.4	318.1	.3				
117.1	1.3	150.0	1.1	181.0	.5	216.0	.0	261.0	.3	319.1	.4				
118.1	.5	151.0	.4	182.1	.4	217.0	.0	262.0	.8	320.1	.3				
119.1	.6	152.0	.3	183.1	.3	218.0	.3	263.0	.3	321.1	.1				
120.0	.4	153.0	.2	184.0	.1	220.0	11.5	264.0	.1	322.1	.0				
121.0	.1	154.0	.1	185.0	.0	221.0	2.6	265.0	.0	323.1	.0				

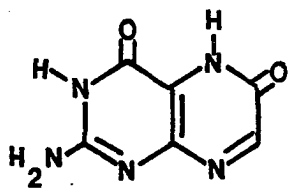
Figure 37. Mass spectrum of an authentic sample of pterin silylated with MTBSTFA. R_t=36.0 minutes in Figure 36.

would immediately be electrooxidized at the potentials used in the electrolysis (0.23-0.26V/SCE). Consequently the possibility exists that the electrolysis product solution should also contain 7,8-dihydroxanthopterin (VII) with a molecular weight of 181 g/mole.



VII

Inspection of Table 6 does not reveal a silylated product which could be a derivative of a molecule with a molecular weight of 181 g/mole. However it does list a molecular ion of a silylated derivative with mass 407 which could be a compound of MW=179 with 2 TBDMS groups. The retention time for this compound is found to be 38.8 minutes from Table 5. Xanthopterin (VIII) has a molecular weight of 179 g/mole and could be formed from 7,8-dihydroxanthopterin by air oxidation during the silylation process.



VIII

Thus an authentic sample of xanthopterin was silylated with MTBSTFA in pyridine at room temperature for ca. 30 minutes. The total ion current chromatogram for xanthopterin is presented in Figure 38.

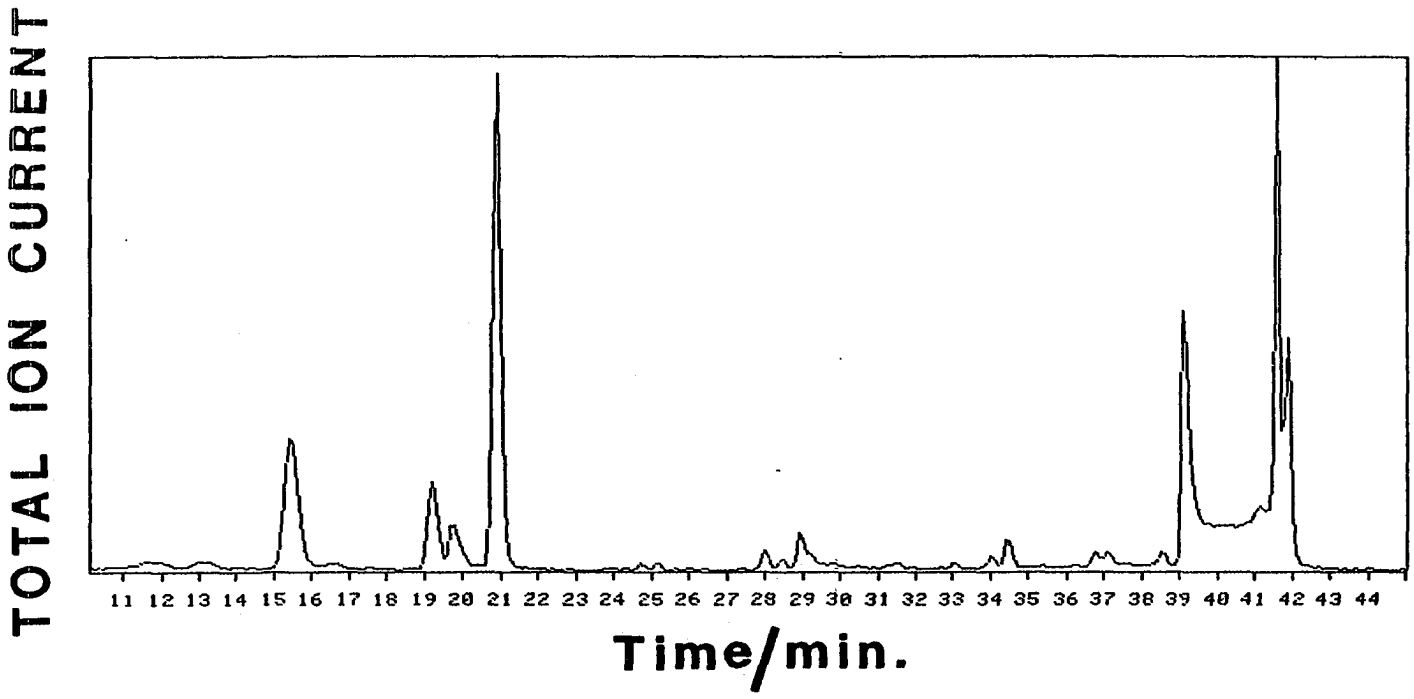
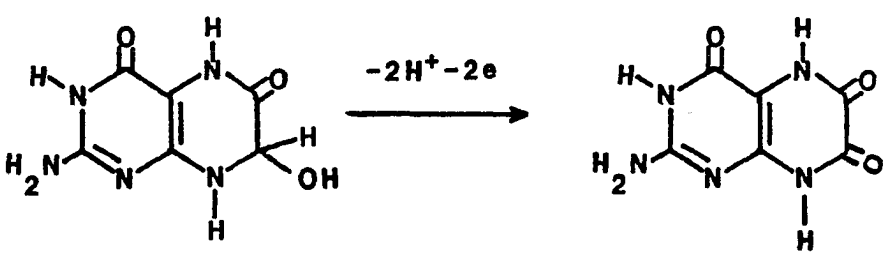


Figure 38. Total ion current chromatogram of an authentic sample of xanthopterin silylated with MTBSTFA in pyridine at room temperature for ca. 30 minutes.

Two peaks are observed at retention times of 39.1 minutes and 41.6 minutes which represent doubly (M^+=407) and triply (M^+=521) silylated derivatives of xanthopterin. Figure 39 shows the mass spectrum of the doubly silylated derivative at a R_t=39.1 minutes. The base peak is at a mass of 350 (M-57). Mass 392 (M-15) and 407 (M^+) are also observed. A peak with an abundance of 6.6% is also observed at mass 464. This is the M-57 peak for triply silylated xanthopterin and is observed because of poor resolution between the gas chromatographic peaks of the doubly and triply silylated derivatives. Comparison of the mass spectrum and retention time of doubly silylated xanthopterin with the mass spectrum and retention time of the peak observed in the silylated electrolysis product mixture is tentative proof of the presence of xanthopterin as one of the products.

Owing to the fact that evidence for xanthopterin was found, the presence of leucopterin (MW=195) in the electrolysis product solution was also suspected. Leucopterin (IX) could be formed from xanthopterin according to the following equation:



hydrated **VIII** **IX**

Indeed a rather large peak is observed in the chromatogram of Figure 32D at a retention time of 39.5 minutes which exhibits a molecular ion of

MASS	%	MASS	%	MASS	%	MASS	%	MASS	%	MASS	%	MASS	%	MASS	%	MASS	%
91.1	.2	125.0	.5	158.0	3.2	192.1	.7	237.1	1.8	296.1	.3	392.1	2.5				
92.1	.2	126.0	.5	159.0	1.0	193.1	.6	238.1	1.3	297.1	.2	393.1	.6				
92.9	.4	127.2	.5	160.1	.4	194.0	.4	239.1	.6	306.1	.2	394.1	.3				
93.8	.2	128.0	.6	161.0	.3	195.1	.2	240.0	.2	308.0	.3	400.9	.2				
95.0	.3	129.0	.6	162.1	.2	196.0	.5	241.2	.2	309.0	.2	406.2	.5				
96.1	.5	129.9	.4	162.9	.3	196.9	.3	248.0	.2	313.3	.2	407.2	2.0				
97.1	.7	131.0	3.5	164.0	.2	198.0	.4	249.1	.2	318.1	.3	408.0	1.0				
98.0	.5	132.0	1.9	165.0	.4	202.0	.3	250.1	.7	319.0	.2	409.1	.6				
99.1	4.7	133.0	4.7	166.1	.6	203.1	.2	251.1	.6	320.1	.2	410.1	.2				
100.1	3.1	134.0	1.0	167.1	.3	204.0	.2	252.1	.3	324.8	.2	422.1	.5				
101.1	.9	135.0	1.0	168.1	.3	205.1	.2	253.1	.2	326.9	.2	423.1	.2				
102.0	.5	136.0	.3	169.0	.6	206.0	.4	262.0	.5	334.1	5.4	429.0	.2				
103.1	.7	137.0	.2	170.1	.2	207.0	2.4	263.0	.2	335.1	1.6	464.2	6.6				
105.0	.4	138.0	.4	171.1	.6	208.0	2.5	264.0	.6	336.1	.8	465.2	3.8				
107.2	.3	138.8	.4	172.0	.2	209.0	1.0	265.0	.8	337.2	.3	466.2	1.1				
108.1	.4	140.1	.2	173.1	.4	210.0	.4	266.0	.4	338.1	.2	467.2	.4				
109.0	.3	140.9	.3	174.0	.3	210.9	.3	266.9	.3	339.3	.5						
110.0	.6	141.9	.5	175.0	.2	212.1	.2	268.0	.2	341.0	.5						
111.1	.8	143.0	.8	176.0	.2	218.0	1.1	269.1	.3	348.0	.3						
112.0	.2	144.0	.8	177.0	.4	219.0	.4	276.0	.5	350.1	100.0						
113.1	.4	145.0	.3	178.0	.2	220.0	.6	278.0	3.9	351.2	28.2						
113.9	.2	146.6	4.9	179.0	.6	221.0	.7	279.0	1.0	352.1	11.1						
115.1	2.2	149.0	.6	180.0	.5	222.0	.3	280.1	.4	353.1	2.1						
116.1	.5	150.0	.3	181.0	1.6	223.0	.7	281.0	.9	354.2	.4						
117.1	1.3	150.9	.3	182.1	.4	224.1	.3	281.9	.3	355.2	.4						
118.1	.3	152.0	.2	183.1	.3	225.0	.3	283.0	.2	357.2	.2						
119.1	.5	152.9	.7	184.0	.2	232.1	.2	290.0	.3	359.1	.2						
120.1	.2	154.0	.6	185.1	.3	233.1	.5	292.1	10.5	365.1	.2						
122.1	.3	155.0	.4	188.9	.2	234.1	.5	293.0	3.8	383.2	1.3						
123.1	.4	156.0	.7	190.1	.3	235.1	1.0	294.0	4.2	384.0	.5						
124.1	.4	157.0	1.7	190.9	.5	236.1	9.4	295.1	1.0	385.0	.2						

Figure 39. Mass spectrum of the doubly silylated derivative of an authentic sample of xanthopterin. R_t=39.1 minutes in Figure 38.

mass 423. This could be a doubly silylated derivative of a molecule with a molecular weight of 195 g/mole.

Authentic leucopterin was silylated with MTBSTFA in pyridine at room temperature for varying periods of time and at 100°C for 15 minutes. In every instance only the triply silylated derivative of leucopterin was observed in the total ion current chromatogram of the GC-MS at a retention time of ca. 42.5 minutes. The molecular ion is at a mass of 537 (195+3(114)=537) and peaks at M-57 (480) and M-15 (522) are also observed. Mass 480 is the base peak in the mass spectrum. It was found that regardless of the silylation procedure used, the process could not be stopped at the point where only two hydrogen atoms are replaced. This shed some doubt on the possibility that the peak observed at 39.5 minutes in Figure 32D with M^+=423 was really a result of leucopterin in the product solution.

Silylation experiments on the total product mixtures of peak I_a electrolyses of 5-MTHP in pH 4.7 NaCl revealed that a number of products could be silylated. This was contradictory to what was observed when the separated products from peak I_a electrolyses of 5-MTHP in pH 4.7 phosphate buffer were subjected to the silylation procedure (vide supra). However the experiments on the total product mixtures revealed that earlier silylations had perhaps been attempted at a temperature which was far too high, particularly in the case of silylation with MTBSTFA. It was found that in many instances room temperature was adequate for performing derivatization with MTBSTFA. In cases where heating was necessary, a temperature of ca. 100°C for ca. 15 minutes was found to accomplish the desired result. Thus it appeared that more study

on the electrooxidation products of 5-MTHP separated using liquid chromatography on Sephadex G-10 was necessary.

Separation of Electrolysis Products by Liquid Chromatography on Sephadex G-10

Separation of products from electrolysis in 0.5 M NaCl solutions. As a result of the dismal success with identification of products from separations of electrolyses performed in pH 4.7 phosphate buffers with an ionic strength of 0.5 M, it was decided to utilize NaCl as the supporting electrolyte. For comparison purposes a typical chromatogram of the separation of products from peak I_a electrolysis (0.20V/SCE) of 5-MTHP in pH 4.7 phosphate is presented in Figure 40. LC peaks 1',2', and 3' which are eluted in a band centered at a retention volume of ca. 250 ml were grossly contaminated with phosphate which has a retention volume of ca. 210 ml. The use of "'", for example 1',2',3', etc., will indicate a peak from separation of products from an electrolysis carried out in phosphate buffer. Peaks 4' and 5' were mostly phosphate free, however they were also quite minor constituents of the product solution as evidenced by low absorbance of the u.v. bands and small quantities of lyophilized material collected. Peaks 6' and 7' eluting with retention volumes of 615 ml and 945 ml respectively were totally phosphate free. These peaks were very broad, however they both exhibited quite strong u.v. spectra and the lyophilized fractions yielded a considerable quantity of products.

Many of the electrolysis solutions in 0.5 M NaCl which had been analyzed before without prior product separation had also been saved.

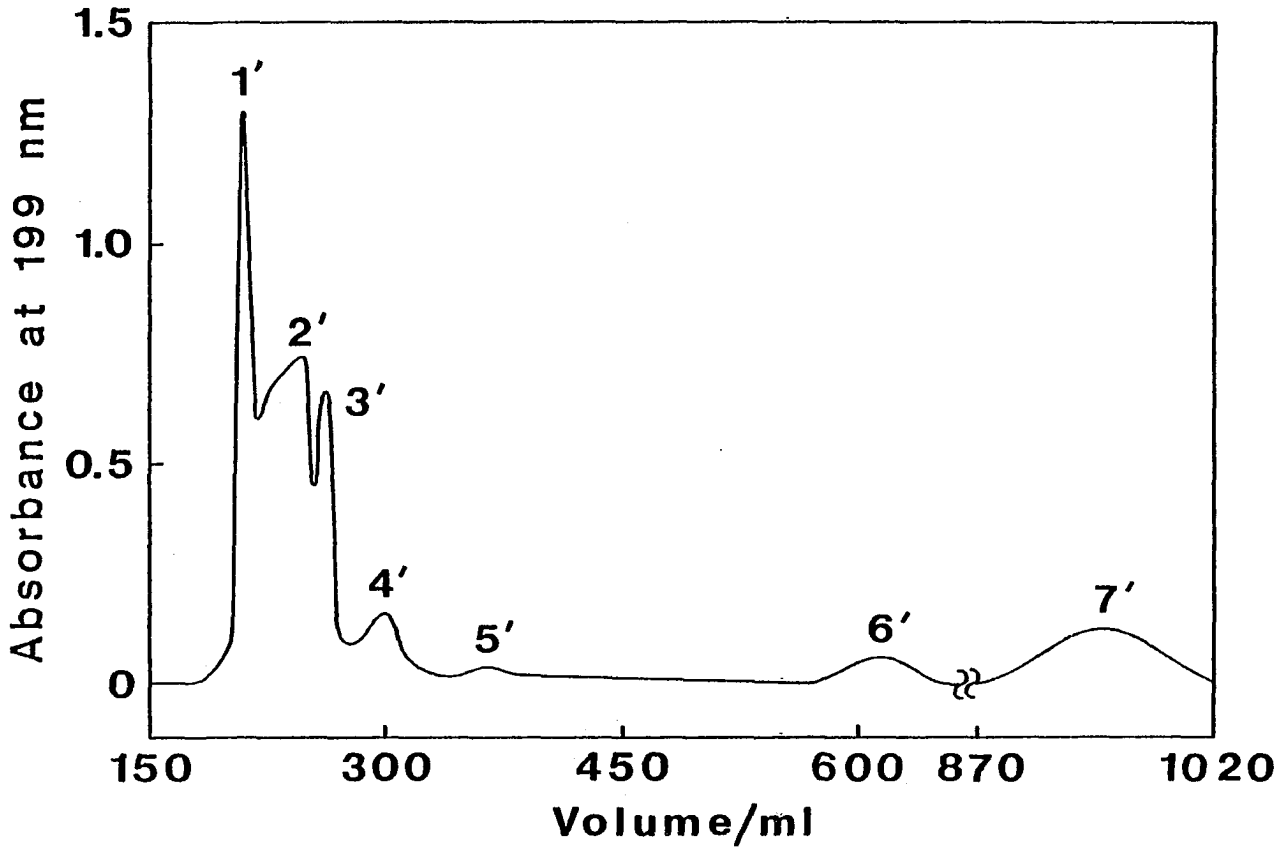


Figure 40. Liquid chromatogram of the products from peak I_a electrooxidation of 0.75 mM 5-MTHP in pH 4.7 phosphate buffer, μ=0.5 M. Separation was accomplished using a 80 cm x 2.5 cm column of Sephadex G-10 resin and eluting with doubly distilled water.

These were now separated utilizing the same liquid chromatographic column of 75 cm x 25 cm Sephadex G-10 resin and eluting with doubly distilled water. None of the fractions of the separated products contained any 5-MTHP. This is a result of the air oxidation of any 5-MTHP which was not electrolyzed prior to placing on the column or during the residence time on the LC column.

Peak I_a electrooxidation of 5-MTHP was carried out at three concentrations: 0.75 mM, 1.5 mM, and 2.3 mM. The supporting electrolyte in all cases was 0.5 M NaCl with the pH maintained at 4.7±0.1 by addition of microliter quantities of ca. 1 N NaOH. Changing the amount of starting material in the electrolysis did not seem to change the products which were observed in the separation on Sephadex G-10. A typical separation is illustrated by the liquid chromatogram in Figure 41. This is the separation of 1/2 of the products from peak I_a electrolysis of 10 mg of 5-MTHP in 25 ml of solution (1.5 mM 5-MTHP). One-half of the products were separated per chromatographic run to prevent overloading the column and increasing the absorbance above the limits of the flow-through detector.

Electrolysis product solutions were concentrated by lyophilization to ca. 3 ml. The concentrated electrolysis product solutions were stored in small screw cap vials. This made it convenient to take one-half of the products to inject on the LC column. Figure 41 illustrates the separation of electrolysis products immediately after concentrating by lyophilization. Figure 42 is a chromatogram of the separation of products which had been stored in solution for several weeks. The amount of starting material and all other conditions were the same as in

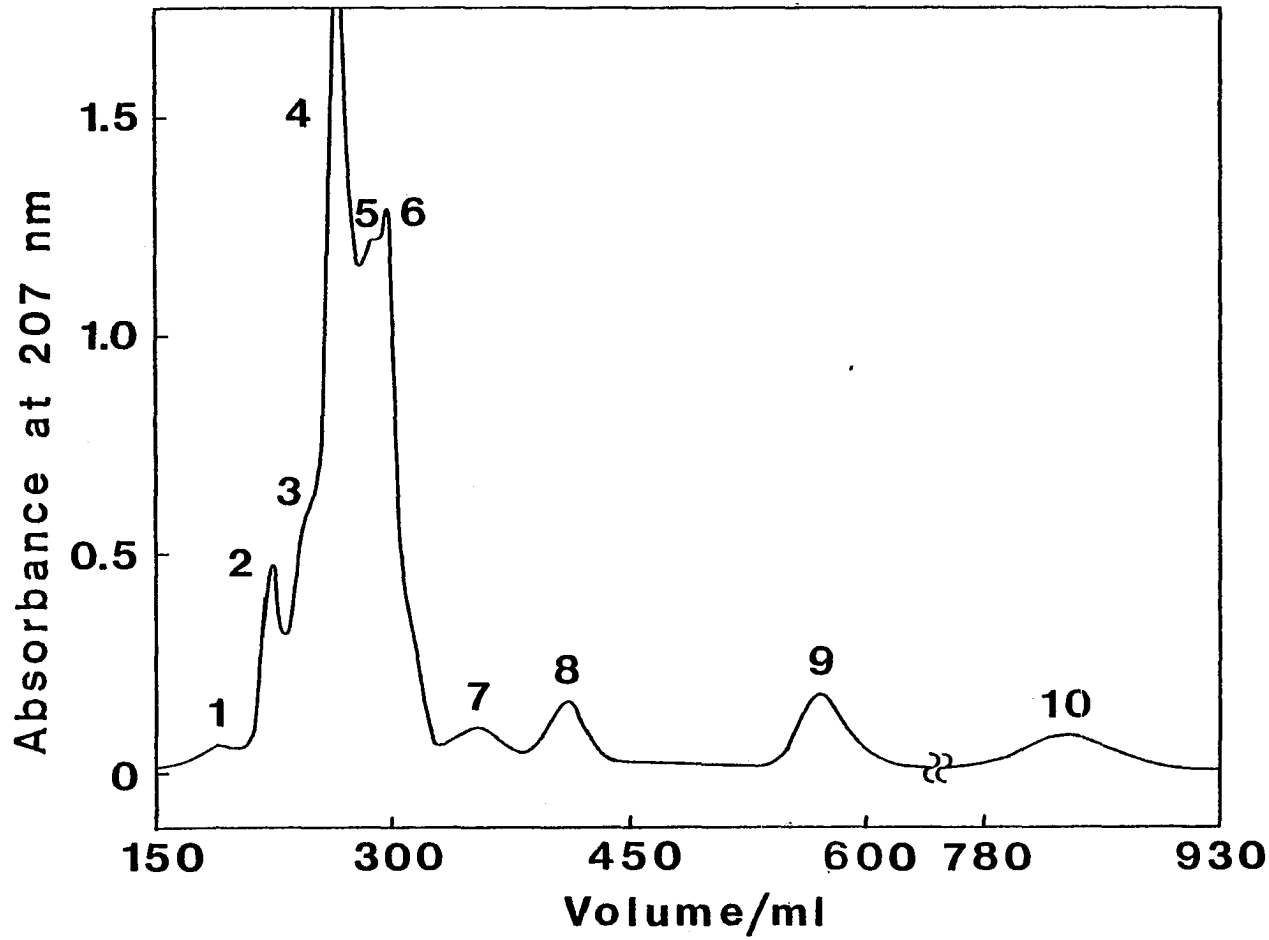


Figure 41. Liquid chromatogram of the products from peak I_a electrooxidation of 1.5 mM 5-MTHP in pH 4.7 ± 0.1 NaCl, 0.5 M. Separation was accomplished on a 75 cm x 2.5 cm column of Sephadex G-10 resin and eluting with doubly distilled water.

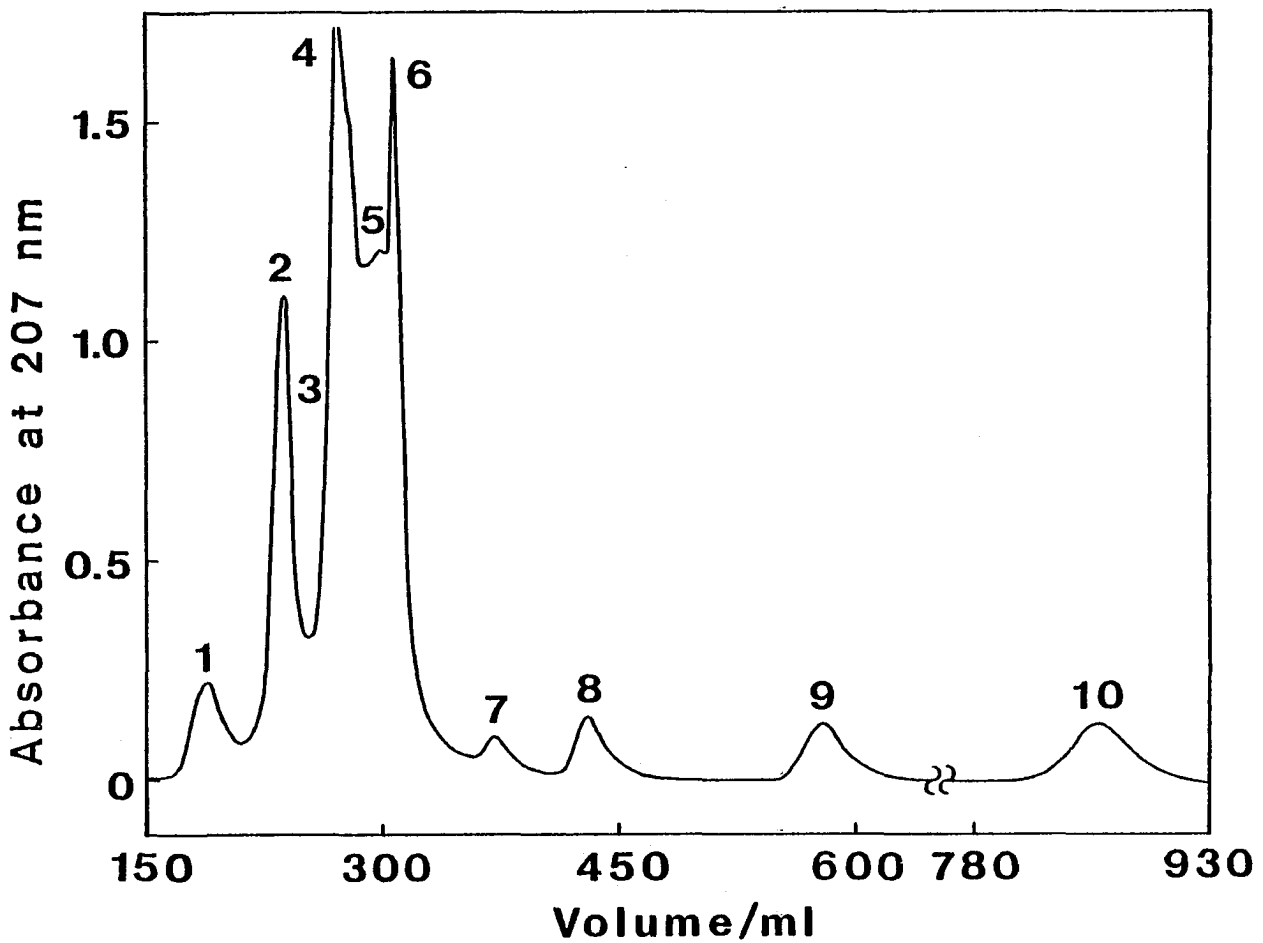


Figure 42. Liquid chromatogram of the products from peak I_a electrooxidation of 1.5 mM 5-MTHP in pH 4.7 ± 0.1 NaCl, 0.5 M. Separation was accomplished on a 75 cm x 2.5 cm column of Sephadex G-10 resin and eluting with doubly distilled water. These products had been stored in solution for several weeks.

the separation depicted in Figure 41. In each case the flow rate was set at ca. 15 ml hr^{-1} until chromatographic peak 6 was eluted. After this the flow rate was increased to 35-40 ml hr^{-1} to decrease the total time for the separation.

Comparing the two separations several differences are noted. The separation of the products which had been stored (Figure 42) illustrates that the compounds responsible for peaks 1, 2, and 6 are present in much larger quantities. Another difference is the decrease in size of peak 3 which is observed as a shoulder on the rising portion of peak 4. The most plausible explanation for the origin of peaks 1, 2, and 6 is that they are decomposition products of other components of the electrolysis product mixture. Since peak 3 decreases in size it seems likely that it decomposes with time perhaps yielding some of the compounds responsible for peaks 1, 2, and 6.

Identification of separated products from electrolyses in 0.5 M NaCl. Since several electrolysis products had been identified in analyses of the total product mixtures, it was decided to determine if any of the separated products were those already identified. Pterin was the first product which was identified in the electrolysis product mixture. Therefore a u.v. spectrum of authentic pterin was run in distilled water and is shown in Figure 43A (λ_{max}=213 nm, 226 nm, 267 nm, and 336 nm). This is slightly different from the values reported for the u.v. bands of pterin at pH 5 (λ_{max}=233 nm, 270 nm, and 339 nm).[40] U.v. spectra of single test tubes at chromatographic peak maxima had been obtained throughout the chromatographic runs of all separations. Because the amount of the various components was greater in the

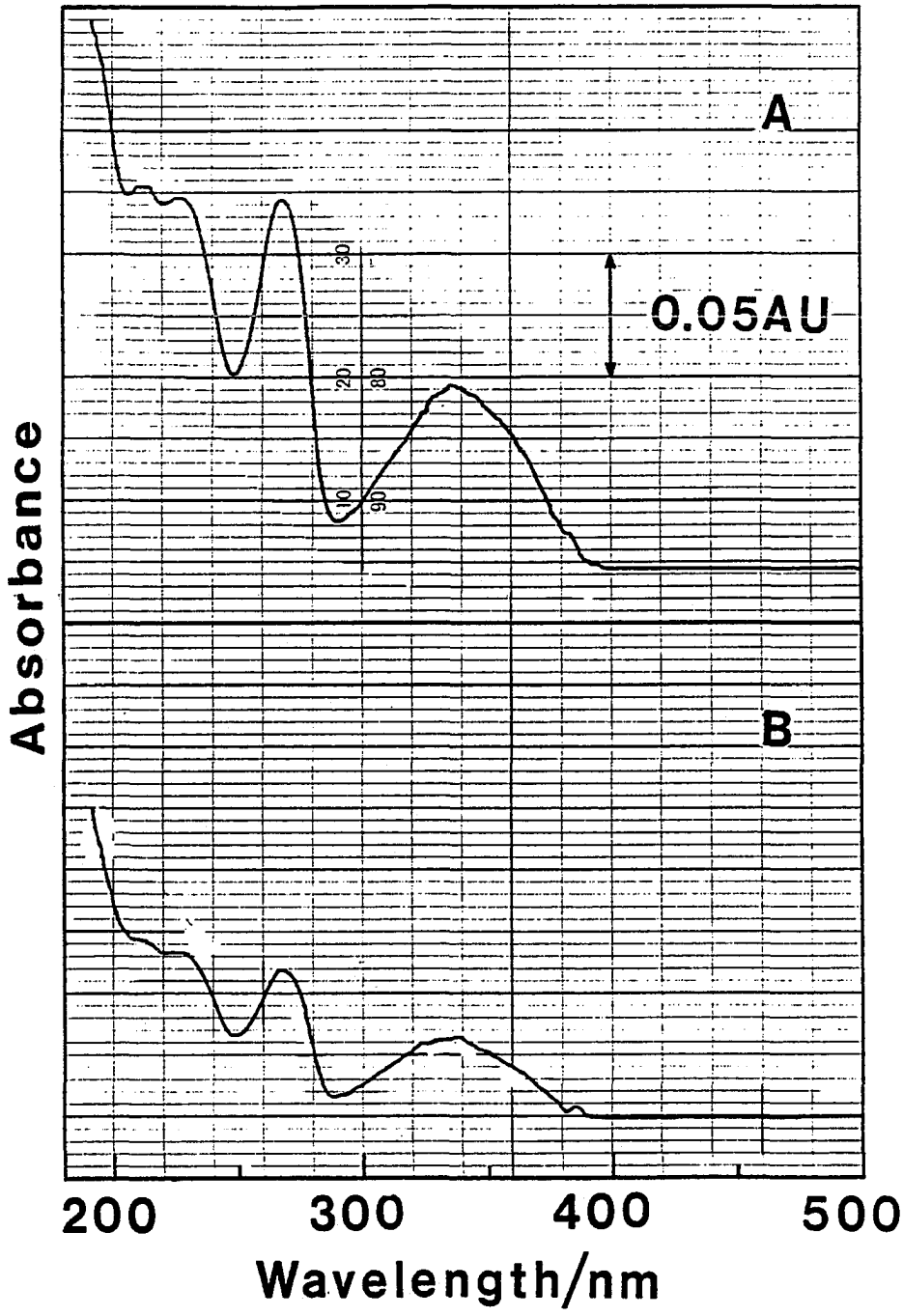


Figure 43. (A) U.v. spectrum of authentic pterin sample dissolved in distilled water. Spectrum obtained in 0.5 cm cells. Scan rate: 200 nm min-1. (B) U.v. spectrum of fraction (574-576 ml) from separation of peak I_a electrolysis of 15 mg 5-MTHP in pH 4.7 NaCl, 0.5 M. Scan rate: 400 nm min-1.

electrolysis of larger amounts of starting material (5-MTHP), the spectra obtained during the separation of 2.3 mM 5-MTHP electrolysis products were examined. The u.v. spectrum of a 3 ml fraction of the LC peak corresponding to peak 9 in Figures 41 and 42 at a retention volume of 576 ml is shown in Figure 43B. It exhibits u.v. peak maxima at λ=213 nm, 226 nm, 267 nm, and 337 nm which is identical to the spectrum of authentic pterin.

However when LC peak 9 was concentrated by lyophilization the u.v. spectrum changed giving new peaks at λ_{max}=248 nm, (268 nm), and 353 nm. Pterin has a pK_a at ca. 8 and it was felt that the pH of the solution might be above the pK_a. To make absolutely certain that the u.v. spectrum of LC peak 9 was identical with pterin, both authentic pterin and the compound isolated from peak 9 were dissolved in pH 4.6 PO_4^{3-}, μ=0.5. The spectra at pH 4.6 are shown in Figures 44A,B and it is obvious they are indeed the same. Authentic pterin has u.v. peaks at λ_{max}=215 nm, 231 nm, 271 nm, and 338 nm at pH 4.6 and LC peak 9 has u.v. peaks at λ_{max}=(212) nm, (229) nm, 271 nm, and 336 nm. The long wavelength peak in each case has a shoulder at ca. 360 nm which is also characteristic for pterin. At very short wavelengths another u.v. peak is observed at ca. 193 nm which is probably due to absorption by the buffer. It was not observed when the spectra were obtained in water.

GC-MS of LC peak 9 product. The total ion current chromatogram of the product isolated from LC peak 9 and silylated with MTBSTFA is shown in Figure 45. A peak is observed at R_t=35.8 minutes (5855 counts) which is ca. the retention time for pterin (see Figure 36). The mass spectrum of the peak at 35.8 minutes is shown in Figure 46. This mass

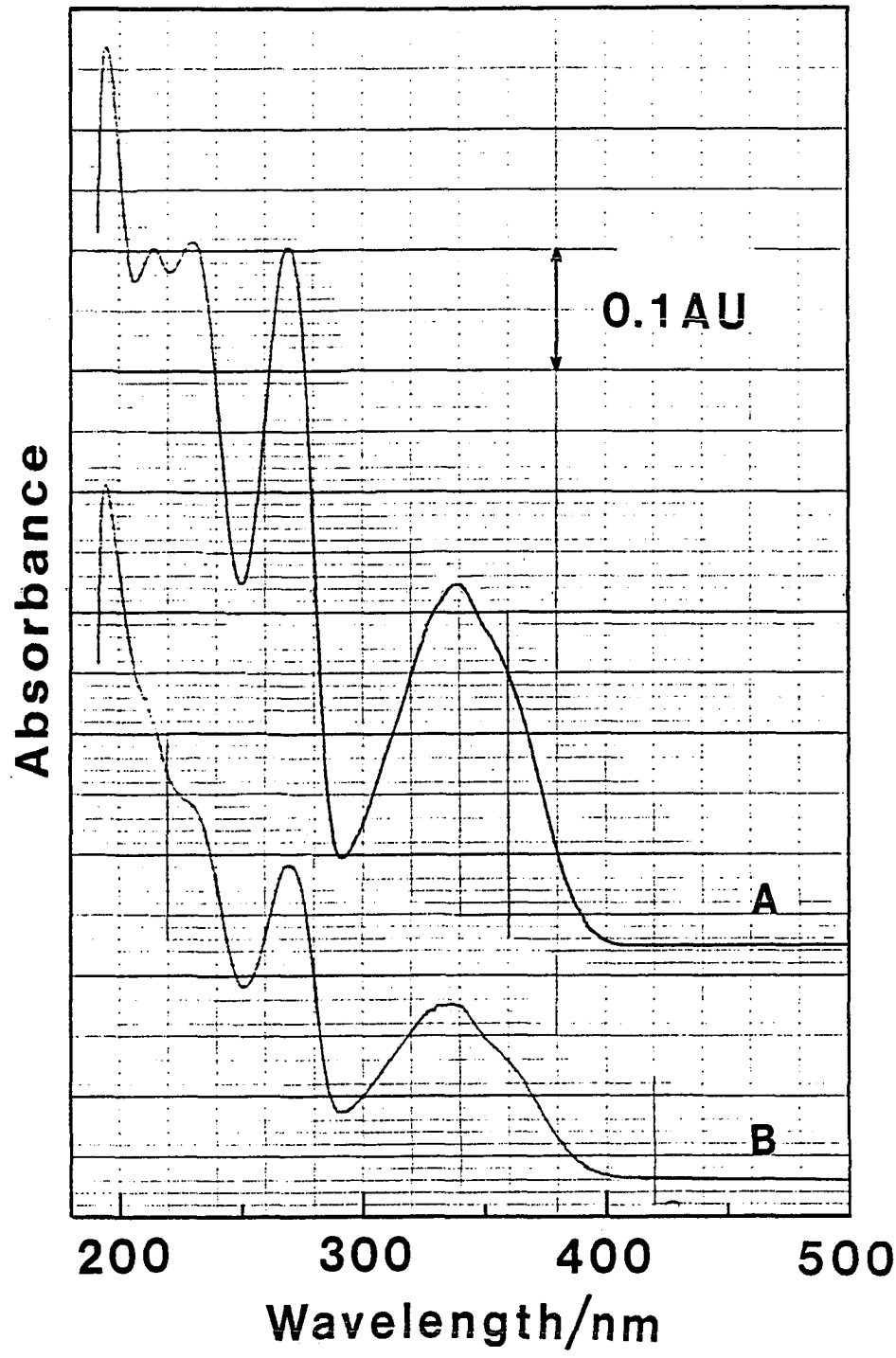


Figure 44. U.v. spectra in pH 4.7 phosphate buffer in 0.5 cm cells. Scan rate: 200 nm min^{-1}. (A) authentic pterin and (B) LC peak 9.

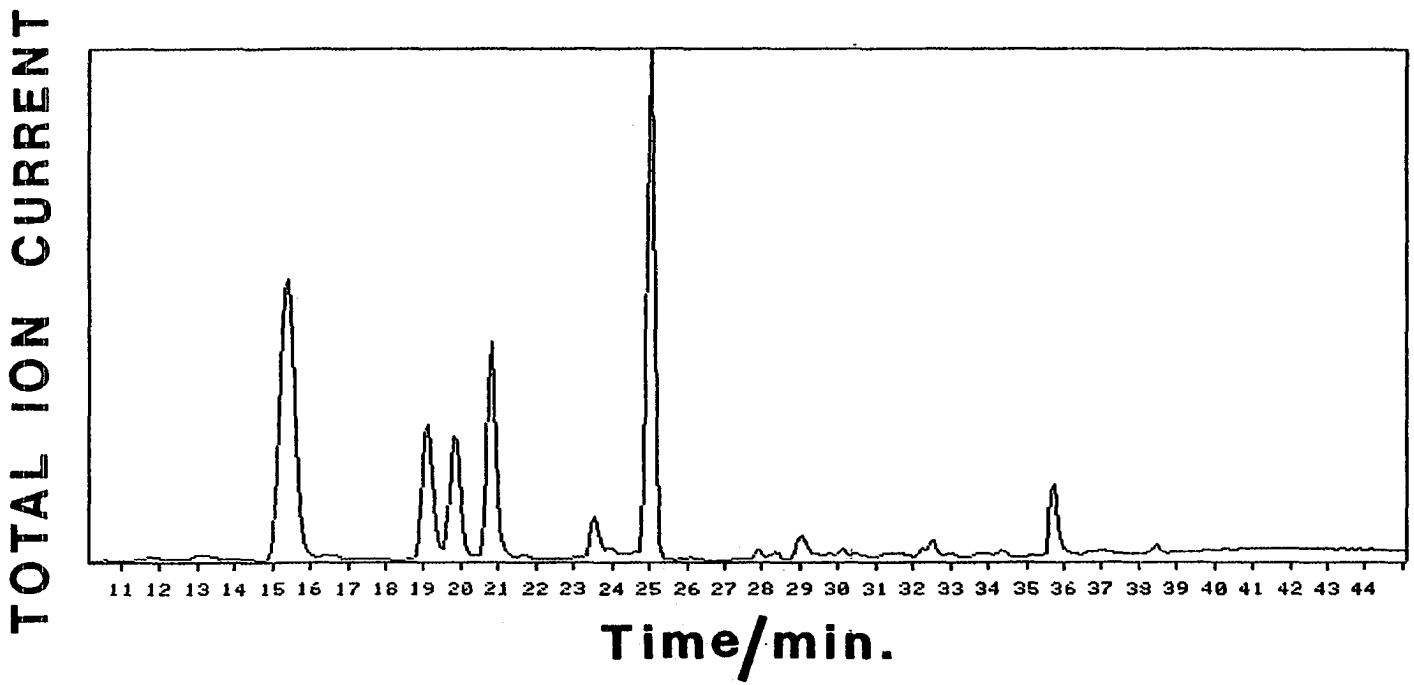


Figure 45. Total ion current chromatogram of product isolated from LC peak 9 and silylated with 50 µl MTBSTFA in 50 µl pyridine at 100°C for 13 minutes.

MASS	%	MASS	%	MASS	%	MASS	%	MASS	%	MASS	%	MASS	%	MASS	%
91.1	.3	124.2	.5	158.0	2.0	194.0	.3	260.0	.4	341.0	.3				
92.1	.3	125.1	.5	159.0	.6	195.0	.3	261.0	.4	355.1	.3				
93.0	.6	126.1	.3	160.0	.2	196.9	.3	262.0	.8	376.2	3.0				
94.1	.4	127.1	.4	160.9	.4	198.0	.8	263.0	.3	377.2	.9				
95.0	.7	128.0	.5	161.8	.2	199.1	.2	264.1	.2	378.2	.4				
96.0	1.2	129.0	.6	163.0	.5	202.0	2.4	264.9	.2	390.1	.2				
97.2	.7	130.9	2.6	165.0	.3	202.9	.6	267.0	.3	391.2	2.6				
98.1	1.1	132.0	1.5	165.9	.2	204.0	.9	276.0	1.0	392.2	.9				
99.1	4.5	132.9	2.2	167.0	.5	205.1	.6	277.0	6.8	393.1	.3				
100.1	2.2	134.0	.7	168.1	.3	205.9	.3	278.0	5.9						
101.0	.6	135.1	.6	169.0	.3	207.0	7.7	279.0	2.3						
102.0	.6	136.1	.4	171.0	1.0	208.0	1.9	280.0	.7						
103.1	.5	137.1	.2	172.1	.3	208.9	1.3	281.0	1.6						
104.1	.6	138.6	5.6	173.0	1.0	210.0	.4	281.9	.4						
105.1	.8	141.0	.4	174.0	.2	218.0	.4	283.0	.4						
107.1	.2	142.0	1.2	175.0	.2	219.1	.2	292.1	.4						
108.9	.4	143.0	.8	176.2	.4	220.0	10.0	293.1	.2						
110.1	.4	143.9	.3	177.0	1.9	221.0	2.1	304.0	.2						
111.2	.5	145.0	.2	178.0	1.2	221.9	.7	315.2	.9						
112.1	.3	146.0	.4	179.1	1.0	223.1	.3	316.2	.2						
113.1	.4	147.0	3.6	180.1	.5	224.1	.2	317.0	.2						
114.1	.2	148.0	.7	181.0	.5	234.0	.3	318.1	.3						
115.1	.9	148.9	1.8	182.0	.3	235.0	3.7	319.2	.4						
116.1	.5	150.0	1.2	183.1	.4	236.0	.9	320.1	.3						
117.1	1.6	150.9	.5	185.1	.2	237.0	.6	327.2	.7						
118.2	.6	152.0	.4	188.1	.2	247.1	.5	328.3	.2						
119.1	.9	152.8	.2	189.1	.2	248.1	.3	334.1	100.0						
120.1	.5	154.0	.3	190.0	.3	248.9	.4	335.1	39.0						
121.0	.2	155.0	.4	191.0	.9	251.1	1.6	336.1	13.0						
122.1	.2	156.0	.5	192.1	.4	252.1	.4	337.1	3.3						
123.1	1.1	157.0	2.5	192.9	.5	253.1	.3	338.1	.6						

Figure 46. Mass spectrum of peak at R_t=35.8 minutes from the chromatogram of LC peak 9 (Figure 41) silylated with MTBSTFA in pyridine.

spectrum is identical with the one obtained for authentic pterin (compare Figure 37) with characteristic ions at mass 334 (M-57), 376 (M-15), and 391 (M^+).

Cyclic voltammetry of LC peak 9 product. Cyclic voltammetry of LC peak 9 and authentic pterin was carried out in pH 4.6 phosphate, μ=0.5 M because voltammetry in the NaCl solution showed broad ill-defined peaks as a result of the lack of buffer capacity. A cyclic voltammogram of LC peak 9 is presented in Figure 47A. The initial sweep toward negative potentials reveals two voltammetric reduction peaks identical to those for pterin in Figure 47B. When the potential sweep is reversed one major voltammetric oxidation peak together with three small oxidation peaks is observed in each case. The large voltammetric oxidation peak at 0.03V is due to the $2e$ - $2H^+$ electrooxidation of tetrahydropterin which is formed in the reduction process at a peak potential of -1.17V/SCE. This oxidation process forms an unstable quinonoid-dihydropterin which undergo a quasi-reversible reduction at a peak potential of ca. 0V. at pH 4.6.[7] Referring to Figure 47 it can be seen that the reverse peak is extremely small at 200 mV s^{-1} indicating most of the quinonoid-dihydropterin has diffused away from the electrode surface and is unavailable for reduction. This can explain why a large voltammetric oxidation peak is observed at ca. 0V/SCE during electrolyses of 5-MTHP in both PO_4^{3-} and Cl^- solutions which appears to lose its reversible characteristics as the electrolysis nears completion (see Figures 12 and 14B).

All of the above data comparing the LC peak 9 product with authentic pterin firmly identifies it as pterin. Comparing the u.v.

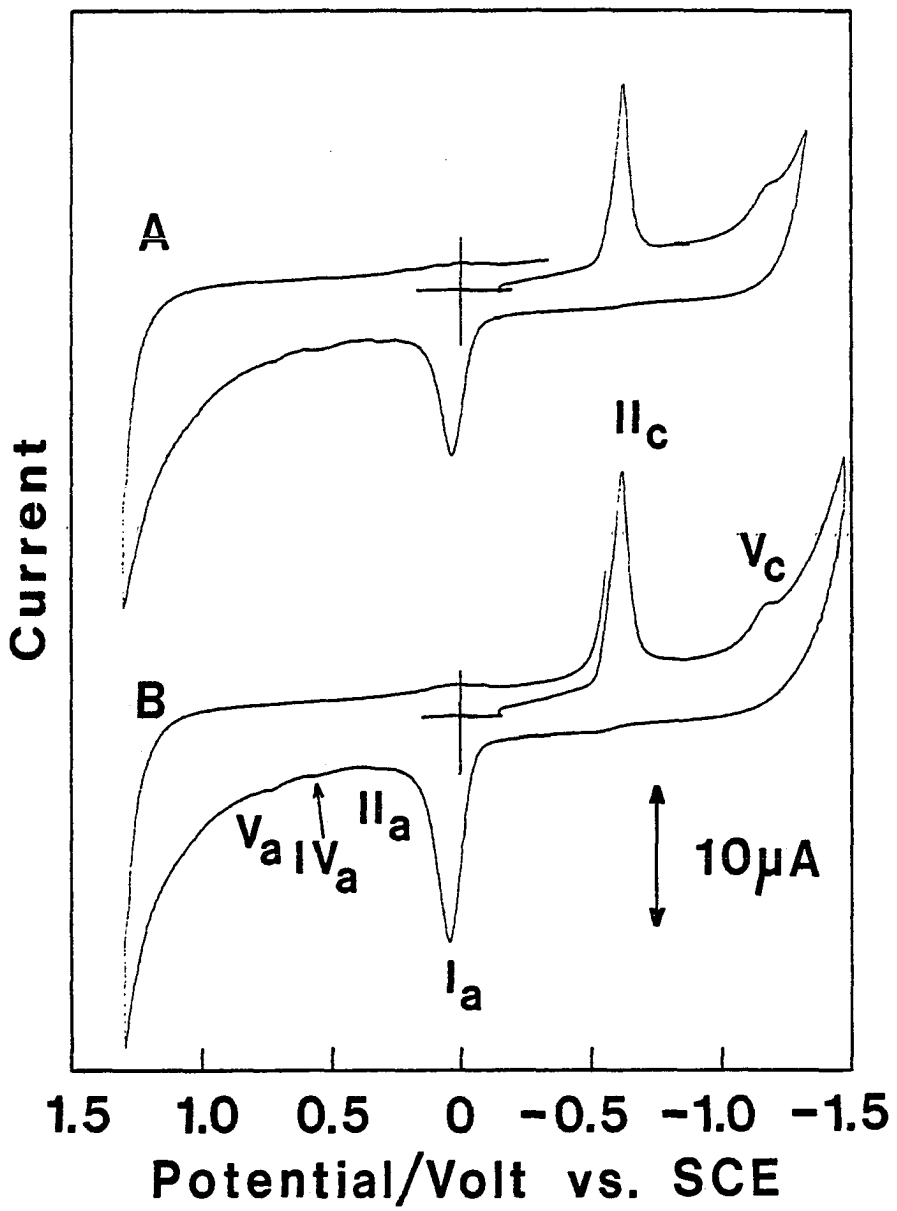


Figure 47. Cyclic voltammograms in pH 4.6 phosphate buffer, μ=0.5 M. Sweep rate: 200 mV s^{-1}. (A) LC peak 9 and (B) authentic pterin.

spectrum and retention volume (615 ml) of LC peak 6' from the separation of products from peak I_a electrolysis in pH 4.7 PO_4^{3-} (Figure 40) with LC peak 9 identifies LC peak 6' as pterin also.

Identification of xanthopterin as one of the electrolysis products. Values for u.v. peak maxima are given as λ=276 nm and 388 nm at pH 4.0 for the non-hydrated species of xanthopterin.[40] At pH 13.0 the values are given as λ_{max}=255 nm, (275) nm, and 394 nm. An u.v. spectrum of an authentic sample of xanthopterin was obtained in both distilled water and pH 4.7 PO_4^{3-}, μ=0.5 M and exhibited peaks at λ_{max}= 212 nm, 276 nm, (300) nm, and 388 nm. A solution of xanthopterin is decidely orangeish-yellow. Several of the components from separation of products from peak I_a electrolysis of 5-MTHP in pH 4.7 PO_4^{3-} were decidedly yellowish. The component which elutes as LC peak 2' in Figure 40 had an u.v. spectrum similar to the u.v. spectrum of xanthopterin. U.v. peaks in distilled water were observed at λ_{max}=258 nm, (276) nm, and 387 nm. This compares quite well with the spectrum reported in the literature at pH 13.0. Once again the pH of the distilled water is not controlled therefore it might have a pH high enough to cause some unusual behavior. However it appears that the peak at λ_{max}= 387 nm is very characteristic for xanthopterin.

Separation of products from peak I_a electrolyses which were carried out in 0.5 M NaCl pH 4.7 showed evidence of only small quantities of xanthopterin. When xanthopterin was observed it was found in fractions eluting in the region of LC peaks 5 and 6 in Figures 41 and 42. These fractions had a component in very low concentration with λ_{max}=258 nm, (~275) nm, and 388 nm. At other times xanthopterin was not observed

at all in the u.v. spectra. This was not surprising in the light of the fact that the GC-MS of the total product mixture (Figure 32D) gave a total of less than 2000 counts for both doubly (mass 407) and triply silylated (mass 523) xanthopterin. The product solution of 5-MTHP electrolyzed at peak I_a in 0.5 M NaCl pH 4.7 did not show nearly the intensity of yellow color as the product solution when electrolyzed in pH 4.7 PO_4^{3-}, μ=0.5 M, indicating that less xanthopterin was probably generated in the NaCl solution.

In an attempt to confirm that the yellowish fraction isolated from electrolyses carried out in pH 4.7 PO_4^{3-} and showing λ_{max}=258 nm, (276) nm, and 387 nm was indeed xanthopterin, a sample was lyophilized and silylated with MTBSTFA. This sample, which eluted at a retention volume of 248 ml (LC peak 2'), was actually from an electrolysis carried out at peak II_a potentials (0.32V/SCE) because more of this component was generated at this potential. As mentioned above all LC peaks at this retention volume were contaminated with phosphate and thus the GC-MS data indicated only the presence of derivatized phosphate. The lyophilized sample appeared to be very hygroscopic because it was always soft and sticky. Samples with phosphate typically exhibit this type of behavior.

It was felt that it might be possible to remove the phosphate from the organic compound by extraction with an organic solvent. Consequently the sample isolated from LC peak 2' was extracted with methanol. The organic compound appeared to dissolve in the methanol as evidenced by the yellowish color of the methanol solution. A white precipitate was left after the methanol extraction which gave a positive phosphate test with acidified ammonium molybdate solution. Unfortunately,

phosphate is also partially soluble in methanol. However, additional phosphate was precipitated from the methanol solution when some of the methanol was allowed to evaporate.

After precipitating the phosphate the methanol extract was once again lyophilized, dissolved in distilled water, and subjected to another pass through the G-10 column. This time a baseline separation was achieved between the remaining phosphate and the sample peak. The material which was isolated from the sample peak on this occasion was a fluffy, orange powder. A small amount of this sample was silylated with MTBSTFA in pyridine at room temperature for ca. 30 minutes and subjected to GC-MS analysis. Figure 48 is the total ion current chromatogram which shows a large peak at 41.8 minutes with a molecular ion of mass 521. It also shows a peak at 29 minutes which is silylated phosphate. The mass spectrum of the peak with R_t=41.8 minutes is presented in Figure 49. This mass spectrum exhibits an identical fragmentation pattern as the mass spectrum of the peak at 41.6 minutes (Figure 50) from the chromatogram of authentic xanthopterin (Figure 38). This is confirmation that LC peak 2' with u.v. peaks at λ_{max}=258 nm, (276) nm, and 387 nm is indeed xanthopterin.

Cyclic voltammetry of xanthopterin. Cyclic voltammetry of xanthopterin in pH 4.7 phosphate is very complex (Figure 51A,B). The initial positive sweep reveals five voltammetric oxidation peaks. Upon reversing the sweep six voltammetric reduction peaks are observed. On the second positive sweep a number of new oxidation peaks are observed (five new peaks). If the initial sweep is toward negative potentials three reduction peaks are observed. Upon reversal of the potential sweep

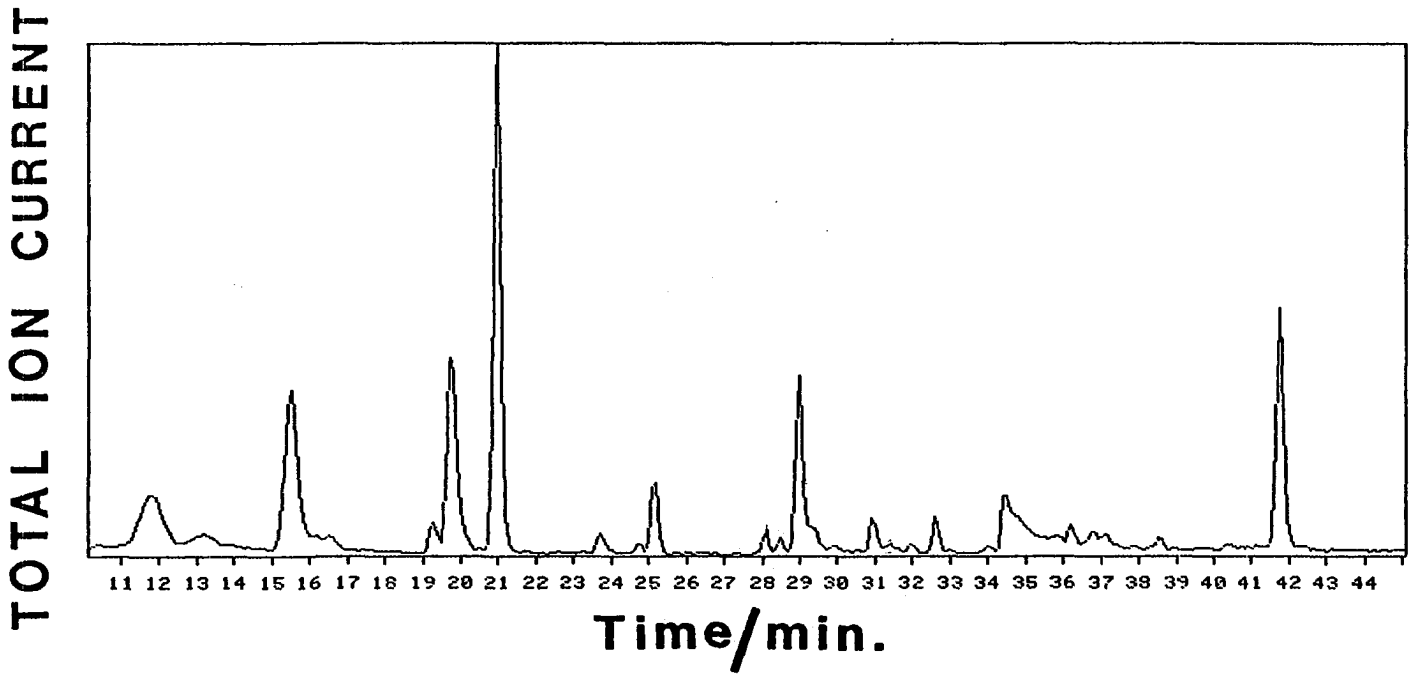


Figure 48. Total ion current chromatogram of product isolated from LC peak 2' and silylated with MTBSTFA in pyridine at room temperature for ca. 30 minutes.

MASS	%	MASS	%	MASS	%	MASS	%	MASS	%	MASS	%	MASS	%	MASS	%
93.2	.5	142.9	.7	202.0	.5	293.0	5.2	448.0	.7						
96.0	.5	144.1	.8	204.0	.4	294.0	2.6	449.2	.7						
96.9	.8	147.0	4.1	207.0	4.4	295.1	.5	450.1	.7						
97.9	.6	148.0	.9	208.1	1.1	306.2	.5	464.2	100.0						
99.1	5.1	149.0	.9	209.0	.7	307.2	.5	465.2	58.2						
100.1	3.5	151.0	.4	213.1	.5	308.0	.5	466.2	21.7						
101.0	.7	154.9	.4	217.0	.6	309.0	.8	467.2	6.2						
101.9	.5	156.1	.8	218.0	1.7	311.2	.4	468.2	1.9						
103.1	.4	156.9	2.4	219.0	.6	318.1	.8	506.3	2.3						
103.4	.4	158.0	5.9	221.0	.4	320.1	.4	507.3	.9						
108.1	.8	159.0	1.5	224.0	.4	323.1	.4	508.2	.5						
111.0	.5	160.0	.3	224.9	.9	325.0	.4	520.4	.5						
113.1	.4	167.9	.4	230.9	.3	332.0	.9	521.3	3.1						
115.1	1.3	169.0	.6	236.1	1.2	334.1	4.4	522.3	1.1						
116.3	.4	171.1	2.6	237.1	.4	335.1	1.1	523.3	.5						
117.1	1.1	172.2	.4	238.1	.5	336.1	1.0								
117.8	.4	173.0	1.3	248.1	.5	338.2	.7								
119.1	.5	173.9	.5	249.0	.4	347.9	.6								
124.1	.5	174.9	.5	251.0	.5	349.0	.6								
127.1	.4	176.0	1.4	252.1	.4	350.1	4.0								
128.0	.4	177.0	.4	262.0	.5	351.1	2.9								
129.1	.5	181.1	.8	264.1	1.4	352.1	1.1								
130.0	.8	182.0	.7	264.9	.6	353.1	.5								
131.0	5.3	184.0	.4	267.0	.8	365.1	.5								
132.1	1.6	190.1	.7	276.0	.7	392.1	.6								
133.0	4.2	191.1	.9	277.0	.6	406.0	1.4								
133.8	.8	192.1	.5	277.9	1.2	407.2	3.7								
135.0	.6	193.0	.7	281.0	1.4	408.0	6.7								
139.1	.4	194.1	.5	282.1	.7	409.1	4.6								
141.0	.5	197.0	.4	290.0	.5	410.1	1.5								
141.9	.7	198.0	.7	292.0	21.7	411.2	.5								

Figure 49. Mass spectrum of peak at R_t=41.8 minutes from the chromatogram of LC peak 2' (Figure 48) silylated with MTBSTFA in pyridine.

MASS	%	MASS	%	MASS	%	MASS	%	MASS	%	MASS	%	MASS	%	MASS	%
97.0	.1	140.9	.2	175.0	.2	208.9	.2	248.1	.3	293.0	4.9	338.1	.6	409.1	5.3
98.0	.2	142.0	.2	176.2	.7	210.0	.1	249.0	.2	294.0	2.4	339.2	.3	410.0	1.6
99.1	1.6	143.1	.2	177.0	.2	211.0	.1	250.0	.3	295.0	.5	340.9	.2	411.1	.7
100.1	.7	144.1	.3	178.0	.2	213.1	.2	251.0	.5	296.1	.4	348.1	.6	422.1	.2
100.9	.1	144.9	.2	180.1	.2	215.1	.2	252.1	.2	297.1	.2	349.0	.4	423.2	.2
102.2	.1	147.1	1.3	181.0	.3	216.0	.2	253.1	.3	298.1	.2	350.1	6.2	434.2	.2
108.0	.2	147.9	.2	182.0	.4	217.0	.2	254.1	.1	302.1	.1	351.1	3.2	448.0	.7
110.1	.1	148.9	.4	182.9	.2	218.0	1.2	256.1	.1	306.0	.2	352.1	1.8	449.2	.5
111.0	.2	149.9	.1	184.0	.1	219.0	.3	261.9	.5	307.1	.2	353.1	.4	450.1	.5
113.0	.1	153.0	.2	184.9	.1	220.0	.2	263.0	.2	308.0	.4	355.0	.1	451.1	.2
115.1	.4	153.9	.2	189.0	.2	221.1	.1	264.0	1.1	309.1	.5	364.0	.5	462.1	.3
116.1	.2	154.9	.2	190.0	.3	222.0	.2	265.0	.4	310.2	.3	365.2	.2	464.1	100.0
117.1	.4	156.1	.3	191.0	.2	223.0	.3	266.0	.3	311.0	.4	366.2	.3	465.1	57.6
119.1	.1	157.0	1.2	192.1	.1	224.1	.2	267.0	.5	312.0	.2	367.1	.1	466.1	24.7
124.1	.1	158.0	3.7	193.0	.3	225.0	.3	268.0	.2	318.0	.6	376.1	.2	467.2	7.3
125.0	.1	159.0	.8	194.1	.2	226.0	.2	269.1	.1	319.0	.3	381.2	.2	468.1	1.9
128.1	.1	160.0	.4	194.9	.1	231.0	.2	276.1	.7	320.1	.2	383.3	.3	469.1	.3
128.9	.1	165.0	.2	197.0	.3	232.1	.2	276.9	.5	321.9	.3	384.0	.2	506.3	2.7
130.0	.4	166.0	.2	198.0	.3	234.1	.2	278.0	.9	323.0	.5	390.0	.2	507.3	1.0
131.0	2.2	167.1	.2	202.0	.2	235.1	.2	279.1	.4	324.9	.3	391.1	.1	508.2	.6
132.0	.7	168.1	.1	203.0	.2	236.1	.9	280.1	.2	332.1	.7	391.9	.4	509.2	.1
133.0	1.3	169.1	.4	204.1	.2	237.1	.4	281.0	.5	333.0	.3	393.0	.4	520.2	.7
134.0	.4	171.1	1.0	204.9	.1	238.0	.3	281.9	.2	334.0	3.7	394.1	.3	521.2	3.0
135.0	.2	172.0	.2	206.0	.1	239.1	.2	290.1	.4	335.1	1.2	406.0	1.4	522.2	1.2
138.0	.1	173.0	.5	207.1	.6	240.0	.2	291.2	.3	336.0	.7	407.1	3.4	523.3	.6
139.0	.1	174.0	.2	208.0	.3	242.0	.2	292.0	18.3	337.0	.3	408.0	6.7	524.2	.1
LAST	32														
408.0	6.7	409.1	5.3	410.0	1.6	411.1	.7	412.1	.1	422.1	.2	423.2	.2	424.0	.1
429.0	.1	434.2	.2	448.0	.7	449.2	.5	450.1	.5	451.1	.2	452.0	.1	462.1	.3
464.1	100.0	465.1	57.6	466.1	24.7	467.2	7.3	468.1	1.9	469.1	.3	490.2	.1	506.3	2.7
507.3	1.0	508.2	.6	509.2	.1	520.2	.7	521.2	3.0	522.2	1.2	523.3	.6	524.2	.1

Figure 50. Mass spectrum of the triply silylated derivative of an authentic sample of xanthopterin. R_t=41.6 minutes in the chromatogram of Figure 38.

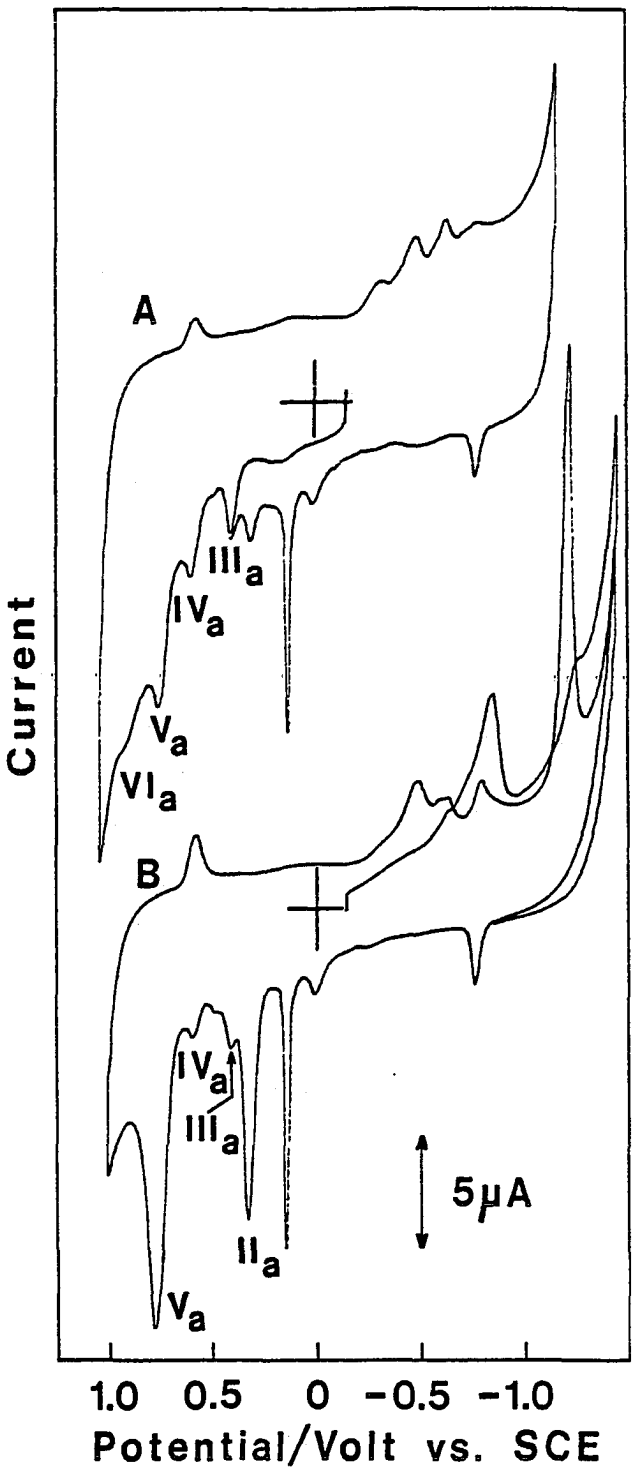


Figure 51. Cyclic voltammograms of authentic xanthopterin in pH 4.7 phosphate buffer, μ=0.3 M. Sweep rate: 200 mV s^{-1}. (A) Initial sweep positive and (B) initial sweep negative.

all ten voltammetric oxidation peaks are observed. The cyclic voltammetry of xanthopterin is very similar to the cyclic voltammetry of the peak I_a electrolysis product mixture of 5-MTHP electrooxidized in pH 4.7 PO_4^{3-}, μ=0.5 M (Figure 12A,B). This suggests that xanthopterin probably accounts for a large fraction of the electroactive products.

Identification of 7,8-dihydroxanthopterin. Identification of 7,8-dihydroxanthopterin is tenuous at best because there is no spectral evidence, u.v. or GC-MS, to support the contention that it is one of the electrolysis products of 5-MTHP. In the voltammetry of xanthopterin, when the negative potential sweep passes through the reduction peak at -0.63 V a new oxidation peak appears at 0.32 V on the ensuing positive sweep. Reduction at -0.63 V in pH 4.7 buffer generates 7,8-dihydroxanthopterin which is reoxidized to xanthopterin at 0.32 V/SCE. In the voltammetry of the electrolysis product mixture an oxidation peak is observed at 0.32 V/SCE on the initial positive sweep. Since no reduction was necessary to observe this peak, 7,8-dihydroxanthopterin might be present in the product mixture, particularly in product solutions from electrolysis in pH 4.7 phosphate.

Identification of LC peak 10. The compound isolated from LC peak 10 in the separation of products from peak I_a electrolysis carried out in 0.5 M NaCl pH 4.7 was silylated with MTBSTFA at room temperature for ca. 20 minutes. The total ion current chromatogram for the GC-MS analysis of LC peak 10 is shown in Figure 52. Three peaks are observed which would correspond to 1, 2, or 3 positions silylated in a molecule of mass 195. They have retention times of 35.8 minutes, 38.7 minutes, and

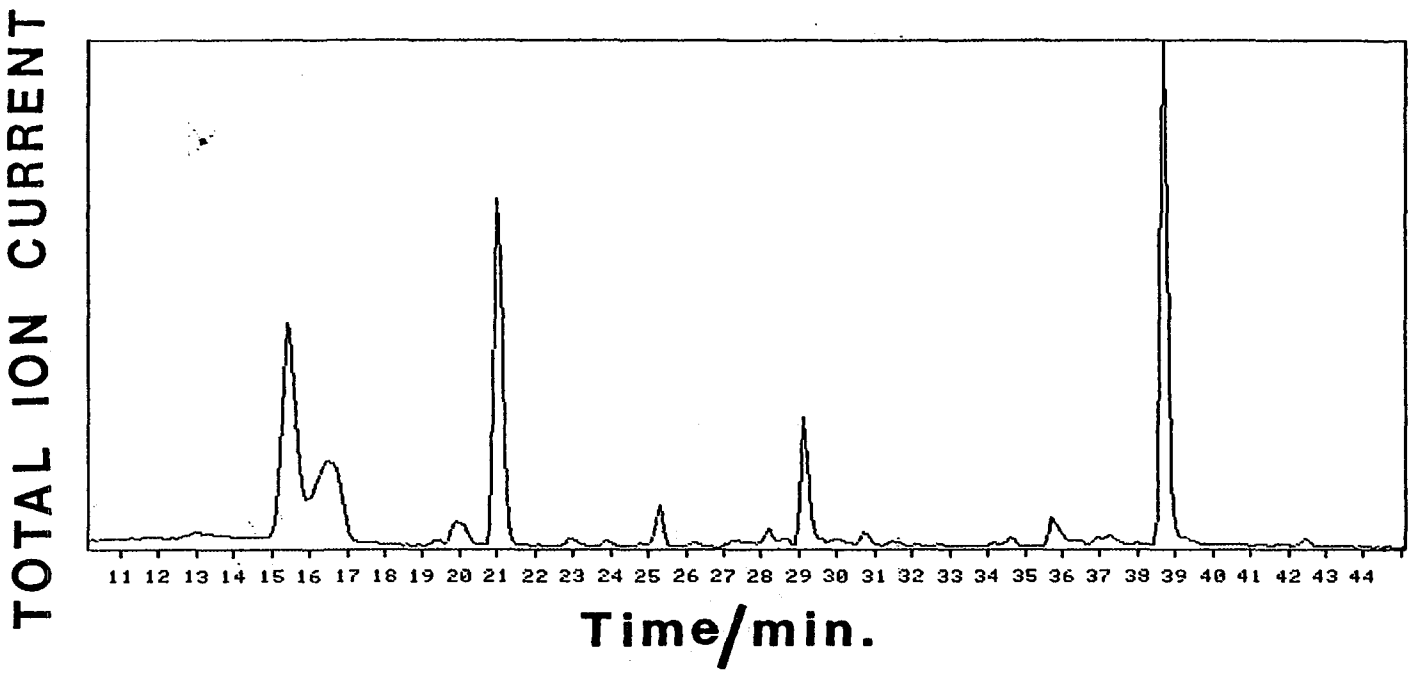


Figure 52. Total ion current chromatogram of product isolated from LC peak 10 and silylated with MTBSTFA in pyridine at room temperature for ca. 20 minutes.

42.4 minutes respectively. The mass spectrum of the doubly silylated derivative at R_t=38.7 minutes is shown in Figure 53 and exhibits a molecular ion of mass 423. Leucopterin (MW=195) has been shown to yield only the triply silylated derivative (M^+=537) (vide supra) even when silylated with MTBSTFA at room temperature.

The reported u.v. spectrum of leucopterin at pH 13 has λ_{max}=240 nm, 285 nm, and 340 nm.[40] An u.v. spectrum of authentic leucopterin in pH 4.7 phosphate was run and peak maxima were observed at λ_{max}=203 nm, 221 nm, 298 nm, and (335) nm. Another spectrum of leucopterin was obtained in pH 11.5 N_aOH and had λ_{max}=240 nm, 287 nm, and 342 nm which is close to the reported values.

The u.v. spectrum of LC peak 10 in pH 4.6 PO_4^{3-} is presented in Figure 54. It has λ_{max}=223 nm, (272) nm, 280 nm, and 302 nm and only two of these are close to that of leucopterin in pH 4.7 phosphate. From the mass spectrometry and u.v. data it appears that LC peak 10 is not leucopterin.

Cyclic voltammetry of product isolated from LC peak 10. The cyclic voltammetry of LC peak 10 was studied at 200 $mV\,s^{-1}$ in pH 4.6 phosphate buffer with an ionic strength of 0.5 M. Rather surprising results were observed as illustrated in Figure 55A,B. The voltammetry looks amazingly similar to the cyclic voltammetry of xanthopterin in Figure 51. Several important differences are noted however, most notably the oxidation peak at 0.34 V/SCE is observed on the initial positive sweep. For xanthopterin it was necessary to sweep negative before the oxidation peak at 0.32 V was observed (vide supra). This oxidation peak was attributed to the oxidation of 7,8-dihydroxanthopterin

MASS	%	MASS	%	MASS	%	MASS	%	MASS	%	MASS	%	MASS	%	MASS	%	MASS	%
91.1	.2	123.1	.5	157.0	1.1	192.1	.6	227.1	.1	279.0	.5	358.3	.5				
92.1	.1	124.2	1.0	158.0	1.4	193.0	.9	232.0	.1	280.1	1.0	359.2	.2				
93.0	.4	125.1	.6	159.2	.7	194.1	1.1	233.0	.1	281.1	.6	361.2	.1				
94.1	.3	126.1	.5	160.1	.7	195.2	1.2	234.1	1.0	282.0	.2	364.1	.3				
95.1	.3	127.2	.4	161.0	.4	196.1	1.1	235.1	3.2	292.1	2.6	366.2	100.0				
96.2	.3	128.1	.4	162.1	1.2	197.0	.7	236.1	2.8	293.1	1.0	367.2	30.4				
97.1	.5	128.9	.6	163.1	.2	198.1	.4	237.1	3.0	294.1	2.5	368.2	11.5				
98.2	.6	130.0	.3	164.0	.2	199.1	.2	238.1	1.6	295.0	.6	369.2	2.1				
99.1	4.9	131.0	1.8	165.0	.5	200.0	.1	239.1	1.2	296.1	2.2	370.2	.4				
100.1	3.0	132.0	.9	166.0	1.5	202.0	.1	240.1	.2	297.2	.5	392.2	.3				
101.1	1.2	133.0	2.7	166.9	.9	203.1	.1	241.1	.1	298.1	.3	393.3	.1				
102.1	.5	134.0	.7	168.1	.7	204.0	.7	248.2	.4	306.1	.2	394.2	.6				
103.2	.4	135.0	.7	169.1	.5	205.0	.3	250.1	9.4	308.1	12.6	395.1	.1				
104.1	.2	136.0	.4	170.1	.2	206.2	.6	251.1	6.4	309.1	5.0	406.2	.2				
105.1	.2	136.9	.3	171.2	.6	207.0	1.4	252.2	10.9	310.2	2.9	407.1	.1				
107.1	.3	138.0	.4	172.1	.2	208.2	2.2	253.2	2.7	311.3	.7	408.2	4.6				
108.2	.3	139.0	.5	173.1	1.0	209.1	1.8	254.2	1.0	312.1	.2	409.2	1.4				
109.2	.2	139.9	.4	174.0	.4	210.0	1.1	255.2	.3	320.1	.2	410.2	.5				
110.2	.4	141.0	.4	175.2	.4	211.1	1.2	261.0	.1	321.1	.1	411.2	.1				
111.2	.7	142.1	.4	176.0	.4	212.1	.3	262.0	.4	322.2	.1	422.3	1.8				
112.2	.5	143.0	.7	177.1	.3	213.1	.2	263.1	.3	324.1	.3	423.3	27.3				
113.1	.8	144.1	.5	178.1	.6	214.1	.1	264.0	.5	325.2	.1	424.2	9.8				
114.0	.4	145.1	.3	179.0	.6	218.1	.4	265.1	.4	334.1	1.1	425.3	3.8				
115.1	1.5	147.1	1.0	180.1	1.0	219.1	.2	266.1	.7	335.1	.3	426.3	.6				
116.1	.4	148.1	.9	181.1	1.1	220.1	1.7	267.1	1.6	336.1	.5	427.3	.1				
117.1	1.0	149.0	1.8	182.1	1.4	221.1	1.0	268.1	1.5	337.1	.2	480.3	.5				
118.1	.3	150.1	.6	183.1	1.4	222.1	7.8	269.1	.6	350.2	9.2	481.3	.2				
119.1	.6	151.0	.4	184.1	.4	223.1	2.4	270.1	.2	351.2	2.6	537.5	.1				
120.1	.3	152.1	.8	185.2	.4	224.1	4.0	276.1	.3	352.1	1.4						
121.1	.2	152.9	.6	190.2	.3	225.1	1.0	277.0	.3	353.1	.3						
122.3	.3	154.6	11.5	191.1	.4	226.0	.3	278.0	1.1	357.3	1.7						

Figure 53. Mass spectrum of the doubly silylated derivative of product isolated from LC peak 10. R_t=38.7 minutes in the chromatogram of Figure 52. Silylation was carried out with MTBSTFA.

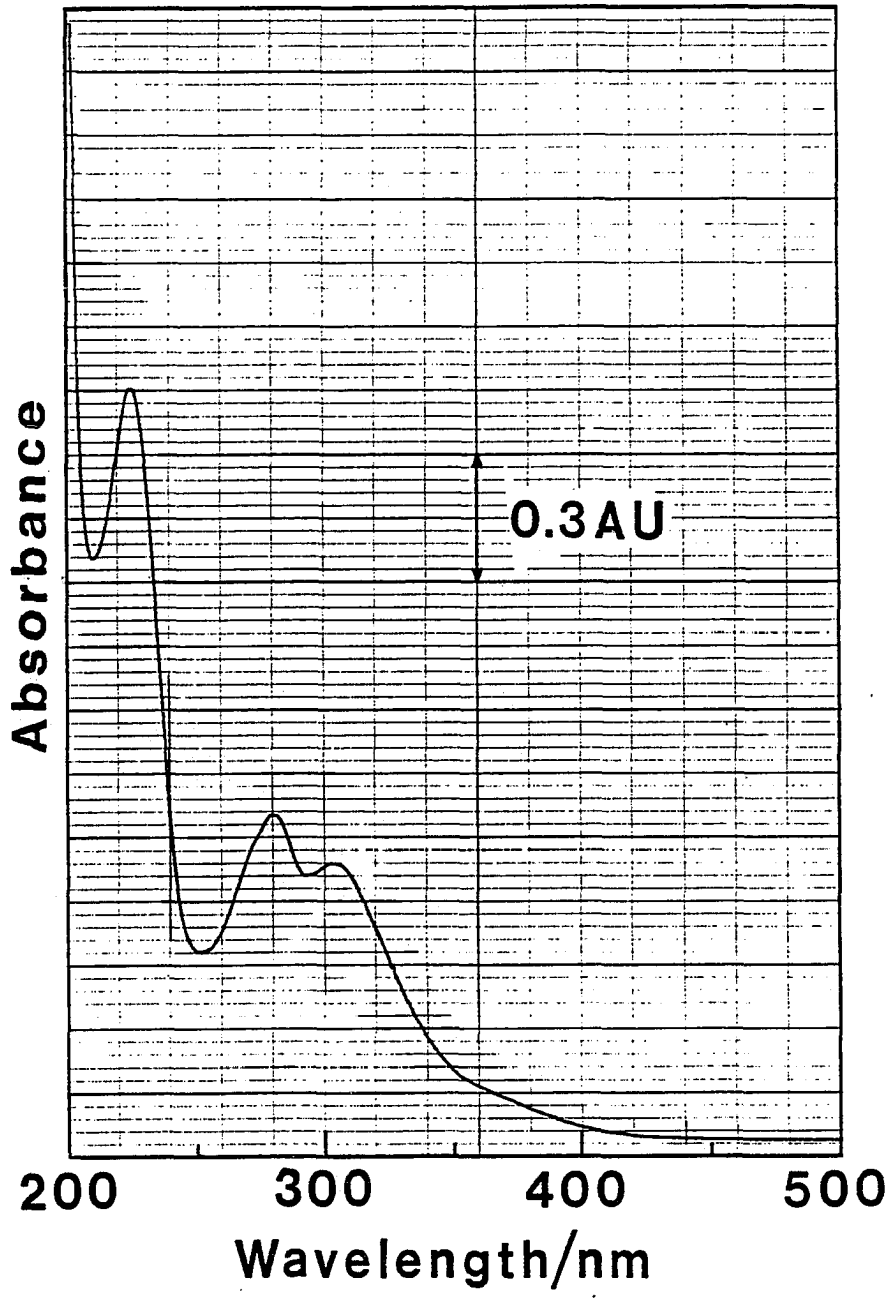


Figure 54. U.v. spectrum of LC peak 10 in pH 4.7 phosphate buffer. Spectrum obtained in 0.5 cm cells at a scan rate of 200 nm min^{-1}.

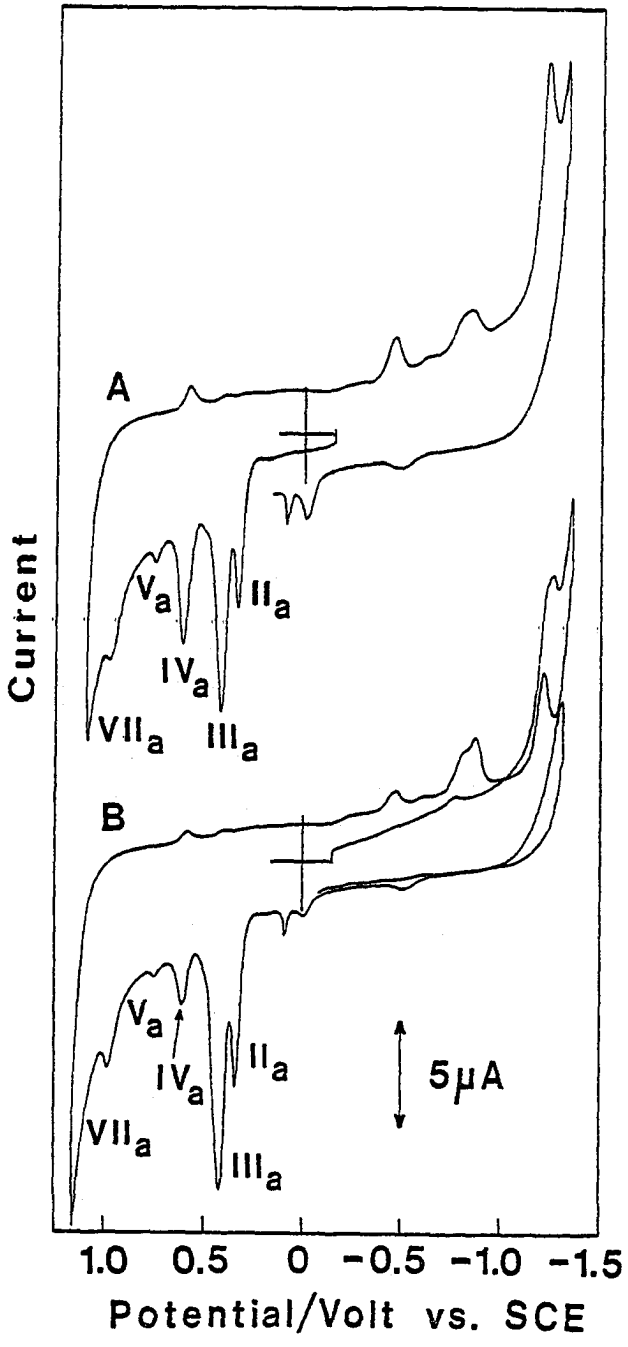
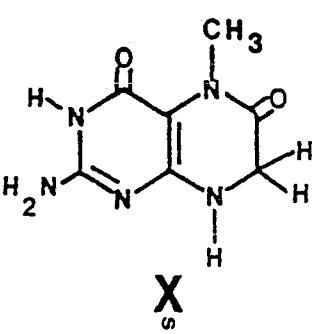


Figure 55. Cyclic voltammograms of LC peak 10 product in pH 4.6 phosphate buffer of ionic strength 0.5 M. Sweep rate: 200 mV s^{-1}. (A) Initial sweep positive and (B) initial sweep negative.

generated on the negative sweep. In the case of LC peak 10 this peak is observed on the initial positive sweep indicating it is probably a substituted 7,8-dihydroxanthopterin.

Another difference noted is the reversal in the size of the oxidation peaks at ca. 0.60 V and 0.75V. In xanthopterin the peak at 0.75 V is by far the largest of the two peaks, but in LC peak 10 the oxidation peak at 0.60 V/SCE is the largest. Also the oxidation peak at 0.98 V is much more clearly defined in the LC peak 10 product. The oxidation peak at 0.42 V in the voltammetry of LC peak 10 also exhibits reversible characteristics (Figure 56) unlike the analogous peak in the voltammetry of xanthopterin. Xanthopterin, however, exhibits a quasi-reversible oxidation peak (-0.75V) for the reduction peak at ca. -0.80V. The analogous oxidation peak in the voltammetry of LC peak 10 is much smaller and is shifted ca. 250 mV to -0.50V/SCE. In other ways the cyclic voltammetry is very similar leading us to believe that the LC peak 10 product was a substituted, 7,8-dihydroxanthopterin. A cyclic voltammogram of leucopterin at pH 4.6 is presented in Figure 57 to illustrate that it is completely different from the voltammetry of LC peak 10.

Another molecule which has a molecular weight of 195 g/mole and could reasonably be expected as a product of electrolysis of 5-MTHP is 5-methyl-7,8-dihydroxanthopterin (5-M-7,8-DXP)(X).



X

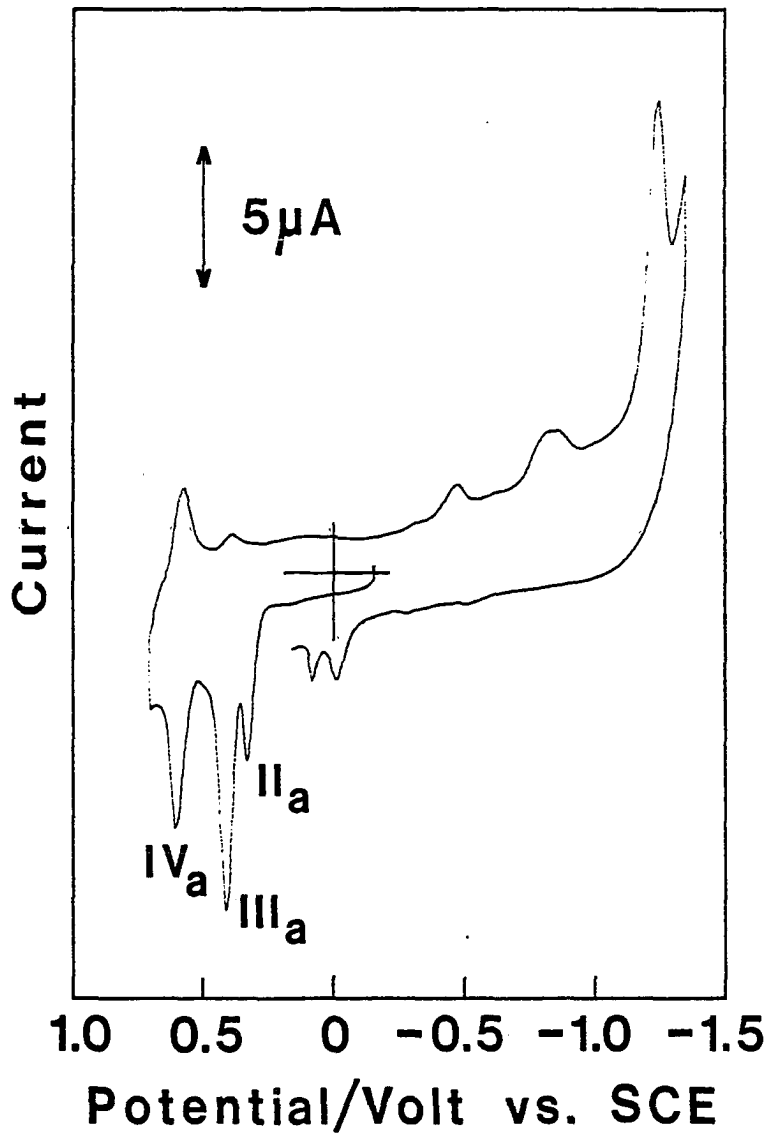


Figure 56. Cyclic voltammogram of LC peak 10 product in pH 4.6 phosphate buffer, μ=0.5 M in which the sweep was reversed immediately after passing through the oxidation peak at 0.42V. Sweep rate: 200 mV s^{-1}.

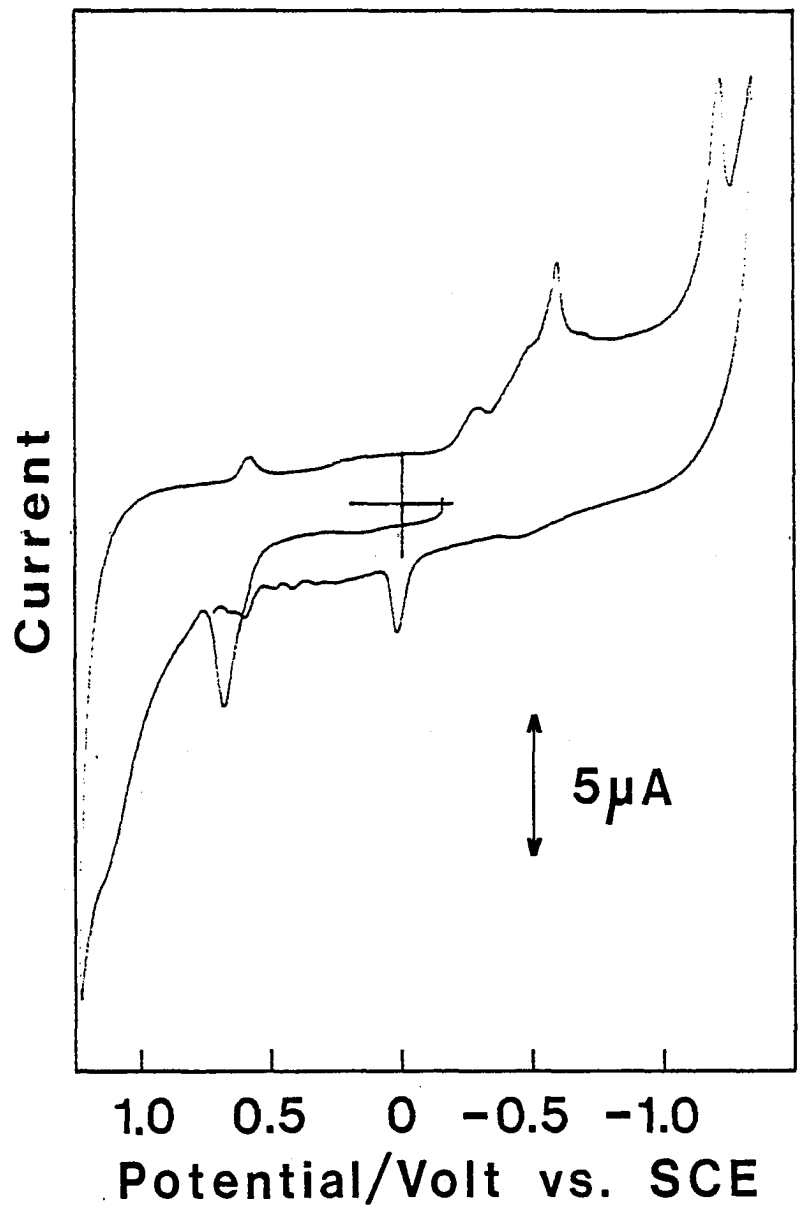


Figure 57. Cyclic voltammogram of a saturated solution of leucopterin in pH 4.6 phosphate buffer of ionic strength 0.5 M. Sweep rate: 200 mV s^{-1}.

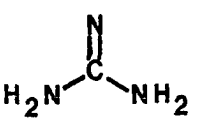
A methyl group replacing a hydrogen atom would not be expected to alter the electrochemical properties of a molecule drastically unless that position is directly involved in the redox reaction. Except for the differences in the cyclic voltammetry noted above, the only other difference observed was a 20-40 mV positive shift in the oxidation peak potentials of 5-M-7,8-DXP relative to xanthopterin.

U.v. spectroscopy. U.v. peak maxima for a number of 7,8-dihydroxanthopterins are reported in the literature.[41] At pH 7 it was found that 5-M-7,8-DXP exhibits u.v. peaks at λ_{max}=223 nm, 270 nm, and 302 nm. Likewise at pH 7, 7,8-dihydroxanthopterin has a very similar spectrum with u.v. peaks at λ_{max}=223 nm, 273 nm, and 308 nm. A spectrum for LC peak 10 is shown in Figure 54 (vide supra) at pH 4.6. The pK_a's of 5-M-7,8-DXP are given as 1.45 and 9.92 therefore the ionic species at pH 4.6 should be the same as at pH 7. A distinction based on the u.v. spectrum would be impossible, however taken together with the GC-MS data and the cyclic voltammetry it is possible to state with considerable certainty that LC peak 10 is 5-methyl-7,8-dihydroxanthopterin. This is supported by the solubility data which indicates leucopterin is practically insoluble while the compound isolated from LC peak 10 is easily soluble.

Identification of electrolysis products present in LC peaks 3-6. LC peaks 3-6 really appear as one large peak because of severe overlapping of the various components (Figure 41). By running u.v. spectra of every second 3 ml fraction across these peaks it was possible to collect several fractions which were relatively free of cross-

contamination. The component designated as LC peak 3 was collected from fractions eluting between 240 ml and 255 ml. LC peak 4 was collected from fractions eluting between 264 ml and 273 ml. Peak 5 with a retention volume of 288 ml was the NaCl used as the supporting electrolyte. Some chloride was found in the eluant as early as 210 ml and as late as 330 ml, but the bulk of it eluted between 264 ml and 324 ml. LC peak 6 was collected from fractions eluting between 291 ml and 300 ml. Peaks 3-6 all gave a positive Cl^- test with dilute silver nitrate solution. However Cl^- does not interfere with the silylation process therefore it was not a big problem.

Identification of product isolated from LC peak 6. It is reported in the literature that guanidine (XI) (MW=59 g/mole) was observed among the degradation products of pterins.[40] Referring to Tables 5 and 6 it can be seen that a peak at R_t=ca. 30 minutes had a molecular ion at mass 401 which could be a molecule of mass 59 with 3 hydrogens replaced by TBDMS groups.



XI

The u.v. spectrum of LC peak 6 is shown in Figure 58 and exhibits one peak at λ_{max}=198 nm. A u.v. spectrum of an authentic sample of guanidine sulphate in water is shown in Figure 59. Authentic guanidine also exhibits a peak at λ_{max}=197-198 nm. Chloride ions in solution are known

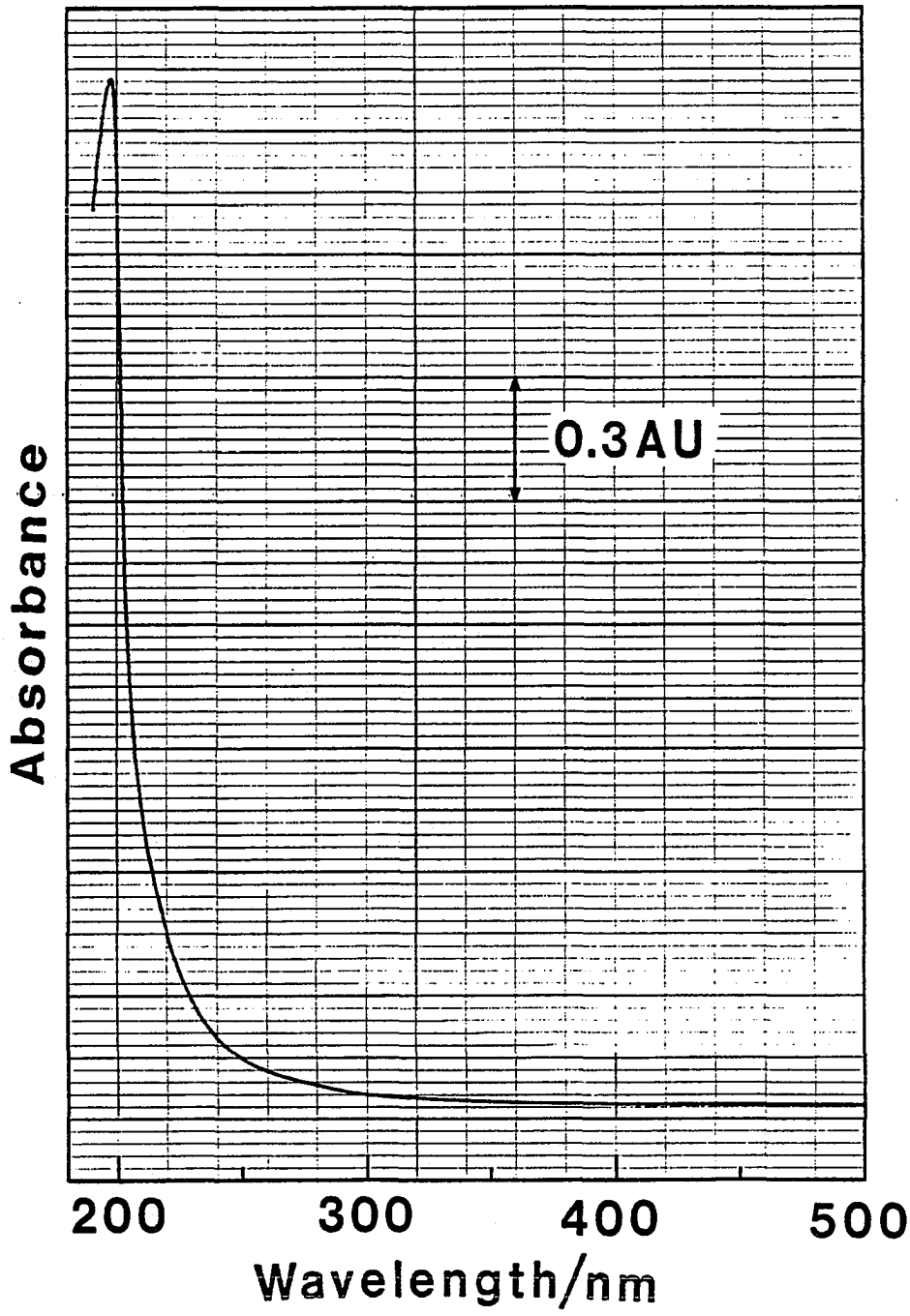


Figure 58. U.v. spectrum of LC peak 6 in H_2O. Spectrum was obtained in 0.5 cm cells at a scan rate of 200 nm min^{-1}.

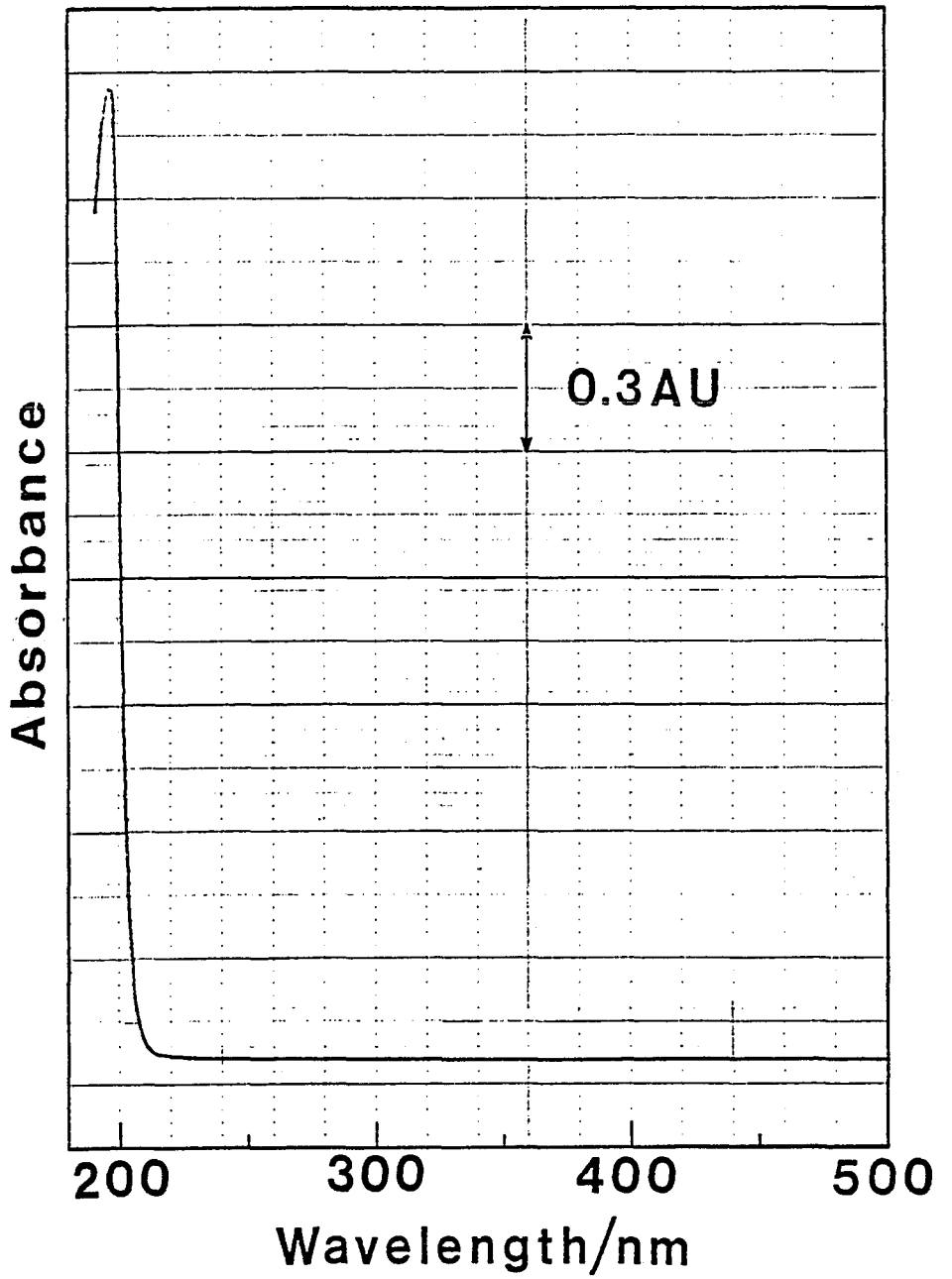


Figure 59. U.v. spectrum of guanidine sulfate in distilled water. Spectrum was obtained in 0.5 cm cells at a scan rate of 200 nm min^{-1}.

to absorb near this wavelength region, however λ_{max} for chloride is ca. 193 nm.

GC-MS data on compound isolated from LC peak 6. The total ion current chromatogram for LC peak 6 silylated with MTBSTFA in pyridine at 85°C for 10 minutes is presented in Figure 60. The peak at R_t=28.4 minutes has a molecular ion of mass 401 and its complete spectrum is presented in Figure 61. The fragmentation pattern of the mass spectrum in Figure 61 is identical with the mass spectrum of authentic guanidine silylated with MTBSTFA (R_t=28.3 minutes) shown in Figure 62. Both spectra exhibit a base peak at mass 344 (M-57), an M-15 peak at mass 386, and the molecular ion at mass 401.

The product from LC peak 6 does not show any oxidation or reduction peaks at the PGE and authentic guanidine likewise did not show any oxidation or reduction peaks in the cyclic voltammetry. An i.r. spectrum of the product isolated from LC peak 6 was not obtained because the sample was contaminated with too much NaCl. All of the data presented confirm that LC peak 6 is really guanidine.

Identification of LC peak 4. LC peak 4 appears to be a major product however it must be noted that it eluted together with chloride and also with the trailing part of LC peak 3. Cyclic voltammetry at 200 mV s^{-1} revealed one very small reduction peak at -0.88V and no oxidation peaks. The u.v. spectrum of LC peak 4 has only one small peak at λ_{max}=340 nm and an inflection at ca. 230-240 nm. In an acidic solution the long wavelength peak shifts to ca. 420 nm. Below 230 nm the absorbance goes off-scale because of the enormous absorbance of chloride which is

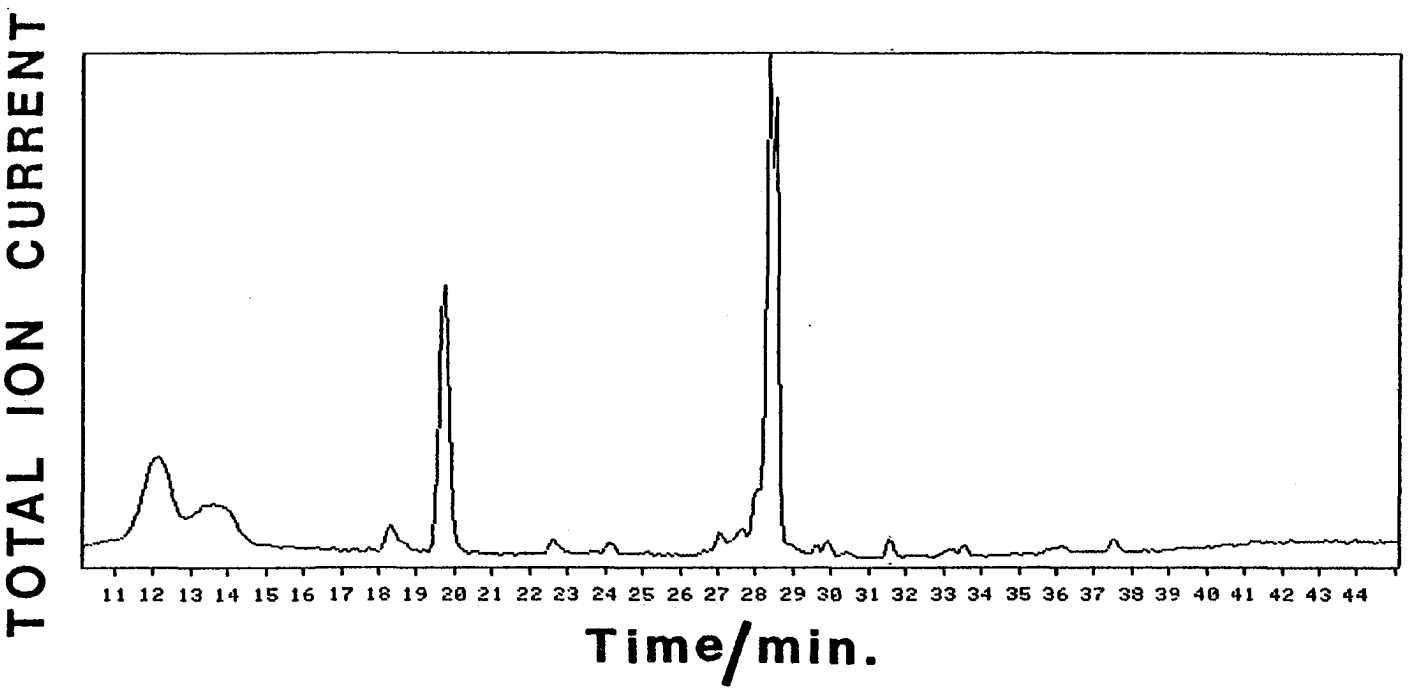


Figure 60. Total ion current chromatogram of product isolated from LC peak 6 and silylated with MTBSTFA in pyridine at 85°C for 10 minutes.

MASS	%	MASS	%	MASS	%	MASS	%	MASS	%	MASS	%	MASS	%	MASS	%
91.0	.2	127.0	.4	173.1	3.5	211.1	.2	261.2	.1	342.4	.1				
93.1	.1	128.0	.4	174.1	1.4	213.1	25.8	263.0	.1	344.3	100.0				
94.8	.1	130.1	51.7	175.0	.4	214.1	11.8	264.8	.1	345.3	34.6				
95.3	.1	131.0	10.7	176.1	.1	215.1	3.8	267.0	.1	346.3	14.7				
95.6	.1	132.0	9.4	177.0	.1	216.1	6.5	269.2	.2	347.3	3.6				
97.1	.2	133.0	1.5	180.9	.1	217.2	1.7	270.0	.4	348.3	.9				
99.1	5.9	134.0	1.4	182.3	.1	218.1	.9	271.2	2.4	349.4	.1				
100.1	7.1	135.1	.2	183.1	.3	219.1	.2	272.2	2.5	355.0	.2				
101.1	1.4	136.0	.1	184.1	.5	221.1	.5	273.2	.7	356.0	.1				
102.1	1.6	138.9	.7	185.1	.2	221.9	.1	274.0	.5	370.3	.2				
103.1	.3	140.0	.3	186.1	1.1	222.9	.1	275.1	.1	371.2	.1				
104.1	.3	141.0	1.4	187.1	1.9	225.7	.1	277.3	.1	384.3	.1				
104.9	.1	142.0	1.3	188.2	9.4	228.2	.4	281.1	.4	386.3	4.8				
105.1	.1	143.1	.7	189.1	5.1	230.1	19.9	282.2	.1	387.3	1.8				
106.9	.1	144.1	.6	190.2	1.3	231.2	5.7	286.1	2.7	388.3	.9				
107.6	.1	146.1	58.8	191.2	.5	232.2	4.2	287.2	1.3	389.3	.2				
108.9	.1	147.1	10.3	192.1	.1	233.1	.8	288.2	13.3	400.2	.5				
110.2	.2	148.1	4.4	192.8	.1	234.2	.4	289.2	4.5	401.2	3.9				
111.1	.4	149.1	1.4	195.8	.1	235.2	.1	290.2	1.6	402.3	1.6				
113.0	2.3	150.0	.1	197.1	1.8	239.2	.1	291.2	.5	403.3	.6				
114.1	2.5	154.1	.2	198.1	.8	241.2	.1	292.1	.1	404.2	.1				
115.2	1.9	155.0	.4	199.0	.4	242.1	.1	297.0	.1	429.1	.1				
116.2	11.3	156.1	3.1	200.0	1.0	244.2	1.3	312.2	.1						
117.2	2.0	157.0	2.7	200.9	.3	245.2	.4	312.9	.1						
118.1	1.2	158.0	1.5	203.1	10.2	246.2	.3	314.1	.2						
119.0	.1	159.1	.6	204.1	2.4	255.3	7.3	317.2	.1						
119.8	.1	160.0	.2	205.1	1.6	256.1	2.0	318.3	.1						
120.6	.1	161.0	.1	206.1	.3	257.1	1.0	328.2	8.3						
122.7	.1	170.0	.5	207.0	.5	258.2	.5	329.2	2.5						
125.1	.2	171.1	10.3	208.0	.1	259.1	.2	330.2	1.4						
126.2	.3	172.1	10.5	209.0	.1	260.1	.1	331.2	.3						

Figure 61. Mass spectrum of peak at 28.4 minutes from the chromatogram of LC peak 6 (Figure 60) silylated with MTBSTFA in pyridine.

MASS	%	MASS	%	MASS	%	MASS	%	MASS	%	MASS	%	MASS	%	MASS	%
91.1	.1	124.1	.2	165.4	.1	213.1	37.7	274.2	.3						
91.8	.2	125.0	.4	167.5	.2	214.0	12.6	280.9	.2						
93.0	.2	126.2	.6	168.5	.1	215.1	4.4	286.2	2.2						
93.3	.2	127.1	.5	171.1	18.1	216.1	4.9	287.2	.7						
94.1	.2	128.1	.6	172.1	9.7	217.0	1.9	288.2	10.3						
95.0	.2	130.0	71.5	173.1	4.2	218.1	.7	289.2	3.4						
96.8	.2	131.1	14.9	174.1	2.0	219.1	.2	290.1	1.6						
98.0	.3	132.0	16.4	175.0	.7	223.1	.2	291.3	.4						
99.1	10.5	133.0	2.8	176.0	.3	228.0	.3	308.2	.1						
100.0	13.3	133.9	1.0	182.0	.2	229.0	.2	314.2	.2						
101.1	2.7	135.1	.2	183.1	.6	230.0	15.0	328.1	6.9						
102.0	2.3	139.0	.8	183.9	.2	231.1	4.1	329.1	2.4						
102.9	.3	139.9	.5	185.1	.3	232.1	2.9	330.1	1.5						
104.0	.6	140.8	2.5	186.1	1.1	233.2	.8	331.1	.2						
105.1	.2	141.9	1.5	187.1	1.7	234.2	.2	332.1	.2						
107.8	.4	142.9	1.2	188.1	12.8	235.2	.2	341.9	.2						
108.7	.1	143.9	.7	189.0	5.9	239.1	.2	344.2	100.0						
109.7	.1	146.0	97.9	190.1	1.4	240.1	.2	345.2	39.8						
111.1	.6	147.0	15.9	191.1	.4	244.2	.9	346.2	16.0						
113.1	3.1	148.1	5.5	197.1	1.6	245.1	.5	347.2	3.7						
114.0	3.9	149.0	5.6	198.1	.8	246.0	.3	348.2	1.1						
115.1	2.8	149.9	.5	199.1	.4	249.2	.2	370.1	.3						
116.1	19.5	150.9	.2	199.9	.4	255.3	7.0	386.2	6.4						
117.1	3.5	155.0	.7	201.0	.2	256.2	1.7	387.2	2.6						
118.1	1.3	156.0	3.8	202.1	.8	257.1	.9	388.2	1.4						
119.2	.3	157.0	4.0	203.1	8.2	258.1	.4	389.0	.2						
120.1	.2	158.0	2.4	204.1	1.8	269.9	.3	400.1	.6						
120.8	.2	158.9	.8	205.0	1.0	271.2	1.5	401.2	5.7						
121.5	.1	160.0	.3	205.9	.2	272.1	1.5	402.3	2.2						
122.7	.3	160.7	.2	206.2	.2	272.9	.6	403.2	.8						
123.4	.1	163.0	.1	207.0	.5	273.9	.3	404.2	.1						

Figure 62. Mass spectrum of the triply silylated derivative of guanidine (MTBSTFA in pyridine at room temperature for 15 minutes). R_t= 28.3 minutes.

present as a contaminant. The lyophilized product was orangeish-yellow and only a small amount of material was collected. It has been observed that the quantity of material collected from LC peak 4 increases according to the length of time elapsed between the electrolysis and the chromatography. This is an indication that it may also be a degradation product (along with peaks 1, 2, and 6, vide supra) of other products in the solution.

GC-MS of LC peak 4. The product isolated from peak 4 was contaminated with chloride, therefore a good melting point was hard to obtain. It does not appear to melt, however it begins to char at ca. 250°C. The direct insertion mass spectrum revealed only peaks which could be attributed to plasticizer.

Fortunately silylation of LC peak 4 was successful with both BSA and MTBSTFA in pyridine. The total ion current chromatogram of the MTBSTFA silylated product is shown in Figure 63. There are three peaks in this chromatogram which are of interest with retention times of 29.6 minutes, 32.1 minutes, and 32.8 minutes. The peak at R_t=29.6 minutes is triply silylated guanidine (M^+=401) and is probably due to cross-contamination with LC peak 6. The GC peaks at R_t=32.1 minutes and 32.8 minutes have molecular ions of mass 266 and 458 respectively. Mass 458 is not observed in the mass spectrum of the peak at 32.8 minutes, however the pattern M-57 (401) and M-15 (443) is very clear.

LC peak 4 was also silylated with BSA in pyridine at room temperature for ca. 1½ hours. Figure 64 illustrates the total ion current chromatogram for the derivatized product. This chromatogram is very clear compared to many other attempts at silylation with BSA. Peaks of

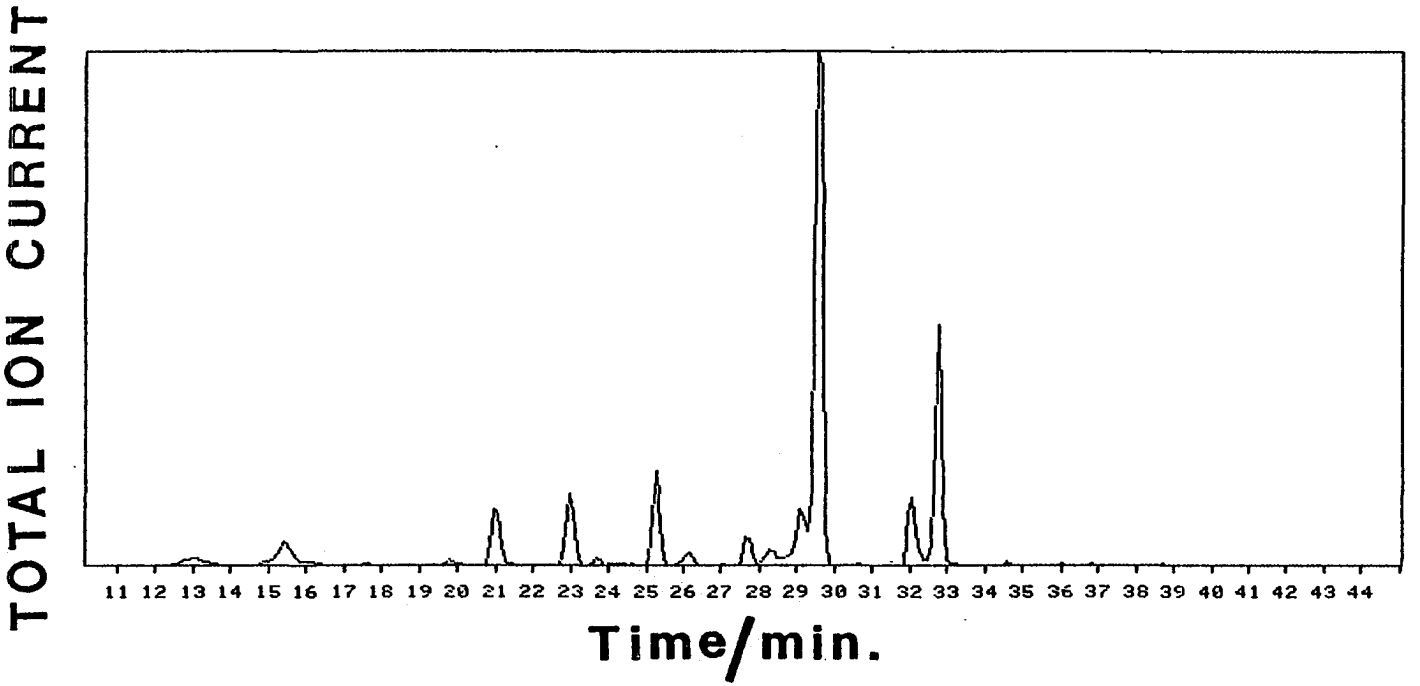


Figure 63. Total ion current chromatogram of product isolated from LC peak 4 and silylated with MTBSTFA in pyridine at room temperature for ca. 30 minutes.

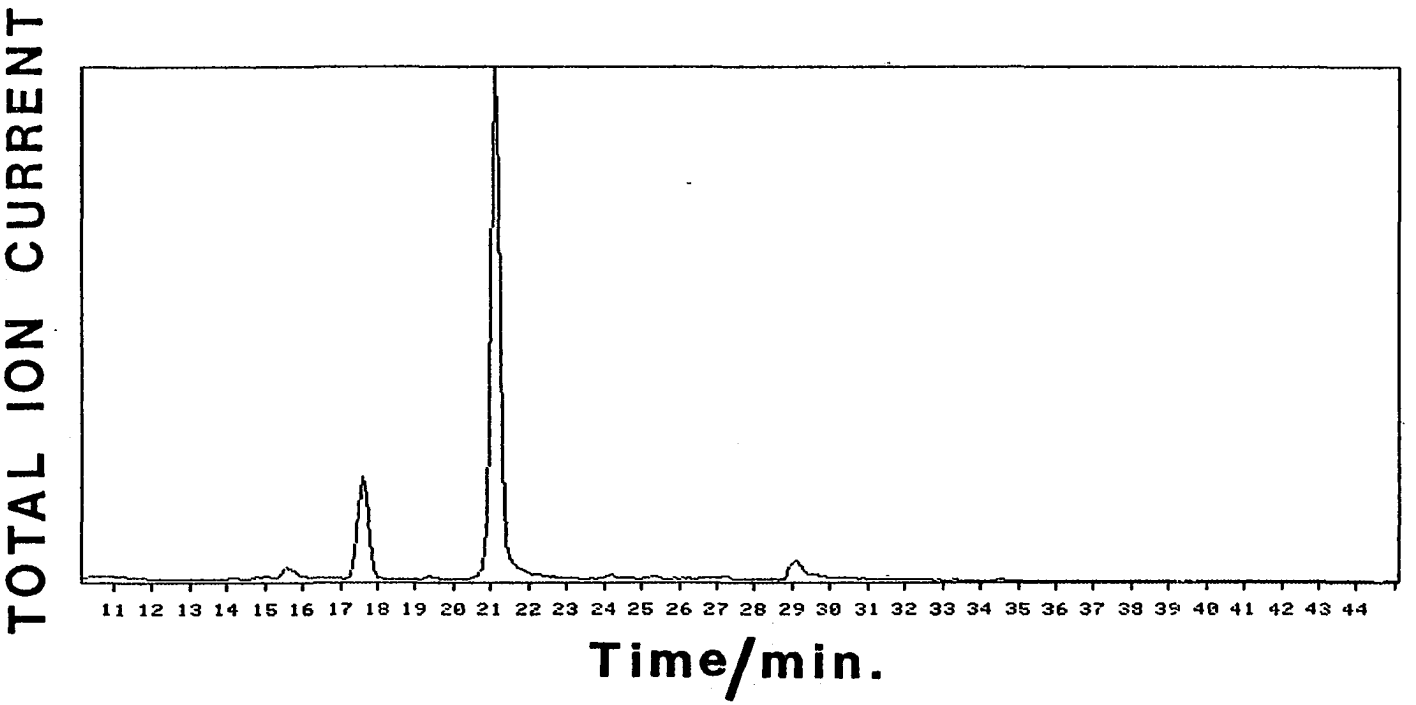


Figure 64. Total ion current chromatogram of product isolated from LC peak 4 and silylated with BSA in pyridine at room temperature for ca. 1½ hours.

interest are those at retention times of 21.2 minutes (M^+=332) and 29.2 minutes (M^+=224) because they are the counterparts to the peaks of the TBDMS derivatives in Figure 63. Using Equation 14 the number of silylatable positions in the underivatized molecule can be calculated:

$$458 - 332 = 126 = 42(n)$$

$$n = 3 \text{ silylatable positions}$$

$$266 - 224 = 42 = 42(n)$$

$$n = 1 \text{ silylatable position}$$

The molecular weights of the underivatized molecules are 458-3(114) = 332-3(72)=116 g/mole and 266-1(114)=224-1(72)=152 g/mole. The peak at 32.8 minutes (M^+=458) in the chromatogram of Figure 63 is the largest peak except for the guanidine peak. Likewise the peak at 21.2 minutes in the chromatogram of the BSA silylated product is by far the largest peak in Figure 64. Therefore it was decided to concentrate on identifying the compound of molecular weight 116.

Use of isotope ratio to give possible molecular formulas. In the absence of other data a list of possible formulas was generated by referring to the mass spectroscopy tables of Beynon and Williams.[42] The number of possibilities was narrowed down by using the Nitrogen rule,[43] i.e., a molecule of even mass must contain no atoms of nitrogen or an even number of nitrogen atoms. If the molecular weight is an odd number the number of nitrogen atoms must be odd. Another piece of data which helped narrow the possibilities was the fact that the product from LC peak 4 was silylated in three positions. Thus it must have at least

three active hydrogen atoms, i.e., hydrogens attached to O, N, S, etc.

After narrowing down the possibilities in this manner the isotope ratio was used to rule out still other possibilities. Table 7 contains a list of possible empirical formulas which meet the criteria

TABLE 7

Possible Empirical Formulas for Molecular Weight = 116 g/mole Containing C, H, N, and O[a]

Formula	P_{M+1}/P_{M+2}[b]
$C_1H_4N_6O$	13.9
$C_2H_4N_4O_2$	8.3
$C_2H_8N_6$	51.6
$C_3H_4N_2O_3$	6.2
$C_3H_8N_4O$	16.4
$C_4H_4O_4$	5.2
$C_4H_8N_2O_2$	10.3
$C_4H_{12}N_4$	38.7
$C_5H_8O_3$	7.7
$C_5H_{12}N_2O$	17.1

[a]Must meet the criteria: 1. An even number of N's or none, 2. At least 3 active H's.

[b]Ratio of the abundance of the M+1 peak to the abundance of the M+2 peak.

given above. Table 8 contains a list of isotopic abundances[43] of the elements which are present in the silylated derivatives. The calculation

was made on the M-57 peak of the MTBSTFA silylated derivative because it has an abundance of 100%. From the GC peak at 32.8 minutes in the chromatogram of Figure 63 the M-57 peak is found to be 401.

MW	Abundance
401	100%
402	35.0%
403	15.5%

$$\frac{P_{M+1}}{P_{M+2}} = 2.26$$

TABLE 8

Isotopic Abundances

Elements	Abundance					
Carbon	^{12}C	100	^{13}C	1.08	^{14}C	*
Hydrogen	^{1}H	100	^{2}H	0.016		
Oxygen	^{16}O	100	^{17}O	0.04	^{18}O	0.20
Nitrogen	^{14}N	100	^{15}N	0.38		
Silicon	^{28}Si	100	^{29}Si	5.10	^{30}Si	3.35

*The contribution of ^{14}C to the M+2 peak can be calculated by Equation 15.

$$\%(M+2) \simeq \frac{(1.1 \times \text{number of C atoms})^2}{200} \qquad (15)$$

Each TBDMS group adds the following percentage to the M+1 peak:

$C_6H_{15}Si$

(6 C's)(1.08)+(15 H's)(0.016)+(1 Si)(5.10) = 11.82%

After the loss of a tertiary butyl group the fragment remaining would contribute the following to the percentage of the M+1 peak:

C_2H_6Si

(2 C's)(1.08)+(6 H's)(0.016)+(1 Si)(5.10) = 7.36%

The contribution to the M+2 peak for a TBDMS group is:

$$(1\ Si)(3.35) + \frac{(6\ C's \times 1.1)^2}{200} = 3.57\%$$

When a tertiary butyl group is missing, the contribution to M+2 is:

$$(1\ Si)(3.35) + \frac{(1.1 \times 2\ C's)^2}{200} = 3.37\%$$

These values were subtracted from the observed values in the mass spectrum to arrive at what should be the correct abundances for the compound of mass 116.

M+1 35.0% - 2 (11.82%) - 1 (7.36%) = 4.0%

M+2 15.5% - 2 (3.57%) - 1 (3.37%) = 5.0%

$$\frac{P_{M+1}}{P_{M+2}} = 0.8$$

Since the ratio of P_{M+1}/P_{M+2} was so low this eliminated all those possibilities in Table 7 except those with the lowest ratios. Table 9 is the list of the possibilities which remained after this analysis. These formulas were subjected to calculation of the isotope ratio after adding the formula for 2 TBDMS groups and 1 group without the tertiary butyl contribution.

$$2(C_6H_{15}Si) + 1\ (C_2H_6Si) = C_{14}H_{36}Si_3$$

TABLE 9

Possible Empirical Formulas with the Lowest

P_{M+1}/P_{M+2} Ratio

Formula	P_{M+1}/P_{M+2}	Formula after adding $C_{14}H_{36}Si_3$ - 3H's replaced
$C_2H_4N_4O_2$	8.3	$C_{16}H_{37}N_4O_2Si_3$
$C_3H_4N_2O_3$	6.2	$C_{17}H_{37}N_2O_3Si_3$
$C_4H_4O_4$	5.2	$C_{18}H_{37}O_4Si_3$
$C_5H_8O_3$	7.7	$C_{19}H_{41}O_3Si_3$

An example of how the expected M+1 and M+2 abundances were calculated is illustrated using $C_2H_4N_4O_2$:

$$M+1 = 16(1.08)+37(0.016)+4(0.38)+2(0.04)+3(5.1) = 34.8\%$$

$$M+2 = \frac{(16x1.1)^2}{200} + 2(0.20)+3(3.35) = 12.0\%$$

$$P_{M+1}/P_{M+2} = 2.90$$

Usually it is observed that experimental isotopic abundances are somewhat greater than calculated values because of other contributions to the observed abundances.[43] Taking into account this fact would seem to lower the probability that either of the last two formulas are the correct ones. If the structure of the other electrolysis products is considered it is only reasonable that the compound of LC peak 4 should contain nitrogen.

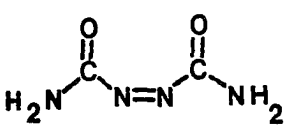
TABLE 10

Calculated Isotopic Abundances for the Silylated Derivatives

Formula	M+1	M+2	P_{M+1}/P_{M+2}
$C_2H_4N_4O_2$	34.8	12.0	2.90
$C_3H_4N_2O_3$	35.1	12.4	2.83
$C_4H_4O_4$	35.5	12.8	2.77
$C_5H_8O_3$	36.6	12.8	2.86

A search of the literature revealed only a limited number of possibilities for the molecular formulas $C_2H_4N_4O_2$ and $C_3H_4N_2O_3$. Table 11 lists the most likely possibilities.

From the fact that LC peak 4 exhibits an u.v. spectrum with the long wavelength peak at 420 nm in acidic solution suggests it must have a conjugated system of several double bonds. The only molecule which meets this criteria is azodicarbonamide (XII).



XII

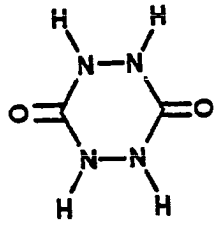
An u.v. absorption spectrum is reported in the literature which has a weak absorption at $\lambda_{max} \simeq 420$ nm and a stronger absorption at shorter wavelengths.[45] A more recent report gives the spectrum in ethanol with $\lambda_{max} = 245$ nm ($\log \varepsilon = 3.33$) and 422 nm ($\log \varepsilon = 1.56$).[46] The melting

TABLE 11

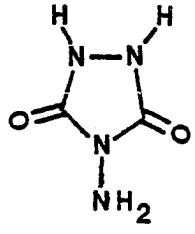
Possibilities for Compounds with Molecular Formulas

$C_2H_4N_4O_2$ and $C_3H_4N_2O_3$

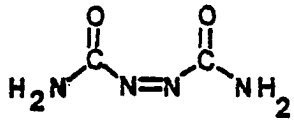
$C_2H_4N_4O_2$



1. diurea[a] (also known as hexahydro-1,2,4,5-tetrazine-3,6-dione, or p-urazine)

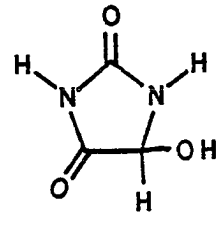


2. 4-aminourazole



3. azodicarbonamide

$C_3H_4N_2O_3$



1. 5-hydroxyhydantoin (also known as 5-hydroxy-2,4-imidazolidinedione)

[a]Reference 44 states that diurea or p-urazine was later determined to be 4-aminourazole.

point is reported as 225°C with decomposition.[47] In the absence of other data it appears that LC peak 4 is probably azodicarbonamide.

Tentative identification of LC peak 3. A positive identification of LC peak 3 was not made, however the data collected allowed a plausible structure to be proposed. LC peak 3 was the fraction collected from 240 ml to 255 ml on the rising section of the group of LC peaks 3-6. When first collected it exhibited a strong u.v. spectrum with λ_{max} = 233 nm. After several days in solution a hypsochromic shift was observed (λ_{max} = 228 nm) and the absorbance decreased. Immediately after lyophilization the fluffy material collected appeared white. After a short time (ca. 6-8 hours) it began to turn yellowish and when redissolved it now exhibited an u.v. spectrum very similar to that for LC peak 4.

It was also found that the compound responsible for the u.v. absorption at λ_{max} = 233 nm could be rapidly decomposed by adding a small amount of a concentrated NaOH solution. The absorbance at 233 nm decreased rapidly and after about 10 minutes the u.v. spectrum exhibited only the characteristic absorption of sodium hydroxide from 210 nm to 190 nm. Lyophilization of the neutralized solution yielded a white powder. Apparently decomposition by using sodium hydroxide yielded a different product from the decomposition in the dry state.

GC-MS analysis of LC peak 3. As a result of the ease of decomposition good GC-MS data was difficult to obtain. Silylation of LC peak 3 was attempted with all three silylation reagents, MTBSTFA, BSA, and BSTFA. Pyridine and acetonitrile were both tried as solvents.

Temperatures from room temperature to 100°C were used with MTBSTFA and as high as 120°C for BSA. Reaction times as long as 30 minutes were used.

Initial silylation attempts with MTBSTFA (100°C, 15 minutes) yielded a total ion current chromatogram which showed a fairly large peak for guanidine (M^+=401) and another peak at 21.6 minutes with a molecular ion of mass 318. This same sample when silylated with MTBSTFA at room temperature did not show the peak at R_t=21.6 minutes (M^+=318) and only a very small guanidine peak. Initial silylation attempts with BSA failed to yield any useful results. These experiments were repeated numerous times and the results seem to be different each time. The only thing which seemed repeatable was the appearance of the guanidine peak at R_t=29.3 minutes.

Finally the procedure which yielded the results given below was determined. The product from LC peak 4 was allowed to remain in solution until ca. 8 hours before the silylation procedure when it was lyophilized. This minimized the decomposition of the sample which was observed in the dry state. Two identical samples were prepared in this manner. One was silylated with MTBSTFA in pyridine at 100°C for 11 minutes (Figure 65). The other sample was silylated with BSA in pyridine at 120°C for 16 minutes (Figure 66). In the total ion current chromatogram of the MTBSTFA silylated product there are several peaks which are not part of the background: R_t=21.3 minutes (M^+=318); 29.5 minutes (M^+=401); 30.9 minutes (M^+=374); and 35.3 minutes (M^+=516). Peaks of interest from the BSA silylated product are: R_t=20.8 minutes (M^+=319); 23.4 minutes (M^+=290); and 29.1 minutes (M^+=223).

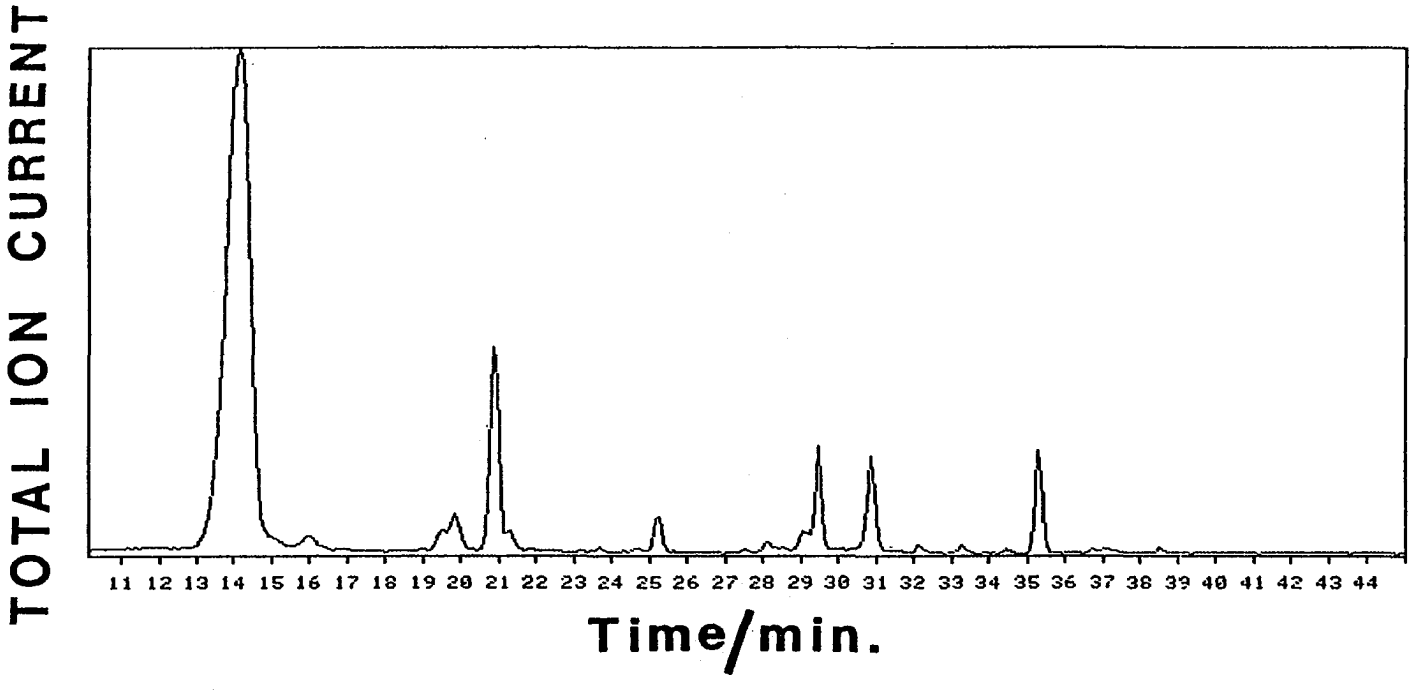


Figure 65. Total ion current chromatogram of product isolated from LC peak 3 and silylated with MTBSTFA in pyridine at 100°C for 11 minutes.

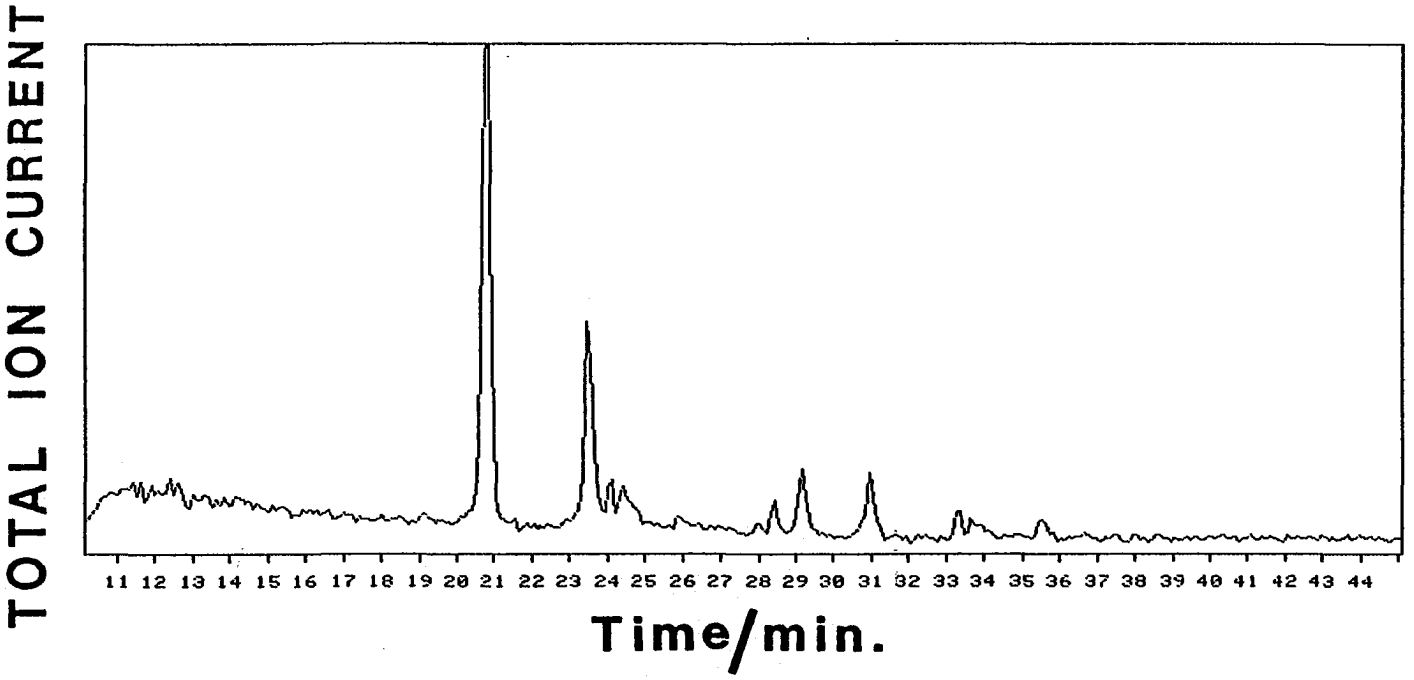


Figure 66. Total ion current chromatogram of product isolated from LC peak 3 and silylated with BSA in pyridine at 120°C for 16 minutes.

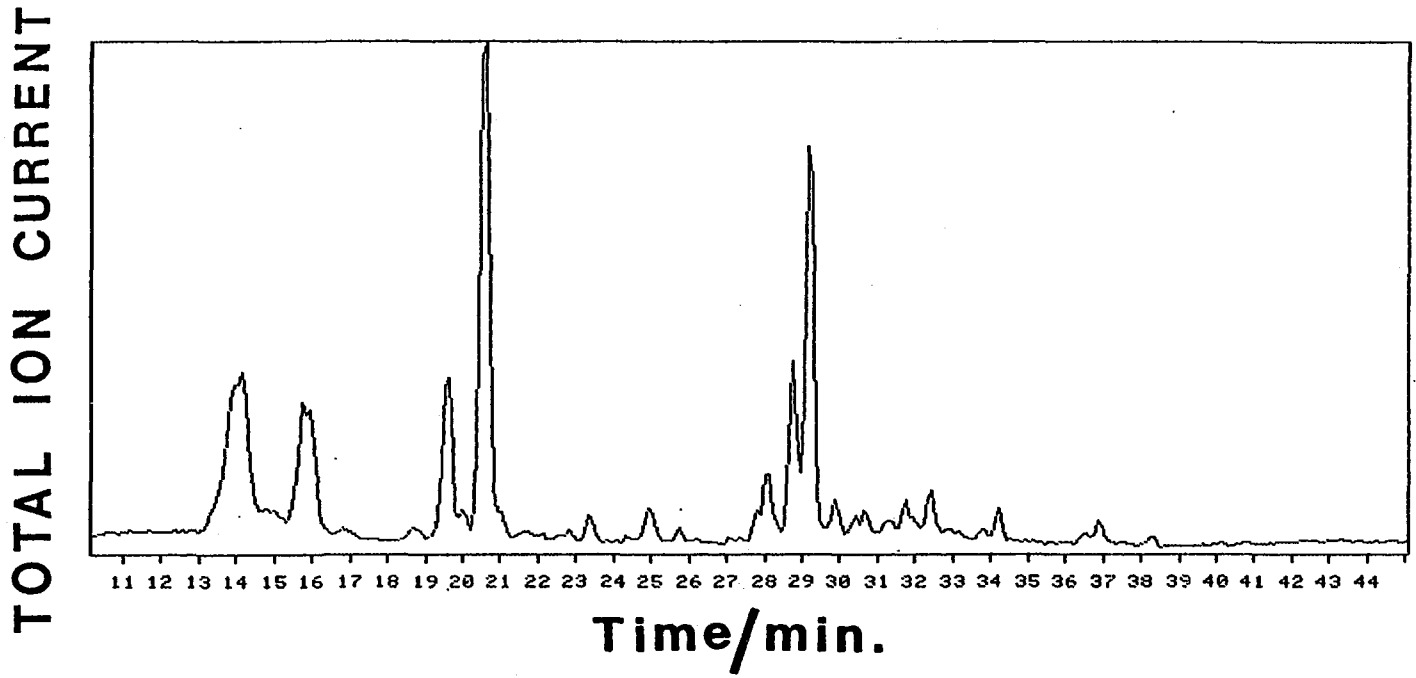


Figure 67. Total ion current chromatogram of the sodium hydroxide decomposed product from LC peak 3. Silylation was carried out with MTBSTFA in pyridine at 85°C for 10 minutes.

There is only one peak in each chromatogram which corresponds to the same compound. This is the peak at 30.9 minutes in the MTBSTFA silylation and the peak at 23.4 minutes in the BSA silylation. The number of silylated positions was calculated from Equation 14:

$$374 - 290 = 42\,(n) = 84$$

$$n = 2 \text{ silylated positions}$$

The molecular weight is found by subtracting the contribution of the silyl groups:

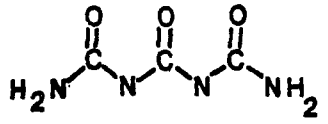
$$MW = 374 - 2(114) = 290 - 2(72) = 146 \text{ g/mole}$$

The sample which was decomposed with sodium hydroxide was also silylated with MTBSTFA in pyridine. Its total ion current chromatogram is entirely different from that of LC peak 3 in Figure 66. The main peaks are at R_t = 19.6 minutes (M^+=318) and 29.3 minutes (M^+=401) which is further evidence that guanidine and the compound represented by mass 318 were really decomposition products of LC peak 3 (Figure 67). There are a number of small peaks in the chromatogram which are probably other decomposition products.

Use of isotope ratio and mass tables. All of the details for limiting the number of possible formulas is analogous to what was presented for LC peak 4 and only the results are presented for LC peak 3. If guanidine was really a decomposition product than the compound isolated from LC peak 3 must contain at least 3 nitrogen atoms. Since the molecular weight is even it must have either 4 or 6 atoms of nitrogen. The most likely molecular formula which met the greatest number of criteria

imposed upon it is $C_3H_6N_4O_3$. Since it has 6 hydrogen atoms it is quite unlikely that it is a ring system, but rather a ring-opened product of one of the pterins identified earlier or one of the intermediates observed in the thin-layer spectroelectrochemistry and cyclic voltammetry.

One possible compound with molecular formula $C_3H_6N_4O_3$ is triuret (XIII).



XIII

It was considered as a possibility if guanidine were to form an oligomer and then hydrolyze. However triuret was reported to be only slightly soluble in cold water and melts with decomposition at 231°C.[48] The product from LC peak 3 was very soluble in cold water and appeared to discolor only slightly when heated to 320°C.

More information about the structure of the LC peak 3 product was obtained from the i.r. spectrum of the KBr disc (Figure 68). A broad band is observed between ca. 3600 cm^{-1} and 2600 cm^{-1} which is characteristic of a carboxylic acid. Two peaks are superimposed on this broad band at 3340 cm^{-1} and 3180 cm^{-1} which are characteristic of a primary amide in the solid state.[43] The strong carbonyl absorption at 1650 cm^{-1} is also characteristic of a carbonyl group in an amide. Primary amides also exhibit CN stretch near 1400 cm^{-1} and a band in Figure 68 is observed at 1380 cm^{-1}.

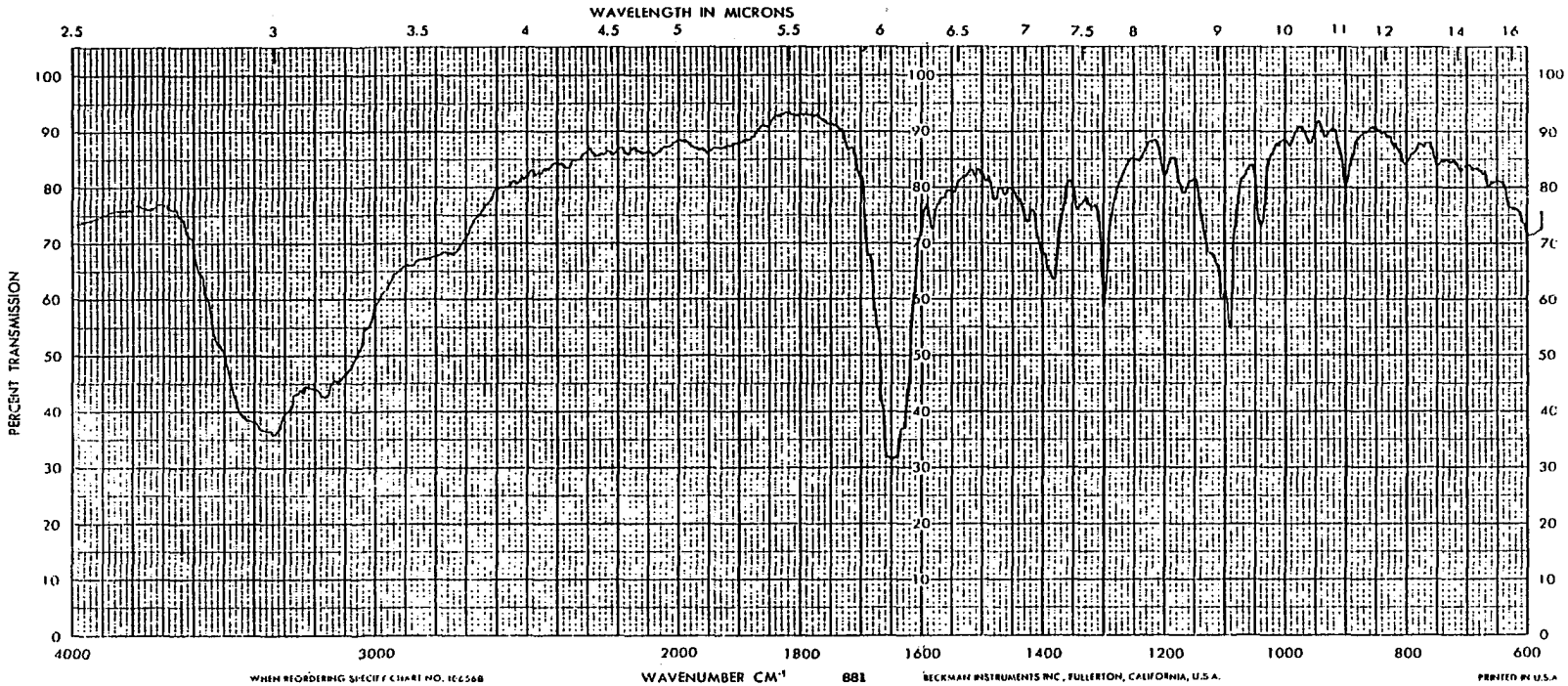
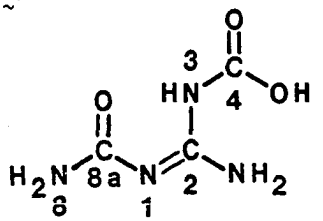


Figure 68. I.r. spectrum of LC peak 3 product. Spectrum was obtained on a KBr disc.

A possible structure of molecular formula $C_3H_6N_4O_3$ which takes into account all of the above facts and considers the origin of the product is structure (XIV).



XIV

The numbering in structure (XIV) refers to the positions these atoms are derived from in the original pterin molecule. This seems a plausible structure which can explain the observed properties.

Minor LC peaks 7 and 8. The products isolated from LC peaks 7 and 8 exhibited very weak u.v. spectra with a short wavelength inflection at ca. 215 nm in each case and a small peak at λ_{max}≃280 nm for LC peak 7 and 265 nm for LC peak 8 in distilled water. Both compounds are electroactive at the PGE. LC peak 7 exhibited a small oxidation peak at 0.49V/SCE in pH 4.7 phosphate buffer. This oxidation peak has a reduction peak associated with it at 0.42V/SCE. LC peak 7 also showed two other very small reduction peaks at -0.63V and -0.94V/SCE. LC peak 8 has only one very small oxidation peak at the PGE in pH 4.7 phosphate with a peak potential of 0.49V/SCE. These two LC peaks appeared to be very minor products which have a very similar structure. LC peaks 7 and 8 as well as LC peaks 1 and 2 were not studied more thoroughly because of the fact they do not appear to account for very much of the total electrolysis products.

Products were found in the electrolysis product solution which could only have been formed by loss of the methyl group at the N(5)-position. N-demethylation of various N-heterocyclic compounds during electrooxidation has been reported in the literature.[49-51] The mechanism proposed for these processes proceeds through an iminium cation which ultimately loses a molecule of formaldehyde. Another possible pathway for the loss of the methyl group is by loss of a methyl carbonium ion. Consequently an experiment was carried out to determine if formaldehyde was a constituent of the electrolysis product solution.

Formaldehyde can be determined in aqueous solutions by the use of the chromotropic acid test. Chromotropic acid forms an intense purple color with formaldehyde which is very specific for formaldehyde.[52] The chromotropic acid test was carried out according to the procedure described by McAllister.[53] Conditions for the electrolysis were chosen to maximize the yield of xanthopterin in the belief that this should be an indication of the amount of 5-MTHP demethylated. The conditions for maximum formation of xanthopterin were found to be an electrolysis potential of 0.32V/SCE in pH 4.7 phosphate buffer with an ionic strength of 0.5 M. No formaldehyde was detected in the electrolysis product solution using the chromotropic acid test. Therefore it was concluded that the methyl group was probably lost during the electrooxidation process *via* a methyl carbonium ion.

Explanation of Observed Properties

The cyclic voltammetry after peak I_a electrolysis suggests that some kind of xanthopterin or 7,8-dihydroxanthopterin species is responsible for the oxidation and reduction peaks observed. (Compare Figure 51 of xanthopterin and Figures 55 and 56 of LC peak 10 with Figures 12 and 13 of peak I_a electrolysis solution.) Since peak II_a is observed on the initial positive sweep in the electrolysis solution this suggests the product isolated from LC peak 10 (identified as 5-methyl-7,8-dihydroxanthopterin) is responsible for this oxidation process. The reversibility of peak III_a also supports the fact that 5-methyl-7,8-dihydroxanthopterin (5-M-7,8-DXP) is a major product because peak III_a of xanthopterin does not exhibit reversible behavior. However peaks IV_a and V_a are very nearly the same size in the cyclic voltammetry of the electrolysis solution, unlike 5-M-7,8-DXP in which peak IV_a is much larger than peak V_a. This suggests that xanthopterin is present because it has a peak V_a oxidation peak which is much larger than peak IV_a, just the opposite of 5-M-7,8-DXP. If both were present in ca. equal quantities then peaks IV_a and V_a would be ca. equal in size.

The possibility of unsubstituted 7,8-dihydroxanthopterin in the electrolysis product mixture cannot be ruled out, however none was isolated during the chromatography and none was observed in the GC-MS of the total product mixture (vide supra). The oxidation peak which occurs at ca. 0V in the electrolysis product solution can be explained by observing the cyclic voltammetry of pterin (Figure 47B), xanthopterin (Figure 51), and 5-M-7,8-DXP (Figures 55 and 56). All three compounds exhibit an oxidation peak near 0V after sweeping toward negative

potentials and then reversing the sweep. This could explain the unusually broad and unsymmetrical shape observed for this peak in the product mixture (Figure 12).

Reduction peaks observed in the voltammetry of the electrolysis product solution (Figure 12) can be explained by observing the voltammetry of pterin, 5-M-7,8-DXP, and xanthopterin. However, this does not explain the first reduction peak observed in Figure 12B on the initial negative sweep. It is entirely possible that the product responsible for this peak decomposes by the time the product separation is complete. None of the separated products was observed which had a reduction peak at this potential supporting this viewpoint.

The thin-layer spectroelectrochemistry suggests that two intermediates are generated when 5-MTHP is electrooxidized at peak I_a. 7,8-DHP is observed to be the final product whenever the potential is applied for only a short time, only long enough to generate a reasonable concentration of intermediate. First order rate constants for the fast step, k_1, at pH 6.9 and 7.8 are within the range of the rate constants for the chemical rearrangement of the quinonoid-dihydropterin of tetrahydropterin.[7] At pH 4.7 only one rate constant is observed which is a factor of 10 smaller than those for the chemical rearrangement of the quinonoid-dihydropterin. The smaller rate constant, k_2, is probably for the rearrangement of the intermediate which gives 5-methyl-7,8-dihydroxanthopterin. Referring back to Table 6 which is the list of the silylated products for peak I_a electrolysis of 5-MTHP in 0.5 M NaCl there is evidence of additional products with a molecular weight of 193, 211, and 209 g/mole. These could correspond to 5-methylxanthopterin,

covalently hydrated 5-methylxanthopterin, and 5-methylleucopterin respectively. They are not observed however in the separated products which were positively identified.

Other products which were identified appear to be fragments of the pterin nucleus. They are probably formed by breakdown of an unstable intermediate, possibly 5-methyl-5,8-dihydropterin. This intermediate may be responsible for the absorbance observed at 246 nm at pH 6.9 and 7.8 during electrolysis of 5-MTHP in the RVC thin-layer cell.

Proposed Reaction Scheme

The linear sweep voltammetry of 5-MTHP in pH 4.7 phosphate buffer exhibits a number of oxidation peaks (Figure 1B). The peak I_a electrooxidation process of 5-MTHP is much more complex than the peak I_a electrooxidation process of other tetrahydropterins recently investigated.[7-10] Peak I_a electrooxidation of 5-MTHP appears to involve several different processes. Figure 69 illustrates the reaction scheme proposed for the pathway in which the methyl group is lost during the oxidation process. Figure 14A, which is a cyclic voltammogram of 5-MTHP in pH 4.7 0.5 M NaCl, illustrates that two processes may be occurring at very nearly the same potential because a shoulder is observed on the rising portion of peak I_a. It is proposed that 5-MTHP (I, Figure 69), which is protonated at pH 4.7, is oxidized in an initial $1e\text{-}1H^+$ process to a cation radical (II, Figure 69). This cation radical may be the species which is quasi-reversibly reduced at peak I_c. The small size of peak I_c even at 20 $V\,s^{-1}$ (Figure 11C) indicates that the species is quite unstable. The air oxidation of 5-methyltetrahydropterins has been

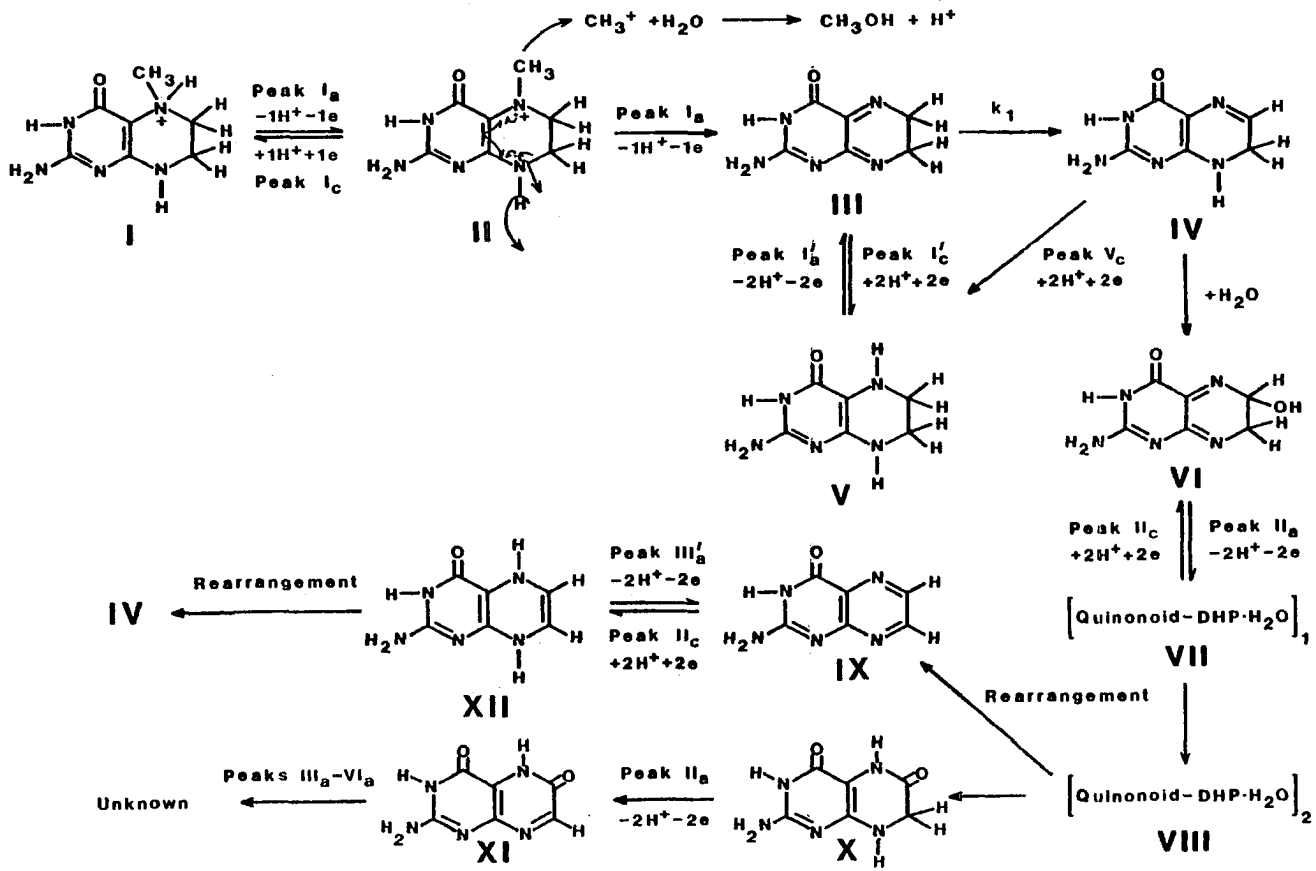


Figure 69. Proposed reaction scheme to explain the observed products for oxidation of 5-MTHP at peak I_a in which the methyl group is lost.

reported to proceed via a cation radical.[36,54] A subsequent 1e-1H$^+$ process occurs immediately, together with the loss of a methyl carbonium ion. The remaining electron of the lone pair of each nitrogen atom and the two electrons in the 4a,8a double bond migrate to form double bonds in the 4a-5 position and the 8-8a position. This proposed compound (III, Figure 69) is one of the possible quinonoids of tetrahydropterin.[7] Quinonoid-dihydropterin (III, Figure 69) is reduced at peak I_c' (see Figure 5) in a 2e-2H$^+$ process to tetrahydropterin (V, Figure 69). Tetrahydropterin (V, Figure 69) is reoxidized at peak I_a' in a 2e-2H$^+$ process to the same quinonoid-dihydropterin (III, Figure 69). This quinonoid-dihydropterin rearranges to 7,8-dihydropterin (IV, Figure 69) characterized by rate constant k_1. 7,8-dihydropterin (IV, Figure 69) undergoes an acid catalyzed hydration (below ca. pH 6) to form the 5,6-covalently hydrated dihydropterin (VI, Figure 69).[7] Compound VI (Figure 69) is electrooxidized in a 2e-2H$^+$ process at peak II_a' (Figure 4A) to another quinonoid species (VII, Figure 69). This quinonoid rearranges to a second, more stable quinonoid (VIII, Figure 69). One or both of these quinonoids is reduced at peak II_c' in a quasi-reversible 2e-2H$^+$ process to the 5,6-covalently hydrated dihydropterin (VI, Figure 69). Quinonoid VIII (Figure 69) was found to break down to pterin (IX, Figure 69) and 7,8-dihydroxanthopterin (X, Figure 69).[7] The rearrangement of quinonoids VII and VIII (Figure 69) was not observed in the thin-layer spectroelectrochemistry because of their low concentration. 7,8-dihydroxanthopterin (X, Figure 69) is oxidized at peak II_a in a 2e-2H$^+$ process to xanthopterin (XI, Figure 69). Xanthopterin is responsible for oxidation peaks III_a-V_a and possibly

peak VI_a (Figure 1B). The reaction scheme from compound III to the end is identical to that reported in reference 7.

Reduction peaks II_c and V_c in cyclic voltammetry of 5-MTHP (Figure 5) are due to reduction of pterin (IX, Figure 69) first to 5,8-dihydropterin (XII, Figure 69) which rearranges to 7,8-dihydropterin (IV, Figure 69). Subsequently 7,8-dihydropterin (IV, Figure 69) is reduced to tetrahydropterin (V, Figure 69) at peak V_c. Peak IV'_c which is only observed at low concentrations of 5-MTHP (Figure 7A) or slow sweep rates (Figure 10B) is probably due to resolution of peak II_c into its diffusion controlled component and adsorption component.[7]

The other reaction scheme proposed is for the pathway where the N(5)-methyl group is retained during the peak I_a oxidation process of 5-MTHP. In this pathway 5-MTHP (I, Figure 70) is proposed to be oxidized in a $2\underline{e}$-$2H^+$ process to the protonated form of 5-methyl-5,8-dihydropterin (II, Figure 70), which subsequently loses the proton. 5-methyl-5,8-dihydropterin (II, Figure 70) is proposed to hydrate across the 6,7-double bond in a process which is characterized by rate constant, k_2. This covalently hydrated 5-methyl-5,8-dihydropterin (III, Figure 70) is proposed to be oxidized in a $2\underline{e}$-$2H^+$ process (near peak I_a potentials) to 5-methyl-7,8-dihydroxanthopterin (IV, Figure 70). 5-methyl-7,8-dihydroxanthopterin (IV, Figure 70) is oxidized at peak II_a to 5-methylxanthopterin (V, Figure 70). Oxidation peaks III_a-V_a and VII_a appear to be a result of further oxidation of 5-methylxanthopterin. Since 5-M-7,8-DXP and xanthopterin both give rise to oxidation peaks at potentials corresponding to peaks III_a-V_a of 5-MTHP, it is entirely possible that oxidation of both compounds (formed by rearrangement of

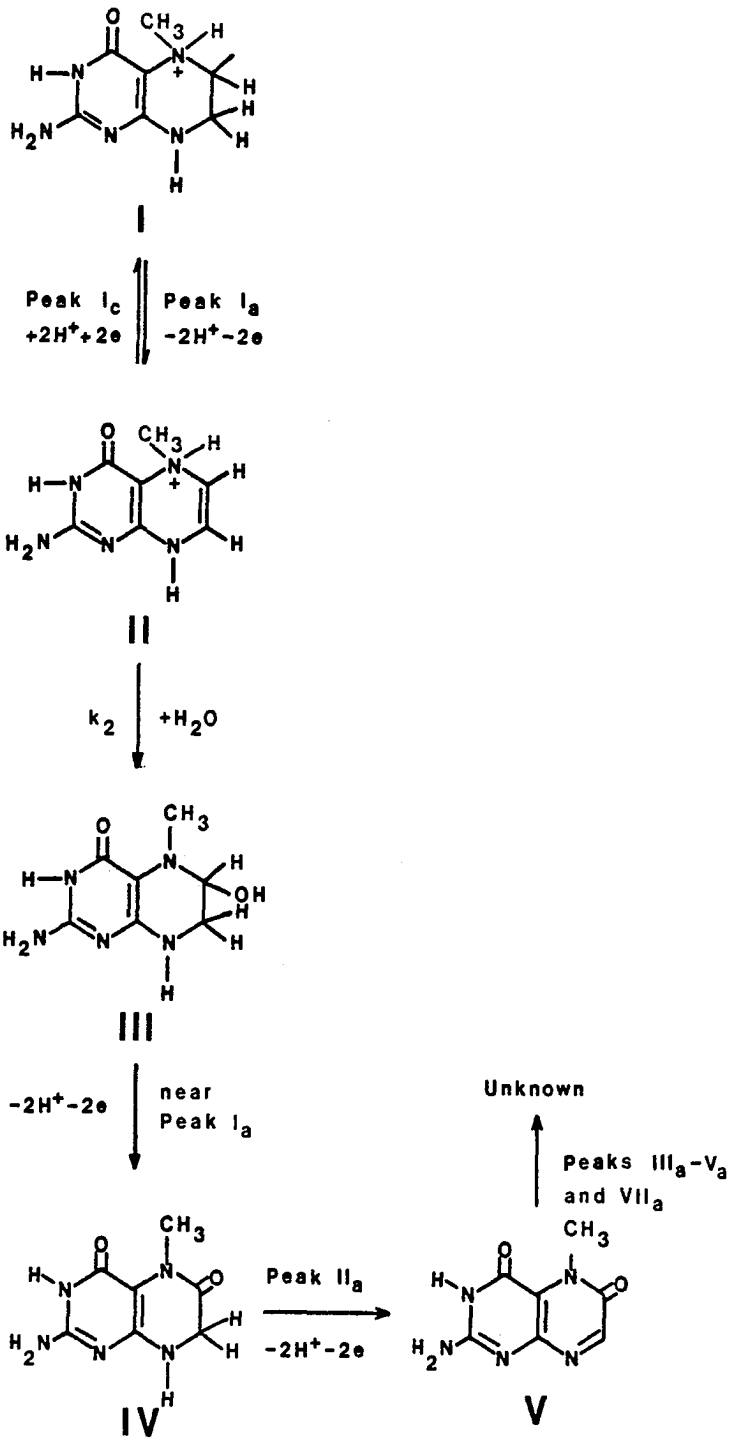


Figure 70. Proposed reaction scheme to explain the observed products for oxidation of 5-MTHP at peak I_a in which the methyl group is retained.

intermediates generated at peak I_a) is occurring simultaneously.

Reduction peaks III_c' and IV_c (Figure 8B) are due to reduction of products from electrooxidation of 5-methyl-7,8-dihydroxanthopterin or 5-methylxanthopterin. Peak III_c is not observed unless the positive sweep in cyclic voltammetry passes through oxidation peak VI_a or VII_a (compare Figures 5 and 8B). This indicates it is probably reduction of a product from further oxidation of 5-methylxanthopterin or xanthopterin.

CHAPTER III

EXPERIMENTAL

Chemicals. 5-methyltetrahydropterin was synthesized via the technique of Matsuura and Sugimoto.[39] Pterin used for the synthesis of 5-MTHP was obtained from Sigma Chemical (St. Louis, MO). Platinum (IV) oxide (Adams' catalyst) was obtained from Aldrich Chemical Co. (Milwaukee, WI). Xanthopterin, leucopterin (Sigma Chemical, St. Louis, MO) and guanidine hydrochloride (Matheson, Coleman, and Bell, Norwood, OH) were used as standards for the GC-MS analyses.

The procedure for recrystallization of 5-MTHP was modified somewhat. The procedure called for dissolving the lyophilized residue in 25 ml of 4 N HCl and concentrating to 5 ml to obtain the product. However, when the concentration step was carried out the product precipitated from solution all at once before the 5 ml volume was attained. Therefore the procedure was modified so that the residue was dissolved in a minimum amount (ca. 9-10 ml) of boiling 4 N HCl. This solution was cooled slowly and a precipitate of large, creamy white crystals separated from the mother liquor. After the solution cooled to room temperature, it was further cooled by refrigeration to obtain the product. The crystals were filtered off and washed with 3 portions of methanol (ca. 2 ml each). The product had a melting point of 245-247°C with decomposition (reported m.p. = 237-239°C).[39] Direct insertion mass spectroscopy

of the product gave a molecular weight of 181 g/mole.

Using the molar absorptivity of 2.63×10^4 at 215 nm in a pH 3.5 solution the molecular weight of the product was determined to be ca. 254 g/mole. The dihydrochloride salt of 5-MTHP, $C_7H_{11}N_5O \cdot 2HCl$ has a calculated molecular weight of 254 g/mole. Thus the product was found to be the dihydrochloride salt of 5-MTHP.

Silylating reagents, bis (trimethylsilyl) trifluoroacetamide (BSTFA), N,O-bis (trimethylsilyl) acetamide (BSA), pyridine, and acetonitrile were obtained from Supelco, Inc. (Belletonte, PA). N-methyl-N-t-butyldimethylsilyl trifluoroacetamide was obtained from Regis Chemical Co. (Morton Grove, IL). 3% SE-30 on Chromosorb W (HP) 80/100 mesh used for gas chromatography was obtained from Supelco, Inc. (Bellefonte, PA). Sephadex G-10 resin used for gel permeation chromatography was obtained from (Pharmacia Fine Chemicals, Piscataway, NJ).

Electrolyses were carried out in sodium phosphate buffers of ionic strength 0.5 M (see Experimental Chapter, Part II) or in 0.5 M NaCl.

Apparatus. The apparatus for voltammetry, coulometry, and thin-layer spectroelectrochemistry is described in Chapter IV of Part II.

Gravity flow chromatographic systems utilized a Pharmacia Model SR 25/100 (2.5 cm x 100 cm) column. The column was generally filled with 75 cm of Sephadex G-10 resin. A Gilson Model HM Uv-vis Holochrome flow-through detector (Gilson Medical Electronics Inc., Middleton, WI) set at 207 nm was used as the detector. The output of the detector was recorded on a Houston Instruments Omniscribe stripchart recorder. 3 ml fractions were collected using either an Isco Model 328 fraction collector

(Instrumentation Specialties Co., Lindoln, NE) or a Buchler Fractomat fraction collector. U.v. spectra of the collected samples were obtained with a Hitachi Model 100-80 Uv-vis Spectrophotometer.

Gas chromatography utilized a Varian Model 2400 gas chromatograph with FID detection (Varian, Palo Alto, CA). Coupled gas chromatography-mass spectrometry utilized a Hewlett-Packard Model 5985 GC-MS.

Procedures. Electrolyses in phosphate-free solutions used 0.5 M NaCl as the supporting electrolyte. The pH was monitored using an Orion Research Model 501 Digital Ionalyzer with an Orion Model 91-04 combination pH electrode. Microliter quantities of ca. 1 N NaOH were added with a syringe to maintain the pH at 4.7±0.1.

Silylation was accomplished using ca. 100 ul of silylating reagent and 100 ul of solvent (generally pyridine) in a 3 ml Reacti-Vial (Pierce Chemical Co., Rockford, IL). When MTBSTFA was used the silylation was generally carried out at room temperature for ca. 30 minutes or 100°C for 15 minutes. With BSA or BSTFA temperatures used were generally 120°C for ca. 20-30 minutes. Samples were generally silylated immediately prior to GC-MS analysis in case the silylated derivatives were unstable.

Chromotropic acid reagent for detection of formaldehyde was prepared according to McAllister[53] (0.1 g of the disodium salt of chromotropic acid in 3.3 ml of water added to 30 ml of concentrated H_2SO_4). 1 ml of the chromotropic acid solution was added to 1 ml of the electrolysis solution in a test tube and the volume made up to 10 ml with concentrated H_2SO_4. The solution was heated in a boiling water bath to develop the color. A water blank and a 1 mM standard formaldehyde solution were carried through the same procedure.

CHAPTER IV

SUMMARY

The peak I_a electrooxidation process of 5-methyltetrahydropterin was investigated using a variety of electrochemical techniques. It was found that the oxidation process was not a simple $2\underline{e}$-$2H^+$ process as in many other tetrahydropterins. In fact the peak I_a process appears to proceed through two pathways, one which retains the methyl group and the other in which the methyl group is lost. The pathway in which the methyl group is lost appears to predominate in phosphate buffer with an ionic strength of 0.5 $\underline{M}$, while the retention of the methyl group is favored during electrolysis in 0.5 $\underline{M}$ NaCl. After the loss of the methyl group the reaction pathway follows the same course as tetrahydropterin. It is also proposed that the degradation products observed are a result of breakdown of the putative 5-methyl-5,8-dihydropterin intermediate which leads to 5-methyl-7,8-dihydroxanthopterin. Thus the peak I_a electrooxidation process has been elucidated in some detail.

CHAPTER V

REFERENCES

1. S. Kaufman, Proc. Nat. Acad. Sci. U.S.A., 50 (1963) 1085.
2. A. R. Brenneman and S. Kaufman, Biochem. Biophys. Res. Commun., 17 (1964) 177.
3. W. Lovenberg, E. Jequier, and A. Sjoerdsma, Science, 155 (1967) 217.
4. F. I. Maclean, Y. Fujita, H. S. Forrest, and J. Myers, Plant Physiol., 41 (1966) 774.
5. A. Tietz, M. Lindberg, and E. P. Kennedy, J. Biol. Chem., 239 (1964) 4081.
6. A. Albert in Chemistry and Biology of Pteridines, W. Pfleiderer (Ed.), W. de Gruyter, Berlin, 1975, p. 1.
7. R. Raghavan and G. Dryhurst, J. Electroanal. Chem., 129 (1981) 189.
8. D. Ege-Serpkenci and G. Dryhurst, Bioelectrochem. Bioenerg., 9 (1982) 175.
9. L. G. Karber and G. Dryhurst, J. Electroanal. Chem., 136 (1982) 271.
10. D. Ege-Serpkenci, Ph.D. Dissertation, University of Oklahoma, 1982.
11. S. Kaufman, Biochim. Biophys. Acta, 27 (1958) 428.
12. S. Kaufman and B. Levenberg, J. Biol. Chem., 234 (1959) 2683.
13. T. Nagatsu, K. Mizutani, I. Nagatsu, S. Matsuura, and T. Sugimoto, Biochem. Pharmacol., 21 (1972) 1945.
14. J. M. Whiteley, J. H. Drais, and F. M. Huennekens, Arch. Biochem. Biophysics, 133 (1969) 436.
15. W. L. F. Armarego and H. Schow, Aust. J. Chem., 31 (1978) 1081.
16. V. Herbert, A. R. Larrabee, and I. M. Buchanan, J. Clin. Invest., 41 (1962) 1134.

17. J. Stavrianopoulos and L. Jaenicke, Eur. J. Biochem., 3 (1967) 95.

18. S. J. Benkovich, Ann. Rev. Biochem., 49 (1980) 227.

19. P. F. Nixon and J. R. Bertino, New Engl. J. Med., 286 (1972) 175.

20. W. A. Bleyer, Cancer, 41 (1978) 36.

21. B. M. Mehta, A. N. Gisolf, D. J. Hutchinson, A. Nirenberg, M. G. Kellick, and G. Rosen, Cancer Treat. Rep., 6 (1978) 345.

22. H. Sauer and W. Wilmanns in Chemistry and Biology of Pteridines, W. Pfleiderer (Ed.), W. de Gruyter, Berlin, 1975, p. 153.

23. M. Viscontini, H. Leidner, G. Mattern, and T. Okada, Helv. Chim. Acta, 49 (1966) 1911.

24. A. Ehrenberg, P. Hemmerich, F. Mueller, T. Okada, and M. Viscontini, Helv. Chim. Acta, 50 (1967) 411.

25. M. Viscontini and T. Okada, Helv. Chim. Acta, 50 (1967) 1492.

26. M. Viscontini and T. Okada, Helv. Chim. Acta, 50 (1967) 1845.

27. A. Ehrenberg, P. Hemmerich, F. Mueller, and W. Pfleiderer, Eur. J. Biochem., 16 (1970) 584.

28. J. A. Jongejan, H. I. X. Mager, and W. Berends in Chemistry and Biology of Pteridines, R. L. Kisluik and G. M. Brown (Eds.), Elsevier, New York, 1979, p. 241.

29. J. A. Jongejan, H. I. X. Mager, and W. Berends, Tetrahedron, 31 (1975) 533.

30. H. von Koningsveld, Tetrahedron, 31 (1975) 541.

31. G. R. Gapski, J. M. Whiteley, and F. M. Huennekens, Biochemistry, 10 (1971) 2930.

32. M. Viscontini and A. Bobst, Helv. Chim. Acta, 48 (1965) 816.

33. J. A. Blair, A. J. Pearson, and A. J. Robb, J. Chem. Soc. Perkin II, 1975, p. 18.

34. T. Maruyama, T. Shiota, and C. L. Krumdieck, Anal. Biochem., 84 (1978) 277.

35. T. L. Deits, A. Russel, K. Fugii, and J. M. Whiteley in Chemistry and Biology of Pteridines, W. Pfleiderer (Ed.), W. de Gruyter, Berlin, 1975, p. 525.

36. M. Viscontini and T. Okada, Helv. Chim. Acta, 52 (1969) 306.

37. M. H. Kim, Ph.D. Dissertation, University of Oklahoma, 1979.

38. R. H. Wopschall and I. Shain, Anal. Chem., 39 (1967) 1514.

39. S. Matsuura and T. Sugimoto, Research Bulletin (Department of General Education, Nagoya University) 13 (1969) 9.

40. R. L. Blakley in The Biochemistry of Folic Acid and Related Pteridines, A. Neuberger and E. L. Tatum (Eds.), North Holland Publishing Co., Amsterdam, 1969, Chapter 3.

41. W. Pfleiderer, Chem. Bev., 107 (1974) 785.

42. J. H. Beynon and A. E. Williams, Mass and Abundance Tables for Use in Mass Spectrometry, Elsevier, Amsterdam, 1963.

43. R. M. Silverstein, G. C. Bassler, and T. C. Morrill, Spectrometric Identification of Organic Compounds, 3rd Edition, John Wiley and Sons, New York, 1974.

44. H. Neunhoeffer and P. F. Wiley in Chemistry of 1,2,3-Triazines and 1,2,4-Triazines, Tetrazines, and Pentazines, Wiley-Interscience, New York, 1978, p. 1076.

45. A. Hantzsch and J. Lifschitz, Chem. Ber., 45 (1912) 3011.

46. R. Andrisano and T. Vitali, Gazz. Chim. Ital., 93 (1963) 493.

47. Physical Properties of Organic Compounds in The CRC Handbook of Chemistry and Physics, 59th Edition, CRC Press, New York, 1979.

48. R. C. Haworth and F. G. Mann, J. Chem. Soc., (1943) 603.

49. H. Sayo and M. Masui, J. Chem. Soc. Perkin II (1973) 1640.

50. M. Masui and H. Sayo, J. Chem. Soc. (B), (1971) 1593.

51. M. Masui, H. Sayo, and Y. Tsuda, J. Chem. Soc. (B), (1968) 973.

52. F. D. Snell and C. T. Snell, Colorimetric Methods of Analysis, 3rd Edition, Volume 3, D. Van Nostrand, Toronto, 1953, p. 256.

53. D. L. McAllister, Ph.D. Dissertation, University of Oklahoma, 1973.

54. A. M. Bobst, Nature, 220 (1968) 164.